



HAL
open science

Microscopic nonlocal potentials for the study of scattering observables of nucleons within the coupled channel framemork

Amine Nasri

► **To cite this version:**

Amine Nasri. Microscopic nonlocal potentials for the study of scattering observables of nucleons within the coupled channel framemork. Nuclear Theory [nucl-th]. Université Paris Saclay (COMUE), 2018. English. NNT: 2018SACLS273 . tel-02111689

HAL Id: tel-02111689

<https://theses.hal.science/tel-02111689>

Submitted on 26 Apr 2019

HAL is a multi-disciplinary open access archive for the deposit and dissemination of scientific research documents, whether they are published or not. The documents may come from teaching and research institutions in France or abroad, or from public or private research centers.

L'archive ouverte pluridisciplinaire **HAL**, est destinée au dépôt et à la diffusion de documents scientifiques de niveau recherche, publiés ou non, émanant des établissements d'enseignement et de recherche français ou étrangers, des laboratoires publics ou privés.

Microscopic nonlocal potentials for the study of scattering observables of nucleons within the coupled channel framework

Thèse de doctorat de l'Université Paris-Saclay
préparée à l'Université Paris-Sud

École doctorale n°576 PHENIICS
Particules, hadrons, énergie et noyau : instrumentation, imagerie,
cosmos et simulation
Spécialité de doctorat : Structure et réactions nucléaires

Thèse présentée et soutenue à l'Institut de Physique Nucléaire d'Orsay, le vendredi
14 Septembre 2018 par

Amine El Mehdi Nasri

Composition du Jury :

Dr. Denis Lacroix Directeur de recherche à l'IPN Orsay	Président
Pr. Marek Płoszajczak Directeur de recherche au GANIL	Rapporteur
Dr. Toshihiko Kawano Directeur de recherche à Los Alamos National Laboratory	Rapporteur
Dr. Jutta Escher Chargée de recherche à Lawrence Livermore National Laboratory	Examinatrice
Dr. Maëlle Kerveno Chargée de recherche à l'Institut Pluridisciplinaire Hubert Curien	Examinatrice
Dr. Eric Bauge Directeur de recherche au CEA	Directeur de thèse
Dr. Marc Dupuis Ingénieur chercheur au CEA	Co-Directeur de thèse

Dedication

To my grandfathers and Titus, who watch over the end of my studies from the other world, and to my father.

Acknowledgments

This Ph.D. thesis was the occasion for me to (at last!) study nuclear physics, the one subject in physics that thrills me the most. And like probably all other people who are doing, who did or who will do a Ph.D., mine required the implication and support of many people. Unfortunately, my list of saints would take the size of a whole thesis if I mentioned them all here, so I ask those who won't be explicitly mentioned to forgive me.

First, I would like to thank my supervisor Marc Dupuis. I genuinely hope more students will be as lucky as me to be supervised by you, your infinite patience and kindness, and your amazing knowledge in nuclear physics. Five years ago, I discovered your existence through your own Ph.D. paper and it was undoubtedly at that moment and thanks to you that I chose to do a thesis in theoretical physics. My deepest thanks go also to Guillaume Blanchon. You set me on the right rails during my first two months, and you showed me how humble a physicist should be during your presentation in Seattle. I give my thanks to Eric Bauge, who kindly accepted to be my director for this work. And my deepest thanks go to Hugo F. Arellano for providing help, support, deep insight on the physics and his computation code.

I am sincerely grateful to the members of my jury Ms. Jutta Escher, Ms. Maëlle Kerveno and M. Denis Lacroix for the interest and the time they put in reviewing my work. Special thanks go to Toshihiko Kawano-san and M. Marek Płoszajczak for accepting to be referees.

I believe that during the 3 years I spent in the Service de Physique Nucléaire, not only was I working with great colleagues but also and mostly with great friends. I thank Noël Dubray and Nathalie Pillet for the support they showed me during the period when my mother was abroad. I also thank Pascal Morel for his jokes and the time we spent together in Los Hbardos. Thank you Audrey, for running with me when I was clearly too slow for you. Thank you Gilbert B. for your jokes (should I really call them so?) and Julien T. for your great performance at the karaoke.

My thanks go to Jean-Paul Ebran for fascinating discussions on many subjects. I hope you and Adeline raise nice, healthy kids. Thank You, Véronique, for the excellent work and support you provide everyone at work. Thank you Gilbert G., for the nice war-games we had. I hope we'll have more in the future. My thanks go to Stéphane Hilaire, Pascal Romain and Benjamin Morillon, who helped me get a position at IRSN. For introducing me to the Boxing club of ASCEA, I thank deeply Pierre-Jacques Dossantos-Uzarralde. I thank also all members of the boxing club, especially Jean-Luc, Christophe, Johann and Philippe.

To Marc Verrière, David Regnier and Guillaume Hupin, thank you for leading the way! And to Pascal Archier and especially Pierre Tamagno, for supervising my internship in Cadarache and for providing help on ECIS-06. Thank you for all you efforts Pierre. All other members of the Service de physique nucléaire with whom I had the chance to spend

time, thank you for bearing me!

My special thanks go to Jacques Raynal for his friendship and his support on his codes.

I give my greatest thanks to Satoshi Kunieda-san, my supervisor and dear friend from Japan. I hope we'll work together again in the future. I am also very grateful to Kazuhito Mizuyama-san whose passion for physics is so communicative. I have many friends in Japan, I would like to thank them all here, they are part of the reason I was able to go this far.

There are also two persons who are extremely important to me and who literally made me survive through certain periods: Aurélien Nouvion and Emma Leclerc. To the both of you, thank you and FIGHT! And to all my friends in Ex Machina also: FIGHT!

Eventually, I want to thank those who had to spend so many long years raising me and helping me to become a young man. Mom, Dad, Yasmine, Nassima, Nicolas, my family in Algeria: thank you. I hope all the efforts you put in me are worth it. Dad, I hope you feel a bit of your dream through me, it only costs 5 €you know. I hope you all are as proud of me as I am of you!

The last thing I want to mention is the Ph.D. itself, for through the long road it contained I met Mathilde, my wife, my dream, my proud, half of my life and all of my happiness. Thank you for your love, your support, all those helpful pancakes (approved by the very Holy Bob Lennon), and thank God I was crazy enough to do a thesis that made me meet you!

Contents

1	Introduction	1
1.1	Many-body aspects of the nucleon-nucleus scattering problem	2
1.2	Coupled channels and DWBA	5
1.3	Computation of the (generalized) optical potential	9
1.4	The nonlocality of the potential	10
2	The GOM: the Feshbach formalism	15
2.1	Projection operators	16
2.2	Properties of the effective Hamiltonian	17
2.3	Effective interaction and optical potential	19
2.4	Simple case of scattering by a central potential	21
2.5	Formulae for the scattering of a nucleon off a target nucleus	22
2.5.1	Coupling of angular momenta and definition of a basis for projections	22
2.5.2	Total wave function, scattering amplitude and cross section	24
3	Treating the radial part of CC equations	29
3.1	Coupled equations in the radial coordinate basis	29
3.2	Multipole expansion	31
3.3	Solving the system of coupled equations	32
4	Derivation of microscopic potentials	37
4.1	Notations	37
4.2	1-body potential from a 2-body interaction	38
4.3	The Melbourne G matrix	40
4.4	Microscopic description of the target nucleus	43
4.4.1	Hartree-Fock description of the structure of a nucleus	43
4.4.2	Generalities on the Random Phase Approximation for nuclear structure	44
4.4.3	RPA states in spherical symmetry	45
4.4.4	Matrix elements of 1-body density matrices	46
4.5	Formula for the optical potential with a 0+ ground state	49
4.6	Coupling potential in a spherical basis: formulae for the most general case	51
4.6.1	Direct term	52
4.6.2	Exchange term	54
5	Presentation of codes ECANOL and MINOLOP	57
5.1	The microscopic nonlocal potentials code MINOLOP	58

5.1.1	Input files required by MINOLOP	58
5.1.2	Specificities of MINOLOP	59
5.1.3	Treatment of the isospin and LDA	60
5.2	ECANOL	61
5.2.1	Input and options	61
5.2.2	Organization of the code through an example	62
5.3	Validation of ECANOL	67
5.3.1	The vibrational model	67
5.3.2	Validation of ECANOL for local potentials by comparison to ECIS-06	70
5.3.3	Validation of both ECANOL and MINOLOP for nonlocal potentials by comparison to the DWBA98 code	73
6	Applications	81
6.1	Preequilibrium stage of a nuclear reaction	82
6.1.1	Multistep Direct and Multistep Compound processes	82
6.1.2	Microscopic formulation of MSD processes	83
6.1.3	Practical calculation for MSD processes	87
6.2	Extending preequilibrium calculations by including 2-step processes	89
6.2.1	Scheme of approximations	89
6.2.2	Illustration through an example	90
6.3	Contribution of 2-phonon states to preequilibrium emission	91
6.3.1	Interference terms	91
6.3.2	Counting of 2-phonon states	92
6.3.3	Results for 2-phonon states	95
6.4	Contribution of uncorrelated 2p2h states to the preequilibrium emission	98
6.4.1	Derivation of reduced matrix elements for 1-body densities	98
6.4.2	Counting of 2p2h states	103
6.5	Comparison between the contributions of 2-phonon and 2p2h states	105
6.5.1	Violation of the Pauli exclusion principle due to the QBA	108
7	Conclusion	109
A	Wigner 3J, 6J and 9J symbols, Clebsch-Gordan coefficients	113
B	The Gogny D1S force	115
C	Slater expansion of a Yukawa form factor	117
D	Matrix elements	119
D.1	Central terms	119
D.1.1	Central terms, spin independent	120
D.1.2	Central terms, spin dependent	120
D.2	Spin-orbit terms	122
D.2.1	1-body L.S term	122
D.2.2	Derivative term	123
D.2.3	X12 and X21 terms	125

E	Demonstrations for uncorrelated 2p2h state	131
F	The Wigner-Eckart Theorem	135
G	Coulomb wave functions and Riccati-Bessel functions	137
H	Resume in French	139
H.1	Dérivation des potentiels	141
H.2	Résolution des équations couplées	142
H.3	Validation des codes de calcul	142
H.4	Applications	144
H.5	Conclusion	145

List of Figures

1.1	Experimental angular distribution [1] for the elastic scattering of neutrons with 20 MeV of kinetic energy off ^{208}Pb . The cross section for forward angles ($\theta < 20$) is up to 1000 times bigger than for backward angles	2
1.2	schematic representation of a nucleon induced reaction on a target nucleus. In a), each individual nucleon is considered separately. In b), all nucleons are folded into a single entity that contains the averaged interactions and form a 1-body potential.	3
1.3	Shell model-based representation of processes that may occur during a collision between a nucleon and a nucleus. Filled shells are represented by hatched areas, solid dots represent valence nucleons and the incident nucleon is drawn as a small circle. On a), the incident nucleon is shape elastically scattered. On b), the projectile interacts with one nucleon of the target, then undergoes a mirror interaction with the same nucleon and leaves the target. On c), the projectile excites one nucleon of the target and leaves it in an excited state. .	4
1.4	Schematic description of the difference between DWBA and CC calculations. Straight arrows depict the existence of a potential connecting one level to another, and circular arrows depict the coupling of partial waves of one level with its other partial waves.	6
1.5	Ratios of direct inelastic scattering cross section to direct elastic scattering cross section for incident neutrons on ^{208}Pb (bottom curve) and ^{238}U (top curve). Black dashed curves were calculated within the DWBA and red full curves within CC formalism.	7
1.6	Schematic description of the difference between DWBA and CC calculations. Straight arrows depict the existence of a potential connecting one level to another, and circular arrows depict the coupling of partial waves of one level with its other partial waves.	7
1.7	Ratios of direct inelastic scattering cross section to direct elastic scattering cross section for incident neutrons on ^{238}U . Blue curves were calculated within the DWBA and black curves within CC formalism.	8
1.8	Total cross section and elastic scattering cross section as a function of the incident energy for incident neutrons on ^{208}Pb (left panel) and ^{238}U (right panel). Blue points are experimental data, red curves are calculations with coupled channel effects, and black dashed curves are calculations without coupled channel effects.	9
1.9	Example of a knock-on exchange process that contributes to elastic scattering.	11
5.1	Part of an input file containing single particle wave functions developed on a harmonic oscillator basis for ^{208}Pb	58

5.2	Input file containing RPA amplitudes of ^{208}Pb of the reduced matrix elements of the transition density $\rho_{\alpha\beta}^{\bar{0}\rightarrow 3^-, J=3}$ with an excitation energy of 2.614 MeV	59
5.3	Relative difference between the angular distribution of a (n,n) reaction on ^{208}Pb computed by ECIS-06 with a given maximum radius rmax, and the reference with rmax=25 fm. The incident energy is 40 MeV.	71
5.4	Relative difference between the angular distribution of a (n,n) reaction on ^{208}Pb computed by ECIS-06 with rmax=20 fm, for various values of the step size. The reference calculation is with h=0.01 fm, and the incident energy is 40 MeV.	72
5.5	Relative difference between the reference angular distribution of a (n,n) reaction on ^{208}Pb computed by ECIS-06 with rmax=20fm and h=0.01fm, and ECANOL calculations for various step sizes. The incident energy is 40 MeV.	73
5.6	Plot of the optical potential for the reaction (n,n) on ^{208}Pb at an incident energy of 40 MeV in the lab frame, as computed by MINOLOP code. On the upper panels for the direct term, the same calculation done with DWBA code is displayed in red for comparison. The exchange term in the bottom panels is for $r = 5$ fm and for partial waves $\{j,l\} = \{\frac{3}{2}, 1\}$	74
5.7	Angular distribution and relative difference between the computation done by DWBA98 and our codes for neutron elastic scattering on ^{90}Zr . The maximum radius and the step size used in both codes are rmax=15 fm and h=0.2 fm.	75
5.8	Angular distribution for (n,n') to the first 5^- state of ^{90}Zr at incident energy of 40 MeV.	79
6.1	Double differential cross sections for (p,xp) off ^{90}Zr at 120 MeV of incident energy. RPA calculations are displayed as full red curves, uncorrelated particle-hole calculations as black dashed curves. Experimental data from references [2] and [3] are depicted as symbols.	88
6.2	Schematic depiction of the couplings leading to an excitation for a 2-step process from excitations of 1-step processes. The full arrows are potentials that are calculated explicitly and included in our calculations, and the dashed arrows represent potentials that are neglected.	90
6.3	Angular distribution to 2-phonon states built by coupling the first, 1-phonon 3^- and 5^- states in ^{90}Zr for an incident neutron. Dotted lines are for the sum of the separate contributions from both 1-phonon states (when A-3 is used), and full curves are for calculations that include interference terms (when A-3 is not used).	91
6.4	Comparison between the number of 1 and 2-phonon states in ^{90}Zr for excitation energies below 30 MeV. The red bars are for 1-phonon states and the black bars are for 2-phonon states. Each bar corresponds to the counting of all states in an energy bin of 0.5 MeV	92
6.5	Angular distribution to 2-phonon states built by coupling the first, 1-phonon 3^- state and 5^- state in ^{90}Zr for an incident neutron. Here, 2-phonon states are populated exclusively from the 1-phonon 3^- state.	93
6.6	Angular distribution to 2-phonon states built by coupling the first, 1-phonon 3^- state and 5^- state in ^{90}Zr for an incident neutron. Here, 2-phonon states are populated exclusively from the 1-phonon 5^- state.	94

-
- 6.7 Contribution of 2-phonon states (discriminated in terms of their spin) to the total inelastic cross section to 2-phonons up to $E^*=14$ MeV. The red bars correspond to the total cross section of 2-phonon states with a given spin, and the blue curve is the cumulative sum of their contributions. 95
- 6.8 Double differential cross section as a function of the angle of emission for a (n,n') reaction with an incident energy of 80 MeV on ^{90}Zr . The black curves are the contribution from 2-phonon states up to 20 MeV of excitation energy, the red curves are the contributions from 1-phonon states up to 20 MeV of excitation energy. Results are displayed for the three outgoing energies $E_{\text{out}} = 74, 71, 68$ MeV, which correspond to excitation energies of 6, 9 and 12 MeV. 96
- 6.9 Double differential cross section as a function of the emission energy for a (n,n') reaction with an incident energy of 80 MeV on ^{90}Zr . The black curves are the contribution from 2-phonon states up to 20 MeV of excitation energy, the red curves are the contributions from 1-phonon states up to 20 MeV of excitation energy. We display results for emission angles $\theta = 15, 90, 130^\circ$ in the center of mass frame. 97
- 6.10 Comparison between the number of 1p1h and 2p2h states in ^{90}Zr for excitation energies below 30 MeV. The red bars correspond to the counting of all 1p1h states and the black bars are for the counting of all 2p2h states, in both cases for an energy bin of 0.5 MeV. 103
- 6.11 Comparison between the angular distribution obtained in a coherent calculation, and the sum of contributions coming from incoherent calculations. The red curve is for the incoherent sum, and the black curve for the coherent calculation. 104
- 6.12 Comparison between the angular distribution obtained in a coherent calculation for 1 (red curves) and 2-phonon states (blue curves), and the sum of contributions coming from incoherent calculations of uncorrelated 2p2h (black curves) states. Each panel displays the angular distribution for preequilibrium emission due to states in a given energy bin. The upper left panel is for states with excitation energy between 0 and 4 MeV, the upper right for excitation energies between 4 and 8 MeV, the bottom left for excitation energies between 8 and 12 MeV, and the bottom right for excitation energies between 12 and 16 MeV. 105
- 6.13 Comparison between the angular distribution obtained in a coherent calculation for 1 (red curves) and 2-phonon states (blue curves), and the sum of contributions coming from incoherent calculations of uncorrelated 2p2h (black curves) states. The excitation energies considered in this calculation range from 0 to 16 MeV. 107

List of Tables

5.1	Table describing the time cost of MINOLOP to compute the central part of microscopic nonlocal potentials.	79
-----	---	----

Chapter 1

Introduction

From the first experiments done by Ernest Rutherford until today, studying nuclear physics often implied and still implies colliding a beam of particles (nucleons, electrons, atomic nuclei...) into a target made of a precisely known composition of nuclei. Both experimental and theoretical understanding of the complex and many phenomena that occur during such collisions have greatly improved. Nuclear reactions involving an incident nucleon with kinetic energy between 100 keV and a few hundred MeV, and a target nucleus that is larger than a few nucleons are, conceptually, divided into three parts:

- A direct component characterized by its brevity ($< 10^{-21}$ s), during which projectile and target interact just once or a few times. Consequently, the momentum exchanged between the projectile and the target is more likely to be small; this is observed experimentally when checking the angular distribution of nucleons scattered off nuclei: the cross sections associated are much stronger for forward angles, as can be seen on figure 1.1.
- A compound component in which the projectile, after having been absorbed by the target, shares most of its energy with it and loses track of its original direction. The compound nucleus that is formed by this absorption decays then (which takes much more time, over 10^{-16} s). In this case, enough energy is shared with the target nucleus to reach excited states in the continuum, and the decaying process of the compound nucleus is characterized by particles emitted with low kinetic energy.
- A hybrid component, during which the projectile interacts quickly with a few nucleons of the target and shares a bit more of its momentum with the target than in the direct part. The number of interactions remains limited, therefore emitted particles from the target keep track of the momentum of the projectile and their angular distribution is still bigger at forward angles. However, enough energy is shared so that excited states lying in the continuum can be reached and this involves the possibility to emit particles with a continuous energy spectrum. This hybrid component of nuclear reactions is often called preequilibrium.

Various tools and models have been developed to provide efficient frameworks for studying more and more complex phenomena occurring during nuclear reactions, such as direct elastic scattering and direct inelastic scattering. The description of these reactions remains a field of intensive research even after 70 years of theoretical and experimental investigation, and it has led to the creation of many mathematical tools that are intricately together. To describe nucleon-nucleus elastic and direct inelastic scattering, one has to solve a many-body problem.

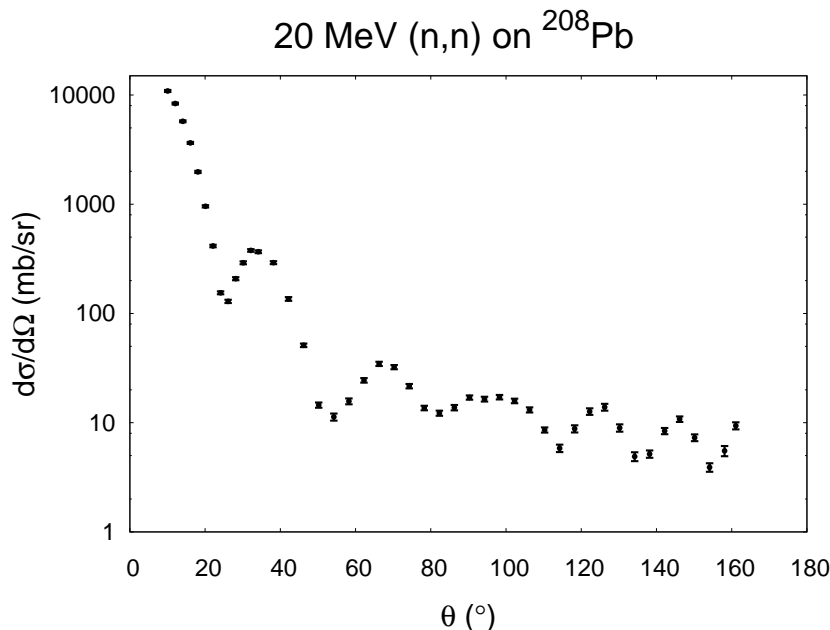


Figure 1.1: Experimental angular distribution [1] for the elastic scattering of neutrons with 20 MeV of kinetic energy off ^{208}Pb . The cross section for forward angles ($\theta < 20^\circ$) is up to 1000 times bigger than for backward angles

So first, we will describe how we can treat the many-body aspect of the physical problem and explain our choice of modeling. We will give some general features associated with the chosen model, and discuss the resolution of its equations. In particular, we will compare the exact treatment of nucleon-nucleus scattering with the Coupled-Channel (CC) formalism, and with the Distorted Wave Born Approximation (DWBA). We shall then discuss the fundamental physical quantity associated with our choice of model: the 1-body potential. This potential can be obtained by different means, and we will give a brief overview of the most classical approaches. Finally, the nonlocality, a particular feature of the potential, will be discussed and we shall proceed on to our calculations.

1.1 Many-body aspects of the nucleon-nucleus scattering problem

Generally speaking, direct reactions involving a nucleon colliding with a nucleus constitute a many-body problem, and there are different ways to solve it, the most fundamental being *ab initio* calculation [4, 5]. This approach uses ingredients derived from Quantum Chromodynamics (QCD) and tries to solve the many-body problem with no approximation. Thus, it is restrained to small systems with a very limited number of nucleons. Great progress has been achieved recently with the increasing of computing power [6–8], but an *ab initio* description of elastic and direct inelastic scattering of a nucleon off an actinide is still out of reach. Another *ab initio* method is based on the explicit inclusion of all couplings in a chosen reaction process within the shell model embedded in the continuum [9–11] or the Coupled-Cluster model [12]

Our purpose in the present work is to study, in a microscopic framework, elastic and direct inelastic scattering of nucleons off any target, including deformed nuclei such as actinides,

thus *ab initio* calculations are excluded.

Instead, one can imagine that all the complicated interactions between the constituents of the target nucleus can be averaged to one large field of interaction, and rather than treating all mutual interactions between the projectile and the target's nucleons, we can simply study the interaction of the projectile with the averaged field: a 2-body problem. This is the approach we have chosen to follow. Combined with an appropriate averaging over the energy, this approach is named the optical model [13].

The optical model is the most common way to treat elastic scattering (whether you use parameter-free ingredients or not). It was first suggested in 1935 by Bethe [14], and comes from a modelization developed in optics: light can be refracted or absorbed by a medium (as for example a crystal) with a complex refractive index. The absorption is taken into account by the imaginary part of the refractive index. In nuclear physics, the “optical” potential that is introduced in the Schrödinger equation is complex, and part of the flux is “absorbed” because of the presence of the imaginary component. First used in a semi-classical analysis as an attempt to make an analogy with optics [15], the optical model showed remarkably good results. Several other phenomenological analysis were done [16] and a solid theoretical basis was given to this model a few years later [17–19] while, in parallel, the theoretical description of inelastic scattering was also developed [17].

In order to give an approximate picture of the optical model and its generalization, let us consider from a semi-classical point of view an elastic scattering reaction between one incident nucleon and a target made of a bulk of nucleons. Each individual nucleon generates a field of interaction - with a finite range - around itself which can overlap with that of its neighbours. Basically, if we want to describe the reaction with no approximation we need to determine the interaction of the projectile with each nucleon of the target and the interaction of each of them with its neighbours, and we are faced with a complicated many-body problem. This situation is depicted on figure 1.2 a).

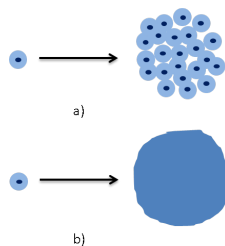


Figure 1.2: schematic representation of a nucleon induced reaction on a target nucleus. In a), each individual nucleon is considered separately. In b), all nucleons are folded into a single entity that contains the averaged interactions and form a 1-body potential.

However, instead of considering each individual nucleon of the target, one may try to find what is the average field of interaction generated by all the nucleons of the target. Finally, the reaction between the projectile and the target is transformed from a many-body calculation to a simple 2-body problem as shown on figure 1.2 b). The average field of interaction, or potential, takes into account in an effective way of all processes besides elastic scattering, and some of these processes imply an absorption of a part of the incident flux.

In our example we have considered only the case of elastic scattering, but of course other reactions may occur during the collision of a nucleon on a nucleus: the projectile can share some of its energy or some of its angular momentum with the target and then leave; the nucleus is in an excited state after the reaction and we call this mechanism inelastic scattering. Or the projectile can be captured by the target and possibly decay by emitting gammas, and so on. In the following developments we will call “channel” a given reaction outcome (inelastic channel, radiative capture channel...). As we have previously said, when using the optical model you focus on the exact description of elastic scattering and take into account in an effective way all other channels. But it is possible to generalize the approach by treating explicitly the elastic channel plus a selection of other channels. Let us return to the simple representation used in figure 1.2. Beside the elastic channel, we assume that the projectile can cause the target to vibrate and that we want to describe explicitly this reaction outcome. It would appear quite natural, then, to treat explicitly the elastic channel and the “vibrational” inelastic channel, and to treat implicitly others channels. The generalized optical model (GOM) [20] is based on this approach, but of course it is not limited to one channel besides the elastic channel. The more channels you add, the more you refine your model and you probe more internal degrees of freedom of the system. However, the more channels you include, the more complicated and long your calculation becomes and the more computing power you need. Depictions such as that of figure 1.2 are useful - though not perfect - to understand how we describe nucleon induced reactions between 100keV and a few hundred MeV: the optical model that we use can be interpreted as an attempt to simplify the complicated many-body problem that arises from a nucleon-nucleus collision into a simple problem of two particles interacting through a potential. As mentioned previously, the optical model treats explicitly only direct elastic scattering, and considers in an effective way the role played by all other reaction mechanisms. To describe a nuclear reaction beyond the elastic channel one must then find other models designed for reaction processes that are not dealt with by the optical model. Our purpose here is not to describe all possible reaction mechanisms but rather to focus on direct elastic and direct inelastic scattering of nucleons off nuclei. A simplified picture of some reaction mechanisms that are involved in them is presented on figure 1.3.

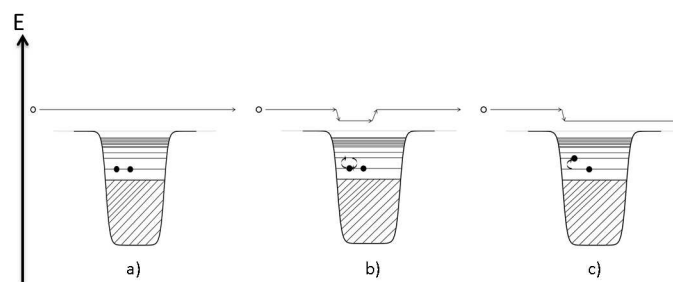


Figure 1.3: Shell model-based representation of processes that may occur during a collision between a nucleon and a nucleus. Filled shells are represented by hatched areas, solid dots represent valence nucleons and the incident nucleon is drawn as a small circle. On a), the incident nucleon is shape elastically scattered. On b), the projectile interacts with one nucleon of the target, then undergoes a mirror interaction with the same nucleon and leaves the target. On c), the projectile excites one nucleon of the target and leaves it in an excited state.

Using a shell-model representation of the target nucleus, direct (also called shape) elastic scattering can be described as an incident nucleon scattered by the target without disturbing any of its constituents (figure 1.3 a). An example of a 2-step process for direct elastic scattering would be that of figure 1.3 b where the incident nucleon shares some energy with one nucleon of the target, and as a second process the energy exchange is reversed. Another possibility is that after sharing some of its energy with the target, the incident nucleon is scattered as shown on figure 1.3 c. In the final state, the target nucleus has received some energy from the projectile and is in an excited state; this is a simple case of inelastic scattering to a single particle discrete excited level. Basically, elastic and inelastic scattering reactions include interactions leading to energy and angular momentum exchanges, and spin flip. Describing these phenomena can be done with the GOM (the optical model itself is restricted to elastic scattering).

1.2 Coupled channels and DWBA

In the GOM framework, we need to compute potentials that connect each channel included in our model with the others. They represent the coupling of one channel with another, which means if we try to describe a reaction with N channels, there are in principle N^2 potentials to compute. Once they are calculated, they are to be inserted in a set of N coupled equations - one equation for one channel. The complexity of this mathematical problem has led physicists to search for approximations, and one is of particular importance in the description of direct inelastic scattering. Let us introduce it by giving a physical example: we want to study the scattering of a neutron on a spherical target nucleus. In particular, we focus on the first excited state of the target nucleus, which consists of a surface vibrational state. We assume that all other reaction mechanisms are taken into account in an effective manner. With these assumptions, we can derive all of the 4 coupling potentials and solve the CC problem, or we can make another hypothesis: surface vibration is a collective state that gives rise to a quite strong inelastic cross section but still much smaller than the cross section for elastic scattering. Speaking in terms of energy, the projectile needs to transfer more than a few keVs to the target in order to excite a state of surface vibration. Thus, the elastic scattering process is not really perturbed by this inelastic process and, in practice, this means that the potential that couples the excited state to the ground state is much smaller than the optical potential. Thanks to this feature, we can first solve the equations for the elastic channel and obtain a distorted wave function, that we then use as input for the inelastic channel instead of solving coupled equations. This computation procedure is strictly equivalent to the DWBA.

The DWBA has been successfully applied to elastic and inelastic scattering of light projectiles off many nuclei [21–23]. But as we have mentioned, the DWBA relies on the assumption that coupling potentials are small compared to the optical potential. The validity of the DWBA for elastic and inelastic scattering has been investigated by studying coupling strength expressed in terms of collective models in the 1960s [24], and although the DWBA was proved to be a good description of reactions involving spherical nuclei, cases where the target nucleus is strongly deformed (with a deformation parameter $\beta > 0.2$) showed that the DWBA is not longer valid [25] and it is necessary to use the CC approach. A comparison between ^{208}Pb , a spherical nucleus and ^{238}U , a strongly deformed nucleus is a good way to illustrate the relevancy of the DWBA. In the case of ^{208}Pb , a doubly closed shell spherical nucleus, the first excited state is one of surface vibrations that requires 2.6 MeV of excitation

energy. The coupling between this excited state and the ground state is weak compared to the optical potential, so the DWBA should be a good approximation. In the case of ^{238}U , the first excited state correspond to a rotational state that requires 46 keV of excitation energy (57 times less than for the 3^- of ^{208}Pb) - you don't need to give a lot of energy to a deformed nucleus to make it rotate. The coupling between this state and the ground state is strong enough that it cannot be neglected compared to the optical potential, so the DWBA shouldn't be a good approximation. More generally, strongly deformed nuclei display a rotational spectrum a low excitation energy. For even-even nuclei with a strong prolate deformation, such as ^{238}U , the low energy states 2^+ , 4^+ , 6^+ , 8^+ (located at 46, 149, 307 and 508 keV, respectively, for ^{238}U) are members of the ground state rotational band which are strongly coupled together. On figure 1.4, we summarize the different terms that are computed by the DWBA and by CC for both nuclei, if we only consider the coupling of the ground state with the first excited state.

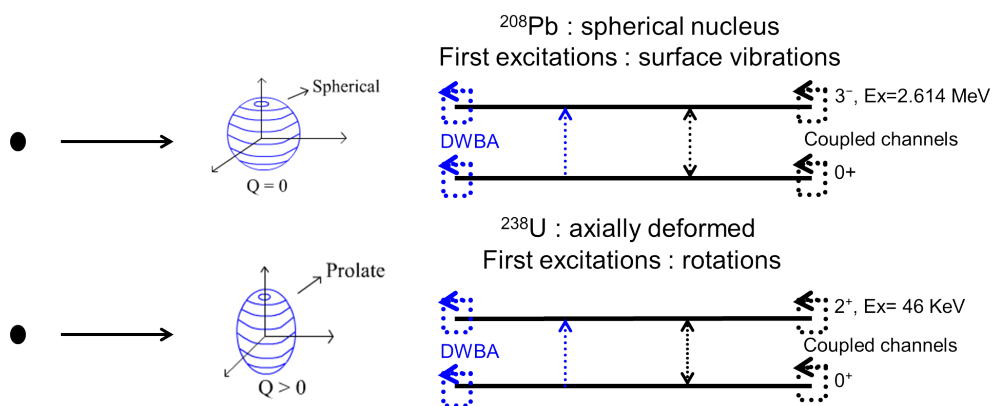


Figure 1.4: Schematic description of the difference between DWBA and CC calculations. Straight arrows depict the existence of a potential connecting one level to another, and circular arrows depict the coupling of partial waves of one level with its other partial waves.

We have computed cross sections for both nuclei to make the comparison and have plotted them on figure 1.5. In the case of ^{208}Pb , a semi-microscopic approach based on the JLM folding model ([26] and references therein) using nuclear structure information calculated within the Random Phase Approximation (RPA [27]) has been applied to elastic and inelastic scattering of neutrons to the 3^- excited state of the target nucleus. The comparison between the ratios of the inelastic and elastic cross sections obtained within DWBA and CC frameworks shows - as expected - a remarkable agreement. We also notice that the cross sections ratio is small ($\sim 10^{-2}$) which confirms the hypothesis used for the DWBA. A similar approach using nuclear structure information calculated within the Hartree-Fock-Bogoliubov method has been done with ^{238}U as target nucleus (see [26] and references therein), considering its first excited state 2^+ . This time, the ratio between inelastic and elastic scattering cross section for CC and DWBA calculations noticeably differs. Furthermore, this time the cross sections average ratio is no longer small (about 10^{-1}), which shows that this inelastic process is not negligible compared to the elastic process. This quantitative observation is consistent with our qualitative prediction: the coupling between the ground state and the 2^+ excited state is too strong to be neglected compared to the optical potential. This calculation shows that the DWBA is not a good approximation to be used in studying nucleon-nucleus scattering for this nucleus.

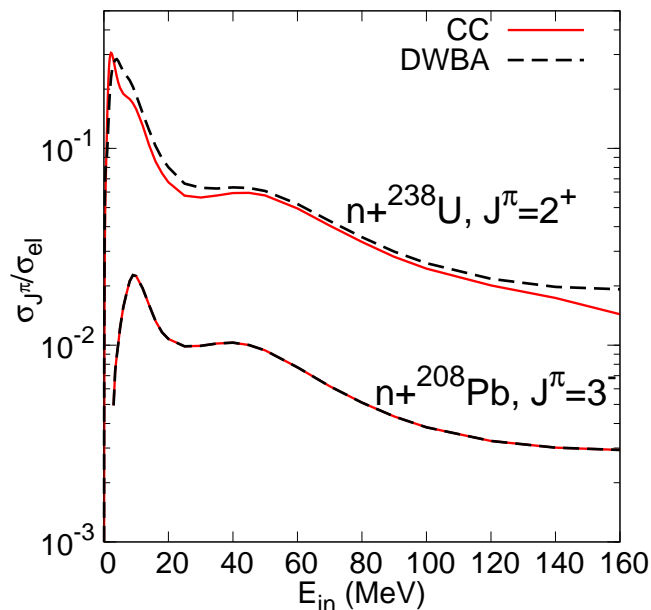


Figure 1.5: Ratios of direct inelastic scattering cross section to direct elastic scattering cross section for incident neutrons on ^{208}Pb (bottom curve) and ^{238}U (top curve). Black dashed curves were calculated within the DWBA and red full curves within CC formalism.

The inadequacy of the DWBA for deformed nuclei is even clearer if we consider several excited states in the coupling scheme of ^{238}U . On figure 1.6, we depict schematically the couplings between the ground state and the three first excited states of ^{238}U .

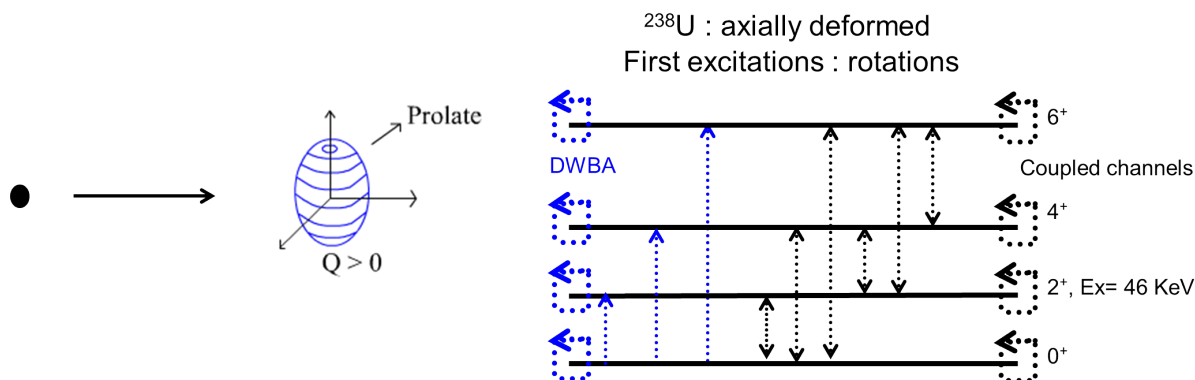


Figure 1.6: Schematic description of the difference between DWBA and CC calculations. Straight arrows depict the existence of a potential connecting one level to another, and circular arrows depict the coupling of partial waves of one level with its other partial waves.

The coupling scheme appears quite more complicated this time, with couplings between excited states that are neglected in the DWBA, and one can expect to see large discrepancies between DWBA and CC calculations (assuming that coupling potentials are not negligible compared to the optical potential). This is indeed the case as can be seen on figure 1.7.

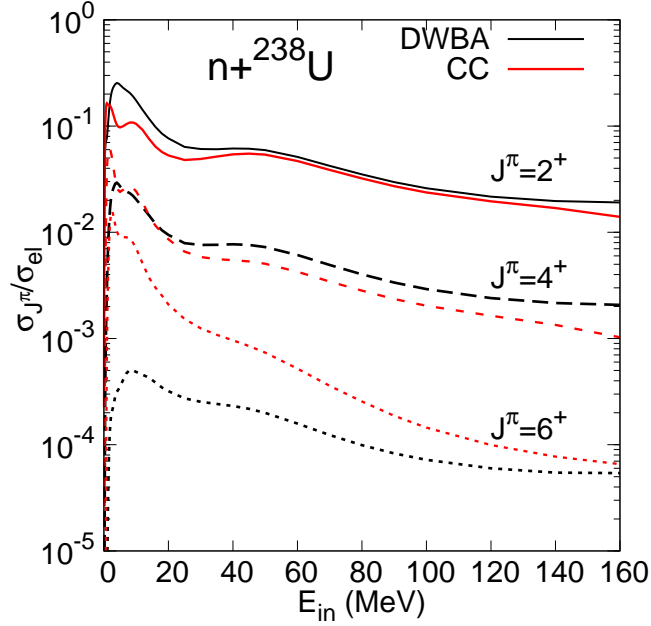


Figure 1.7: Ratios of direct inelastic scattering cross section to direct elastic scattering cross section for incident neutrons on ^{238}U . Blue curves were calculated within the DWBA and black curves within CC formalism.

In this calculation, we observe the same kind of discrepancies as depicted on figure 1.5 for each excited state. Another interesting phenomenon appears here: if we focus only on the CC calculation, we see that for low incident energies (<20 MeV) there is one order of magnitude between the curves of the 2^+ and the 6^+ states. On the other hand, if we look at the DWBA results, there is more than two orders of magnitude between the two states, and the cross section for the 6^+ computed with the DWBA is much smaller than when computed with CC. This shows another interesting feature: the DWBA considers only couplings between the ground state and one excited state, but it is a known fact that excited states are populated in a somewhat sequential way. In the present case, it means that first, the flux that is lost from the elastic channel is used to populate the 2^+ state, then part of this flux is taken to populate the 4^+ state, and the flux that goes to the 4^+ is partly used to populate the 6^+ . Only in the CC framework can such a sequential process be reproduced.

Finally, we display on figure 1.8 the total cross section and the direct elastic scattering cross section for ^{208}Pb (left panel) and ^{238}U (right panel), comparing calculations with and without considering coupled channel effects. For ^{208}Pb , the coupling between the ground state and the first excited state (a 3^-) is considered, and in the case of ^{238}U the couplings between the states 0^+ , 2^+ , 4^+ , 6^+ and 8^+ are included. The experimental total cross section is displayed for both nuclei. Again, we see that observables for ^{238}U can be well described only if coupled channel effects are correctly accounted for.

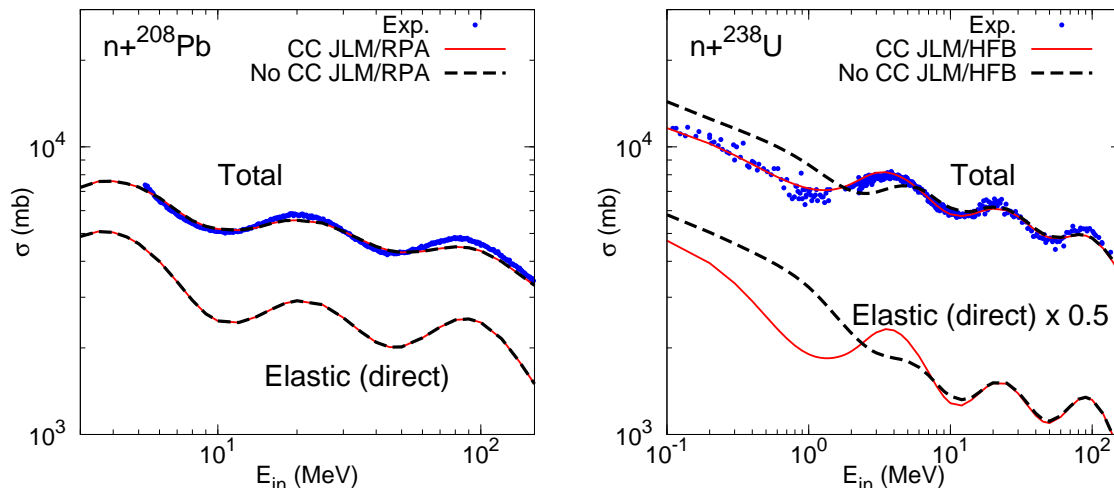


Figure 1.8: Total cross section and elastic scattering cross section as a function of the incident energy for incident neutrons on ^{208}Pb (left panel) and ^{238}U (right panel). Blue points are experimental data, red curves are calculations with coupled channel effects, and black dashed curves are calculations without coupled channel effects.

Because of all these considerations, if we want to describe elastic and inelastic scattering of a nucleon on a deformed nucleus then we must use CC formalism. In the GOM, the key element of the calculation - whether it is done with CC or DWBA - is the potential.

1.3 Computation of the (generalized) optical potential

All the complexity of the many-body nature of the problem, and of all the reaction mechanisms that are not treated explicitly is included in this potential. Therefore all the quality of the model relies on our capacity to build good potentials. Historically, the first potentials that were used were phenomenological [14, 15]: by first assuming a functional form with a set of parameters, and then adjusting these parameters to fit experimental data, it is possible to build a potential. By nature, this method is very versatile since it allows more or less complicated functional forms and sets of parameters to reproduce any set of data, and its successes are numerous. The Morillon-Romain [28], Koning-Delaroche [29], Varner [30] and Barbieri-Dickhoff [31] are some famous examples of global phenomenological potentials that assume a functional form with a simple, local dependence on radial coordinates: they can be written, in the radial coordinates basis $\{|\vec{r}\rangle\}$, as a linear combination of functions $f(r)$. There also exists phenomenological potentials with more complex functional forms; it is possible to assume a potential which is nonlocal: it is a linear combination of functions $g(r, r')$ that are not diagonal in the radial coordinates basis. One of the earliest phenomenological nonlocal study of elastic scattering of a nucleon on various nuclei is that of Perey and Buck [32], but there exists more recent studies like that of Dickhoff *et al.*, who published a nonlocal extension [33] of the Barbieri-Dickhoff potential.

Phenomenological potentials are robust and reliable tools in the domains where their parameters have been adjusted, but extrapolating them to other domains is risky. This is why other approaches that (in principle) do not need to be adjusted to experimental data have been developed. They are based on two fundamental elements: the effective nucleon-nucleon

(NN) interaction and a detailed description of the nuclear structure. Various methods exist to compute a potential from the effective NN interaction; potentials obtained with these methods are called microscopic. We present here a brief overview of some up-to-date technics to compute microscopic potentials:

- The nuclear matter method

The idea here is to compute the potential starting from the free NN interaction. Since the free NN interaction has a strong repulsive core that makes it unpractical, an effective NN interaction - called G matrix - is derived from the free NN interaction in a medium made of infinite nuclear matter at various densities. This G matrix is then convoluted with a nuclear density obtained separately. Good results were achieved with this method as early as in the 1970s [34] and, in the 1990s, parameter-free nuclear matter calculations were able to reproduce experimental data for the first time [35, 36]. In 2000, the Melbourne group derived a G matrix that was able to reproduce scattering observables between 60 MeV and 350 MeV [37]. This microscopic method is, to this day [38], the one that was applied with success to the largest number of nuclei but fails to reproduce experimental data at low incident energies.

- The nuclear structure method (NSM)

Instead of computing separately the NN effective interaction and the nuclear density, one can think of using the same ingredients to build both elements. The NSM was built on this idea by N. Vinh Mau [39] and has been successfully applied to the study of the elastic scattering of nucleons with low kinetic energy ($<30\text{MeV}$) off doubly closed shell nuclei such as ^{40}Ca [40] [41–43], ^{48}Ca [44] and ^{208}Pb [45], but it is yet to be extended to other types of nuclei, such as spherical nuclei experiencing pairing correlations.

Other methods that are more or less related to the nuclear matter method or the NSM [46] also exist, but have been used in less studies. As aforementioned, we aim at describing in a parameter-free framework the elastic and direct inelastic scattering of nucleons off any nucleus, including deformed nuclei. Considering the progress of each method, we have chosen to follow the nuclear matter approach to derive potentials required in the GOM. Regardless of how you compute them, potentials should have special features that stem directly from their theoretical construction and one is of particular importance here: the nonlocality.

1.4 The nonlocality of the potential

In the generalized optical model framework of Feshbach [20], a total wave function and interacting potentials for the system {projectile ; target} are introduced, and these are quantum objects that have a spacial expansion; in classical mechanics, this system would be represented by two small spherical objects (one for the neutron and one for the nucleus) that have precise, finite sizes. We know this modelization to be wrong: neutrons and nuclei are quantum particles described by wave functions, mathematical objects describing the quantum state of the system and that are related to the probability to find the system in a given configuration. And the potential that embodies the interaction of the projectile with the target doesn't have a simple radial dependence. When we derive equations to describe elastic scattering, such complicated dependence appears in the radial Schrödinger equation as:

$$\hat{T}\varphi(r) + \int U(r, r')\varphi(r')dr' = E\varphi(r) \quad (1.4.1)$$

with \widehat{T} the kinetic energy operator, U the potential of interaction between projectile and target, E the energy of the system and φ the radial wave function of the relative motion. From (1.4.1) we can formally write an equation for φ :

$$\varphi(r) = \frac{\int U(r, r')\varphi(r')dr'}{E - \widehat{T}} \quad (1.4.2)$$

This formal expression clearly shows that, in order to know the value of the radial wave function at a given position r , you need information on it everywhere in space. The key element here is the potential $U(r, r')$: it connects the value taken by the radial wave function at point r to its value everywhere in space. Because of it the value taken by the radial wave function doesn't depend only on the local state of the system at position r , but on the state of the system everywhere in space by connection to the potential. The potential, which is responsible for this behavior, is thus nonlocal. Nonlocality is not a trivial physical property, easily viewable. But sources of nonlocality in the scattering of a nucleon on a target nucleus can be identified. One source is directly related to the fact that nucleons are fermions. According to the Pauli exclusion principle their wave function must be antisymmetrized and this leads, even at a mean field approximation level such as Hartree-Fock (HF), to an exchange term in the potential [47, 48]. A schematic way of visualizing the exchange term is by returning to the modeling used in figure 1.3 as shown on figure 1.9:

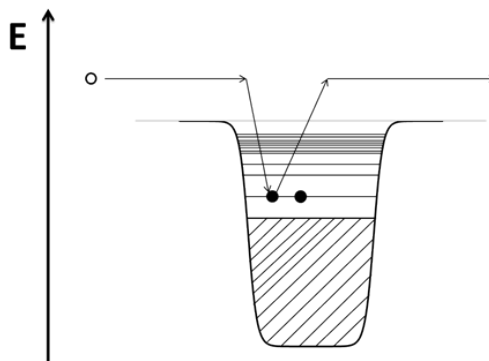


Figure 1.9: Example of a knock-on exchange process that contributes to elastic scattering.

The projectile knocks out a similar nucleon of the target nucleus and it is impossible, after the reaction, to know which nucleon is measured by the detector. If the effective NN interaction used to build the potential is nonlocal itself, or local with a finite range, then the exchange term won't be diagonal in the radial basis which makes it nonlocal. Another source of nonlocality can be understood from multiple scattering theory [49, 50]: the target nucleus contains A nucleons and each can be considered as a scattering centre, and the nucleon-nucleus potential must take into account the possibility to be scattered by several nucleons of the target. This can also be understood as channel coupling effects: let us suppose that as a first step of the collision, the projectile is scattered at position \vec{r} and excites the target into a channel that is treated explicitly (or not) in our model. Let us suppose that, as a second step, the reaction is inverted: at position \vec{r}' , the excited target transfers back all its excitation energy and angular momentum to the projectile, leading to elastic scattering as represented on figure 1.3 b. Nonlocality appears because the particle in the elastic channel moves under the influence of coupling to the other channels. This source of nonlocality in the nucleon-nucleus potential [48] is usually called dynamical polarization;

its contribution to the nucleon-nucleus potential has been investigated in the 1970s [51], the 1980s [52], the 1990s [53], and more recently by Keeley *et al* [54] in (p,d) reactions using the DWBA framework. They have shown that dynamical polarization contributes significantly enough that it should not be neglected, and proposed ways to calculate its contribution.

However, in most reaction analyzes, potentials that are used are local. Perey *et al* developed a localization procedure [32] that makes it possible to build a local potential that gives the same scattering matrix as its nonlocal equivalent potential in the case of nucleon-nucleus elastic scattering. Their prescription, called the Perey correction factor, allows to partly include nonlocal effects by adding energy dependence on the potential. This way, nonlocality can be taken into account in an efficient way for elastic scattering and avoids us the complicated treatment of an integrodifferential problem. But this procedure includes only partially nonlocal effects and by an ad-hoc phenomenological method. Any direct link to a microscopic source of nonlocality is thus difficult. In order to lift this problem, there exists methods to localize a potential computed microscopically [55]. However, in both microscopic and phenomenological approaches, only the asymptotic part of the wave function is correctly constrained. The consequence is that the wave function obtained with a nonlocal potential is equivalent to a wave function obtained with the local equivalent potential only far from the interacting area [56, 57]. Therefore, computing observables that depend on the value of the wave function inside the interacting area will give different result depending on which kind of potential is used. Furthermore, while localization procedures yield good results for elastic scattering, the situation is much less satisfactory for inelastic scattering [55]. It appears thus necessary to treat explicitly the nonlocality and solve the integrodifferential form of the Schrödinger equation in studies on inelastic scattering.

One major issue is that, to this day and to our knowledge, there exists only one open source calculation - published in 2016 - code that solves the CC integrodifferential equations with nonlocal potentials stemming from the theoretical description of a collision involving a nucleon and a nucleus [58], and it has only been used for *ab initio* calculations. Widely used computation codes like FRESCO [59] or ECIS [60] solve CC differential equations with local potentials while other codes like DWBA98 [61] use nonlocal potentials but within the DWBA formalism which prevents us from using them for deformed nuclei. A lot of work and efforts has been put in the last ten years by various laboratories to develop computation codes for elastic and inelastic scattering using nonlocal potentials as input. Especially, our collaborator H. Arellano has written a CC code for charge-exchange reactions and has successfully used it for quasi elastic (p,n) reactions [62]. Moreover, Titus *et al* [63] have developed NLAT, a code using nonlocal potentials to study transfer reactions with the DWBA and the adiabatic distorted wave approximation. The results obtained in these studies only increases the desirability of CC codes for nucleon-nucleus elastic and inelastic scattering with nonlocal potentials.

Because of all these considerations on the importance of nonlocality, the wider range of use of CC calculations over DWBA, and the available codes on the market, we have decided to start the development of our computation code that is able to solve CC equations with nonlocal potentials for direct elastic and inelastic scattering of incident nucleons. Our collaborator has kindly provided us with his code, HYDRA, that he used to study charge exchange reactions with nonlocal potentials [62], and with some derivations associated with the method he uses in his code to solve coupled equations for charge exchange reactions.

HYDRA was designed to study reactions with no spin transfer and with target nuclei in a 0^+ ground state. We have extended his method to the case of elastic and inelastic scattering of a nucleon off any target nucleus, and have written the computation code ECANOL - Equations Couplées Avec NOn Localité - to solve CC equations with nonlocal potentials for nucleon-nucleus elastic and inelastic scattering. In parallel to this, we have worked on the derivation of microscopic nonlocal potentials and a code to compute them, MINOLOP (Microscopic NOnLocal Potentials) that produces inputs for ECANOL. Using the nuclear matter approach, Dupuis *et al.* have folded the Melbourne G matrix with nuclear densities computed microscopically to calculate potentials and study elastic and direct inelastic scattering of nucleons off ^{208}Pb [23, 64]. The good results they obtained fostered us to extend their method to CC calculations. As a validation step, we can compare our calculations to theirs before expanding our modeling to study nuclei like ^{238}U that have, to our knowledge, never been studied in an entirely microscopic framework.

We have organized our dissertation as follows: in chapter 2, after an introduction on the formalism of the generalized optical model, we detail properties of the effective operator introduced in this procedure and explain their origins. We also present the particular case of nucleon-nucleus collisions modeled with the Feshbach method, and remind basic concepts of the scattering theory by a central potential. We then expand this simple formalism to the case of nucleon-nucleus scattering by taking into account angular momentum coupling.

Chapter 3 is dedicated to the derivation of coupled-channel equations, their projection on an appropriate basis and the presentation of our extension of the method proposed by Arellano to solve these equations for nonlocal potentials.

Then, we present in chapter IV the nuclear matter approach: from the 1-body potentials we introduced in our derivations in chapter 3, we describe how we can link them to a potential computed from a 2-body interaction and a 1-body density. We then briefly present how a G matrix can be constructed from a free NN interaction and some features of the Melbourne G matrix, which was computed from such an approach. Next, we remind some derivations of the RPA implemented with the Gogny D1S force, and we calculate coupling densities between 1 and 2-phonon states. Combining what we presented of the Melbourne G matrix and the target's structure description with the RPA, we derive as a first, simple example the optical potential for a nucleus that has a 0^+ ground state. We then give the full derivation of the most general coupling potential in which one initial state $|\psi_i\rangle$ is coupled to a final state $|\psi_f\rangle$.

The formulae given in chapter 4 are the fundamental objects used to write ECANOL and MINOLOP codes. In chapter 5, we present these two programs by detailing the inputs they require and by showing the validation process we followed for them. In particular, we derive local, macroscopic potentials within the vibrational model that we used to validate ECANOL against ECIS-06. We also show some results regarding the convergence of calculations done with ECIS-06 as a function of the cutoff radius and the stepsize.

The first physical application done with the two new codes concerns the contribution of 2-phonon states to preequilibrium emission, which we describe in chapter 6. After giving a short review of microscopic approaches to preequilibrium calculations, we explain how 2-phonon contributions can be taken into account and the motivations for each approximation

we did in our modeling. We justify them by comparing observables computed with them and without them. We then show our results and give some analysis regarding the enrichment of the microscopic modeling of preequilibrium emissions. The improvement we could achieve using our new tools MINOLOP and ECANOL encourage us in completing these tools with remaining parts of the NN interaction and using them to describe direct elastic and inelastic scattering of nucleons off deformed nuclei.

Chapter 2

The GOM: the Feshbach formalism

We have introduced the generalized optical model by using simplified depictions to ease the understanding of the relevant physics of the model, but we also mentioned that it has a solid theoretical basis [20] that is useful for understanding - from a theoretical point of view - the underlying physics of the system, and also for practical calculations. Our purpose in the present section is to briefly give both mathematical and physical explanations of the ingredients of the generalized optical model, and give a starting point of oncoming calculations. We consider the case in which a non-relativistic nucleon with energy $E_{C.M.}$ in the center of mass frame hits a nucleus in its ground state. The evolution of the projectile's wave packet, represented by the wave function Ψ is given by the time-dependent Schrödinger equation (for a detailed discussion on wave packets in nuclear physics, see [65]):

$$i\hbar\frac{\partial\Psi}{\partial t} = \hat{H}\Psi \quad (2.0.1)$$

where \hat{H} is the total Hamiltonian of the system. If we know the decomposition of the wave function on its stationary scattering states, we can easily obtain its time evolution. These quantum stationary states are solutions of the time-independent Schrödinger equation:

$$\hat{H}|\Psi\rangle = E|\Psi\rangle \quad (2.0.2)$$

where $|\Psi\rangle$ is the total vector state describing both the relative motion of the target and the incident nucleon and their internal structure. In the case of pure elastic scattering of an incoming wave packet of average momentum \vec{k} , the energy eigenvalue of the wave packet is $E = E_{C.M.} = \frac{\hbar^2 k^2}{2\mu}$, with μ the reduced mass of the system {projectile; target}. If we choose a complete set of single particle state vectors and neglect the indistinguishability of the incident nucleon with those of the target, then we may write the total wave function of the A+1 nucleons as:

$$|\Psi\rangle = \sum_i |\psi_i\rangle \otimes |w_i\rangle \quad (2.0.3)$$

$\{|\psi_i\rangle\}$ is an orthonormal basis of the state vectors describing the internal state of the target and $\{|w_i\rangle\}$ a complete basis of state vectors describing the relative motion of the projectile and the target, and the intrinsic state of the projectile. For simplicity, we haven't considered excited states of the continuum in the expansion of the state vector of the target but in principle, we should consider them by adding an integral term. From these simple definitions, we will use projection operator formalism to derive expressions that give some insight on the physics involved in this model.

2.1 Projection operators

Let us assume that $E_{C.M.}$ is high enough to ensure channels noted $\{1, 2, \dots, N\}$ are open. Let P be an operator that projects the target nucleus to a selected subspace of n states that couple strongly to the ground state, $n \leq N$ and Q the operator projecting it to all the other states:

$$P = \sum_{i=0}^n |\psi_i\rangle\langle\psi_i| \quad Q = \sum_{j>n} |\psi_j\rangle\langle\psi_j| \quad (2.1.1)$$

It is important to note here that the Q operator projects the system to open channels j that verify $n < j \leq N$ and to all other channels, which means that some open channels that couple weakly to the ground state can be contained in the space spanned by the Q operator, and also all closed channels that can cause virtual excitations and that are usually associated with compound processes are contained in this space. By construction of the operators, P and Q satisfy the relations:

$$P^2 = P \quad Q^2 = Q \quad P + Q = \mathbb{1} \quad PQ = QP = 0 \quad (2.1.2)$$

with $\mathbb{1}$ the identity operator. We will use these operators so as to recast the time-independent many-body Schrödinger equation (2.0.2) and define an effective Hamiltonian. From equation (2.1.2), it is obvious that:

$$\hat{H}|\Psi\rangle = E|\Psi\rangle \quad \Leftrightarrow \quad \hat{H}(P + Q)|\Psi\rangle = E(P + Q)|\Psi\rangle$$

Now, by applying the P operator on the left of this formula and using again (2.1.2), we can find:

$$(\hat{H}_{PP} - E)P|\Psi\rangle = -\hat{H}_{PQ}Q|\Psi\rangle \quad (2.1.3)$$

with the obvious notation $\hat{H}_{XY} = X\hat{H}Y$. This equation gives some basic information on the physics of the scattering process: the \hat{H}_{PP} term couples the n open channels that we treat explicitly in our model, including elastic scattering. \hat{H}_{PQ} has matrix elements that connect the aforementioned channels to all the others. As we seek only for $P|\Psi\rangle$, we need to eliminate $Q|\Psi\rangle$ in equation (2.1.3). In order to do so, we may follow the procedure applied with the P operator, but now with the Q operator so as to obtain:

$$(\hat{H}_{QQ} - E)Q|\Psi\rangle = -\hat{H}_{QP}P|\Psi\rangle \quad (2.1.4)$$

$Q|\Psi\rangle$ includes only channels with outgoing waves, and capture channels (bound states). Therefore, a formal solution of equation (2.1.4) can be expressed simply as:

$$Q|\Psi\rangle = \frac{1}{E - \hat{H}_{QQ} + i\varepsilon} \hat{H}_{QP}P|\Psi\rangle \quad (2.1.5)$$

in which the infinitesimal $i\varepsilon$ is here to ensure we obtain only outgoing waves in channels of the Q space. We may note here that for channels in which the projectile is captured by the target, the addition of $i\varepsilon$ is not required. Now we may eliminate $Q|\Psi\rangle$ in the equation for $P|\Psi\rangle$:

$$\begin{aligned} (\hat{H}_{PP} - E)P|\Psi\rangle &= -\hat{H}_{PQ}Q|\Psi\rangle \\ (\hat{H}_{PP} - E)P|\Psi\rangle &= -\hat{H}_{PQ} \frac{1}{E - \hat{H}_{QQ} + i\varepsilon} \hat{H}_{QP}P|\Psi\rangle \\ (\hat{H}_{PP} + \hat{H}_{PQ} \frac{1}{E - \hat{H}_{QQ} + i\varepsilon} \hat{H}_{QP})P|\Psi\rangle &= EP|\Psi\rangle \end{aligned}$$

which we can rewrite as:

$$(\hat{H}_{PP} + \hat{\mathcal{O}}_{\text{eff}})P|\Psi\rangle = EP|\Psi\rangle \quad (2.1.6)$$

with the effective operator:

$$\hat{\mathcal{O}}_{\text{eff}} = \hat{H}_{PQ} \frac{1}{E - \hat{H}_{QQ} + i\varepsilon} \hat{H}_{QP} \quad (2.1.7)$$

Thus, we have been able to recast equation (2.0.2) into an apparently simpler form in which, instead of having to compute the total wave function $|\Psi\rangle$, we only need to compute its projection in the P space $P|\Psi\rangle$. However, the efficiency of this procedure depends on our capacity to construct good models for the effective Hamiltonian $\hat{H}_{\text{eff}} = \hat{H}_{PP} + \hat{\mathcal{O}}_{\text{eff}}$. Equation (2.1.7) is a suitable form, though, to discuss properties that the effective operator must have.

2.2 Properties of the effective Hamiltonian

The effective Hamiltonian built within this framework has some features and properties that have been discussed in details by Feshbach [17]. We remind here some of the most important properties, and discuss in particular the nonlocality.

The most obvious property of the effective operator is its energy dependence, as it appears explicitly in equation (2.1.7). It can readily be understood because channels can be considered open only if the energy of the system is high enough.

Another property of the effective operator is its complex nature: \hat{H}_{PP} connects directly, as we mentioned earlier, the various states spanned by the P operator. Only a limited number of states are included in the $P|\Psi\rangle$ space, which means we do not treat explicitly all the possible states. The second term, $\hat{\mathcal{O}}_{\text{eff}}$ is here to compensate for the states that we do not consider explicitly, which form the $Q|\Psi\rangle$ space. The inclusion of $\hat{\mathcal{O}}_{\text{eff}}$ is necessary when we calculate transitions between states contained in $P|\Psi\rangle$ because it accounts for virtual intermediate states. Besides, if $Q|\Psi\rangle$ contains one or more open channels, then part of the incoming flux must be lost from the channels in $P|\Psi\rangle$ to these open channels in $Q|\Psi\rangle$. Therefore, \hat{H}_{eff} must be absorptive which means it has to be complex, thus non-hermitian. Such a property emerges in an obvious way when considering the formal relation:

$$\lim_{\varepsilon \rightarrow \infty} \frac{1}{E - \hat{H}_{QQ} + i\varepsilon} = \mathcal{P} \left(\frac{1}{E - \hat{H}_{QQ}} \right) - i\pi\delta(E - \hat{H}_{QQ}) \quad (2.2.1)$$

where \mathcal{P} is the Cauchy principal value. What must be understood from this relation is that the absorption is here to account for the flux that is lost from the entrance channel to channels in the Q space.

The last property we want to focus on is the nonlocal nature of the effective operator. In order to show explicitly the nonlocality, let us introduce eigenstates of \hat{H}_{QQ} :

$$\hat{H}_{QQ}|\Phi_q\rangle = E_q|\Phi_q\rangle \quad (2.2.2)$$

$|\Phi_q\rangle$ represents the incident nucleon bound to an excited state of the target nucleus. In principle, These $|\Phi_q\rangle$ should include bound states in the continuum, but in equation (2.0.3),

we haven't considered them in the expansion of the total wave function. We do the same here in the expansion of the effective Hamiltonian on eigenstates of \hat{H}_{QQ} :

$$\hat{\mathcal{O}}_{\text{eff}} = \sum_q \frac{\hat{H}_{PQ}|\Phi_q\rangle\langle\Phi_q|\hat{H}_{QP}}{E - E_q + i\varepsilon} \quad (2.2.3)$$

Let f be a function in the space of the relative motion. If we let \hat{H}_{eff} operate on f , its nonlocality appears explicitly:

$$\begin{aligned} \langle\vec{r}|\hat{\mathcal{O}}_{\text{eff}}|f\rangle &= \sum_q \langle\vec{r}|\frac{\hat{H}_{PQ}|\Phi_q\rangle\langle\Phi_q|\hat{H}_{QP}|f\rangle}{E - E_q + i\varepsilon} \\ &= \sum_q \frac{\hat{H}_{PQ}(\vec{r})\Phi_q(\vec{r}) \int \Phi_q^*(\vec{r}')\hat{H}_{QP}(\vec{r}')f(\vec{r}')d\vec{r}'}{E - E_q + i\varepsilon} \end{aligned} \quad (2.2.4)$$

To obtain the right part of this equation, we inserted a closure relation on radial coordinates. This equation shows that even if the underlying Hamiltonian is itself local, the optical potential should be nonlocal. It can be readily understood by looking at equation (2.2.4) and linking it to figure 1.3 b: a system that is excited into one of the states included in $Q|\Psi\rangle$ because of an interaction at point \vec{r} can reappear in a state of $P|\Psi\rangle$ due to another interaction at point \vec{r}' .

In the GOM, it is assumed that the projectile cannot be scattered before it reaches the target: this is the requirement of causality [66]. Because of this property, the effective operator must satisfy a dispersion relation of the form:

$$Re(\hat{\mathcal{O}}_{\text{eff}}) = \sum_q \frac{\hat{H}_{PQ}|\Phi_q\rangle\langle\Phi_q|\hat{H}_{QP}}{E - E_q} - \frac{1}{\pi} \mathcal{P} \int \frac{Im(\hat{\mathcal{O}}_{\text{eff}})}{E - E_q} dE_q \quad (2.2.5)$$

Modern phenomenological approaches based on such dispersion relation can reproduce very accurately scattering observables for specific cases like the work of Dickhoff *et al.* on ^{40}Ca and ^{48}Ca [67], but also for a large number of nuclei and energies like the global dispersive optical potential of Morillon [68] and the dispersive potential for actinides of Capote *et al.* [69]. Microscopic studies also achieve some nice successes using dispersive optical potentials in ab initio calculations [12, 70] and also with nuclear matter approaches [38].

The question of dispersive interactions was studied by Hodgson [66]. In his paper, he makes the following considerations: physically, the dispersion relation gives the effect of the coupling of non-elastic channels on the real part of the potential. Such effects are very important when the projectile's incident energy is close to the energies of the non-elastic channels, and more specifically the most significant contributions come from the coupling to low lying collective states. We expect then the effects of their contribution on the real part of the potential to be strong for incident energies below a few MeV, but weaker for higher energies. In particular, calculations made with effective operators that don't satisfy such dispersion relation can't predict single particle energies and occupation numbers as precisely as when using dispersive operators [67, 71]. In our work, we study reactions involving a projectile that has a high kinetic energy (> 50 MeV). At such energies, the effect of the coupling to low lying collective states on the real part of the potential is weak, and if we are able to reproduce correctly the experimental data for elastic scattering observables, then we

can assume that non-elastic processes are correctly taken into account in the imaginary part of the potential. Therefore, we do not address problems linked to the dispersive character of the effective operator, but keeping in mind that they should be dealt with in order to improve our modeling.

One last property of importance is the resonant nature of the effective operator. Indeed, let us consider a closed channel in $Q|\Psi\rangle$, which we label “c”. Then, the effective operator for this particular channel reads:

$$\hat{\mathcal{O}}_{\text{eff}}^c = \frac{\hat{H}_{PQ}|\Phi_c\rangle\langle\Phi_c|\hat{H}_{QP}}{E - E_c} \quad (2.2.6)$$

If $E \rightarrow E_c$ then $\hat{\mathcal{O}}_{\text{eff}}$ diverges and has a resonant behavior. This can be immediately attributed to quasi bound states stemming from couplings to the bound states of \hat{H}_{QQ} , and these resonances represent compound nucleus formation. By a proper treatment of these resonances (including an energy averaging), it is possible to account for them which leads - as a consequence - to more absorption in the effective operator [17] [72]. We do not refer to this property in our study, but it is an important feature of the effective operator worth mentioning. Now, if we resume ourselves, the effective operator introduced by the optical model must be:

- Energy dependent
- Nonlocal
- Resonant (it is possible to transform this property into more absorption)
- Complex
- Dependent on our choice of projection operators P and Q

More details on the properties of the effective Hamiltonian are given in references [11, 20, 73] and an extensive discussion on the nonlocality and its consequences on the total wave function can be found in [65]. We have given general features of the generalized optical model, so let us now give a more precise formalism for nucleon-nucleus elastic and inelastic scattering, our cases of interest.

2.3 Effective interaction and optical potential

It is possible to expand the total Hamiltonian of equation (2.0.2) into:

$$\hat{H} = \hat{T} + \hat{H}_A + \hat{V} \quad (2.3.1)$$

where \hat{T} is the kinetic energy operator for the projectile-target relative motion, \hat{V} is a NN potential of interaction that connects the projectile with one nucleon of the target in the interaction area, and \hat{H}_A is the intrinsic Hamiltonian of the target nucleus which obeys the equation:

$$\hat{H}_A|\psi_i\rangle = E_i|\psi_i\rangle, \quad \langle\psi_i|\psi_j\rangle = \delta_{ij} \quad (2.3.2)$$

with E_i the energy of the $|\psi_i\rangle$ state. Using these definitions and those of equation (2.1.2), we can write:

$$\begin{aligned}
 \hat{H}_{PP} &= P\hat{H}P = P(\hat{T} + \hat{H}_A + \hat{V})P = \sum_{i=0}^n \sum_{j=0}^n |\psi_i\rangle\langle\psi_i|(\hat{T} + \hat{H}_A + \hat{V})|\psi_j\rangle\langle\psi_j| \\
 &\Leftrightarrow \hat{H}_{PP} = \sum_{i=0}^n \sum_{j=0}^n |\psi_i\rangle \left(\langle\psi_i|\hat{T}|\psi_j\rangle + \langle\psi_i|\hat{H}_A|\psi_j\rangle + \langle\psi_i|\hat{V}|\psi_j\rangle \right) \langle\psi_j| \\
 &\Leftrightarrow \hat{H}_{PP} = \sum_{i=0}^n \sum_{j=0}^n |\psi_i\rangle \left(\hat{T}\delta_{ij} + E_j\delta_{ij} + \langle\psi_i|\hat{V}|\psi_j\rangle \right) \langle\psi_j| \\
 &\Leftrightarrow \hat{H}_{PP} = \sum_{i=0}^n (\hat{T} + E_i)|\psi_i\rangle\langle\psi_i| + \sum_{i=0}^n \sum_{j=0}^n |\psi_i\rangle\langle\psi_i|\hat{V}|\psi_j\rangle\langle\psi_j|
 \end{aligned}$$

So the operator \hat{H}_{PP} is expanded into a more suitable form for calculations:

$$\hat{H}_{PP} = (\hat{T} + \hat{H}_A)P + P\hat{V}P \quad (2.3.3)$$

Similarly, we can show that formulae for the other operators in \hat{H}_{eff} read:

$$\begin{aligned}
 \hat{H}_{QQ} &= (\hat{T} + \hat{H}_A)Q + Q\hat{V}Q \\
 \hat{H}_{PQ} &= P\hat{V}Q \\
 \hat{H}_{QP} &= Q\hat{V}P
 \end{aligned}$$

and finally, we can rewrite the equation for $P|\Psi\rangle$ and proceed with some algebra:

$$\begin{aligned}
 &\left(\hat{H}_{PP} + \hat{H}_{PQ} \frac{1}{E - \hat{H}_{QQ} + i\varepsilon} \hat{H}_{QP} \right) |\Psi\rangle = EP|\Psi\rangle \\
 &\Leftrightarrow \left((\hat{T} + \hat{H}_A)P + P\hat{V}P + P\hat{V}Q \frac{1}{E - \hat{H}_A - \hat{T} - Q\hat{V}Q + i\varepsilon} Q\hat{V}P \right) P|\Psi\rangle = EP|\Psi\rangle \\
 &\Leftrightarrow \left(\hat{T} + \hat{H}_A + P\hat{V}P + P\hat{V}Q \frac{1}{E - \hat{H}_A - \hat{T} - Q\hat{V}Q + i\varepsilon} Q\hat{V}P \right) P|\Psi\rangle = EP|\Psi\rangle \quad (2.3.4)
 \end{aligned}$$

With this form, we can define a NN effective interaction operator:

$$\hat{V}_{\text{eff}} = P\hat{V}P + P\hat{V}Q \frac{1}{E - \hat{H}_A - \hat{T} - Q\hat{V}Q + i\varepsilon} Q\hat{V}P \quad (2.3.5)$$

The complications of the many-body problem are contained in this effective operator, so the usefulness of the whole approach - meaning of the generalized optical model - depends on our capability to build simple and accurate models for it. Here, \hat{V}_{eff} is the interaction that connects the incident nucleon with nucleons of the target in the nuclear medium. This ingredient conditions greatly the accuracy of the predictions done within a microscopic framework; that is why many efforts have been put in deriving simple yet accurate effective NN interactions for nucleon-nucleus scattering. We give some details of such interactions in section 4.3. For the moment, let us derive formulae for elastic scattering of a spinless projectile on a central potential.

2.4 Simple case of scattering by a central potential

The formal theory of elastic scattering of a spinless particle on a central potential is critical to understand the physical phenomena that govern such reactions. However, it has been presented thoroughly in many textbooks [72] [74], so our purpose here is to give at first a simple form of some equations that we generalize in later sections. Let us start our description from the definition (2.3.1) and assume that the potential V_{eff} doesn't act on spin variables:

$$\hat{H} = \hat{T} + \hat{H}_A + \hat{V}_{\text{eff}} \quad (2.4.1)$$

We define the projection operators for the present derivation as:

$$P = |\psi_0\rangle\langle\psi_0| \quad Q = \sum_{i>0} |\psi_i\rangle\langle\psi_i|$$

If \hat{V}_{eff} vanishes, equation (2.0.2) reads:

$$(E - \hat{T} - \hat{H}_A)|\Psi_0\rangle = 0 \quad (2.4.2)$$

$|\Psi_0\rangle$ is the solution of the homogeneous form of equation (2.0.2). We can also define the free-particle Green's function G as (written in radial coordinates):

$$(E + \frac{\hbar^2}{2\mu} \vec{\nabla}^2 - E_A)G(\vec{r} - \vec{r}') = \delta(\vec{r} - \vec{r}') \quad (2.4.3)$$

where E_A is the intrinsic energy of the target and μ the reduced mass of the system {projectile+target}. When $\hat{V}_{\text{eff}} \neq 0$, a formal solution of equation (2.0.2) reads:

$$|\Psi\rangle = |\Psi_0\rangle + \frac{1}{E - \hat{T} - \hat{H}_A \pm i\epsilon} \hat{V}_{\text{eff}}|\Psi\rangle \quad (2.4.4)$$

In order to compute the solution wave function for elastic scattering, we need to project this equation on the ground state of the target nucleus $|\psi_0\rangle$:

$$\langle\psi_0|\Psi\rangle = \langle\psi_0|\Psi_0\rangle + \langle\psi_0|\frac{1}{E - \hat{T} - \hat{H}_A \pm i\epsilon} \hat{V}_{\text{eff}}|\Psi\rangle \quad (2.4.5)$$

we then insert a closure relation (on internal states of the target) on each side of \hat{V}_{eff} and use orthonormality of states defined in (2.3.2) to reduce this equation to:

$$\langle\psi_0|\Psi\rangle = \langle\psi_0|\Psi_0\rangle + \frac{1}{E - \hat{T} - E_A \pm i\epsilon} \langle\psi_0|\hat{V}_{\text{eff}}|\psi_0\rangle \langle\psi_0|\Psi\rangle = \Psi_0^{\text{elastic}} + \frac{1}{E - \hat{T} - E_A \pm i\epsilon} \hat{U}_{\text{eff}}\Psi^{\text{elastic}} \quad (2.4.6)$$

in which we labeled the optical potential operator $\langle\psi_0|\hat{V}_{\text{eff}}|\psi_0\rangle$ as \hat{U}_{eff} . We can project this equation on space coordinates to solve it. In this basis, the Green's function can be shown to be equal to:

$$\langle\vec{r}|\frac{1}{E + \frac{\hbar^2}{2\mu} \vec{\nabla}^2 - E_A \pm i\epsilon}|\vec{r}'\rangle = -\frac{2\mu}{\hbar^2} \frac{1}{4\pi} \frac{e^{\pm ik_i|\vec{r}-\vec{r}'|}}{|\vec{r}-\vec{r}'|} \quad (2.4.7)$$

with μ the reduced mass of the system and k_i the wave number of the system in the entrance channel. Boundary conditions impose scattered outgoing waves only, so the \pm sign reduces

to +. Given this result, we can project equation (2.4.6) on the radial coordinates basis. We insert closure relation of this basis on both sides of \hat{U}_{eff} and obtain the Dyson equation:

$$\Psi^{\text{elastic}}(\vec{r}) = \Psi_0^{\text{elastic}}(\vec{r}) - \frac{2\mu}{\hbar^2} \frac{1}{4\pi} \int \frac{e^{ik_i|\vec{r}-\vec{r}'|}}{|\vec{r}-\vec{r}'|} d\vec{r}' \int \hat{U}_{\text{eff}}(\vec{r}', \vec{r}'') \Psi^{\text{elastic}}(\vec{r}'') d\vec{r}'' \quad (2.4.8)$$

For \vec{r} sufficiently large we have:

$$\begin{aligned} |\vec{r}| &\gg |\vec{r}'| \\ |\vec{r} - \vec{r}'| &\approx r - \vec{u} \cdot \vec{r}' \quad , \quad \vec{u} = \frac{\vec{r}}{r} \\ \frac{1}{|\vec{r} - \vec{r}'|} &\approx \frac{1}{r} \end{aligned}$$

which leads, once inserted in the previous equation, to the asymptotic form:

$$\begin{aligned} \Psi^{\text{elastic}}(\vec{r}) &\underset{\infty}{=} \Psi_0^{\text{elastic}}(\vec{r}) - \frac{e^{ik_i r}}{r} \frac{\mu}{2\pi\hbar^2} \int e^{i\vec{k}_i' \cdot \vec{r}'} d\vec{r}' \int \hat{U}_{\text{eff}}(\vec{r}', \vec{r}'') \Psi^{\text{elastic}}(\vec{r}'') d\vec{r}'' \\ &\underset{\infty}{=} \Psi_0^{\text{elastic}}(\vec{r}) + f(\vec{k}_i, \vec{k}_i') \frac{e^{ik_i r}}{r} \end{aligned} \quad (2.4.9)$$

where $\vec{k}_i' = k_i \vec{u}$. We have defined the scattering amplitude $f(\vec{k}, \vec{k}')$, and we can show [74] that it is related to the differential cross section by:

$$\frac{d\sigma}{d\Omega} = |f(\vec{k}_i, \vec{k}_i')|^2 \quad (2.4.10)$$

We can similarly derive formulae for the more complicated case of nucleon-nucleus scattering, taking into account the spin of the projectile and some excited states of the projectile.

2.5 Formulae for the scattering of a nucleon off a target nucleus

The simple definitions that we gave for the scattering amplitude and the differential cross section in the previous section still hold in the case of nucleon-nucleus scattering with inclusion of spins, provided we take into account the coupling of angular momenta. Such work is done in several textbooks [72, 75], but sign and coupling conventions (among other things) vary from one book to another. We have chosen to give details about our convention choices and associated derivations to obtain a global, consistent description. In order to do this, we will start by expressing our choice of angular momentum coupling scheme, then we will give the generalized formula of the total wave function of the total system {projectile + target}. From this definition, we will deduce the scattering amplitude's formula and, after explaining how the radial part of the scattering amplitude is computed, we will link it to the differential cross section.

2.5.1 Coupling of angular momenta and definition of a basis for projections

So first, we must give our coupling scheme. We have chosen to couple the spin of the projectile \vec{s} and its orbital angular momentum \vec{l} to \vec{j} , and couple this total spin of the

projectile with the total spin of the target \vec{J} to obtain the total angular momentum of the system \vec{I} , which is a good quantum number for the case of nucleon-nucleus scattering. Our choice of coupling scheme can be summarized as:

$$\vec{l} + \vec{s} = \vec{j} \quad \vec{j} + \vec{J} = \vec{I} \quad (2.5.1)$$

Moreover, we shall denote m_i the projection of the angular momentum i on the quantization axis. Furthermore, the total parity π of the system is also conserved during nucleon-nucleus scattering. So we shall label the parity of the target nucleus by Π (the parity of the relative motion function is simply $(-1)^l$). With these definitions, we will rewrite the total wave function of the system and include explicitly all couplings of angular momenta. If we consider the projectile with spin and spin projection $|\frac{1}{2}m_p\rangle$ colliding with a target nucleus in its ground state defined by total spin, total spin projection and parity $|\psi_i \in J_i M_i \Pi_i\rangle$, the asymptotic form of the total wave function of the system can be written, in analogy with (2.4.9):

$$\begin{aligned} \Psi_{m_p, M_i} \sim & e^{i\vec{k}_i \cdot \vec{r}} |\frac{1}{2}m_p\rangle |\psi_i \in J_i M_i \Pi_i\rangle + \\ & \sum_{m'_p, M'_i} \frac{e^{ik_i r}}{r} f_{m_p m'_p}^{\psi_i \rightarrow \psi_i}(\vec{k}_i, \vec{k}'_i) |\frac{1}{2}m'_p\rangle |\psi_i \in J_i M'_i \Pi_i\rangle + \\ & \sum_{\substack{m'_p, M'_f \\ k_f \neq k_i \\ \psi_f \neq \psi_i}} \frac{e^{ik_f r}}{r} f_{m_p m'_p}^{\psi_i \rightarrow \psi_f}(\vec{k}_i, \vec{k}_f) |\frac{1}{2}m'_p\rangle |\psi_f \in J_f M_f \Pi_f\rangle \end{aligned} \quad (2.5.2)$$

with \vec{k}_i the incident wave vector, \vec{k}'_i the wave vector of the outgoing wave in the elastic channel, \vec{k}_f the wave vector of the outgoing wave in inelastic channels, f the scattering amplitude. The solution for the homogeneous equation is taken - just like for the scattering of a spinless particle on a central potential - to be simply a plane wave, and the presence of the interacting potential V generates scattered spherical waves. In order to account for the coupling of angular momenta, we need to rewrite the total wave function in a way that clearly shows the couplings. Given our choice of coupling scheme, we can expand the wave function on the spin-angular function basis, which are related to spherical harmonics and spinors by the relation:

$$Y_m^{l\frac{1}{2}j}(\Omega, \sigma) = \sum_{m_l m_s} \langle l m_l \frac{1}{2} m_s | j m \rangle i^l Y_{m_l}^l(\Omega) \chi_{\frac{1}{2}m_p}^{\frac{1}{2}}(\sigma) = \left[\overline{Y}_l(\Omega) \otimes \overline{\chi}_{\frac{1}{2}}(\sigma) \right]_m^j \quad (2.5.3)$$

where $\langle l m_l \frac{1}{2} m_s | j m \rangle$ is a Clebsch-Gordan coefficient (see Appendix A), \overline{Y} an irreducible tensor operator, $\chi_{\frac{1}{2}m_p}^{\frac{1}{2}}$ a spinor defined formally by $\chi_{\frac{1}{2}m_p}^{\frac{1}{2}}(\sigma) = \langle \sigma | \frac{1}{2}m_p \rangle$ and finally Y_m^l a spherical harmonic. Spin-angular functions obey the orthogonality relation:

$$\int Y_{m'}^{l'\frac{1}{2}j'^*}(\Omega, \sigma) Y_m^{l\frac{1}{2}j}(\Omega, \sigma) d\Omega d\sigma = \delta_{jj'} \delta_{ll'} \delta_{mm'} \quad (2.5.4)$$

It is also useful to define, for oncoming derivations, a generalized function that results from the tensor product of a spin-angular function with the target's internal state $|\psi \in JM\Pi\rangle$:

$$\begin{aligned} \mathcal{Y}_{(l\frac{1}{2})j, J}^{I, \mu}(\Omega, \sigma, x) &= \langle \Omega \sigma x | [(l\frac{1}{2})j, J], I \mu \rangle = \left[Y^{l\frac{1}{2}j}(\Omega, \sigma) \otimes \psi^J(x) \right]_{\mu}^I \\ &= \sum_{m, M} \langle j m J M | I \mu \rangle Y_m^{l\frac{1}{2}j}(\Omega, \sigma) \psi_{JM\Pi}(x) \end{aligned} \quad (2.5.5)$$

where $\psi_{JM\Pi}(x) = \langle x|\psi \in JM\Pi\rangle$, with x labeling the internal variables of the target. Similarly, these functions obey the orthogonality relation:

$$\int \mathcal{Y}_{(l'\frac{1}{2})j',J'}^{l',\mu'^*}(\Omega, \sigma, x) \mathcal{Y}_{(l\frac{1}{2})j,J}^{l,\mu}(\Omega, \sigma, x) d\Omega d\sigma dx = \delta_{l'l'} \delta_{\mu\mu'} \delta_{J'J} \delta_{j'j} \delta_{l'l'} \quad (2.5.6)$$

and the inverse relation of equation (2.5.5) reads:

$$Y_m^{l\frac{1}{2}j}(\Omega, \sigma) \psi_{JM\Pi}(x) = \sum_{I\mu} \langle jmJM|I\mu\rangle \mathcal{Y}_{(l\frac{1}{2})j,J}^{I,\mu}(\Omega, \sigma, x) \quad (2.5.7)$$

Expanding the total wave function on such basis enables us to use the Racah algebra, thus allowing us to write formulae for the total wave function in which angular and radial variables are explicitly separated.

2.5.2 Total wave function, scattering amplitude and cross section

First, let us consider the case when there is no interaction between the projectile and the target. In this case, the quantum states describing the relative motion and the target are unchanged and quantum numbers are conserved. We can write the expansion (2.0.3) as:

$$|\Psi\rangle = \sum_i |\vec{k}_i m_p\rangle \otimes |\psi_i \in J_i M_i \Pi_i\rangle \quad (2.5.8)$$

where \vec{k} is the wave vector of the relative motion, $m_p = \pm\frac{1}{2}$ the projection of the projectile's spin on the quantization axis, J_i the spin of target, M_i its projection on the quantization axis and Π_i its parity. Since there is no interaction, the wave function for the relative motion is simply a plane wave. The multipole expansion of a plane wave reads:

$$e^{i\vec{k}\cdot\vec{r}} = 4\pi \sum_{lm_l} j_l(k, r) i^l Y_{m_l}^{l*}(\Omega_k) Y_{m_l}^l(\Omega_r) \quad (2.5.9)$$

with j_l the spherical Bessel function of the first kind. If we write the total wave function in the initial state as $|\Psi_i\rangle = |\vec{k}_i m_p\rangle \otimes |\psi_i \in J_i M_i \Pi_i\rangle$, then using the multipole expansion of a plane wave we can write this total wave function in the $\{|\vec{r}, \sigma, x\rangle\}$ basis as:

$$\begin{aligned} \langle \vec{r}, \sigma, x | \Psi_i \rangle &= \Psi_{m_p, i}^{\text{Veff}=0}(\vec{r}, \sigma, x) = \langle \vec{r}, \sigma | \vec{k}_i m_p \rangle \langle x | \psi_i \in J_i M_i \Pi_i \rangle \\ &= 4\pi \sum_{lm_l} j_l(k, r) i^l Y_{m_l}^{l*}(\Omega_k) Y_{m_l}^l(\Omega_r) \chi_{m_p}^{\frac{1}{2}}(\sigma) \psi_{JM\Pi}(x) \end{aligned}$$

We use the inverse relation of equation (2.5.3) to insert the spin-angular functions:

$$\Psi_{m_p, i}^{\text{Veff}=0}(\vec{r}, \sigma, x) = 4\pi \sum_{\substack{lm_l \\ jm}} j_l(k, r) i^l Y_{m_l}^{l*}(\Omega_k) \left\langle lm_l \frac{1}{2} m_p | jm \right\rangle Y_m^{l\frac{1}{2}j}(\Omega_r, \sigma) \psi_{JM\Pi}(x)$$

We notice here that m_p is fixed, and $m = m_l + m_p$ because of the Clebsch-Gordan coefficients which means the sum over m is redundant with that of m_l . Now we use the relation of equation (2.5.7) to obtain finally:

$$\Psi_{m_p, i}^{\text{Veff}=0}(\vec{r}, \sigma, x) = 4\pi \sum_{\substack{l j I \\ m_l \mu}} j_l(k, r) Y_{m_l}^{l*}(\Omega_k) \left\langle lm_l \frac{1}{2} m_p | jm \right\rangle \langle jm J_i M_i | I \mu \rangle \mathcal{Y}_{(l\frac{1}{2})j, J_i}^{I, \mu}(\Omega_r, \sigma, x)$$

with I the total angular momentum of the system as defined in (2.5.1). We derived this formula by assuming there was no interaction between the projectile and the target. When such is not the case, the radial function j_l is modified and outgoing spherical waves are generated in partitions $|\Psi_{i \neq i}\rangle$. Furthermore, the quantum numbers of the initial state are not necessarily conserved during the reaction (except for I and μ) which leads to:

$$\Psi_{m_p, i}(\vec{r}, \sigma, x) = \frac{4\pi}{k_i r} \sum_{i', m'_p} \sum_{\substack{l j I \\ m_l \mu}} \left\langle l m_l \frac{1}{2} m_p | j m \right\rangle \langle j m J_i M_i | I \mu \rangle Y_{m_l}^{l*}(\Omega_k) \quad (2.5.10)$$

$$\sum_{l' j'} \mathcal{Y}_{(l' \frac{1}{2}) j', J'_i}^{I, \mu}(\Omega_r, \sigma, x) \phi_{[(l' \frac{1}{2}) j', J'_i], [(l \frac{1}{2}) j, J_i]}^I(k, r)$$

where $\phi_{[(l' \frac{1}{2}) j, J_i], [(l \frac{1}{2}) j', J'_i]}^I$ contains the radial dependence of $|\Psi_i\rangle$ and i' labels a sum over the states $|\psi_{i'}\rangle$ of the target. If the projectile undergoes elastic scattering, then its spin can be reoriented and the target is unchanged except for its spin orientation, which corresponds to the second line of equation (2.5.2) (meaning the sum over i' is simply a sum over M'_i). Finally, the inelastic scattering case that corresponds to the third line of equation (2.5.2) is when the sum over i' consists of a sum over all quantum numbers describing the target's states in the expansion (2.5.8).

We can expand the general function \mathcal{Y} in (2.5.10) and use selection rules of the Clebsch-Gordan coefficients to show explicitly the projections of angular momenta, which is useful in order to make the link with the asymptotic form and the scattering amplitude. In order to make the difference between the initial state labeled i and the other states i' , we will henceforth label these other states f . Equation (2.5.10) reads now:

$$\Psi_{m_p, i}(\vec{r}, \sigma, x) = \frac{4\pi}{k_i r} \sum_{\substack{l' j j' \\ m'_p M_f}} \left\langle l m_l \frac{1}{2} m_p | j m_l + m_p \right\rangle \langle j J_i m_l + m_p M_i | I m_l + m_p + M_i \rangle Y_m^{l*}(\Omega_{k_i})$$

$$\left\langle l' m_l + m_p + M_i - m'_p - M_f \frac{1}{2} m'_p | j' m_l + m_p + M_i - M_f \right\rangle$$

$$\langle j' J_f m_l + m_p + M_i - M_f M_f | I m_l + m_p + M_i \rangle$$

$$i^{l'} Y_{m_l + m_p + M_i - m'_p - M_f}^{l'}(\Omega_r) \phi_{[(l' \frac{1}{2}) j', J'_f], [(l \frac{1}{2}) j, J_i]}^I(k_f, r) \chi_{m'_p}^{\frac{1}{2}}(\sigma) \psi_{J_f M_f \Pi_f}(x) \quad (2.5.11)$$

The Clebsch-Gordan coefficients resume well the couplings involved in the reaction: the entrance channel, characterized by the partial wave $|(l \frac{1}{2}) j\rangle$ and the target in the state $|J_i M_i \Pi_i\rangle$ couples to partial waves $|(l' \frac{1}{2}) j'\rangle$ in the exit channel and the target in a state $|J_f M_f \Pi_f\rangle$. The selection of partial waves that couple to each other follows selection rules of the Clebsch-Gordan coefficients, and the quantum numbers that are conserved during the whole process are the total angular momentum I and total parity π of the system. There is one function containing the radial dependence of the total wave function for each combination of partial waves, target nucleus state and total angular momentum and parity. The computation of geometric terms is made rather easy thanks to the Racah algebra, but the radial dependence remains.

The radial part is obtained by solving a system of coupled equations as presented in chapter 3. The asymptotic part of this solution wave function can be directly linked to the scattering amplitude, and consequently the cross section. Using the phase shifts method,

one can show that in the case of nucleon-nucleus collision, the asymptotic form of the radial wave function is expressed by [76]:

$$\phi_{[(l'\frac{1}{2})j',J_f],[(l\frac{1}{2})j,J_i]}^I(k_f,r) = \frac{1}{2}ie^{i\sigma_l} \left(H_l^*(k_i r) \delta_{jj'} \delta_{ll'} \delta_{\psi_i \psi_f} - S_{[(l'\frac{1}{2})j',J_f],[(l\frac{1}{2})j,J_i]}^I H_{l'}(k_f r) \right) \quad (2.5.12)$$

where $\sigma_{l'}$ is the Coulomb phase shift [77], H is the Hankel function (G.0.3), S is the scattering matrix. This form shows that the only incoming spherical waves are in the elastic channel, while there are outgoing spherical waves in all other open channels. Once the system of coupled equations is solved and we have calculated the radial wave function, we can use equation (2.5.12) to compute the scattering matrix, which is directly linked to the scattering amplitude. In the most general case, the potential used to compute the solution wave function is made of a short range component - the hadronic part - and a long range component, the Coulomb component. This structure is conserved when expressing the scattering amplitude in terms of the scattering matrix:

$$\begin{aligned} f_{m_p, m'_p}^{\psi_i \rightarrow \psi_f}(\vec{k}_i, \vec{k}_f) &= f_{\text{Coulomb}}(\vec{k}_i, \vec{k}_f) \delta_{m_p m'_p} \delta_{M_i M_f} + \\ &\frac{2\pi}{k_i} \sum_{\substack{l, j \\ l', j'}} \left\langle l m_l \frac{1}{2} m_p | j m_l + m_p \right\rangle \left\langle j J_i m_l + m_p M_i | I m_l + m_p + M_i \right\rangle \\ &\left\langle l' m_l + m_p + M_i - m'_p - M_f \frac{1}{2} m'_p | j' m_l + m_p + M_i - M_f \right\rangle \\ &\left\langle j' J_f m_l + m_p + M_i - M_f M_f | I m_l + m_p + M_i \right\rangle \\ &ie^{i(\sigma_l + \sigma_{l'})} \left(\delta_{m_p m'_p} \delta_{jj'} \delta_{ll'} \delta_{\psi_i \psi_f} - S_{[(l'\frac{1}{2})j',J_f],[(l\frac{1}{2})j,J_i]}^I \right) \\ &Y_{m_l}^{l*}(\Omega_{k_i}) Y_{m_l + m_p + M_i - m'_p - M_f}^{l'}(\Omega_{k_f}) \end{aligned} \quad (2.5.13)$$

where the Coulomb scattering amplitude is (for any angle θ):

$$f_{\text{Coulomb}}(\theta) = -\frac{\eta}{2k \sin^2(\frac{\theta}{2})} e^{-i\eta \ln(\sin^2(\frac{\theta}{2})) + 2i\sigma_0}, \quad \sigma_0 = \arg \Gamma(1 + i\eta), \quad \eta = \frac{Z_{\text{projectile}} Z_{\text{target}} e^2 \mu}{\hbar^2 k}$$

with η the usual Sommerfeld parameter. This formula can be somewhat simplified by taking the axis of quantization - the $(0 \vec{z})$ axis in the lab frame - parallel to the direction of the incident particle momentum \vec{k}_i . Indeed, in this case the projection of the orbital angular momentum for the incident partial wave is zero ($m_l = 0$) which yields:

$$\begin{aligned} f_{m_p, m'_p}^{\psi_i \rightarrow \psi_f}(\vec{k}_i, \vec{k}_f) &= f_{\text{Coulomb}}(\Omega_{k_f}) \delta_{m_p m'_p} \delta_{M_i M_f} + \\ &\frac{2\pi}{k_i} \sum_{\substack{l, j \\ l', j'}} \left\langle l 0 \frac{1}{2} m_p | j m_p \right\rangle \left\langle j J_i m_p M_i | I m_p + M_i \right\rangle \\ &\left\langle l' m_p + M_i - m'_p - M_f \frac{1}{2} m'_p | j' m_p + M_i - M_f \right\rangle \\ &\left\langle j' J_f m_p + M_i - M_f M_f | I m_p + M_i \right\rangle \\ &ie^{i(\sigma_l + \sigma_{l'})} \left(\delta_{m_p m'_p} \delta_{jj'} \delta_{ll'} \delta_{\psi_i \psi_f} - S_{[(l'\frac{1}{2})j',J_f],[(l\frac{1}{2})j,J_i]}^I \right) \\ &\sqrt{\frac{2l+1}{4\pi}} Y_{m_l + m_p + M_i - m'_p - M_f}^{l'}(\Omega_{k_f}) \end{aligned} \quad (2.5.14)$$

The final step is to write the differential cross section. The inclusion of spin variables modifies slightly formula (2.4.10) to:

$$\boxed{\frac{d\sigma}{d\Omega}(\theta) = \frac{1}{(2s_p + 1)(2J_i + 1)} \sum_{\substack{m_p, M_i, \\ m'_p, M_f}} \left| f_{\text{Coulomb}}(\theta) \delta_{m_p m'_p} \delta_{M_i M_f} + f_{m_p, m'_p}^{\psi_i \rightarrow \psi_f}(\theta) \right|^2} \quad (2.5.15)$$

Using this procedure we are able to separate angular and radial coordinates, and the Racah algebra eases the integration over angular variables. The scattering matrix can be evaluated once we know the radial wave functions, taking a large value for the matching radius r_∞ and inverting formula (2.5.12) to:

$$S_{[(l'\frac{1}{2})j', J_f], [(l\frac{1}{2})j, J_i]}^I = \frac{k_i (F_l(k_i r_\infty) + 2i \phi_{[(l'\frac{1}{2})j', J_f], [(l\frac{1}{2})j, J_i]}^I(k_f r_\infty))}{k_f H_l(k_f r_\infty)} \quad (2.5.16)$$

with F_l the regular Coulomb function defined in appendix G. The radial wave functions are thus necessary to compute the differential cross section, and in the next section we derive a set of coupled radial equations for which these radial wave functions are solution. We also describe a simple way to solve these coupled equations.

Chapter 3

Treating the radial part of CC equations

In the previous section, we have introduced the generalized optical model and we have derived the generalized optical potential. After giving some insight of physics contained in this potential and presenting its features, we introduced its use in the theory of scattering in the simple case of a spinless projectile on a central potential. Then, we gave formulae for the total wave function, the scattering amplitude and the differential cross section. These quantities can be computed using Racah algebra, once we know the radial wave functions. In the present section, we derive CC equations using the coupling scheme described in section II.E, and introduce a simple way to solve these coupled equations to obtain the radial wave functions. We will give quite many details needed for our computational work so as to ease any process of reproduction.

3.1 Coupled equations in the radial coordinate basis

In order to avoid unnecessary complications, we will derive coupled equations involving the ground state of the target nucleus, denoted as $|\psi_0\rangle$, and a selection of discrete states denoted $|\psi_i\rangle$ but we will write the associated equation of only the last of these states, labeled $|\psi_N\rangle$. By doing this, we assume that the coupling to all other states $|\psi_{j>N}\rangle$ is taken into account effectively by using the complex effective nucleon-nucleus interaction. In a mathematical formulation, the P space contains the ground state plus $N-1$ excited states, and the Q space contains in principle all other states. Thus, using the expansion (2.0.3) of the total wave function, the P and Q operators read:

$$P = \sum_{i=0}^N |\psi_i\rangle\langle\psi_i| \qquad Q = \sum_{j>N} |\psi_j\rangle\langle\psi_j| \qquad (3.1.1)$$

so the part of the total wave function that we will treat explicitly reads:

$$P|\Psi\rangle = \sum_{i=0}^N |\psi_i\rangle \otimes |w_i\rangle \qquad (3.1.2)$$

and we remind the equation for which $P|\Psi\rangle$ is solution in the center of mass (CM) frame of reference:

$$\left(\hat{T} + \hat{H}_A + \hat{V}\right) P|\Psi\rangle = E_{C.M.} P|\Psi\rangle \qquad (3.1.3)$$

with \hat{V} the effective operator defined in equation (2.3.5) (we shall omit the label “eff” for this interaction in the following derivations). We project (3.1.3) on $|\psi_0\rangle$ the ground state of

the target and on its excited state $|\psi_N\rangle$ (it is also valid for the other states $\psi_{i<N}$):

$$\mathcal{S} : \begin{cases} \hat{T}\langle\psi_0|\Psi\rangle + \langle\psi_0|\hat{H}_A|\Psi\rangle + \langle\psi_0|\hat{V}|\Psi\rangle = E_{CM}\langle\psi_0|\Psi\rangle \\ \hat{T}\langle\psi_N|\Psi\rangle + \langle\psi_N|\hat{H}_A|\Psi\rangle + \langle\psi_N|\hat{V}|\Psi\rangle = E_{CM}\langle\psi_N|\Psi\rangle \end{cases}$$

We separate diagonal components from off-diagonal ones, using (3.1.2):

$$\mathcal{S} : \begin{cases} \hat{T} \sum_i \langle\psi_0|\psi_i\rangle|w_i\rangle + \langle\psi_0|\hat{H}_A|\psi_0\rangle|w_0\rangle + \langle\psi_0|\hat{V}|\psi_0\rangle|w_0\rangle + \sum_{i\neq 0} \langle\psi_0|\hat{H}_A|\psi_i\rangle|w_i\rangle + \\ \sum_{i\neq 0} \langle\psi_0|\hat{V}|\psi_i\rangle|w_i\rangle = E_{CM} \sum_i \langle\psi_0|\psi_i\rangle|w_i\rangle \\ \hat{T} \sum_i \langle\psi_N|\psi_i\rangle|w_i\rangle + \langle\psi_N|\hat{H}_A|\psi_N\rangle|w_N\rangle + \langle\psi_N|\hat{V}|\psi_N\rangle|w_N\rangle + \sum_{i\neq N} \langle\psi_N|\hat{H}_A|\psi_i\rangle|w_i\rangle + \\ \sum_{i\neq N} \langle\psi_N|\hat{V}|\psi_i\rangle|w_i\rangle = E_{CM} \sum_i \langle\psi_N|\psi_i\rangle|w_i\rangle \end{cases}$$

then we use orthonormality properties of the state vectors $|\psi_i\rangle$ and relation (2.3.2) to reduce the system to:

$$\mathcal{S} : \begin{cases} (E - \hat{T} - \langle\psi_0|\hat{V}|\psi_0\rangle) |w_0\rangle = \sum_{i\neq 0} \langle\psi_0|\hat{V}|\psi_i\rangle|w_i\rangle \\ (E' - \hat{T} - \langle\psi_N|\hat{V}|\psi_N\rangle) |w_N\rangle = \sum_{i\neq N} \langle\psi_N|\hat{V}|\psi_i\rangle|w_i\rangle \end{cases}$$

in which we defined $E = E_{CM} - E_0$, $E' = E_{CM} - E_N$. From this general system, we can derive coupled equations in any complete basis. We choose radial coordinates, so we project the system \mathcal{S} on the complete basis $\{|\vec{r}, \sigma\rangle\}$. Also, we write the kinetic operator in the space coordinates:

$$\mathcal{S} : \begin{cases} \langle\vec{r}, \sigma|(E + \frac{\hbar^2}{2\mu}\vec{\nabla}^2 - \langle\psi_0|\hat{V}|\psi_0\rangle) |w_0\rangle = \langle\vec{r}, \sigma| \sum_{i\neq 0} \langle\psi_0|\hat{V}|\psi_i\rangle|w_i\rangle \\ \langle\vec{r}, \sigma|(E' + \frac{\hbar^2}{2\mu}\vec{\nabla}^2 - \langle\psi_N|\hat{V}|\psi_N\rangle) |w_N\rangle = \langle\vec{r}, \sigma| \sum_{i\neq N} \langle\psi_N|\hat{V}|\psi_i\rangle|w_i\rangle \end{cases}$$

Using orthonormality properties of the basis $\{|\vec{r}, \sigma\rangle\}$, we can write the system as:

$$\mathcal{S} : \begin{cases} Ew^0(\vec{r}, \sigma) + \frac{\hbar^2}{2\mu}\vec{\nabla}^2(w^0(\vec{r}, \sigma)) - \int U^{00}(\vec{r}, \sigma, \vec{r}', \sigma')w^0(\vec{r}', \sigma')d\vec{r}'d\sigma' = \\ \sum_{i\neq 0} \int U^{0i}(\vec{r}, \sigma, \vec{r}', \sigma')w^i(\vec{r}', \sigma')d\vec{r}'d\sigma' \\ E'w^N(\vec{r}, \sigma) + \frac{\hbar^2}{2\mu}\vec{\nabla}^2(w^N(\vec{r}, \sigma)) - \int U^{NN}(\vec{r}, \sigma, \vec{r}', \sigma')w^N(\vec{r}', \sigma')d\vec{r}'d\sigma' = \\ \sum_{i\neq N} \int U^{Ni}(\vec{r}, \sigma, \vec{r}', \sigma')w^i(\vec{r}', \sigma')d\vec{r}'d\sigma' \end{cases}$$

where we introduced for simplicity $U^{ab}(\vec{r}, \sigma, \vec{r}', \sigma') = \langle\vec{r}, \sigma|\langle\psi_a|\hat{V}|\psi_b\rangle|\vec{r}', \sigma'\rangle$. The structure of the system exhibits some features that we discussed in the previous section but that appear more clearly here: U^{00} is the potential that couples the ground state to itself so it contains the physics of shape elastic scattering; it is what is usually called the optical potential. U^{NN} couples the excited state $|\psi_N\rangle$ to itself and treats the virtual shape elastic reaction in which the kinetic energy of the projectile is E' and the target is in its excited state. Reactions that

feed elastic scattering such as transitions from one excited state $|\psi_i\rangle$ to the ground state are represented by $U^{0i, i \neq 0}$, and the opposite process during which the transition goes from the ground state $|\psi_0\rangle$ or one excited state $|\psi_{i < N}\rangle$ to $|\psi_N\rangle$ is contained in $U^{Ni, i \neq N}$. Now, we need to calculate each integral term to solve this system and since we have chosen the space coordinate basis, let us separate spin and angular variables from radial ones by doing a multipole expansion on the spin-angular functions basis.

3.2 Multipole expansion

Choosing the initial direction of the projectile as a quantization axis for the angular momentum, we develop the wave functions $w^i(\vec{r}, \sigma)$ and the potential $U^{ab}(\vec{r}, \sigma, \vec{r}', \sigma')$ on the function basis that we have defined in equation (2.5.5). The angular momenta that appear are those defined in equation (2.5.1). The expansion of $P|\Psi\rangle$ reads:

$$\langle \Omega \sigma x | P | \Psi \rangle = \frac{4\pi}{k_b r} \sum_{l j I} \left\langle l 0 \frac{1}{2} m_p | j m \right\rangle \langle j m J_b M_b | I \mu \rangle \sqrt{\frac{2l+1}{4\pi}} \sum_{l' j' a} \mathcal{Y}_{(l' \frac{1}{2}) j', J_a}^{I, \mu}(\Omega, \sigma, x) \phi_{[(l' \frac{1}{2}) j', J_a], [(l \frac{1}{2}) j, J_b]}^I(k, r) \quad (3.2.1)$$

and the coupling potential, taken between an initial state $[(l \frac{1}{2}) j, J_b], I \mu\rangle$ and a final state $[(l' \frac{1}{2}) j', J_a], I \mu\rangle$ and integrated over all but radial variables reads:

$$U_{[(l' \frac{1}{2}) j', J_a], [(l \frac{1}{2}) j, J_b]}^{I, ab}(r, r') = \langle [(l' \frac{1}{2}) j', J_a], I \mu | \widehat{V}_{\text{eff}} | [(l \frac{1}{2}) j, J_b], I \mu \rangle \quad (3.2.2)$$

Here, the bra-ket embody the integration over internal coordinates of the target's nucleons and the projectile's, and over angular variables of the relative motion. By applying the Wigner-Eckart theorem (F.0.2) to this formula, we can show that U does not depend on the projection μ of the total angular momentum which is why we do not write this quantum number in the left hand side of equation (3.2.2).

We use the expansion of $P|\Psi\rangle$ in the system \mathcal{S} , then we project the system on one element $[(l' \frac{1}{2}) j', J] I, \mu\rangle$. We use orthogonality relation (2.5.6) to simplify the integrals over angular, spin and internal variables to obtain:

$$\mathcal{S}: \left\{ \begin{array}{l} \left(E + \frac{\hbar^2}{2\mu} \left(\frac{d^2(r.)}{r dr^2} - \frac{l'(l'+1)}{r^2} \right) \right) \varphi_{[(l' \frac{1}{2}) j', J_0], [(l \frac{1}{2}) j', J_0]}^{I, 0}(r) - \sum_{j l} \int U_{[(l' \frac{1}{2}) j', J_0], [(l \frac{1}{2}) j, J_0]}^{I, 00}(r, r') \varphi_{[(l' \frac{1}{2}) j', J_0], [(l \frac{1}{2}) j, J_0]}^{I, 0}(r') r'^2 dr' \\ = \sum_{i \neq 0} \sum_{j l} \int U_{[(l' \frac{1}{2}) j', J_0], [(l \frac{1}{2}) j, J_i]}^{I, 0i}(r, r') \varphi_{[(l' \frac{1}{2}) j', J_0], [(l \frac{1}{2}) j, J_i]}^{I, i}(r') r'^2 dr' \\ \left(E' + \frac{\hbar^2}{2\mu} \left(\frac{d^2(r.)}{r dr^2} - \frac{l'(l'+1)}{r^2} \right) \right) \varphi_{[(l' \frac{1}{2}) j', J_N], [(l \frac{1}{2}) j', J_N]}^{I, N}(r) - \sum_{j l} \int U_{[(l' \frac{1}{2}) j', J_N], [(l \frac{1}{2}) j, J_N]}^{I, NN}(r, r') \varphi_{[(l' \frac{1}{2}) j', J_N], [(l \frac{1}{2}) j, J_N]}^{I, N}(r') r'^2 dr' \\ = \sum_{i \neq N} \sum_{j l} \int U_{[(l' \frac{1}{2}) j', J_N], [(l \frac{1}{2}) j, J_i]}^{I, Ni}(r, r') \varphi_{[(l' \frac{1}{2}) j', J_N], [(l \frac{1}{2}) j, J_i]}^{I, i}(r') r'^2 dr' \end{array} \right.$$

Finally, we multiply the system by r , and use the substitution $\phi(r) = r\varphi(r)$ to get a very general form of coupled channel equations (3.2.3). From this mathematical formulation of

the scattering of a nucleon off a target nucleus, we need to extract relevant physical quantities including the scattering matrix. We present next our way of doing so.

$$\mathcal{S} : \left\{ \begin{aligned} & \left(E + \frac{\hbar^2}{2\mu} \left(\frac{d^2}{dr^2} - \frac{l'(l'+1)}{r^2} \right) \right) \phi_{[(l'\frac{1}{2})j', J_0], [(l\frac{1}{2})j, J_0]}^{I,0}(r) - \sum_{jl} \int U_{[(l'\frac{1}{2})j', J_0], [(l\frac{1}{2})j, J_0]}^{I,00}(r, r') \phi_{[(l'\frac{1}{2})j', J_0], [(l\frac{1}{2})j, J_0]}^{I,0}(r') rr' dr' \\ & = \sum_{i \neq 0} \sum_{jl} \int U_{[(l'\frac{1}{2})j', J_0], [(l\frac{1}{2})j, J_i]}^{I,0i}(r, r') \phi_{[(l'\frac{1}{2})j', J_0], [(l\frac{1}{2})j, J_i]}^{I,i}(r') rr' dr' \\ & \left(E' + \frac{\hbar^2}{2\mu} \left(\frac{d^2}{dr^2} - \frac{l'(l'+1)}{r^2} \right) \right) \phi_{[(l'\frac{1}{2})j', J_N], [(l\frac{1}{2})j', J_N]}^{I,N}(r) - \sum_{jl} \int U_{[(l'\frac{1}{2})j', J_N], [(l\frac{1}{2})j, J_N]}^{I,NN}(r, r') \phi_{[(l'\frac{1}{2})j', J_N], [(l\frac{1}{2})j, J_N]}^{I,N}(r') rr' dr' \\ & = \sum_{i \neq N} \sum_{jl} \int U_{[(l'\frac{1}{2})j', J_N], [(l\frac{1}{2})j, J_i]}^{I, Ni}(r, r') \phi_{[(l'\frac{1}{2})j', J_N], [(l\frac{1}{2})j, J_i]}^{I,i}(r') rr' dr' \end{aligned} \right. \quad (3.2.3)$$

3.3 Solving the system of coupled equations

So far in our derivation, we have written the coupled equations for the ground state $|\psi_0\rangle$ and the excited state $|\psi_N\rangle$. We did not include the equations for the other $|\psi_{i,0 < i < N}\rangle$ states to avoid unnecessary complications. We can further simplify the situation here: we can choose to treat only the ground state with quantum numbers $|J_0 M_0 \Pi_0\rangle$ and one excited state $|\psi_N\rangle$ with quantum numbers $|J_N M_N \Pi_N\rangle$, and consider that the effect of the coupling to the other states is accounted for in the effective interaction. The effect of this hypothesis can be seen now: the sum over i states is reduced to one term: $|\psi_N\rangle$ in the upper equation and $|\psi_0\rangle$ in the bottom equation. The system reads now:

$$\mathcal{S} : \left\{ \begin{aligned} & \left(E + \frac{\hbar^2}{2\mu} \left(\frac{d^2}{dr^2} - \frac{l'(l'+1)}{r^2} \right) \right) \phi_{[(l'\frac{1}{2})j', J_0], [(l\frac{1}{2})j, J_0]}^{I,0}(r) - \sum_{jl} \int U_{[(l'\frac{1}{2})j', J_0], [(l\frac{1}{2})j, J_0]}^{I,00}(r, r') \phi_{[(l'\frac{1}{2})j', J_0], [(l\frac{1}{2})j, J_0]}^{I,0}(r') rr' dr' \\ & = \sum_{jl} \int U_{[(l'\frac{1}{2})j', J_0], [(l\frac{1}{2})j, J_N]}^{I,0N}(r, r') \phi_{[(l'\frac{1}{2})j', J_0], [(l\frac{1}{2})j, J_N]}^{I,N}(r') rr' dr' \\ & \left(E' + \frac{\hbar^2}{2\mu} \left(\frac{d^2}{dr^2} - \frac{l'(l'+1)}{r^2} \right) \right) \phi_{[(l'\frac{1}{2})j', J_N], [(l\frac{1}{2})j', J_N]}^{I,N}(r) - \sum_{jl} \int U_{[(l'\frac{1}{2})j', J_N], [(l\frac{1}{2})j, J_N]}^{I,NN}(r, r') \phi_{[(l'\frac{1}{2})j', J_N], [(l\frac{1}{2})j, J_N]}^{I,N}(r') rr' dr' \\ & = \sum_{jl} \int U_{[(l'\frac{1}{2})j', J_N], [(l\frac{1}{2})j, J_0]}^{I,N0}(r, r') \phi_{[(l'\frac{1}{2})j', J_N], [(l\frac{1}{2})j, J_0]}^{I,0}(r') rr' dr' \end{aligned} \right.$$

We can rewrite this system as:

$$\left\{ \begin{aligned} & D_{l'}(E) \phi_{[(l'\frac{1}{2})j', J_0], [(l\frac{1}{2})j, J_0]}^{I,0}(r) - \sum_{jl} \int U_{[(l'\frac{1}{2})j', J_0], [(l\frac{1}{2})j, J_0]}^{I,00}(r, r') \phi_{[(l'\frac{1}{2})j', J_0], [(l\frac{1}{2})j, J_0]}^{I,0}(r') rr' dr' \\ & = \sum_{jl} \int U_{[(l'\frac{1}{2})j', J_0], [(l\frac{1}{2})j, J_N]}^{I,0N}(r, r') \phi_{[(l'\frac{1}{2})j', J_0], [(l\frac{1}{2})j, J_N]}^{I,N}(r') rr' dr' \\ & D_{l'}(E') \phi_{[(l'\frac{1}{2})j', J_N], [(l\frac{1}{2})j', J_N]}^{I,N}(r) - \sum_{jl} \int U_{[(l'\frac{1}{2})j', J_N], [(l\frac{1}{2})j, J_N]}^{I,NN}(r, r') \phi_{[(l'\frac{1}{2})j', J_N], [(l\frac{1}{2})j, J_N]}^{I,N}(r') rr' dr' \\ & = \sum_{jl} \int U_{[(l'\frac{1}{2})j', J_N], [(l\frac{1}{2})j, J_0]}^{I,N0}(r, r') \phi_{[(l'\frac{1}{2})j', J_N], [(l\frac{1}{2})j, J_0]}^{I,0}(r') rr' dr' \end{aligned} \right.$$

with the differential operator $D_l(E) = E + \frac{\hbar^2}{2\mu} \left(\frac{d^2}{dr^2} - \frac{l(l+1)}{r^2} \right)$. As we said in the previous section, in general the nuclear interaction used to obtain U^{ij} potentials contains a Coulomb term due to the charge distribution of the target nucleus, which can be written (in a local form):

$$U^{ij}(\vec{r}, \vec{r}') = U_{\text{hadronic}}^{ij}(\vec{r}, \vec{r}') + U_{\text{Coulomb}}^{ij}(r) \delta(\vec{r}, \vec{r}') \quad (3.3.1)$$

It is difficult to treat at the same time the hadronic part of the potential, which is a short range contribution, and the Coulomb part which is not a short range contribution. Following a method developed and proposed by Arellano [78], we can rewrite this equation as:

$$\begin{aligned} U^{ij}(\vec{r}, \vec{r}') &= U_{\text{hadronic}}^{ij}(\vec{r}, \vec{r}') + \left(U_{\text{Coulomb}}^{ij}(r) - \frac{ZZ'e^2}{r} \right) \delta(\vec{r}, \vec{r}') + \frac{ZZ'e^2}{r} \delta(\vec{r}, \vec{r}') \\ &= U_{\text{shortrange}}^{ij} + \frac{ZZ'e^2}{r} \delta(\vec{r}, \vec{r}') \end{aligned} \quad (3.3.2)$$

where Z is the target proton number, Z' is the projectile proton number, e is the elementary electric charge. Rewriting things this way, we create a short range equivalent of the charge density dependent Coulomb potential and incorporate it in the hadronic potential. Finally, a simple point (or uniformly charged sphere) Coulomb potential remains to be treated. Given this algebraic transformation, we write the new form of the differential operator:

$$D_l(E) = E + \frac{\hbar^2}{2\mu} \left(\frac{d^2}{dr^2} - \frac{l(l+1)}{r^2} - \frac{ZZ'e^2 2\mu}{r\hbar^2} \right) \quad (3.3.3)$$

The transformation done on the Coulomb potential doesn't change the system \mathcal{S} , which reads in a matrix form:

$$\begin{pmatrix} D(E) & 0 \\ 0 & D(E') \end{pmatrix} \begin{pmatrix} \phi^0 \\ \phi^N \end{pmatrix} = \begin{pmatrix} U^{00} & U^{0N} \\ U^{N0} & U^{NN} \end{pmatrix} \begin{pmatrix} \phi^0 \\ \phi^N \end{pmatrix} \quad (3.3.4)$$

where we used a condensed notation for potentials and wave functions. The solutions of the homogeneous equation are the regular and irregular Coulomb functions F and G (see appendix G) related to the Hankel function H as defined in equation (G.0.3):

$$D \begin{pmatrix} F_l(kr) \\ G_l(kr) \end{pmatrix} = 0 \quad (3.3.5)$$

These Coulomb functions already contain the treatment of the point Coulomb potential. Since the boundary conditions for the wave functions impose their regularity at the origin, the irregular Coulomb function G is eliminated. We can now give a formal solution of the matrix equation in terms of the Coulomb Green's operator \mathcal{G} :

$$\begin{pmatrix} \phi^0 \\ \phi^N \end{pmatrix} = \begin{pmatrix} \frac{F}{k_i} \\ 0 \end{pmatrix} + \begin{pmatrix} \mathcal{G}(k_i) U^{00} & \mathcal{G}(k_i) U^{0N} \\ \mathcal{G}(k_f) U^{N0} & \mathcal{G}(k_f) U^{NN} \end{pmatrix} \begin{pmatrix} \phi^0 \\ \phi^N \end{pmatrix} \quad (3.3.6)$$

This is a Lippman-Schwinger equation with the ground state and one excited state, written in a matrix form. In order to give the explicit form of the Coulomb Green's operator, let us

write the solution radial wave function ϕ^0 for one partial wave:

$$\begin{aligned} \phi_{[(l\frac{1}{2})j, J_0], [(l\frac{1}{2})j, J_0]}^{I,0}(r) &= \frac{F_l(k_i r)}{k_i} + \int g_l(r, r', k_i) \frac{2\mu}{\hbar^2} \sum_{j'l'} \left(\int U_{[(l'\frac{1}{2})j', J_0], [(l\frac{1}{2})j, J_0]}^{I,00}(r', r'') \right. \\ &\quad \left. \phi_{[(l'\frac{1}{2})j', J_0], [(l\frac{1}{2})j, J_0]}^{I,0}(r'') r' r'' dr'' \right) dr' \\ &\quad + \int g_l(r, r', k_i) \frac{2\mu}{\hbar^2} \sum_{j'l'} \left(\int U_{[(l'\frac{1}{2})j', J_0], [(l\frac{1}{2})j, J_i]}^{I,0i}(r', r'') \right. \\ &\quad \left. \phi_{[(l'\frac{1}{2})j', J_0], [(l\frac{1}{2})j, J_i]}^{I,i}(r'') r' r'' dr'' \right) dr' \end{aligned} \quad (3.3.7)$$

with the Coulomb propagator:

$$g(r, r', k) = -\frac{F(kr_{\text{inf}})}{k} (G(kr_{\text{sup}}) + iF(kr_{\text{sup}})) \quad , \quad r_{\text{inf}} = \min(r, r') \quad r_{\text{sup}} = \max(r, r')$$

The solution wave functions can be obtained formally with a matrix inversion:

$$\begin{pmatrix} \phi^0 \\ \phi^N \end{pmatrix} = \left(\mathbf{1} - \begin{pmatrix} \mathcal{G}(k_i) U^{00} & \mathcal{G}(k_i) U^{0N} \\ \mathcal{G}(k_f) U^{N0} & \mathcal{G}(k_f) U^{NN} \end{pmatrix} \right)^{-1} \begin{pmatrix} \frac{F}{k_i} \\ 0 \end{pmatrix} \quad (3.3.8)$$

As we have previously mentioned, the total angular momentum and parity I^π are conserved during the reaction, and we can define one matrix equation for each I^π . Let us do it here in the most general case. First, we must specify the selection rules for partial waves that will couple:

$$\begin{cases} |I^\pi - J_0^{\Pi_0}| \leq j \leq I^\pi + J_0^{\Pi_0} \\ (-)^l * (\Pi_0) = \pi \\ |I^\pi - J_N^{\Pi_N}| \leq j' \leq I^\pi + J_N^{\Pi_N} \\ (-)^{l'} * (\Pi_N) = \pi \end{cases} \Rightarrow \begin{cases} \{j, l\} \subset \left\{ \{j_1, l_1\}, \{j_2, l_2\}, \dots, \{j_f, l_f\} \right\} \\ \{j', l'\} \subset \left\{ \{j'_1, l'_1\}, \{j'_2, l'_2\}, \dots, \{j'_f, l'_f\} \right\} \end{cases} \quad (3.3.9)$$

then we write the system for one given I^π (see next page for the matrix equation) and solve it, which provides the radial wave functions. Finally we can calculate the scattering matrix thanks to the formula (2.5.16) and therefore obtain the scattering amplitude of equation (2.5.14). In order to obtain a converged value of the scattering amplitude, we will have to solve the matrix equation for enough values of I^π , so that we can use the scattering amplitude to evaluate the angular dependent differential cross section of equation (2.5.15).

Now, let us summarize some features associated with this method: it requires two integrations due to the Coulomb Green propagator and the resolution of a large matrix equation per value of I^π , but allows us to solve coupled channel equations describing elastic and inelastic scattering of a nucleon off a target nucleus using nonlocal potentials. With the help of our collaborator Arellano, we have written a calculation code - ECANOL - that follows the aforementioned computing procedure and that evaluates scattering observables with nonlocal potentials as input. We describe this code in details in section 5. In parallel, we have also developed a code that calculates the various potentials needed as input for ECANOL, with a microscopic approach using the Melbourne G matrix effective interaction. In the following section, we derive formulae of the microscopic potentials that we need to compute and give as input to ECANOL.

$$\begin{pmatrix} \phi_{j_1, l_1}^{I,0} \\ \dots \\ \phi_{j_f, l_f}^{I,0} \\ \phi_{j'_1, l'_1}^{I,N} \\ \dots \\ \phi_{j'_f, l'_f}^{I,N} \end{pmatrix} = \mathbb{1} - \left(\begin{pmatrix} \mathcal{G}_{l_1}(k_i) U_{[(l_1 \frac{1}{2})j_1, J_0], [(l_1 \frac{1}{2})j_1, J_0]}^{I,00} & \dots & \mathcal{G}_{l_1}(k_i) U_{[(l_1 \frac{1}{2})j_1, J_0], [(l_f \frac{1}{2})j_f, J_0]}^{I,00} & \mathcal{G}_{l_1}(k_i) U_{[(l_1 \frac{1}{2})j_1, J_0], [(l'_1 \frac{1}{2})j'_1, J_N]}^{I,0N} & \dots & \mathcal{G}_{l_1}(k_i) U_{[(l_1 \frac{1}{2})j_1, J_0], [(l'_f \frac{1}{2})j'_f, J_N]}^{I,0N} \\ \dots & \dots & \dots & \dots & \dots & \dots \\ \mathcal{G}_{l_f}(k_i) U_{[(l_f \frac{1}{2})j_f, J_0], [(l_1 \frac{1}{2})j_1, J_0]}^{I,00} & \dots & \mathcal{G}_{l_f}(k_i) U_{[(l_f \frac{1}{2})j_f, J_0], [(l_f \frac{1}{2})j_f, J_0]}^{I,00} & \mathcal{G}_{l_f}(k_i) U_{[(l_f \frac{1}{2})j_f, J_0], [(l'_1 \frac{1}{2})j'_1, J_N]}^{I,0N} & \dots & \mathcal{G}_{l_f}(k_i) U_{[(l_f \frac{1}{2})j_f, J_0], [(l'_f \frac{1}{2})j'_f, J_N]}^{I,0N} \\ \mathcal{G}_{l'_1}(k_f) U_{[(l'_1 \frac{1}{2})j'_1, J_N], [(l_1 \frac{1}{2})j_1, J_0]}^{I,N0} & \dots & \mathcal{G}_{l'_1}(k_i) U_{[(l'_1 \frac{1}{2})j'_1, J_N], [(l_f \frac{1}{2})j_f, J_0]}^{I,N0} & \mathcal{G}_{l'_1}(k_i) U_{[(l'_1 \frac{1}{2})j'_1, J_N], [(l'_1 \frac{1}{2})j'_1, J_N]}^{I,NN} & \dots & \mathcal{G}_{l'_1}(k_i) U_{[(l'_1 \frac{1}{2})j'_1, J_N], [(l'_f \frac{1}{2})j'_f, J_N]}^{I,NN} \\ \dots & \dots & \dots & \dots & \dots & \dots \\ \mathcal{G}_{l'_f}(k_f) U_{[(l'_f \frac{1}{2})j'_f, J_N], [(l_1 \frac{1}{2})j_1, J_0]}^{I,N0} & \dots & \mathcal{G}_{l'_f}(k_f) U_{[(l'_f \frac{1}{2})j'_f, J_N], [(l_f \frac{1}{2})j_f, J_0]}^{I,N0} & \mathcal{G}_{l'_f}(k_f) U_{[(l'_f \frac{1}{2})j'_f, J_N], [(l'_1 \frac{1}{2})j'_1, J_N]}^{I,NN} & \dots & \mathcal{G}_{l'_f}(k_f) U_{[(l'_f \frac{1}{2})j'_f, J_N], [(l'_f \frac{1}{2})j'_f, J_N]}^{I,NN} \end{pmatrix} \right)^{-1} \begin{pmatrix} \frac{F_{l_1}^0}{k_i} \\ \dots \\ \frac{F_{l_f}^0}{k_i} \\ 0 \\ \dots \\ 0 \end{pmatrix}$$

Chapter 4

Derivation of microscopic potentials

One main objective of this work is to develop tools that allow for a study of different aspects of nucleon-nucleus direct reactions, implying microscopic potentials and the CC framework. In the introduction of this work, we mentioned and briefly discussed some methods that exist to compute potentials: phenomenology, *ab initio*, nuclear structure method, nuclear matter approach. We have chosen to use a description of the 2-body effective interaction between the projectile and a nucleon of the target obtained with the nuclear matter approach. Since we want to be able to study nucleon-nucleus scattering for a large variety of targets up to actinides, a mean field and beyond description of the target's structure seems reasonable. The G-matrix folding approach with the Melbourne G matrix as NN effective interaction and a HF + RPA description of the target was used successfully in the study of nucleon scattering off medium and heavy mass nuclei [23, 64, 79], which demonstrates the pertinence of the approach for such kind of targets.

In the present section, we describe how a potential can be computed using a 2-body interaction. We then give some features of the Melbourne G matrix, and we remind briefly some important results of the RPA. Finally, we derive general formulae for microscopic potentials obtained from the folding of any 2-body effective interaction and any structure description. We also show a comparison between our calculation of the optical potential obtained by folding the Melbourne G matrix with the RPA ground state of ^{208}Pb , and the optical potential computed (using the same ingredients) by the DWBA98 code, which makes an excellent basis for validations. Before we start, we would like to draw the reader's attention on the fact that these derivations are quite technical, despite our best efforts to simplify them. The most important formulae are framed, while the derivation process and important steps are described and discussed so that reproducibility is easily achievable, as well as extending the computation to other approaches like the nuclear structure method. We give first some notations we will use throughout the rest of this paper.

4.1 Notations

We denote one given state of the target nucleus with the simplified notation:

$$|\psi_N \in n_N J_N M_N \Pi_N\rangle = |J_N M_N\rangle \quad (4.1.1)$$

A single particle state that is above the Fermi level (a particle state) is labeled p , and it is labeled h if it lies under the Fermi level (a hole state). The single particle wave functions

that are solution of a spherical mean field are written (following the coupling scheme of equation (2.5.1) as:

$$\varphi_{\alpha \equiv n_{\alpha} j_{\alpha} l_{\alpha} m_{\alpha}}(\vec{r}, \sigma) = i^{l_{\alpha}} \phi_{n_{\alpha} j_{\alpha} l_{\alpha}}(r) \left[Y_{m_{\alpha}}^{l_{\alpha}}(\Omega) \otimes \chi_{\frac{1}{2} m_s}^{\frac{1}{2}}(\sigma) \right]_{m_{\alpha}}^{j_{\alpha}} \quad (4.1.2)$$

in which we did not write the isospin dependence, and where $\phi_{n_{\alpha} j_{\alpha} l_{\alpha}}(r)$ is real. The matrix elements of a 1-body density operator will be written:

$$\rho_{\alpha\beta}^{N_i \rightarrow N_f} = \langle J_f M_f | a_{\alpha}^{\dagger} a_{\beta} | J_i M_i \rangle \quad (4.1.3)$$

An operator that creates a pair $1\alpha-1\beta$ coupled to a total spin J and projection M will be written:

$$A_{JM}^{\dagger}(\alpha, \beta) = [a_{\alpha}^{\dagger} \otimes a_{\beta}]_M^J = \sum_{m_{\alpha} m_{\beta}} (-)^{j_{\beta} - m_{\beta}} \langle j_{\alpha} m_{\alpha} j_{\beta} - m_{\beta} | JM \rangle a_{\alpha}^{\dagger} a_{\beta} \quad (4.1.4)$$

The matrix elements of a 1-body density matrix coupled to J and M read:

$$\rho_{\alpha\beta}^{N_i \rightarrow N_f, JM} = \langle J_f M_f | A_{JM}^{\dagger}(\alpha, \beta) | J_i M_i \rangle \quad (4.1.5)$$

Following the definition of Talmi [80] reminded in appendix F, the reduced matrix elements of a coupled 1-body density matrix will be written:

$$\rho_{\alpha\beta}^{N_i \rightarrow N_f, J} = \frac{\langle J_f M_f | A_{JM}^{\dagger}(\alpha, \beta) | J_i M_i \rangle}{\langle J_i M_i JM | J_f M_f \rangle \widehat{J}_f^{-1}} \quad (4.1.6)$$

4.2 1-body potential from a 2-body interaction

In our derivations of the system \mathcal{S} , we have introduced potentials with various subscripts representing the couplings involved in the calculation of each potential. These labels are quite general and don't depend on the method chosen to compute potentials. Here, we write explicitly the various couplings in a way that the resulting potentials to calculate can be obtained from various approaches, whether they are microscopic or not. In the most general case, potentials we need to calculate contain the physics that connect an initial state $|J_i M_i\rangle$ to a final state $|J_f M_f\rangle$ and their associated partial waves (in our choice of spherical basis). So first, we need to specify the couplings involving the total angular momentum and parity I^{π} of the system {projectile;target} and the initial and final states. By doing so, we will relieve the potential of its dependence on I^{π} :

$$\begin{aligned} U_{[(l' \frac{1}{2}) j', J_f], [(l \frac{1}{2}) j, J_i]}^{I, f i}(r, r') &= \left\langle [(l' \frac{1}{2}) j', J_f] I^{\pi}, \mu \left| \widehat{V}_{\text{eff}} \right| [(l \frac{1}{2}) j, J_i] I^{\pi}, \mu \right\rangle \\ &= \sum_{m M_f m' M_i} \langle j' m' J_f M_f | I \mu \rangle \langle j m J_i M_i | I \mu \rangle \langle j' m', J_f M_f | \widehat{V}_{\text{eff}} | j m, J_i M_i \rangle \\ &= \sum_{\substack{m M_N \\ m' M_i}} \langle j' m' J_f M_f | I \mu \rangle \langle j m J_i M_i | I \mu \rangle \langle j' m' | \langle J_f M_f | \widehat{V}_{\text{eff}} | J_i M_i \rangle | j m \rangle \end{aligned} \quad (4.2.1)$$

Here, we have uncoupled the potential from the total angular momentum I , and thus we don't have to consider these quantum numbers in further derivations. We have written the

last line of the equation in a way that helps the reader distinguish the various elements and steps of the calculation: the first step consists of defining \widehat{V}_{eff} , the effective operator. Then, to compute matrix elements as $\langle J_f M_f | \widehat{V}_{\text{eff}} | J_i M_i \rangle$, we need a model to describe internal states of the target. In chapter 3, we projected the potential on our basis of choice, in this work we have chosen the radial coordinates and we separated radial and angular variables. So first, let us describe \widehat{V}_{eff} . We derived in chapter 2 its general expression (2.3.5) in the Feshbach formalism but this form not suitable for practical calculations. In our case, we use an effective interaction which is a 2-body force acting between the projectile and one nucleon of the target in the nuclear medium. In second quantization, this reads:

$$\begin{aligned} \widehat{V}_{\text{eff}} &= \sum_{kk'\alpha\beta} \langle k'\alpha | V_{\text{eff}} | \widetilde{k\beta} \rangle a_{k'}^\dagger a_k a_\alpha^\dagger a_\beta = \sum_{kk'\alpha\beta} \left(\langle k'\alpha | V_{\text{eff}} | k\beta \rangle a_{k'}^\dagger a_k a_\alpha^\dagger a_\beta - \langle k'\alpha | V_{\text{eff}} | \beta k \rangle a_{k'}^\dagger a_k a_\alpha^\dagger a_\beta \right) \\ &= \widehat{V}_{\text{eff,direct}} + \widehat{V}_{\text{eff,exchange}} \end{aligned} \quad (4.2.2)$$

In this form, k represents the incident particle, β a nucleon of the target before interacting with the projectile, V_{eff} is the in-medium 2-body effective interaction between the projectile and one nucleon of the target, k' labels the ejectile, and α the target's nucleon after the interaction. $|\widetilde{k\beta}\rangle$ means $|k\beta\rangle - |\beta k\rangle$, a^\dagger is a creation operator and a its associated annihilator. We have separated the potential into a direct and an exchange term, that comes from antisymmetrization. In section 3.1, we identified the potentials that enter in the definition of the CC equations as the matrix elements of the effective interaction \widehat{V}_{eff} between two states of the target nucleus as $U^{ab} = \langle \psi_a | \widehat{V}_{\text{eff}} | \psi_b \rangle$. Note that \widehat{V}_{eff} as defined in (4.2.2) is a one body operator in the space of the target wave functions. Using the separation between the direct and the exchange terms, we can display the nonlocality of the potential that is due to the Pauli exclusion principle mentioned in the introduction 1.4. We do this with the ansatz of a local, finite range, spin independent 2-body interaction. In this case, the direct term reads:

$$\widehat{V}_{\text{eff,direct}} = \sum_{kk'\alpha\beta} \langle k'\alpha | V_{\text{eff}} | k\beta \rangle a_{k'}^\dagger a_k a_\alpha^\dagger a_\beta \quad (4.2.3)$$

We use the condensed notation $\vec{x} = \{\vec{r}, \sigma\}$ to describe the space and spin coordinates of a single particle state (the isospin dependence is treated in chapter 5). We insert closure relations on 2-particle wave functions in the matrix element of (4.2.3):

$$\begin{aligned} \widehat{V}_{\text{eff,direct}} &= \sum_{kk'\alpha\beta} a_\alpha^\dagger a_\beta \iint \langle k' | \vec{x}_1 \rangle \langle \alpha | \vec{x}_2 \rangle \langle \vec{x}_1, \vec{x}_2 | V_{\text{eff}} | \vec{x}_1, \vec{x}_2 \rangle \langle \vec{x}_1 | k \rangle \langle \vec{x}_2 | \beta \rangle a_{k'}^\dagger a_k d\vec{x}_1 d\vec{x}_2 \\ \Leftrightarrow \widehat{V}_{\text{eff,direct}} &= \sum_{\alpha\beta} a_\alpha^\dagger a_\beta \int \varphi_\alpha^*(\vec{x}_2) \left(\int \sum_{kk'} a_{k'}^\dagger \varphi_{k'}^*(\vec{x}_1) V_{\text{eff}}(\vec{x}_1, \vec{x}_2) a_k \varphi_k(\vec{x}_1) d\vec{x}_1 \right) \varphi_\beta(\vec{x}_2) d\vec{x}_2 \end{aligned}$$

Here, we have used $\langle \vec{x}_1 \vec{x}_2 | V_{\text{eff}} | \vec{x}_3 \vec{x}_4 \rangle = \langle \vec{x}_1 \vec{x}_2 | V_{\text{eff}} | \vec{x}_3 \vec{x}_4 \rangle \delta(\vec{x}_1 - \vec{x}_3) \delta(\vec{x}_2 - \vec{x}_4)$ in agreement with our initial ansatz of a finite range, local, spin independent interaction. Using the expansions $\Psi(\vec{x}) = \sum_k a_k \varphi_k(\vec{x})$ and $\Psi^\dagger(\vec{x}) = \sum_{k'} a_{k'}^\dagger \varphi_{k'}^*(\vec{x})$ we insert creation and annihilation operators that depend on \vec{x} coordinates and we simplify the equation:

$$\widehat{V}_{\text{eff,direct}} = \sum_{\alpha\beta} a_\alpha^\dagger a_\beta \iint \varphi_\alpha^*(\vec{x}_2) \Psi_{k'}^\dagger(\vec{x}_1) V_{\text{eff}}(\vec{x}_1, \vec{x}_2) \Psi_k(\vec{x}_1) \varphi_\beta(\vec{x}_2) d\vec{x}_1 d\vec{x}_2 \quad (4.2.4)$$

The same exact procedure can be followed for $\widehat{V}_{\text{eff,exchange}}$:

$$\begin{aligned}
 \widehat{V}_{\text{eff,exchange}} &= \sum_{kk'\alpha\beta} a_\alpha^\dagger a_\beta \iint \langle k' | \vec{x}_1 \rangle \langle \alpha | \vec{x}_2 \rangle \langle \vec{x}_1, \vec{x}_2 | V_{\text{eff}} | \vec{x}_1, \vec{x}_2 \rangle \langle \vec{x}_1 | \beta \rangle \langle \vec{x}_2 | k \rangle a_k^\dagger a_k d\vec{x}_1 d\vec{x}_2 \\
 \Leftrightarrow \widehat{V}_{\text{eff,exchange}} &= \sum_{\alpha\beta} a_\alpha^\dagger a_\beta \iint \sum_{kk'} \varphi_\alpha^*(\vec{x}_2) a_{k'}^\dagger \varphi_{k'}^*(\vec{x}_1) V_{\text{eff}}(\vec{x}_1, \vec{x}_2) a_k \varphi_k(\vec{x}_2) \varphi_\beta(\vec{x}_1) d\vec{x}_1 d\vec{x}_2 \\
 \Leftrightarrow \widehat{V}_{\text{eff,exchange}} &= \sum_{\alpha\beta} a_\alpha^\dagger a_\beta \iint \varphi_\alpha^*(\vec{x}_2) \Psi_{k'}^\dagger(\vec{x}_1) V_{\text{eff}}(\vec{x}_1, \vec{x}_2) \Psi_k(\vec{x}_2) \varphi_\beta(\vec{x}_1) d\vec{x}_1 d\vec{x}_2 \quad (4.2.5)
 \end{aligned}$$

Now, we project equations (4.2.4) and (4.2.5) on states $\langle \vec{r}, \sigma |$ and $|\vec{r}', \sigma'\rangle$ to obtain:

$$\langle \vec{r}, \sigma | \widehat{V}_{\text{eff,direct}} | \vec{r}', \sigma' \rangle = \sum_{\alpha\beta} a_\alpha^\dagger a_\beta \delta(\vec{r} - \vec{r}') \delta_{\sigma\sigma'} \int \varphi_\alpha^*(\vec{r}_2, \sigma_2) V_{\text{eff}}(\vec{r}, \sigma, \vec{r}_2, \sigma_2) \varphi_\beta(\vec{r}_2, \sigma_2) d\vec{r}_2 d\sigma_2 \quad (4.2.6)$$

$$\langle \vec{r}, \sigma | \widehat{V}_{\text{eff,exchange}} | \vec{r}', \sigma' \rangle = \sum_{\alpha\beta} a_\alpha^\dagger a_\beta \varphi_\alpha^*(\vec{r}', \sigma') V_{\text{eff}}(\vec{r}, \sigma, \vec{r}', \sigma') \varphi_\beta(\vec{r}, \sigma) \quad (4.2.7)$$

We saw in equation (4.2.1) that the potentials needed in the coupled equations correspond to matrix elements of (4.2.6) and (4.2.7) between two target states. If we choose an initial state $|J_i M_i\rangle$ and a final state $|J_f M_f\rangle$, then the contraction reads:

$$\boxed{
 \langle J_f M_f | \langle \vec{r}, \sigma | \widehat{V}_{\text{eff}} | \vec{r}', \sigma' \rangle | J_i M_i \rangle = \sum_{\alpha\beta} \rho_{\alpha\beta}^{N_i \rightarrow N_f} \left[\delta(\vec{r} - \vec{r}') \delta_{\sigma\sigma'} \int \varphi_\alpha^*(\vec{r}_2, \sigma_2) V_{\text{eff}}(\vec{r}, \sigma, \vec{r}_2, \sigma_2) \varphi_\beta(\vec{r}_2, \sigma_2) d\vec{r}_2 d\sigma_2 - \varphi_\alpha^*(\vec{r}', \sigma') V_{\text{eff}}(\vec{r}, \sigma, \vec{r}', \sigma') \varphi_\beta(\vec{r}, \sigma) \right] \quad (4.2.8)$$

in which $\rho_{\alpha\beta}^{N_i \rightarrow N_f}$ defined in (4.1.3) is the nuclear structure input we need for our calculations. So we see with this derivation that the potential ends as a sum of a local term (usually called the direct - or Hartree - term) and a nonlocal term (usually called exchange - or Fock - term). We can add that if we had considered a contact (0-range) interaction, the Fock term would be local as well. On the contrary, if we had chosen a nonlocal 2-body interaction, the simplification in equation (4.2.4) wouldn't have been valid any longer, and the Hartree term would have been nonlocal as well. To finish, the second source of nonlocality mentioned in section 1.4 is here contained in the energy dependence of V_{eff} , which is explicit in equation (2.3.5).

With these definitions, it is now time to describe the effective NN interaction and the microscopic description of the target's structure that we have chosen.

4.3 The Melbourne G matrix

The choice of NN effective interaction V_{eff} is a very important element in microscopic approaches. There are different categories of NN effective interactions, that were designed to study (in principle) particular phenomena: interactions obtained from Energy and Density Functional Theories (EDFT) like the various Skyrme forces and the Gogny forces were

designed mostly to reproduce nuclear structure properties such as nuclear radii and saturation properties. However, we would like to mention that it has been demonstrated that such kind of interaction can also be applied successfully to the study of nucleon-nucleus elastic scattering [43–46].

Other approaches are based on the derivation of a NN effective interaction from the free NN interaction. These interactions are fitted so as to reproduce the results of nucleon-nucleon scattering experiments and are well suited for studying nucleon-nucleus scattering. We have chosen to use a NN effective interaction, the Melbourne G matrix, obtained with such a method. The entire derivation of this interaction is a long and tedious work that is already well documented in [37]. Therefore, here we will only give a quick overview of the process that helps us link the interaction to fundamental aspects of the Feshbach formalism depicted in chapter 3.

First, let us take a look at equation (2.3.5): in this equation, the free NN interaction V is not known exactly. Many of its features are known though, like its strong repulsive core. Groups of scientists have formulated functional forms (with parameters) of approximate free NN interactions that reproduce these features. They fitted the parameters of these forces so as to reproduce deuteron properties and the results of nucleon-nucleon scattering experiments at various energy ranges and obtained, in the end, good parameterizations of the real free NN interaction in a wide range of energies. Some famous examples of parameterized free NN forces are Argonne V18 [81], the Nijmegen potential [82], the CD-Bonn force [83] and so on. But the problem with equation (2.3.5) is that, as long as the free NN interaction you use has a strong repulsive core, the development in series of equation (2.3.5) diverges. This issue can be tackled by reordering the terms of the sum, as was done by Watson [50]. Using Watson's multiple scattering theory, Brueckner [84], Bethe [85] and Goldstone [86] studied the many-body problem starting from the free NN interaction and it led to the definition of the so-called G matrix, solution of the Bethe-Goldstone equation:

$$G_{ij} = V_{ij} + \frac{Q}{E - H_0} G_{ij} \quad , \quad H_0 = \sum_{j=1}^A T_j + U_j \quad (4.3.1)$$

i labels the incident nucleon and j a nucleon of the target. Q is an operator that projects the system out of its ground state, the Hamiltonian H_0 is the sum of the kinetic energy of the j^{th} nucleon and U_j the mean field acting on it. Generalizing this equation to the case of nucleon scattering is done by considering an unbound nucleon. Boundary conditions are then inserted in the propagator as $+i\epsilon$. If we expand the propagator on eigenstates of H_0 , then the G matrix reads:

$$G(E) = V(E) + V(E) \sum_{a,b > K_F} \frac{V|a,b\rangle \langle a,b|G(E)}{E - e(a) - e(b) + i\epsilon} \quad (4.3.2)$$

where $|a\rangle$ and $|b\rangle$ are single particle states with their associated energies $e(a)$ and $e(b)$. K_F is the Fermi momentum, E the energy of the incident nucleon. The solutions of this equation satisfy the dispersion relation given in [87]. The action of the Q operator, which projects the system out of its ground state, is embodied by the condition $a, b > K_F$. Indeed, all single particle states with momentum lower than the Fermi momentum are considered occupied in the ground state, therefore only states with a momentum bigger than K_F are accessible to the

projectile (Q acts as a Pauli blocking operator). This dependence on the Fermi momentum can be directly translated into a nuclear density dependence due to the equation:

$$\rho_{K_F} = \frac{2}{3\pi^2} K_F^3 \quad (4.3.3)$$

Thus, the G matrix should be both energy and density dependent. In infinite nuclear matter, its computation is much more tractable than in finite nuclei, since eigenvectors $|a\rangle$ and $|b\rangle$ are simply plane waves. But if one wants to use the G matrix obtained in infinite nuclear matter for calculations in finite nuclei, there is an ambiguity on how to define the nuclear density at which the G matrix should be evaluated. One way to deal with this problem is to assume that regions where nucleons interact can be considered locally as behaving like infinite nuclear matter. This hypothesis is known as the Local Density Approximation (LDA). It is within this framework that the Melbourne G matrix was derived, with some particular features that should be mentioned. This interaction was computed from the Bonn-B free NN interaction [88], which was computed for incident nucleons with kinetic energy below the pion threshold (< 250 MeV). The Bonn-B force is a sum of a central, 2-body spin orbit, tensor and higher order terms, and the Melbourne G matrix conserves the central, spin orbit and tensor terms in its structure. It is a local, finite range interaction, parameterized in radial coordinates as a linear combination of Yukawa form factors. Furthermore, since the G matrix is density dependent, the practical version of it we have available to use is given on a density mesh [89]. Last, because of the localization procedure, the Melbourne G matrix does not rigorously satisfy the dispersion relation [87].

At this point, it is important to give a few details regarding the LDA. The Melbourne G matrix is a local finite range interaction; it has a simple dependence on the nuclear density. But since it is a 2-body force, it involves two particles that are not necessarily at the same density. This can be seen formally in equation (4.2.8): the density at position \vec{r} and at position \vec{r}' is not necessarily the same. So, there is an ambiguity regarding the choice of density at which the interaction should be computed. We can tackle this issue by considering that the approximate density should be that at the halfway between particles $\rho(\frac{\vec{r}+\vec{r}'}{2})$, or by taking an average of the densities. In the derivation of the Melbourne G matrix reported in [37], the geometric average $\sqrt{\rho(\vec{r})\rho(\vec{r}')}$ was used. We have included in our code the possibility to use also the arithmetic average $\frac{\rho(\vec{r})+\rho(\vec{r}')}{2}$. In summary, the Melbourne G matrix is a local finite range interaction parameterized as a sum of Yukawa form factors:

$$G(\vec{r}, \vec{r}', \rho, E) = \sum_j G_j(\rho, E) \frac{e^{-\frac{|\vec{r}-\vec{r}'|}{\mu_j}}}{|\vec{r}-\vec{r}'|} \quad (4.3.4)$$

with μ_j denoting the range of the interaction, and where the energy and density dependent amplitudes $G_j(\rho, E)$ are complex. This G matrix can be written as:

$$\begin{aligned} G(\vec{r}, \vec{r}', \rho, E) = & \sum_{S,T=0,1} G_{cent}^{ST}(\vec{r}, \vec{r}', \rho, E) P^S P^T \\ & + \sum_{T=0,1} G_{so}^T(\vec{r}, \vec{r}', \rho, E) \vec{L}_{12} \cdot \vec{S} P^T \\ & + \sum_{T=0,1} G_{tens}^T(\vec{r}, \vec{r}', \rho, E) S_{12} P^T \end{aligned} \quad (4.3.5)$$

with projection operators defined by:

$$\begin{aligned}
 P^{S=0} &= \frac{1 - P_\sigma}{2} & P^{S=1} &= \frac{1 + P_\sigma}{2} & P^{T=0} &= \frac{1 - P_\tau}{2} & P^{T=1} &= \frac{1 + P_\tau}{2} \\
 P_\sigma &= \frac{1 + \vec{\sigma}_1 \cdot \vec{\sigma}_2}{2} & P_\tau &= \frac{1 + \vec{\tau}_1 \cdot \vec{\tau}_2}{2}
 \end{aligned}$$

and 2-body spin-orbit and tensor operators expressed as:

$$\begin{aligned}
 \vec{L}_{12} \cdot \vec{S} &= (\vec{r}_1 - \vec{r}_2) \times (\vec{\nabla}_1 - \vec{\nabla}_2) \cdot (\vec{s}_1 - \vec{s}_2) \\
 S_{12} &= 3(\vec{\sigma}_1 \cdot (\vec{r}_1 - \vec{r}_2))(\vec{\sigma}_2 \cdot (\vec{r}_1 - \vec{r}_2)) - (\vec{r}_1 - \vec{r}_2)^2 \cdot (\vec{\sigma}_1 \cdot \vec{\sigma}_2)
 \end{aligned} \tag{4.3.6}$$

where particles 1 and 2 are labeled by their number. Details on the calculation of matrix elements for each operator of the Melbourne G matrix are given in appendix D. Now that we have defined the NN effective interaction of our choice, we must specify the ingredients used to obtain nuclear densities for the folding.

4.4 Microscopic description of the target nucleus

The second ingredient of the nuclear matter approach to compute microscopic potentials is the description of the target's structure. We can see explicitly where it intervenes in equation (4.2.8): single particle wave functions φ_i and the one body density ρ . Various microscopic technics exist to calculate structure elements, depending on properties of the target nucleus of interest. The first applications of the tools we develop will be for ^{208}Pb , a doubly closed shell spherical nucleus. A good description of this kind of nuclei can be achieved by using the RPA. We will not give here a derivation of RPA equations, it has been done thoroughly elsewhere [27, 90]. Instead, we will remind some basic concepts of the Hartree-Fock and RPA theories that we use in our calculations, and write down the most important formulae for our needs.

4.4.1 Hartree-Fock description of the structure of a nucleus

The HF description of a nucleus relies on a series of simple assumptions that constrain the form of a solution wave function [91, 92]. The first hypothesis is the assumption of particles moving independently in a mean field. The 1-body potential felt by one nucleon is that generated by the other $A - 1$ nucleons. Nucleons being fermions, the HF total wave function is a Slater determinant. In second quantization, it reads:

$$|\psi\rangle = \prod_{i=1}^A a_i^\dagger |-\rangle \tag{4.4.1}$$

$|-\rangle$ is the void of particles, a_i^\dagger is the operator creating a fermion in state i and a_i annihilates it. These two operators follow anti-commutation rules:

$$\{a_i^\dagger, a_j\} = \delta_{ij} \quad , \quad \{a_i^\dagger, a_j^\dagger\} = 0 \quad , \quad \{a_i, a_j\} = 0 \tag{4.4.2}$$

The HF method aims at computing the optimized set of single particle wave functions so that the independent particle representation of equation (4.4.1) reproduces best the properties

of the system in its ground state. The system follows the Schrödinger equation with an effective Hamiltonian of the form (in second quantization):

$$H = \sum_{\alpha\beta} T_{\alpha\beta} a_{\alpha}^{\dagger} a_{\beta} + \frac{1}{4} \sum_{\alpha\beta\gamma\delta}^N \left(\langle \alpha\beta | V(\rho) | \gamma\delta \rangle - \langle \alpha\beta | V(\rho) | \delta\gamma \rangle \right) a_{\alpha}^{\dagger} a_{\beta}^{\dagger} a_{\delta} a_{\gamma} \quad (4.4.3)$$

with T the kinetic operator and V the in-medium effective interaction between two nucleons. The accuracy of the HF method relies very much on the effective interaction, and in our case this interaction is the Gogny D1S force [93].

The HF ground state is obtained by minimizing the energy of the system given by:

$$\delta \frac{\langle \psi_{HF} | H | \psi_{HF} \rangle}{\langle \psi_{HF} | \psi_{HF} \rangle} = 0 \quad (4.4.4)$$

where $|\psi_{HF}\rangle$ is the HF ground state. Details on the resolution of this equation can be found in [94]. For our needs, we write down the matrix elements of the 1-body density operator obtained with the Hartree-Fock method:

$$\rho_{\alpha\beta}^{GS \rightarrow GS} = \langle \psi_{HF} | a_{\alpha}^{\dagger} a_{\beta} | \psi_{HF} \rangle = \delta_{\alpha\beta} \delta_{\beta h} \quad (4.4.5)$$

where h labels a hole state. Thus, the HF wave function for the ground state reads:

$$|\psi_{HF}\rangle = \prod_{h=1}^{h_{Fermi}} a_h^{\dagger} |-\rangle \quad (4.4.6)$$

with h_{Fermi} the last hole state before the Fermi energy.

4.4.2 Generalities on the Random Phase Approximation for nuclear structure

With an adequate NN effective interaction, the HF theory is able to describe rather well some properties of doubly closed shell nuclei in their ground state, but fails to describe excited states. In particular, we would like to be able to describe low energy, collective states and giant resonances. Such excitations can be described by the RPA, which we can obtain with the following reasoning: the density computed with the HF method contains correlations between holes $1h1h'$ and describes only the system in its ground state. From this starting point, one can apply a small perturbation to this density. The simplest excitation one can build is the promotion of a nucleon “ h ” below the Fermi energy (a hole state) to an orbit above it “ p ” (a particle state). A mixing of these $1p1h$ configurations is what constitutes the Tamm-Dandoff approximation for collective states. But one can also consider a correlated ground state $|\psi_0\rangle$ which differs from $|\psi_{HF}\rangle$ and which contains multiple particle-hole components. In such case, the simplest possible excitation corresponds to a particle-hole creation or annihilation on this correlated ground state. The notion of correlation is here understood as those beyond the mean-field HF approximation. Some of these correlations (often labeled as “long range” correlations) can be incorporated within the RPA framework. Formal derivations associated to this reasoning can be found in textbooks and references [27, 90]. Let us give here important definitions and formulae of the RPA that will be useful for our calculations.

Let $|\psi_0\rangle$ denote the void of phonon, describing the ground state of the nucleus. We define Θ_N^\dagger the operator that creates a phonon labeled $|\psi_N\rangle$. We associate to the creation operator its adjoint operator Θ_N that annihilates the vibrational mode N . Formally, these definitions read:

$$|\psi_N\rangle = \Theta_N^\dagger |\psi_0\rangle \quad , \quad \langle \psi_N | \Theta_N = \langle \psi_0 | \quad , \quad \langle \psi_0 | \Theta_N^\dagger = 0 \quad , \quad \Theta_N |\psi_0\rangle = 0 \quad (4.4.7)$$

and in terms of amplitudes $X_{ph}^N = \langle \psi_N | a_p^\dagger a_h | \psi_0 \rangle$ and $Y_{ph}^N = \langle \psi_N | a_h^\dagger a_p | \psi_0 \rangle$, which are probability amplitudes to find, within the state $|\psi_N\rangle$, a particle-hole pair excitation on the ground state $|\psi_0\rangle$, we can write Θ_N^\dagger (and its adjoint operator) as a linear combination of particle-hole pairs creation and annihilation operators:

$$\begin{aligned} \Theta_N^\dagger &= \sum_{ph} X_{ph}^N a_p^\dagger a_h - Y_{ph}^N a_h^\dagger a_p \\ \Theta_N &= \sum_{ph} X_{ph}^{N*} a_h^\dagger a_p - Y_{ph}^{N*} a_p^\dagger a_h \end{aligned} \quad (4.4.8)$$

4.4.3 RPA states in spherical symmetry

In spherical symmetry, we associate to the 1-phonon states quantum numbers: total spin J_N , spin projection M_N , parity Π_N and energy $E_N = \hbar\omega_N$, with ω_N the frequency of the phonon. The phonon state can be written as $|\psi_N \in E_N J_N M_N \Pi_N\rangle$. The single particle wave functions that are solution of a spherical mean field are given in equation (4.1.2). In our convention, the time-reversal operator applied to $|\varphi_\alpha\rangle$ yields:

$$T|\varphi_\alpha\rangle = T|n_\alpha(l_\alpha \frac{1}{2})j_\alpha m_\alpha\rangle = (-)^{j_\alpha - m_\alpha} |n_\alpha(l_\alpha \frac{1}{2})j_\alpha - m_\alpha\rangle \quad (4.4.9)$$

It is possible to define an operator that creates a pair $1p$ - $1h$ with a given total angular momentum J and projection M that we write as:

$$A_{J,M}^\dagger(p, h) = \sum_{m_p m_h} (-)^{j_h - m_h} \langle j_p m_p j_h - m_h | JM \rangle a_p^\dagger a_h \quad (4.4.10)$$

where p and h label respectively $|\varphi_p\rangle$ and $|\varphi_h\rangle$. The adjoint operator that annihilates such a pair reads:

$$A_{J,M}(p, h) = \sum_{m_p m_h} (-)^{j_h - m_h} \langle j_p m_p j_h - m_h | JM \rangle a_h^\dagger a_p \quad (4.4.11)$$

Using the time-reversal operator, we can write:

$$T^\dagger A_{J,M}(p, h) T = (-)^{J-M} A_{J,-M}(p, h) = A_{J,\overline{M}}(p, h) \quad (4.4.12)$$

and we can inverse the two previous equations to obtain:

$$a_p^\dagger a_h = \sum_{JM} (-)^{j_h - m_h} \langle j_p m_p j_h - m_h | JM \rangle A_{J,M}^\dagger(p, h) \quad (4.4.13)$$

$$a_h^\dagger a_p = \sum_{JM} (-)^{J+j_h-j_p} (-)^{j_p - m_p} \langle j_p m_p j_h - m_h | J - M \rangle A_{J,\overline{M}}(p, h) \quad (4.4.14)$$

Then, using some simple Racah Algebra, we can write this operator as:

$$\begin{aligned} A_{J,\overline{M}}(p, h) &= (-)^{J-M} \sum_{m_p m_h} (-)^{j_h - m_h} \langle j_p m_p j_h - m_h | J - M \rangle a_h^\dagger a_p \\ &= (-)^{J+j_h-j_p} A_{J,M}^\dagger(h, p) \end{aligned} \quad (4.4.15)$$

and consequently, a $1\alpha-1\beta$ creation-annihilation operator can be written as:

$$a_\alpha^\dagger a_\beta = \sum_{JM} (-)^{j_\beta - m_\beta} \langle j_\alpha m_\alpha j_\beta - m_\beta | JM \rangle A_{J,M}^\dagger(\alpha, \beta), \quad \{\alpha, \beta\} = \{p, h\} \text{ or } \{h, p\} \quad (4.4.16)$$

We can use these definitions to write the phonon creation and annihilation operators in a coupled form:

$$\begin{aligned} \Theta_N^\dagger &= \sum_{ph \in (J_N, M_N, \Pi_N)} X_{ph}^N A_{J,M}^\dagger(p, h) - Y_{hp}^N A_{J,\overline{M}}(p, h) \\ \Theta_N &= \sum_{ph \in (J_N, M_N, \Pi_N)} X_{ph}^N A_{J,M}(p, h) - Y_{hp}^N A_{J,\overline{M}}^\dagger(p, h) \end{aligned} \quad (4.4.17)$$

where N stands now for E_N, J_N, M_N , and Π_N . We notice here that it is possible to define a probability amplitude $Z_{\alpha\beta}^N$ associated to finding a pair $1\alpha-1\beta$, without assuming if α is a particle or a hole:

$$\begin{aligned} Z_{ph}^N &= X_{ph}^N \\ Z_{hp}^N &= (-)^{J+j_p-j_h} Y_{ph}^N \end{aligned} \quad (4.4.18)$$

and we can use the new labels to rewrite the formula of the phonon creation/annihilation operators:

$$\begin{aligned} \Theta_N^\dagger &= \sum_{ph \in (J_N, M_N, \Pi_N)} Z_{ph}^N A_{J,M}^\dagger(p, h) - Z_{hp}^N A_{J,M}^\dagger(h, p) \\ \Theta_N &= \sum_{ph \in (J_N, M_N, \Pi_N)} Z_{ph}^N A_{J,M}(p, h) - Z_{hp}^N A_{J,M}(h, p) \end{aligned} \quad (4.4.19)$$

These very important formulae can be inverted so that we can express an operator like $A_{J,M}^\dagger(p, h)$ as a linear combination of 1-phonon creation and annihilation operators. And equation (4.4.10) can also be inverted so that we can write a formula for $a_\alpha^\dagger a_\beta$:

$$\boxed{a_\alpha^\dagger a_\beta = \sum_{JM} (-)^{j_\beta - m_\beta} \langle j_\alpha m_\alpha j_\beta - m_\beta | JM \rangle \sum_N Z_{\alpha\beta}^N \Theta_N^\dagger + Z_{\beta\alpha}^N \Theta_N, \quad \{\alpha, \beta\} = \{p, h\} \text{ or } \{h, p\}} \quad (4.4.20)$$

4.4.4 Matrix elements of 1-body density matrices

The formulae we presented can be used to evaluate the matrix elements of 1-body density matrices. The derivations done within the Quasi-Boson Approximation (QBA) for the ground state density matrix as well as the transition density coupling the ground state to a 1-phonon excited state can be found in [95] and [23], while a discussion on the impact of the QBA is given in chapter 6. We give here the results, first for the ground state:

$$\left\{ \begin{array}{l} \rho_{pp'}^{\tilde{0} \rightarrow \tilde{0}} = \langle \psi_{\tilde{0}} | a_p^\dagger a_{p'} | \psi_{\tilde{0}} \rangle = \sum_{N,h,j_h} Y_{ph}^N Y_{ph'}^N + \Delta \rho_{pp'} \\ \rho_{hh'}^{\tilde{0} \rightarrow \tilde{0}} = \langle \psi_{\tilde{0}} | a_h^\dagger a_{h'} | \psi_{\tilde{0}} \rangle = (2j_h + 1) \delta_{hh'} - \sum_{N,p,j_p} Y_{ph}^N Y_{ph'}^N + \Delta \rho_{hh'} \\ \rho_{ph}^{\tilde{0} \rightarrow \tilde{0}} = \langle \psi_{\tilde{0}} | a_p^\dagger a_h | \psi_{\tilde{0}} \rangle = 0 \\ \rho_{hp}^{\tilde{0} \rightarrow \tilde{0}} = \langle \psi_{\tilde{0}} | a_h^\dagger a_p | \psi_{\tilde{0}} \rangle = 0 \end{array} \right. \quad (4.4.21)$$

in which $\Delta \rho_{\alpha\alpha'}$ is a correction due to double counting when using the QBA, and that is derived in [96]. It is worth to note that for $\rho_{pp'}^{\tilde{0} \rightarrow \tilde{0}}$ we also have the conditions $j_p = j_{p'}$ and $m_p = m_{p'}$ (and similarly for $\rho_{hh'}^{\tilde{0} \rightarrow \tilde{0}}$). The transition density from the ground state to an excited state N reads:

$$\left\{ \begin{array}{l} \rho_{pp'}^{\tilde{0} \rightarrow N} = \langle \psi_N | a_p^\dagger a_{p'} | \psi_{\tilde{0}} \rangle = 0 \\ \rho_{hh'}^{\tilde{0} \rightarrow N} = \langle \psi_N | a_h^\dagger a_{h'} | \psi_{\tilde{0}} \rangle = 0 \\ \rho_{\alpha\beta}^{\tilde{0} \rightarrow N, J=J_N, M=M_N} = \langle \psi_N | a_\alpha^\dagger a_\beta | \psi_{\tilde{0}} \rangle = \langle j_\alpha m_\alpha j_\beta - m_\beta | JM \rangle (-)^{j_\beta - m_\beta} Z_{\alpha\beta}^N, \alpha\beta = ph \text{ or } hp \end{array} \right. \quad (4.4.22)$$

and finally, we give here the matrix elements of the coupled 1-body density matrix defined in (4.1.5) for a 0^+ ground state:

$$\rho_{\alpha\beta}^{0 \rightarrow 0,00} = \frac{1}{J_\beta} \rho_{\alpha\beta}^{0 \rightarrow 0} \quad (4.4.23)$$

with the notation $\hat{x} = \sqrt{2x+1}$ that we will use henceforth. It is interesting to note here that when the ground state has a spin and parity 0^+ , the reduced matrix elements of the 1-body density matrix of equation (4.1.6) is equal to the matrix elements themselves:

$$\rho_{\alpha\beta}^{0 \rightarrow 0,00} = \rho_{\alpha\beta}^{0 \rightarrow 0,0} \quad (4.4.24)$$

These formulae can be inserted in equation (4.2.8) to derive a microscopic optical potential (using the ground state density matrix elements) and microscopic transition potentials from the ground state to an excited state made of 1 phonon. But we can go even further, and consider an excited state made of 2 phonons coupled together. Let us denote by $|\psi_{N_3}\rangle$ an excited state made of the combination of one phonon $|\psi_{N_1}\rangle$ and another $|\psi_{N_2}\rangle$. This reads:

$$|\psi_{N_3}\rangle = n \left[\Theta_{N_2}^\dagger \otimes \Theta_{N_1}^\dagger \right]_{M_3}^{J_3} |\psi_{\tilde{0}}\rangle \quad (4.4.25)$$

with n a normalization factor, J_3 the total angular momentum of the 2-phonon state, M_3 its projection on the quantization axis. The normalization factor was calculated elsewhere [95], and by definition of the tensor product we can write the 2-phonon states as:

$$|\psi_{N_3}\rangle = \frac{1}{\sqrt{1 + \delta_{N_1 N_2}}} \sum_{M_1 M_2} \langle J_2 M_2 J_1 M_1 | J_3 M_3 \rangle \Theta_{N_2}^\dagger \Theta_{N_1}^\dagger |\psi_{\tilde{0}}\rangle \quad (4.4.26)$$

with the condition that J_3 must be even if $N_1 = N_2$. In order to derive formulae for transitions from the ground state (or from a 1-phonon excited state) to a 2-phonon excited state, we remind here that the quasi-boson approximation leads to:

$$[\Theta_{N_1}^\dagger, \Theta_{N_2}] = \delta_{N_1 N_2} \quad , \quad [\Theta_{N_1}^\dagger, \Theta_{N_2}^\dagger] = [\Theta_{N_1}, \Theta_{N_2}] = 0 \quad (4.4.27)$$

Formulae for matrix elements coupling the ground state to the 2-phonon excitation have been derived in reference [95], let us remind them here:

$$\left\{ \begin{array}{l} \rho_{pp'}^{\tilde{0} \rightarrow N_3, J_3 M_3} = -\frac{1}{\sqrt{1 + \delta_{N_1 N_2}}} \widehat{J}_1 \widehat{J}_2 (-)^{j_p - j_h} \sum_h \left((-)^{J_1} X_{ph}^{N_1} Y_{p'h}^{N_2} \left\{ \begin{array}{ccc} J_1 & J_2 & J_3 \\ j_{p'} & j_p & j_h \end{array} \right\} + \right. \\ \left. (-)^{J_2} X_{ph}^{N_2} Y_{p'h}^{N_1} \left\{ \begin{array}{ccc} J_2 & J_1 & J_3 \\ j_{p'} & j_p & j_h \end{array} \right\} \right) \\ \rho_{hh'}^{\tilde{0} \rightarrow N_3, J_3 M_3} = \frac{1}{\sqrt{1 + \delta_{N_1 N_2}}} \widehat{J}_1 \widehat{J}_2 (-)^{j_p - j_{h'}} \sum_p \left((-)^{J_2} X_{ph'}^{N_1} Y_{ph}^{N_2} \left\{ \begin{array}{ccc} J_1 & J_2 & J_3 \\ j_{h'} & j_h & j_p \end{array} \right\} + \right. \\ \left. (-)^{J_1} X_{ph'}^{N_2} Y_{ph}^{N_1} \left\{ \begin{array}{ccc} J_2 & J_1 & J_3 \\ j_{h'} & j_h & j_p \end{array} \right\} \right) \\ \rho_{ph}^{\tilde{0} \rightarrow N_3, J_3 M_3} = \rho_{hp}^{\tilde{0} \rightarrow N_3, J_3 M_3} = 0 \end{array} \right. \quad (4.4.28)$$

Next, we present the procedure to derive matrix elements for transitions from a 1-phonon state to a 2-phonon one, using the QBA. The 1-body transition density matrix between the initial one phonon state $|\psi_{N_1}\rangle$ and the final 2-phonon state $|\psi_{N_3}\rangle$ is:

$$\rho_{\alpha\beta}^{N_1 \rightarrow N_3, J, M} = \langle \psi_{N_3} | A_{JM}^\dagger(\alpha, \beta) | \psi_{N_1} \rangle \quad (4.4.29)$$

and the reduced 1-body transition density matrix elements by:

$$\rho_{\alpha\beta}^{N_1 \rightarrow N_3, J} = \frac{\langle \psi_{N_3} | A_{JM}^\dagger(\alpha, \beta) | \psi_{N_1} \rangle}{\langle J_1 M_1 J M | J_3 M_3 \rangle \widehat{J}_3^{-1}} \quad (4.4.30)$$

Given the definition of equation (4.4.26), we can develop the reduced transition density to:

$$\rho_{\alpha\beta}^{N_1 \rightarrow N_3, J} = \frac{1}{\sqrt{1 + \delta_{N_1 N_2}}} \sum \frac{\langle J_1 M'_1 J_2 M_2 | J_3 M_3 \rangle \langle \psi_{\tilde{0}} | \Theta_{N'_1} \Theta_{N_2} A_{JM}^\dagger(\alpha, \beta) \Theta_{N_1}^\dagger | \psi_{\tilde{0}} \rangle}{\langle J_1 M_1 J M | J_3 M_3 \rangle \widehat{J}_3^{-1}} \quad (4.4.31)$$

in which $\Theta_{N'_1}$ is the phonon annihilation operator of the state $|\psi_{N'_1} \in E_{N_1} J_{N_1} M'_{N_1} \Pi_{N_1}\rangle$, which is the $|\psi_{N_1}\rangle$ state but with another orientation of its total spin, and where the sum runs over M'_1 and M_2 . Cases in which $\alpha, \beta = p, p'$ and h, h' vanish when using the QBA. Using the reverse form of equation (4.4.15) and combining it with equations (4.4.20) and (4.4.27), we can show that if $\psi_{N_1} \neq \psi_{N_2}$:

$$\langle \psi_{\tilde{0}} | \Theta_{N'_1} \Theta_{N_2} A_{JM}^\dagger(\alpha, \beta) \Theta_{N_1}^\dagger | \psi_{\tilde{0}} \rangle = \delta_{J_2 J} \delta_{M_2 M} \delta_{M'_1 M_1} Z_{\alpha\beta}^{N_1} \quad (4.4.32)$$

And of course, we can derive similarly an equation for the case when $\psi_{N_1} = \psi_{N_2}$. Finally, we sum up our derivations and give the formula for the reduced transition density matrix elements between a 1-phonon excited state $|\psi_{N_1}\rangle$ and a 2-phonon excited state $|\psi_{N_3}\rangle = |[\psi_{N_1} \otimes \psi_{N_2}]_{M_3}^{J_3}\rangle$:

$$\left\{ \begin{array}{l} \rho_{\alpha\beta}^{N_1 \rightarrow N_3, J} = \frac{\langle \psi_{\tilde{0}} | [\Theta_{N_2} \otimes \Theta_{N_1}]_{M_3}^{J_3} A_{JM}^\dagger(\alpha, \beta) \Theta_{N_1}^\dagger | \psi_{\tilde{0}} \rangle}{\langle J_1 M_1 J M | J_3 M_3 \rangle \widehat{J}_3^{-1}} = \delta_{J_2 J} \widehat{J}_3 Z_{\alpha\beta}^{N_2}, \quad N_2 \neq N_1, \alpha\beta = ph \text{ or } hp \\ \rho_{\alpha\beta}^{N_1 \rightarrow N_3, J} = \frac{\langle \psi_{\tilde{0}} | [\Theta_{N_1} \otimes \Theta_{N_1}]_{M_3}^{J_3} A_{JM}^\dagger(\alpha, \beta) \Theta_{N_1}^\dagger | \psi_{\tilde{0}} \rangle}{\langle J_1 M_1 J M | J_3 M_3 \rangle \widehat{J}_3^{-1}} = \sqrt{2} \delta_{J_1 J} \widehat{J}_3 Z_{\alpha\beta}^{N_1}, \quad (-)^{J_3} = 1, \alpha\beta = ph \text{ or } hp \\ \rho_{pp'}^{N_1 \rightarrow N_3, J} = \rho_{hh'}^{N_1 \rightarrow N_3, J} = 0 \end{array} \right. \quad (4.4.33)$$

It is worth to remind, as we used equation (4.4.27) to obtain this result, that this comes from the fact that we use the QBA. Using this approximation can lead to a strong violation of the Pauli exclusion principle when using these 2-phonon states.

Now, let us summarize the situation a bit: we have derived formula (4.2.8) which is the general form of a microscopic potential computed from an effective, 2-body, finite range interaction. We have given the most important features of the effective NN interaction we have chosen to use for our study. And we have briefly presented microscopic theories we have chosen to use to derive nuclear structure information. Furthermore, we have given the form of the effective NN interaction and of the nuclear structure input to use in equation (4.2.8). Now, we can combine all these ingredients and derive formulae for microscopic potentials. As a first, simple step, we will derive the optical potential for a nucleus with a 0^+ ground state.

4.5 Formula for the optical potential with a 0^+ ground state

We do not specify the target nucleus, but we impose that its ground state is a 0^+ . We start our derivation from equation (4.2.1). In this equation, the potential is coupled to total angular momentum and parity I^π . The first step we need to do to compute it is to uncouple relevant quantum numbers. In the case of the optical potential with a $|\psi_0 \in J_0 M_0 \Pi_0\rangle = |00+\rangle$ ground state, the uncoupling (done by the use of Clebsch-Gordan coefficients) reads:

$$\begin{aligned} U_{[(l'\frac{1}{2})j',0],[(l\frac{1}{2})j,0]}^{I,00}(r,r') &= \left\langle [(l'\frac{1}{2})j',0]I^\pi, \mu \left| \widehat{V}_{\text{eff}} \right| [(l\frac{1}{2})j,0]I^\pi, \mu \right\rangle \\ &= \sum_{mm'} \langle j'm'00|I\mu\rangle \langle jm00|I\mu\rangle \langle j'm'|\langle\psi_0|\widehat{V}_{\text{eff}}|\psi_0\rangle|jm\rangle \\ &= \langle jm|\langle\psi_0|\widehat{V}_{\text{eff}}|\psi_0\rangle|jm\rangle \delta_{Ij} \delta_{Ij'} \delta_{m\mu} \end{aligned}$$

in which we use simplifications given in appendix (A.0.4). The condition $l = l'$ comes from the fact that \widehat{V}_{eff} conserves the parity, and that in the entrance channel the parity of the partial wave is $(-)^l$, and also that we have $\delta_{Ij} \delta_{Ij'}$. In the following, we will write the radial part of the optical potential as $U_{[(l\frac{1}{2})j,0],[(l\frac{1}{2})j,0]}^{j,00}(r,r')$, and we will denote the ground state as $|\psi_0\rangle$ without writing down all its quantum numbers. The second step is to introduce nuclear structure ingredients: the matrix elements of the 1-body density.

$$\begin{aligned} \langle\psi_0|\langle\vec{r},\sigma|\widehat{V}_{\text{eff}}|\vec{r}',\sigma'\rangle|\psi_0\rangle &= \sum_{\alpha\alpha'} \rho_{\alpha\alpha'}^{0\rightarrow 0} \left[\delta(\vec{r}-\vec{r}') \delta_{\sigma\sigma'} \int \varphi_\alpha^*(\vec{r}_2, \sigma_2) V_{\text{eff}}(\vec{r}, \sigma, \vec{r}_2, \sigma_2) \right. \\ &\quad \left. \varphi_{\alpha'}(\vec{r}_2, \sigma_2) d\vec{r}_2 d\sigma_2 \right. \\ &\quad \left. - \varphi_\alpha^*(\vec{r}', \sigma') V_{\text{eff}}(\vec{r}, \sigma, \vec{r}', \sigma') \varphi_{\alpha'}(\vec{r}, \sigma) \right] \end{aligned} \quad (4.5.1)$$

where $\varphi_\alpha(\vec{r}, \sigma)$ is defined by equation (4.1.2) and the sum over $\alpha\alpha'$ runs over all quantum numbers of these states. Now, in order to shorten a bit equations to be derived, we will treat separately the direct term and the exchange term.

The third step is to project the previous equation on the spin-angular functions basis (2.5.3). The finite range NN effective interaction needs also to be expanded in multipoles (as

presented in appendix C) to ease the computation of its matrix elements when it is projected on the spin-angular functions basis. We begin with the direct term:

$$\langle jm|\langle\psi_0|\widehat{V}_{\text{eff}}|\psi_0\rangle|jm\rangle_{\text{direct}} = \sum_{k\alpha\alpha'} i^{l+l'_\alpha-l_\alpha-l} \rho_{\alpha\alpha'}^{0\rightarrow 0} (jj_\alpha|V_{\text{eff}}^k|jj'_\alpha) \frac{\delta(r-r')}{rr'} \int \phi_\alpha(r_2) V_{\text{eff}}^k(r, r_2) \phi_{\alpha'}(r_2) r_2^2 dr_2$$

in which $\phi_\alpha = \phi_{n_\alpha j_\alpha l_\alpha}$ is the real function as defined in (4.1.2), and where $(jj_\alpha|V_{\text{eff}}|jj'_\alpha)$ is a shortened notation for $((l_\alpha \frac{1}{2})jm, (l_\alpha \frac{1}{2})j_\alpha m_\alpha|V_{\text{eff}}|(l'_\alpha \frac{1}{2})jm', (l'_\alpha \frac{1}{2})j'_\alpha m'_\alpha)$ the angular integrated matrix element that we can calculate with the Racah algebra. Now for the exchange term:

$$\langle jm|\langle\psi_0|\widehat{V}_{\text{eff}}|\psi_0\rangle|jm\rangle_{\text{exchange}} = \sum_{k\alpha\alpha'} i^{l'+l-l_\alpha-l} \rho_{\alpha\alpha'}^{0\rightarrow 0} (jj_\alpha|V_{\text{eff}}^k|j_\alpha'j) \phi_\alpha(r') V_{\text{eff}}^k(r, r') \phi_{\alpha'}(r)$$

For a 0^+ ground state as mentioned in the previous subsection, we have the condition $j_\alpha = j_{\alpha'}$ and $m_\alpha = m_{\alpha'}$ and we can use henceforth the reduced matrix elements:

$$\langle jm|\langle\psi_0|\widehat{V}_{\text{eff}}|\psi_0\rangle|jm\rangle_{\text{direct}} = \sum_{\substack{kn_\alpha n_{\alpha'} \\ j_\alpha l_\alpha m_\alpha}} i^{l+l_\alpha-l_\alpha-l} \frac{\rho_{\alpha\alpha'}^{0\rightarrow 0,0}}{\widehat{j}_\alpha} (jj_\alpha|V_{\text{eff}}^k|jj_\alpha) \frac{\delta(r-r')}{rr'} \int \phi_{n_\alpha j_\alpha l_\alpha}(r_2) V_{\text{eff}}^k(r, r_2) \phi_{n_{\alpha'} j_\alpha l_\alpha}(r_2) r_2^2 dr_2 \quad (4.5.2)$$

$$\langle jm|\langle\psi_0|\widehat{V}_{\text{eff}}|\psi_0\rangle|jm\rangle_{\text{exchange}} = \sum_{\substack{kn_\alpha n_{\alpha'} \\ j_\alpha l_\alpha m_\alpha}} i^{l'+l-l_\alpha-l} \frac{\rho_{\alpha\alpha'}^{0\rightarrow 0,0}}{\widehat{j}_\alpha} (jj_\alpha|V_{\text{eff}}^k|j_\alpha j) \phi_{n_\alpha j_\alpha l_\alpha}(r') V_{\text{eff}}^k(r, r') \phi_{n_{\alpha'} j_\alpha l_\alpha}(r) \quad (4.5.3)$$

In principle, it is possible to evaluate numerically the optical potential by using the two previous equations. But it will be much easier to evaluate geometric matrix elements of the interaction if we couple partial wave quantum number j with j_α to a total J' :

$$|jj_\alpha\rangle = \sum_{J'M'} \langle jm j_\alpha m_\alpha | J'M' \rangle |j j_\alpha J'M'\rangle$$

Using the Wigner-Eckart theorem (F.0.2), it is possible to show that matrix elements such as $(j j_\alpha J'M'|V_{\text{eff}}^k|j' j'_\alpha J'M')$ do not depend on the total spin projection M' , and we use this property to simplify our labeling of these matrix elements to $(j j_\alpha J'|V_{\text{eff}}^k|j' j'_\alpha J')$ in the rest of this paper. Formulae for these matrix elements are available in Appendix D for an interaction containing the operators of equation (4.3.5). Let us show the recoupling procedure here for the direct term:

$$\begin{aligned} \sum_{m_\alpha} (jj_\alpha|V_{\text{eff}}^k|jj_\alpha) &= \sum_{J'M'm_\alpha} \langle jm j_\alpha m_\alpha | J'M' \rangle \langle jm j_\alpha m_\alpha | J'M' \rangle (jj_\alpha J'|V_{\text{eff}}^k|jj_\alpha J') \\ &= \sum_{J'M'm_\alpha} \widehat{J}'^2 \begin{pmatrix} j & j_\alpha & J' \\ m & m_\alpha & -M' \end{pmatrix}^2 (jj_\alpha J'|V_{\text{eff}}^k|jj_\alpha J') \\ &= \sum_{J'} \frac{\widehat{J}'^2}{\widehat{j}^2} (jj_\alpha J'|V_{\text{eff}}^k|jj_\alpha J') \end{aligned}$$

Following the same procedure for the exchange term yields:

$$\begin{aligned}
 \sum_{m_\alpha} \langle j j_\alpha | V_{\text{eff}}^k | j_\alpha' j \rangle &= \sum_{J' M' m_\alpha} \langle j m j_\alpha m_\alpha | J' M' \rangle \langle j_\alpha m_\alpha j m | J' M' \rangle (j j_\alpha J' | V_{\text{eff}}^k | j_\alpha' j J') \\
 &= \sum_{J' M' m_\alpha} (-)^{j_\alpha' + j + J'} \langle j m j_\alpha m_\alpha | J' M' \rangle \langle j m j_\alpha m_\alpha | J' M' \rangle (j j_\alpha J' | V_{\text{eff}}^k | j_\alpha' j J') \\
 &= \sum_{J'} (-)^{j_\alpha' + j + J'} \frac{\widehat{J}'^2}{\widehat{j}^2} (j j_\alpha J' | V_{\text{eff}}^k | j_\alpha' j J')
 \end{aligned}$$

The recoupling to J' has considerably simplified the formula for the optical potential, which we can now summarize:

$$\begin{aligned}
 U_{[(l\frac{1}{2})j,0],[(l\frac{1}{2})j,0]}^{I,00}(r,r')_{\text{direct}} &= \sum_{\substack{kn_\alpha n_{\alpha'} \\ j_\alpha l_\alpha J'}} \frac{\widehat{J}'^2}{\widehat{j}^2 \widehat{j}_\alpha} \rho_{\alpha\alpha'}^{0 \rightarrow 0,0} (j j_\alpha J' | V_{\text{eff}}^k | j j_\alpha J') \frac{\delta(r-r')}{r r'} \int \phi_{n_\alpha j_\alpha l_\alpha}(r_2) V_{\text{eff}}^k(r, r_2) \\
 &\quad \phi_{n_{\alpha'} j_\alpha l_\alpha}(r_2) r_2^2 dr_2 \\
 U_{[(l\frac{1}{2})j,0],[(l\frac{1}{2})j,0]}^{I,00}(r,r')_{\text{exchange}} &= \sum_{\substack{kn_\alpha n_{\alpha'} \\ j_\alpha l_\alpha J'}} \frac{\widehat{J}'^2}{\widehat{j}^2 \widehat{j}_\alpha} \rho_{\alpha\alpha'}^{0 \rightarrow 0,0} (-)^{j_\alpha' + j + J'} (j j_\alpha J' | V_{\text{eff}}^k | j_\alpha' j J') \phi_{n_\alpha j_\alpha l_\alpha}(r') V_{\text{eff}}^k(r, r') \\
 &\quad \phi_{n_{\alpha'} j_\alpha l_\alpha}(r)
 \end{aligned} \tag{4.5.4}$$

The computation of the optical potential using this formula and results given in Appendix D is now possible and straightforward.

The derivation of formulae for the optical potential, in the case of a nucleus with a 0^+ ground state like ^{208}Pb is rather simple in a spherical basis thanks to the simplifications of the Clebsch-Gordan coefficients, but the situation is more complicated if we consider the more general case of equation (4.2.1): instead of coupling a 0^+ ground state with itself, we need to couple an initial state $|N_i \in J_i \Pi_i M_i\rangle$ to a final state $|N_f \in J_f \Pi_f M_f\rangle$, and more work on the geometric coefficients is involved.

4.6 Coupling potential in a spherical basis: formulae for the most general case

We begin the derivation by focusing on equation (4.2.1). This equation is the most general formulation of a coupling potential between an initial and a final state within the framework of CC equations we derived in the previous section. But this general formula needs to be recast in order to find simplifications. In terms of 3j coefficients, this equation reads:

$$\begin{aligned}
 U_{[(l'\frac{1}{2})j',J_f],[(l\frac{1}{2})j,J_i]}^{I,f_i}(r,r') &= \left\langle [(l'\frac{1}{2})j', J_f] I^\pi, \mu \left| \widehat{V}_{\text{eff}} \right| [(l\frac{1}{2})j, J_i] I^\pi, \mu \right\rangle \\
 &= \sum_{\substack{m M_f \\ m' M_i}} \langle j' m' J_f M_f | I \mu \rangle \langle j m J_i M_i | I \mu \rangle \langle j' m' | \langle J_f M_f | \widehat{V}_{\text{eff}} | J_i M_i \rangle | j m \rangle \\
 &= \sum_{\substack{m M_f \\ m' M_i}} (-)^{j' + j - J_i - J_f + 2\mu} \widehat{I}^2 \begin{pmatrix} j' & J_f & I \\ m' & M_f & -\mu \end{pmatrix} \begin{pmatrix} j & J_i & I \\ m & M_i & -\mu \end{pmatrix} \\
 &\quad \langle j' m' | \langle J_f M_f | \widehat{V}_{\text{eff}} | J_i M_i \rangle | j m \rangle
 \end{aligned} \tag{4.6.1}$$

We need to compute $\langle j' m' | \langle J_f M_f | \widehat{V}_{\text{eff}} | J_i M_i \rangle | j m \rangle$. We will do so by starting from equation (4.2.8) and by defining the reduced 1-body transition density matrix elements.

4.6.1 Direct term

We denote the nuclear states with the labeling defined in (4.1.1). The direct part of equation (4.2.8) reads:

$$\langle J_f M_f | \langle \vec{r}, \sigma | \widehat{V}_{\text{eff}} | \vec{r}', \sigma' \rangle_{\text{direct}} | J_i M_i \rangle = \sum_{\alpha\beta} \langle J_f M_f | a_\alpha^\dagger a_\beta | J_i M_i \rangle \delta(\vec{r} - \vec{r}') \delta_{\sigma\sigma'} \\ \int \varphi_\alpha^*(\vec{r}_2, \sigma_2) V_{\text{eff}}(\vec{r}, \sigma, \vec{r}_2, \sigma_2) \varphi_\beta(\vec{r}_2, \sigma_2) d\vec{r}_2 d\sigma_2$$

by projecting this equation on a the generalized spherical harmonics basis of equation (2.5.3), we obtain:

$$\langle j' m' | \langle J_f M_f | \widehat{V}_{\text{eff}} | J_i M_i \rangle | j m \rangle_{\text{direct}} = \sum_{\alpha\beta k} \langle J_f M_f | a_\alpha^\dagger a_\beta | J_i M_i \rangle i^{l_\beta - l_\alpha + l - l'} (j' j_\alpha | V_{\text{eff}}^k | j j_\beta) \frac{\delta(r - r')}{r r'} \\ \int \phi_\alpha(r_2) V_{\text{eff}}^k(r, r_2) \phi_\beta(r_2) r_2^2 dr_2$$

Now, we transform the tensor operator $a_\alpha^\dagger a_\beta$ into a product of irreducible spherical tensors using equations (4.1.5) and (4.4.10), which yields:

$$\langle j' m' | \langle J_f M_f | \widehat{V}_{\text{eff}} | J_i M_i \rangle | j m \rangle_{\text{direct}} = \sum_{\alpha\beta k} \langle J_f M_f | A_{JM}^\dagger(\alpha, \beta) | J_i M_i \rangle i^{l_\beta - l_\alpha + l - l'} (-)^{j_\beta - m_\beta} \\ \sum_{JM} \langle j_\alpha m_\alpha j_\beta - m_\beta | JM \rangle (j' j_\alpha | V_{\text{eff}}^k | j j_\beta) \\ \frac{\delta(r - r')}{r r'} \int \phi_\alpha(r_2) V_{\text{eff}}^k(r, r_2) \phi_\beta(r_2) r_2^2 dr_2 \quad (4.6.2)$$

By doing this preliminary work, we extracted a geometric coefficient from the transition density. Now, like we did in the previous subsection, we will couple j' and j_α to a total J' , and the coefficient we just extracted will help us in simplifying the resulting formula. The recoupling reads (we write only geometric terms):

$$\sum_{m_\alpha m_\beta} (-)^{j_\beta - m_\beta} \langle j_\alpha m_\alpha j_\beta - m_\beta | JM \rangle (j' j_\alpha | V_{\text{eff}}^k | j j_\beta) \\ = \sum_{\substack{m_\alpha m_\beta \\ J' M'}} \langle j_\alpha m_\alpha j_\beta - m_\beta | JM \rangle (-)^{j_\beta - m_\beta} \langle j' m' j_\alpha m_\alpha | J' M' \rangle \langle j m j_\beta m_\beta | J' M' \rangle (j' j_\alpha J' | V_{\text{eff}}^k | j j_\beta J') \\ = \sum_{\substack{m_\alpha m_\beta \\ J' M'}} (-)^{j' + j - j_\beta + M + 2M' - m_\beta} \widehat{J} \widehat{J}'^2 \begin{pmatrix} j_\alpha & j_\beta & J \\ m_\alpha & -m_\beta & -M \end{pmatrix} \begin{pmatrix} J' & j_\alpha & j' \\ M' & -m_\alpha & -m' \end{pmatrix} \begin{pmatrix} j_\beta & J' & j \\ m_\beta & -M' & m \end{pmatrix} \\ (j' j_\alpha J' | V_{\text{eff}}^k | j j_\beta J') \\ = \sum_{\substack{m_\alpha m_\beta \\ J' M'}} (-)^{j_\alpha + j_\beta + J' + m_\alpha + m_\beta + M'} \begin{pmatrix} j_\alpha & j_\beta & J \\ m_\alpha & -m_\beta & -M \end{pmatrix} \begin{pmatrix} J' & j_\alpha & j' \\ M' & -m_\alpha & -m' \end{pmatrix} \begin{pmatrix} j_\beta & J' & j \\ m_\beta & -M' & m \end{pmatrix} \widehat{J} \widehat{J}'^2 \\ (-)^{j' + j - j_\alpha - 2j_\beta - J' + M + M' - m_\alpha - 2m_\beta} (j' j_\alpha J' | V_{\text{eff}}^k | j j_\beta J')$$

We have a sum in which a phase is multiplied by a product of three Wigner 3J coefficients, followed by remaining terms among which the second phase reduces to $(-)^{j' + j - j_\alpha - J' + M + m'}$. Thus, the remaining terms do not depend on m_α , m_β or M' . Therefore, we can proceed with the summing over these three variables, and use (A.0.13) to simplify the formula to:

$$\sum_{m_\alpha m_\beta} (-)^{j_\beta - m_\beta} \langle j_\alpha m_\alpha j_\beta - m_\beta | JM \rangle (j' j_\alpha | V_{\text{eff}}^k | j j_\beta) = \sum_{J'} (-)^{j' + j - j_\alpha - J' + m} \widehat{J} \widehat{J}'^2 \begin{pmatrix} j & j' & J \\ m & -m' & -M \end{pmatrix} \\ \left\{ \begin{matrix} j & j' & J \\ j_\alpha & j_\beta & J' \end{matrix} \right\} (j j_\alpha J' | V_{\text{eff}}^k | j' j_\beta J') \quad (4.6.3)$$

Now, we need to inverse the signs of the projections in the new Wigner 3J symbols for later factorization, and we can insert (4.6.3) in (4.6.2) and therefore give a complete formula of

the direct term of the coupling potential between the initial state $|J_i M_i\rangle$ and the final state $|J_f M_f\rangle$:

$$\begin{aligned} \langle j' m' | \langle J_f M_f | \widehat{V}_{\text{eff}} | J_i M_i \rangle | j m \rangle_{\text{direct}} = & \sum_{\substack{\bar{\alpha}\bar{\beta}k \\ J'JM}} \langle J_f M_f | A_{JM}^\dagger(\alpha, \beta) | J_i M_i \rangle (-)^{J-j_\alpha-J'+m} \begin{pmatrix} j & j' & J \\ -m & m' & M \end{pmatrix} \\ & \begin{Bmatrix} j & j' & J \\ j_\alpha & j_\beta & J' \end{Bmatrix} i^{l_\beta-l_\alpha+l-l'} (j' j_\alpha J' | V_{\text{eff}}^k | j j_\beta J') \widehat{J} \widehat{J}'^2 \\ & \frac{\delta(r-r')}{rr'} \int \phi_{n_\alpha j_\alpha l_\alpha}(r_2) V_{\text{eff}}^k(r, r_2) \phi_{n_\beta j_\beta l_\beta}(r_2) r_2^2 dr_2 \end{aligned} \quad (4.6.4)$$

where $\bar{\alpha} = n_\alpha, j_\alpha, l_\alpha$ and $\bar{\beta} = n_\beta, j_\beta, l_\beta$. The last step is to introduce (4.6.4) in equation (4.6.1) to have the entire formula of the direct term of the coupling potential that appear in \mathcal{S} and reduce the formula as much as possible:

$$\begin{aligned} U_{[(l' \frac{1}{2}) j', J_f], [(l \frac{1}{2}) j, J_i]}^{I, f i}(r, r') = & \sum_{\substack{mm' \\ M_i M_f \\ J'JM \\ \bar{\alpha}\bar{\beta}k}} (-)^{j'+j-j_\alpha+J-J_i-J_f-J'+m+2\mu} \widehat{I}^2 \widehat{J} \widehat{J}'^2 i^{l_\beta-l_\alpha+l-l'} (j' j_\alpha J' | V_{\text{eff}}^k | j j_\beta J') \\ & \begin{pmatrix} j & j' & J \\ -m & m' & M \end{pmatrix} \begin{pmatrix} j' & J_f & I \\ m' & M_f & -\mu \end{pmatrix} \begin{pmatrix} j & J_i & I \\ m & M_i & -\mu \end{pmatrix} \begin{Bmatrix} j & j' & J \\ j_\alpha & j_\beta & J' \end{Bmatrix} \\ & \langle J_f M_f | A_{JM}^\dagger(\alpha, \beta) | J_i M_i \rangle \frac{\delta(r-r')}{rr'} \int \phi_{n_\alpha j_\alpha l_\alpha}(r_2) V_{\text{eff}}^k(r, r_2) \\ & \phi_{n_\beta j_\beta l_\beta}(r_2) r_2^2 dr_2 \end{aligned}$$

We sum over μ , and divide by \widehat{I}^2 to compensate:

$$\begin{aligned} U_{[(l' \frac{1}{2}) j', J_f], [(l \frac{1}{2}) j, J_i]}^{I, f i}(r, r') = & \sum_{\substack{mm'\mu \\ M_i M_f \\ M J' J \\ \bar{\alpha}\bar{\beta}k}} (-)^{j'+j+I-m-m'-\mu} \begin{pmatrix} j & j' & J \\ -m & m' & M \end{pmatrix} \begin{pmatrix} j' & I & J_f \\ -m' & \mu & -M_f \end{pmatrix} \begin{pmatrix} I & -\mu & j \\ J_i & m & M_i \end{pmatrix} \\ & \frac{\widehat{I}^2 \widehat{J} \widehat{J}'^2}{\widehat{I}^2} i^{l_\beta-l_\alpha+l-l'} (-)^{-j_\alpha+J-J_i-J_f-J'-I+m'+2m+3\mu} \begin{Bmatrix} j & j' & J \\ j_\alpha & j_\beta & J' \end{Bmatrix} \\ & (j' j_\alpha J' | V_{\text{eff}}^k | j j_\beta J') \langle J_f M_f | A_{JM}^\dagger(\alpha, \beta) | J_i M_i \rangle \frac{\delta(r-r')}{rr'} \\ & \int \phi_{n_\alpha j_\alpha l_\alpha}(r_2) V_{\text{eff}}^k(r, r_2) \phi_{n_\beta j_\beta l_\beta}(r_2) r_2^2 dr_2 \end{aligned}$$

The second phase can be simplified as $(-)^{-j_\alpha+J-J_i-J_f-J'-I-M_f-1}$ and the three 3J can be simplified (A.0.13) so that we find for the direct term of a potential coupling two states $|J_i M_i\rangle$ and $|J_f M_f\rangle$:

$$\begin{aligned} U_{[(l' \frac{1}{2}) j', J_f], [(l \frac{1}{2}) j, J_i]}^{I, f i}(r, r')_{\text{direct}} = & \sum_{\substack{M_i M_f \\ M J' J \\ \bar{\alpha}\bar{\beta}k}} (-)^{-j_\alpha+J-J_i-J_f-J'-I-M_f-1} \begin{pmatrix} J_f & J_i & J \\ -M_f & M_i & M \end{pmatrix} \begin{Bmatrix} J_f & J_i & J \\ j & j' & I \end{Bmatrix} \\ & \begin{Bmatrix} j & j' & J \\ j_\alpha & j_\beta & J' \end{Bmatrix} \langle J_f M_f | A_{JM}^\dagger(\alpha, \beta) | J_i M_i \rangle \widehat{J} \widehat{J}'^2 i^{l_\beta-l_\alpha+l-l'} \\ & (j' j_\alpha J' | V_{\text{eff}}^k | j j_\beta J') \frac{\delta(r-r')}{rr'} \int \phi_{n_\alpha j_\alpha l_\alpha}(r_2) V_{\text{eff}}^k(r, r_2) \phi_{n_\beta j_\beta l_\beta}(r_2) \\ & r_2^2 dr_2 \end{aligned} \quad (4.6.5)$$

This version is almost suitable for numerical calculations, but we can go further and simplify it even more by using the preliminary work in which we defined a tensor operator for the matrix elements of the 1-body transition density. In particular, a formula that doesn't

depend on spin projections is highly desirable for time cost considerations. Therefore, let us focus on the operator $\langle J_f M_f | A_{JM}^\dagger(\alpha, \beta) | J_i M_i \rangle$, with J an integer number. Using equation (4.1.6), we expand it in terms of the reduced transition density matrix elements:

$$\begin{aligned} \langle J_f M_f | A_{JM}^\dagger(\alpha, \beta) | J_i M_i \rangle &= \frac{\langle J_i M_i | JM | J_f M_f \rangle}{\widehat{J}_f} \rho_{\alpha\beta}^{N_i \rightarrow N_f, J} \\ &= (-)^{J_i - J + M_f} \begin{pmatrix} J_i & J & J_f \\ M_i & M & -M_f \end{pmatrix} \rho_{\alpha\beta}^{N_i \rightarrow N_f, J} \end{aligned} \quad (4.6.6)$$

We rotate the Wigner 3J symbol and insert this relation in the previous formula:

$$\begin{aligned} U_{[(l' \frac{1}{2}) j', J_f], [(l \frac{1}{2}) j, J_i]}^{I, f i}(r, r')_{\text{direct}} &= \sum_{\substack{M_i M_f \\ M' J' J \\ \bar{\alpha} \bar{\beta} k}} (-)^{-j_\alpha - J_f - J' - I - 1} \begin{pmatrix} J_f & J_i & J \\ -M_f & M_i & M \end{pmatrix}^2 \begin{Bmatrix} J_f & J_i & J \\ j & j' & I \end{Bmatrix} \begin{Bmatrix} j & j' & J \\ j_\alpha & j_\beta & J' \end{Bmatrix} \\ &\quad \rho_{\alpha\beta}^{N_i \rightarrow N_f, J} \widehat{J} \widehat{J}'^2 i^{l_\beta - l_\alpha + l - l'} (j' j_\alpha J' | V_{\text{eff}}^k | j j_\beta J') \\ &\quad \frac{\delta(r - r')}{r r'} \int \phi_{n_\alpha j_\alpha l_\alpha}(r_2) V_{\text{eff}}^k(r, r_2) \phi_{n_\beta j_\beta l_\beta}(r_2) r_2^2 dr_2 \end{aligned}$$

We sum over M_i , M_f and M to simplify the Wigner 3J symbol:

$$\boxed{U_{[(l' \frac{1}{2}) j', J_f], [(l \frac{1}{2}) j, J_i]}^{I, f i}(r, r')_{\text{direct}} = \sum_{\substack{J' J \\ \bar{\alpha} \bar{\beta} k}} (-)^{-j_\alpha - J_f - J' - I - 1} \begin{Bmatrix} J_f & J_i & J \\ j & j' & I \end{Bmatrix} \begin{Bmatrix} j & j' & J \\ j_\alpha & j_\beta & J' \end{Bmatrix} \rho_{\alpha\beta}^{N_i \rightarrow N_f, J} \widehat{J} \widehat{J}'^2 i^{l_\beta - l_\alpha + l - l'} (j' j_\alpha J' | V_{\text{eff}}^k | j j_\beta J') \frac{\delta(r - r')}{r r'} \int \phi_{n_\alpha j_\alpha l_\alpha}(r_2) V_{\text{eff}}^k(r, r_2) \phi_{n_\beta j_\beta l_\beta}(r_2) r_2^2 dr_2} \quad (4.6.7)$$

This formula for the direct part of a potential coupling an initial state $|N_i \in J_i \Pi_i M_i\rangle$ to a final state $|N_f \in J_f \Pi_f M_f\rangle$ is - in the case of a local, finite range 2-body interaction - completely general and it is straightforward to code it. It does not depend on projections of angular momenta, and geometric terms can be computed with the Racah algebra. Now, we do the same derivation procedure for the exchange term.

4.6.2 Exchange term

Equation (4.6.1) is the same for direct and exchange term, so we begin with showing that we can define the same tensor operator for the transition density that we did for the direct term. The first steps are quite identical, so we will give less details. The exchange term of equation (4.2.8) reads:

$$\langle J_f M_f | \langle \vec{r}, \sigma | \widehat{V}_{\text{eff}} | \vec{r}', \sigma' \rangle_{\text{exchange}} | J_i M_i \rangle = \sum_{\alpha\beta} \langle J_f M_f | a_\alpha^\dagger a_\beta | J_i M_i \rangle \varphi_\alpha^*(\vec{r}', \sigma') V_{\text{eff}}(\vec{r}, \sigma, \vec{r}', \sigma') \varphi_\beta(\vec{r}, \sigma)$$

We project on the spin-angular functions basis, then we transform the creation-annihilation operator into a coupled irreducible spherical tensor which leads to the same tensor operator for the transition density that we defined for the direct term:

$$\begin{aligned} \langle j' m' | \langle J_f M_f | \widehat{V}_{\text{eff}} | J_i M_i \rangle | j m \rangle_{\text{exchange}} &= \sum_{\substack{\alpha\beta k \\ JM}} \langle J_f M_f | A_{JM}^\dagger(\alpha, \beta) | J_i M_i \rangle i^{l_\beta - l_\alpha + l - l'} (-)^{j_\beta - m_\beta} \\ &\quad \langle j_\alpha m_\alpha j_\beta - m_\beta | JM \rangle \\ &\quad (j' j_\alpha | V_{\text{eff}}^k | j_\beta j) \phi_\alpha(r') V_{\text{eff}}^k(r, r') \phi_\beta(r) \end{aligned} \quad (4.6.8)$$

We proceed with the recoupling of j' and j_α to J' , writing only geometric terms:

$$\begin{aligned}
 & \sum_{m_\alpha m_\beta} (-)^{j_\beta - m_\beta} \langle j_\alpha m_\alpha j_\beta - m_\beta | JM \rangle \langle j' j_\alpha | V_{\text{eff}}^k | j_\beta j \rangle \\
 &= \sum_{\substack{m_\alpha m_\beta \\ J' M'}} \langle j_\alpha m_\alpha j_\beta - m_\beta | JM \rangle (-)^{j_\beta - m_\beta} \langle j' m' j_\alpha m_\alpha | J' M' \rangle \langle j_\beta m_\beta j m | J' M' \rangle \langle j' j_\alpha J' | V_{\text{eff}}^k | j_\beta j J' \rangle \\
 &= \sum_{\substack{m_\alpha m_\beta \\ J' M'}} \langle j_\alpha m_\alpha j_\beta - m_\beta | JM \rangle (-)^{j_\beta - m_\beta} \langle j' m' j_\alpha m_\alpha | J' M' \rangle (-)^{j + j_\beta + J'} \langle j m j_\beta m_\beta | J' M' \rangle \\
 & \quad \langle j j_\alpha J' | V_{\text{eff}}^k | j_\beta j J' \rangle \\
 &= \sum_{\substack{m_\alpha m_\beta \\ J' M'}} (-)^{j_\alpha + j_\beta + J' + m_\alpha + m_\beta + M'} \begin{pmatrix} j_\alpha & j_\beta & J \\ m_\alpha & -m_\beta & -M \end{pmatrix} \begin{pmatrix} J' & j_\alpha & j' \\ M' & -m_\alpha & -m' \end{pmatrix} \begin{pmatrix} j_\beta & J' & j \\ m_\beta & -M' & m \end{pmatrix} \widehat{J} \widehat{J}'^2 \\
 & \quad (-)^{j' + 2j - j_\alpha - j_\beta + M + M' - m_\alpha - 2m_\beta} \langle j' j_\alpha J' | V_{\text{eff}}^k | j_\beta j J' \rangle
 \end{aligned}$$

The second phase can be simplified as $(-)^{j' - j_\alpha - j_\beta + m}$, and the first phase with the three Wigner 3J can be simplified using formula (A.0.13), so that we finally find:

$$\begin{aligned}
 \sum_{m_\alpha m_\beta} (-)^{j_\beta - m_\beta} \langle j_\alpha m_\alpha j_\beta - m_\beta | JM \rangle \langle j' j_\alpha | V_{\text{eff}}^k | j_\beta j \rangle &= \sum_{J'} (-)^{j' - j_\alpha - j_\beta + m} \widehat{J} \widehat{J}'^2 \begin{pmatrix} j & j' & J \\ m & -m' & -M \end{pmatrix} \\
 & \quad \left\{ \begin{matrix} j & j' & J \\ j_\alpha & j_\beta & J' \end{matrix} \right\} \langle j' j_\alpha J' | V_{\text{eff}}^k | j_\beta j J' \rangle
 \end{aligned} \tag{4.6.9}$$

We inverse the signs of the projections in the Wigner 3J symbols for later factorization, and now we can insert equation (4.6.9) in equation (4.6.8) and therefore give a formula for the exchange term of the coupling potential:

$$\begin{aligned}
 \langle j' m' | \langle J_f M_f | \widehat{V}_{\text{eff}} | J_i M_i \rangle | j m \rangle_{\text{exchange}} &= \sum_{\substack{\bar{\alpha} \bar{\beta} k \\ J' J M}} (-)^{2j' + j + J - j_\alpha - j_\beta + m} \begin{pmatrix} j & j' & J \\ -m & m' & M \end{pmatrix} \left\{ \begin{matrix} j & j' & J \\ j_\alpha & j_\beta & J' \end{matrix} \right\} \\
 & \quad \langle J_f M_f | A_{JM}^\dagger(\alpha, \beta) | J_i M_i \rangle i^{l_\beta - l_\alpha + l - l'} \\
 & \quad \langle j' j_\alpha J' | V_{\text{eff}}^k | j_\beta j J' \rangle \widehat{J} \widehat{J}'^2 \phi_{n_\alpha j_\alpha l_\alpha}(r') V_{\text{eff}}^k(r, r') \phi_{n_\beta j_\beta l_\beta}(r)
 \end{aligned} \tag{4.6.10}$$

Finally, as for the direct term, we combine equation (4.6.10) with equation (4.6.1):

$$\begin{aligned}
 U_{[(l' \frac{1}{2}) j', J_f], [(l \frac{1}{2}) j, J_i]}^{I, f i}(r, r')_{\text{exchange}} &= \sum_{\substack{m m' \\ M_i M_f \\ M J' J \\ \bar{\alpha} \bar{\beta} k}} (-)^{3j' + 2j - j_\alpha - j_\beta + J - J_i - J_f + m + 2\mu} \widehat{I}^2 \widehat{J} \widehat{J}'^2 i^{l_\beta - l_\alpha + l - l'} \\
 & \quad \langle j' j_\alpha J' | V_{\text{eff}}^k | j_\beta j J' \rangle \langle J_f M_f | A_{JM}^\dagger(\alpha, \beta) | J_i M_i \rangle \\
 & \quad \begin{pmatrix} j & j' & J \\ -m & m' & M \end{pmatrix} \begin{pmatrix} j' & J_f & I \\ m' & M_f & -\mu \end{pmatrix} \begin{pmatrix} j & J_i & I \\ m & M_i & -\mu \end{pmatrix} \\
 & \quad \left\{ \begin{matrix} j & j' & J \\ j_\alpha & j_\beta & J' \end{matrix} \right\} \phi_{n_\alpha j_\alpha l_\alpha}(r') V_{\text{eff}}^k(r, r') \phi_{n_\beta j_\beta l_\beta}(r)
 \end{aligned}$$

We sum over μ , and divide by \widehat{I}^2 to compensate:

$$\begin{aligned}
 U_{[(l'\frac{1}{2})j',J_f],[(l\frac{1}{2})j,J_i]}^{I,fi}(r,r')_{\text{exchange}} &= \sum_{\substack{mm'\mu \\ M_iM_f \\ MJ'J \\ \bar{\alpha}\bar{\beta}k}} (-)^{j'+j+I-m'-m-\mu} \begin{pmatrix} j & j' & J \\ -m & m' & M \end{pmatrix} \begin{pmatrix} j' & I & J_f \\ -m' & \mu & -M_f \end{pmatrix} \\
 &\quad i^{l_\beta-l_\alpha+l-l'} \langle J_f M_f | A_{JM}^\dagger(\alpha, \beta) | J_i M_i \rangle \frac{\widehat{I}^2 \widehat{J} \widehat{J}'^2}{\widehat{I}^2} \\
 &\quad (-)^{2j'+j+J-j_\alpha-j_\beta-J_i-J_f-I+m'+2m+3\mu} (j' j_\alpha J' | V_{\text{eff}}^k | j_\beta j J') \\
 &\quad \left\{ \begin{matrix} j & j' & J \\ j_\alpha & j_\beta & J' \end{matrix} \right\} \phi_{n_\alpha j_\alpha l_\alpha}(r') V_{\text{eff}}^k(r, r') \phi_{n_\beta j_\beta l_\beta}(r)
 \end{aligned}$$

The second phase can be simplified as $(-)^{2j'+j+J-j_\alpha-j_\beta-J_i-J_f-I-M_f-1}$ and the three Wigner 3J symbols can be reduced using (A.0.13) so that we find the general formula for the exchange term of a potential coupling two states $|J_i M_i\rangle$ and $|J_f M_f\rangle$:

$$\begin{aligned}
 U_{[(l'\frac{1}{2})j',J_f],[(l\frac{1}{2})j,J_i]}^{I,fi}(r,r')_{\text{exchange}} &= \sum_{\substack{M_iM_f \\ MJ'J \\ \bar{\alpha}\bar{\beta}k}} (-)^{2j'+j-j_\alpha-j_\beta+J-J_i-J_f-I-M_f-1} \begin{pmatrix} J_f & J_i & J \\ -M_f & M_i & M \end{pmatrix} \\
 &\quad \left\{ \begin{matrix} J_f & J_i & J \\ j & j' & J \end{matrix} \right\} \left\{ \begin{matrix} j & j' & J \\ j_\alpha & j_\beta & J' \end{matrix} \right\} \langle J_f M_f | A_{JM}^\dagger(\alpha, \beta) | J_i M_i \rangle \widehat{J} \widehat{J}'^2 \\
 &\quad i^{l_\beta-l_\alpha+l-l'} (j' j_\alpha J' | V_{\text{eff}}^k | j_\beta j J') \phi_{n_\alpha j_\alpha l_\alpha}(r') V_{\text{eff}}^k(r, r') \phi_{n_\beta j_\beta l_\beta}(r)
 \end{aligned} \tag{4.6.11}$$

We finish, like for the direct term, by applying the Wigner-Eckart theorem to the tensor operator $\langle J_f M_f | A_{JM}^\dagger(\alpha, \beta) | J_i M_i \rangle$, and inserting the resulting expression in the previous formula so as to find, after simplification and summation over M_i , M_f and M :

$$\begin{aligned}
 U_{[(l'\frac{1}{2})j',J_f],[(l\frac{1}{2})j,J_i]}^{I,fi}(r,r')_{\text{exchange}} &= \sum_{\substack{J'J \\ \bar{\alpha}\bar{\beta}k}} (-)^{2j'+j-j_\alpha-j_\beta-J_f-I-1} \left\{ \begin{matrix} J_f & J_i & J \\ j & j' & I \end{matrix} \right\} \left\{ \begin{matrix} j & j' & J \\ j_\alpha & j_\beta & J' \end{matrix} \right\} \rho_{\alpha\beta}^{N_i \rightarrow N_f, J} \\
 &\quad \widehat{J} \widehat{J}'^2 i^{l_\beta-l_\alpha+l-l'} (j' j_\alpha J' | V_{\text{eff}}^k | j_\beta j J') \phi_{n_\alpha j_\alpha l_\alpha}(r') V_{\text{eff}}^k(r, r') \\
 &\quad \phi_{n_\beta j_\beta l_\beta}(r)
 \end{aligned} \tag{4.6.12}$$

Formulae (4.6.7) and (4.6.12) are very important results: they can be used to compute any potential appearing in the system of coupled equations \mathcal{S} that we derived in the previous section. Moreover, coding these equations is rather straightforward and allows for a clear separation between the geometric part of the potential and the radial part. However, we cannot validate this derivation by direct comparison because we do not have access to any code performing such calculation. Instead, we chose to use again the DWBA code written by Raynal. This code computes the transition amplitude from $|\widetilde{0}\rangle$ the ground state of a nucleus to $|N\rangle$ one of its excited states, and we can use this feature to validate our derivation as presented in the next chapter.

Chapter 5

Presentation of codes ECANOL and MINOLOP

As we previously mentioned, studies on the scattering involving nonlocal potentials have been done since the 1960s and allowed to put in evidence important effects related to the nonlocality of the potential such as the Perey effect [24, 32]. Since then, numerous other studies related to the same phenomenon have been carried out in different conditions: studying deuteron scattering and transfer reactions within the DWBA [57], nucleon direct elastic scattering [43, 44, 67, 97] with the optical model, charge exchange reactions [62], nucleon direct elastic and inelastic scattering [23, 79].

One purpose of this thesis is to develop tools that allow for the study of nucleon-nucleus direct elastic and inelastic scattering within the CC framework for any target nucleus, using nonlocal potentials derived with a microscopic approach. In practice, this means developing one code to compute potentials and one code to solve the system of coupled integrodifferential equation. In order to validate our developments, we could rely on existing tools like the DWBA98 [61] and the ECIS-06 [60] codes of Raynal.

From the DWBA98 code, it is possible to extract the optical potential obtained by folding the Melbourne G matrix with reduced matrix elements of the 1-body density for a nucleus with a 0^+ ground state. It is also possible to extract the direct part of transition potentials from the ground state to an excited state, but not the exchange part. We can then compare what we can extract with the result of a calculation done by MINOLOP. We can also use DWBA98 to calculate the cross section for elastic scattering using the microscopic optical potential, and the cross section for inelastic scattering using whether only the direct part of the transition potential, or both its direct and exchange parts.

As for the ECIS-06 code, we can calculate scattering observables within the DWBA or the CC framework, but it is limited to local potentials.

We have chosen to develop our codes using a uniform radial mesh, which allows for direct validation against qualified codes like ECIS-06 and DWBA98. Following this idea, we have written two softwares: MINOLOP computes potentials that appear in CC equations using the Melbourne G matrix as the NN effective interaction and nuclear structure input given under the form of 1-body reduced density matrices as presented in chapter 4.5, and ECANOL solves CC equations for nonlocal potentials given on a radial mesh. In this chapter we explain first how MINOLOP works, starting by a description of inputs it requires, then

we explain how we partly validated the code by comparing, when possible, optical and transition potentials for various specific cases to those extracted from the DWBA98 code. Afterwards, we present ECANOL first by detailing its inputs, then by explaining the series of calculations it does through an example. Finally, we introduce the vibrational model that we used for validations against ECIS-06 in the CC case, and final validations of MINOLOP and ECANOL for inelastic scattering using nonlocal potentials.

5.1 The microscopic nonlocal potentials code MINOLOP

5.1.1 Input files required by MINOLOP

MINOLOP can calculate nonlocal potentials for a complex, energy and density dependent NN effective interaction made of a central term with the 4 ST channels. The structure of the code was thought to easily include 2-body spin orbit and tensor terms. In particular, the geometric matrix elements for the 2-body spin orbit have been partly implemented but not yet validated. The effective interaction needs to be a local, finite-range one parameterized as a sum of Yukawa form factors. It is of course the case for the Melbourne G matrix with which we designed the code. MINOLOP could easily be extended to other form factors though (Gaussian,...). The code requires the next few input files: one input file should contain HF single particle wave functions expanded on a harmonic oscillator basis. We give here part of this file for ^{208}Pb as an example on figure 5.1:

```

1 0 1 8
0.45669209E+00 0.8993277-0.4276234 0.0887508 0.0197671-0.0068436-0.0043783-0.0016712-0.0034091
1 1 1 7
0.45669209E+00 0.9090613-0.4129847 0.0459566 0.0305342 0.0001861-0.0025848 0.0004585
1 1 -1 7
0.45669209E+00 0.9174065-0.3956590 0.0318173 0.0282246 0.0029510-0.0012323 0.0002657
1 2 1 7
0.45669209E+00 0.9295392-0.3674480 0.0026084 0.0297834 0.0056507-0.0024029 0.0026889
1 2 -1 7
0.45669209E+00 0.9443395-0.3278946-0.0155267 0.0200732 0.0076612 0.0007016 0.0022151
1 0 1 8
0.45669209E+00-0.4258340-0.8132145 0.3954174-0.0042718-0.0301758-0.0041290 0.0063937 0.0024122
1 3 1 6
0.45669209E+00 0.9496883-0.3107762-0.0302058 0.0223897 0.0090277-0.0038756
1 3 -1 6
0.45669209E+00 0.9680367-0.2471593-0.0418146 0.0044348 0.0067673 0.0018183
1 1 1 7
0.45669209E+00-0.4007475-0.8398894 0.3639939 0.0222229-0.0272191-0.0147542 0.0065764
1 1 -1 7
0.45669209E+00-0.3824673-0.8572941 0.3426230 0.0289088-0.0181427-0.0144345 0.0013345
1 4 1 6
0.45669209E+00 0.9658554-0.2535055-0.0498776 0.0121698 0.0138633-0.0054881
    
```

Figure 5.1: Part of an input file containing single particle wave functions developed on a harmonic oscillator basis for ^{208}Pb

The file is organized as follows: each HF single particle wave function is described by 2 lines. The first one contains, in order from left to right, a computation logical, the orbital angular momentum of the HF single particle wave function, a “+1” if the total angular momentum is $j = l + \frac{1}{2}$ or “-1” if the total angular momentum is $j = l - \frac{1}{2}$, and the number of harmonic oscillator wave functions on which the HF single particle is built. The files we used for our studies on spherical nuclei were obtained with a code that uses the Gogny D1S force, and the maximum orbital angular momentum l_{max} allowed for a single particle is given in the input file.

Another input file that is directly associated to HF single particle wave functions is the file containing reduced transition/coupling density matrix elements. Indeed, these matrix elements are given in the basis of HF single particle wave functions we just described. They are gathered in files and organized as follows: each HF single particle wave function in the first file can be labeled by its order of appearance in the file. Using this way of labeling, the first line of the density matrix elements contains two integer numbers labeling two HF single particle wave functions that form a pair $\alpha\beta$ (pp' or hh' or ph or hp). The second line contains the reduced density matrix elements $Z_{\alpha\beta}$ and $Z_{\beta\alpha}$. part of the file containing the reduced transition density matrix elements coupling the 0^+ ground state to the first 3^- state of ^{208}Pb is given on figure 5.2.

```

32 1
-8.66692730e-04 -3.11486360e-04
47 1
-5.31036000e-04 -3.54252280e-05
32 6
6.82795630e-04 3.16010480e-04
72 6
-1.41300170e-03 8.28304500e-04
104 6
8.62527870e-04 -1.04571470e-03
72 15
1.47077550e-03 2.04938360e-04
104 15
-3.52456910e-03 1.61167620e-04
138 121
-2.42921490e-03 -2.20037510e-03
    
```

Figure 5.2: Input file containing RPA amplitudes of ^{208}Pb of the reduced matrix elements of the transition density $\rho_{\alpha\beta}^{\tilde{0} \rightarrow 3^-, J=3}$ with an excitation energy of 2.614 MeV

The last two input files that are required contain the effective interaction. In a first, short file, the ranges for each term of the interaction are gathered. In the second file, the Melbourne G matrix is given on a density mesh. This interaction consists of a sum of a central, a 2-body spin-orbit and a tensor terms and for each case, the interaction is given in a given channel of total spin S and isospin T ($S = 0, 1$ $T = 0, 1$ for the central term, $S = 1$ $T = 0, 1$ for the spin orbit and the tensor terms). Thus, the input file containing the G matrix is a list of arrays with labels to indicate which part of the interaction is considered and labels for the channel ST .

5.1.2 Specificities of MINOLOP

MINOLOP is written in FORTRAN 90, except for one file written in C++ which can be used to compute various Wigner symbols. All real variables are double precision. We wrote most of MINOLOP's routines ourselves, but not all of them. The program uses two routines that compute modified Bessel functions K and I for which details can be found in [98] [99]. We also extracted some routines from the DWBA98 code that compute Wigner 6J coefficients, because for an equal accuracy we found out they cost much less computation time than other routines we tested. We wrote all the other routines of MINOLOP.

In order to save computation time, particle-hole pairs that have the same quantum numbers j and l are factorized, so that the number of calculations of geometric terms is reduced. Moreover, the Wigner 3J and 9J symbols are tabulated by the code and then arrays are transmitted to routines for geometric matrix elements.

5.1.3 Treatment of the isospin and LDA

In section 4.3, we mentioned the necessity to do a LDA in order to fix the density for practical calculations. This is of particular importance for the exchange term of the central part of our potentials. When we compute a potential using the interaction between two protons or two neutrons, then the total isospin for the channel must be $T = 1$ and the interaction we need to consider reduces to (for both the direct and the exchange term):

$$\begin{aligned}\langle pp|V_{\text{eff}}|pp\rangle &= \langle T = 1M_T = -1|V_{\text{eff}}|T = 1M_T = -1\rangle = V_{\text{eff}}^{T=1,S} \\ \langle nn|V_{\text{eff}}|nn\rangle &= \langle T = 1M_T = 1|V_{\text{eff}}|T = 1M_T = 1\rangle = V_{\text{eff}}^{T=1,S}\end{aligned}\quad (5.1.1)$$

but when we consider the interaction between a proton and a neutron, then two values $T = 0, 1$ of the total isospin are possible and the interaction we need to consider for the exchange term is different from that of the direct term:

$$\begin{aligned}\langle pn|V_{\text{eff}}|pn\rangle_{\text{direct}} &= \frac{1}{2}\langle T = 1M_T = 0|V_{\text{eff}}|T = 1M_T = 0\rangle + \frac{1}{2}\langle T = 0M_T = 0|V_{\text{eff}}|T = 0M_T = 0\rangle \\ &= \frac{1}{2}V_{\text{eff}}^{T=1,S} + \frac{1}{2}V_{\text{eff}}^{T=0,S} \\ \langle pn|V_{\text{eff}}|np\rangle_{\text{exchange}} &= \frac{1}{2}\langle T = 1M_T = 0|V_{\text{eff}}|T = 1M_T = 0\rangle - \frac{1}{2}\langle T = 0M_T = 0|V_{\text{eff}}|T = 0M_T = 0\rangle \\ &= \frac{1}{2}V_{\text{eff}}^{T=1,S} - \frac{1}{2}V_{\text{eff}}^{T=0,S}\end{aligned}\quad (5.1.2)$$

At least two prescriptions can be taken given this situation: the first prescription is to do the LDA on each channel ST to generate $V^{ST}(\rho(r), \rho(r'))$, then proceed with the computation of matrix elements in each channel using (4.6.7) and (4.6.12), and finally take into account equation (5.1.2). The other prescription is to take into account this equation as soon as when doing the LDA: instead of doing the LDA in each channel ST , we define an interaction for two identical particles and an interaction for two different particles using equation (5.1.2) and we do the LDA on this newly defined interaction which leads (for the exchange term) to $\frac{1}{2} \left(V_{\text{eff}}^{T=1,S} - V_{\text{eff}}^{T=0,S} \right) (\rho(r), \rho(r'))$.

In practice, the LDA done in DWBA98 is based on the geometric average using the second prescription but with a particularity: instead of computing the effective interaction at the geometric average of the densities as follows:

$$\left(V_{\text{eff}}^{T=1,S} - V_{\text{eff}}^{T=0,S} \right) \left(\sqrt{\rho(r)\rho(r')} \right) \quad (5.1.3)$$

The code calculates the geometric average of the interaction taken at $\rho(r)$ and $\rho(r')$:

$$\sqrt{\left(V_{\text{eff}}^{T=1,S}(\rho(r)) - V_{\text{eff}}^{T=0,S}(\rho(r)) \right) \left(V_{\text{eff}}^{T=1,S}(\rho(r')) - V_{\text{eff}}^{T=0,S}(\rho(r')) \right)} \quad (5.1.4)$$

and we follow the same prescription to ease the validation process when comparing our potentials to those calculated by the DWBA98 code. The main advantage of this second technique is that it can save computation time, but it would be interesting to see how this choice affects the value of cross sections we compute from it. In this work, we chose to stick to the prescription used by Raynal in his DWBA98 code and we wrote our code so that implementing other methods for the LDA can be done easily.

5.2 ECANOL

One very important objective of this Ph.D. project was the development of a code that could solve coupled channel equations with nonlocal potentials for the study of nucleon-nucleus direct elastic and inelastic scattering. Particular features were required: the code was to be written in a modern language, it was required to be adaptable to super-computers, and it needed to be written in a clear way so that adding new features to it would be straightforward. The last and most important point was that the code should be well documented so that all conventions and numerical choices done in it could be found easily and well explained. Fortunately, we did not have to start from scratch: indeed, our collaborator Arellano kindly provided us with his code HYDRA, which can be used to compute observables from nonlocal potentials for nucleon-nucleus elastic scattering and charge exchange. It was noticeably used in reference [62]. Basically, HYDRA was designed to treat only 0^+ excitations, and the ordering in partial waves $\{[(l, \frac{1}{2})j, J]I\}$ of the matrix equation p 35 was not explicitly done. From this excellent basis, we wrote our own code dedicated to nucleon-nucleus direct elastic and inelastic scattering in FORTRAN 90, with the same C++ routine for Wigner 3J coefficient as that inside MINOLOP code. In particular, we extended the resolution method to any spin-parity J^Π for excited states, we reordered the calculation using the coupling scheme $\{[(l, \frac{1}{2})j, J]I\}$ to optimize the computation time, and we included some important numerical corrections in the resolution of the Lippman-Schwinger equation (3.3.7). Let us describe how ECANOL is built and what it exactly does.

5.2.1 Input and options

Usual information such as the projectile, the target, the discrete excited states to consider with their excitation energy, spin and parity must be specified by the user. There is the possibility to specify as input the masses that should be used when computing kinematic factors, or let the code do it by itself using experimental values of observables stored in a text file. Furthermore, the user can choose between kinematic factors computed with classical mechanics or relativistic mechanics. This can have a large impact on the angular distribution (up to tens of percents) for incident energies above 50 MeV. Moreover, kinematic constants like the fine structure constant are set as fixed parameters in a module. We have chosen the same values as those used in DWBA98 and ECIS-06 for validation of our code, but the user can change them to newer values, measured with a better accuracy.

ECANOL solves equations for direct elastic and inelastic scattering projected on radial coordinates, and we have chosen to divide the space with a constant mesh which means the user must specify a maximum radius and a step size. We give some recommendations on the choice of step size and maximum radius to choose, basing ourselves on comparisons with the code ECIS-06 [60]. Another important option for the user is the possibility to choose between a full coupled channel calculation or the DWBA. Basically, the DWBA calculation

could be made much faster than the CC case. Indeed, in the DWBA the transition amplitude for inelastic scattering reads:

$$T = \langle \chi_{k_f}^- | U_{\text{transition}} | \chi_{k_i}^+ \rangle \quad (5.2.1)$$

where T is the transition amplitude, $\chi_{k_f}^-$ the distorted wave in the inelastic channel, $\chi_{k_i}^+$ the distorted wave in the elastic channel and U the transition potential. In practice, we could compute first the two distorted waves by solving two simple matrix equations, then we could calculate the transition amplitude using (5.2.1). This possibility could well be included in future enhancements of ECANOL, but for now we have chosen to treat the DWBA case like the CC case, by solving the matrix equation as displayed on p 35. This choice was made in order to ease the validation of our code, as will be explain later.

Finally, we have included the possibility for the user to use whether her/his own potentials (given on the radial mesh she/he specified in the input) or to use a macroscopic model based on Woods-Saxon densities and the collective vibrational model for excited states. The user can specify real and imaginary parameters for a volume and a surface term of a central potential, as well as deformation parameters. This feature was of particular importance when validating ECANOL by comparison to ECIS-06 in the case of coupled channels. Now, let us explain what steps are followed by the program when a calculation is launched.

5.2.2 Organization of the code through an example

Let us consider the case in which we want to compute the cross section of elastic and inelastic scattering of a neutron on ^{208}Pb to its first 1^- and 2^+ excited states. We will label them as $N_1 \equiv J_{N_1}^{\Pi N_1} = 1^-$ and $N_2 \equiv J_{N_2}^{\Pi N_2} = 2^+$. Of course, we already mentioned that the ground state of this nucleus is 0^+ . From the information given by the user in the input file, ECANOL computes first kinematic factors associated to each channel to consider. Then, it computes partial waves that couple to each other up to a maximum value of total orbital angular momentum specified by the user. The most general case associated to this coupling is given in equation (3.3.9) ; if we keep only N_1 and if we consider just one value of the total angular momentum of the system $I^\pi = \frac{1}{2}^+$, then equation (3.3.9) reduces to:

$$\left\{ \begin{array}{l} |I^\pi - J_0^{\Pi_0}| \leq j' \leq I^\pi + J_0^{\Pi_0} \\ (-)^{l'} * (+1) = +1 \\ |I^\pi - J_N^{\Pi N}| \leq j \leq I^\pi + J_N^{\Pi N} \\ (-)^l * (-1) = +1 \end{array} \right. \Leftrightarrow \left\{ \begin{array}{l} \frac{3}{2} \leq j' \leq \frac{5}{2} \\ l' = 2 \\ \frac{1}{2} \leq j \leq \frac{3}{2} \\ l = 1 \end{array} \right. \Leftrightarrow \left\{ \begin{array}{l} \{j', l'\} = \{ \{\frac{3}{2}, 2\}, \{\frac{5}{2}, 2\} \} \\ \{j, l\} = \{ \{\frac{1}{2}, 1\}, \{\frac{3}{2}, 1\} \} \end{array} \right. \quad (5.2.2)$$

Let us give another example: we will now consider the case in which we compute the couplings with both N_1 and N_2 . The total angular momentum of the system for which we want to compute the couplings is set to $I^\pi = \frac{3}{2}^+$. Then, with this setup, (3.3.9) reduces to:

$$\begin{aligned}
 & \begin{cases} \{j', l'\} = \{\frac{3}{2}, 2\} \\ |I^\pi - J_{N_1}^{\Pi_{N_1}}| \leq j \leq I^\pi + J_{N_1}^{\Pi_{N_1}} \\ (-)^l * (-1) = +1 \\ |I^\pi - J_{N_2}^{\Pi_{N_2}}| \leq j \leq I^\pi + J_{N_2}^{\Pi_{N_2}} \\ (-)^l * (-1) = +1 \end{cases} \Leftrightarrow \begin{cases} \{j', l'\} = \{\frac{3}{2}, 2\} \\ \frac{1}{2} \leq j \leq \frac{5}{2} \\ l = 1 \text{ or } l = 3 \\ \frac{1}{2} \leq j \leq \frac{7}{2} \\ l = 0 \text{ or } l = 2 \text{ or } l' = 4 \end{cases} \\
 & \Leftrightarrow \begin{cases} \{j', l'\} = \{\frac{3}{2}, 2\} \\ \{j, l\}_1 = \{\{\frac{1}{2}, 1\}, \{\frac{3}{2}, 1\}, \{\frac{5}{2}, 3\}\} \\ \{j, l\}_2 = \{\{\frac{1}{2}, 0\}, \{\frac{3}{2}, 2\}, \{\frac{5}{2}, 2\}, \{\frac{7}{2}, 4\}\} \end{cases} \quad (5.2.3)
 \end{aligned}$$

ECANOL uses this exact basis to compute the couplings between partial waves. The next step consists of reading or computing potentials. The first case is when the user chooses to use potentials he computed himself with another code. In this case, the user includes files in which potentials coupling each channel are given on the same radial mesh and in the same order as in the input file for ECANOL. If the step size is small and many channels are included, this can lead to a large number of sizable files (>100 Mb per file) which is not always easy to handle. Therefore, the user can use a simple property of tensor operators to divide by almost 2 the number of potentials she/he needs to give: If you want to calculate the transition from f to i using what has been done for i to f , then you can use simple properties:

$$\left\langle [(l' \frac{1}{2})j', J_i] I^\pi, \mu \left| \widehat{V}_{\text{eff}} \right| [(l \frac{1}{2})j, J_f] I^\pi, \mu \right\rangle^* = \left\langle [(l' \frac{1}{2})j', J_f] I^\pi, \mu \left| \widehat{V}_{\text{eff}}^\dagger \right| [(l \frac{1}{2})j, J_i] I^\pi, \mu \right\rangle \quad (5.2.4)$$

$$\Leftrightarrow \left\langle [(l' \frac{1}{2})j', J_i] I^\pi, \mu \left| \widehat{V}_{\text{eff}} \right| [(l \frac{1}{2})j, J_f] I^\pi, \mu \right\rangle = \left\langle [(l' \frac{1}{2})j', J_f] I^\pi, \mu \left| \widehat{V}_{\text{eff}}^\dagger \right| [(l \frac{1}{2})j, J_i] I^\pi, \mu \right\rangle^* \quad (5.2.5)$$

So by inverting partial wave quantum numbers, taking the adjoint of the effective interaction and finally the conjugate of the potential we can obtain the transition from f to i directly from the inverse transition. ECANOL uses this property in the particular case of a scalar, complex effective interaction which corresponds to the Melbourne G matrix with which we derived our own potentials. The second case is when the user chooses to use the macroscopic model included in ECANOL. It follows the same logic as for user-defined potentials so that the only real difference lies in the ingredients used to compute them, which we describe in a later subsection.

Now that potentials are stored in an array, ECANOL builds the matrix form of the Lippman-Schwinger equation (3.3.7). During this process, the integral over r' is done. This integral is computed with a trapezoidal method and much attention is given to the treatment of the discontinuities of the integrand (discontinuities due to the Green's operator). Returning to the small example on ^{208}Pb , if we construct the matrix equation associated to the couplings written in equation (5.2.2), we obtain:

$$\begin{pmatrix} \phi_{\frac{1}{2},0}^{\frac{1}{2}+} \\ \phi_{\frac{1}{2},1}^{\frac{1}{2}+,N_1} \\ \phi_{\frac{3}{2},1}^{\frac{1}{2}+,N_1} \end{pmatrix} = \mathbf{1} - \begin{pmatrix} \mathcal{G}_0(k_i)U_{[(0,\frac{1}{2})\frac{1}{2},0],[(\frac{1}{2})\frac{1}{2},0]}^{\frac{1}{2}+,00} & \mathcal{G}_0(k_i)U_{[(0,\frac{1}{2})\frac{1}{2},0],[(\frac{1}{2})\frac{1}{2},1]}^{\frac{1}{2}+,0N_1} & \mathcal{G}_0(k_i)U_{[(0,\frac{1}{2})\frac{1}{2},0],[(\frac{1}{2})\frac{3}{2},1]}^{\frac{1}{2}+,0N_1} \\ \mathcal{G}_1(k_f)U_{[(1,\frac{1}{2})\frac{1}{2},1],[(\frac{1}{2})\frac{1}{2},0]}^{\frac{1}{2}+,N_10} & \mathcal{G}_1(k_f)U_{[(1,\frac{1}{2})\frac{1}{2},1],[(\frac{1}{2})\frac{1}{2},1]}^{\frac{1}{2}+,N_1N_1} & \mathcal{G}_1(k_f)U_{[(1,\frac{1}{2})\frac{1}{2},1],[(\frac{1}{2})\frac{1}{2},0]}^{\frac{1}{2}+,N_1N_1} \\ \mathcal{G}_1(k_f)U_{[(1,\frac{1}{2})\frac{3}{2},1],[(\frac{1}{2})\frac{1}{2},0]}^{\frac{1}{2}+,00} & \mathcal{G}_1(k_f)U_{[(1,\frac{1}{2})\frac{3}{2},1],[(\frac{1}{2})\frac{1}{2},1]}^{\frac{1}{2}+,N_1N_1} & \mathcal{G}_1(k_f)U_{[(1,\frac{1}{2})\frac{3}{2},1],[(\frac{1}{2})\frac{3}{2},1]}^{\frac{1}{2}+,N_1N_1} \end{pmatrix}^{-1} \begin{pmatrix} F_0^0 \\ k_i \\ 0 \\ 0 \end{pmatrix} \quad (5.2.6)$$

The apparent simplicity and small size of this matrix equation can be misleading: equation (5.2.6) is only one member of a series of equations (one for each value of the total angular momentum and parity I^π of the system) that need to be solved. Moreover, the case we just presented contains only one excited state. If we add N_2 to it and use the couplings given in equation (5.2.3) and write the matrix equation for this situation, the result is shown on equation (5.2.7) (next page) and still, this is a simple case of CC equations in which only two excited states are treated together with the ground state.

$$\begin{pmatrix} \phi_{\frac{3}{2}, \frac{3}{2}}^{3+,0} \\ \phi_{\frac{1}{2}, 1}^{3+,N_1} \\ \phi_{\frac{3}{2}, 1}^{3+,N_1} \\ \phi_{\frac{3}{2}, 3}^{3+,N_1} \\ \phi_{\frac{1}{2}, 0}^{3+,N_2} \\ \dots \\ \phi_{\frac{7}{2}, 4}^{3+,N_2} \end{pmatrix} = \mathbf{1} - \left(\begin{pmatrix} \mathcal{G}_2(k_i)U_{[(2, \frac{1}{2})\frac{3}{2}, 0], [(2, \frac{1}{2})\frac{3}{2}, 0]}^{\frac{3+}{2}, 00} & \mathcal{G}_2(k_i)U_{[(2, \frac{1}{2})\frac{3}{2}, 0], [(1, \frac{1}{2})\frac{1}{2}, 1]}^{\frac{3+}{2}, 0N_1} & \mathcal{G}_2(k_i)U_{[(2, \frac{1}{2})\frac{3}{2}, 0], [(1, \frac{1}{2})\frac{3}{2}, 1]}^{\frac{3+}{2}, 0N_1} & \dots & \mathcal{G}_2(k_i)U_{[(2, \frac{1}{2})\frac{3}{2}, 0], [(4, \frac{1}{2})\frac{7}{2}, 2]}^{\frac{3+}{2}, 0N_2} \\ \mathcal{G}_1(k_1)U_{[(1, \frac{1}{2})\frac{1}{2}, 1], [(2, \frac{1}{2})\frac{3}{2}, 0]}^{\frac{3+}{2}, N_10} & \mathcal{G}_1(k_1)U_{[(1, \frac{1}{2})\frac{1}{2}, 1], [(1, \frac{1}{2})\frac{1}{2}, 1]}^{\frac{3+}{2}, N_1N_1} & \mathcal{G}_1(k_1)U_{[(1, \frac{1}{2})\frac{1}{2}, 1], [(1, \frac{1}{2})\frac{3}{2}, 1]}^{\frac{3+}{2}, N_1N_1} & \dots & \mathcal{G}_1(k_1)U_{[(1, \frac{1}{2})\frac{1}{2}, 1], [(4, \frac{1}{2})\frac{7}{2}, 2]}^{\frac{3+}{2}, N_1N_2} \\ \dots & \dots & \dots & \dots & \dots \\ \dots & \dots & \dots & \dots & \dots \\ \mathcal{G}_0(k_2)U_{[(0, \frac{1}{2})\frac{1}{2}, 2], [(2, \frac{1}{2})\frac{3}{2}, 0]}^{\frac{3+}{2}, N_20} & \mathcal{G}_0(k_2)U_{[(0, \frac{1}{2})\frac{1}{2}, 2], [(1, \frac{1}{2})\frac{1}{2}, 1]}^{\frac{3+}{2}, N_2N_1} & \mathcal{G}_0(k_2)U_{[(0, \frac{1}{2})\frac{1}{2}, 2], [(1, \frac{1}{2})\frac{3}{2}, 1]}^{\frac{3+}{2}, N_2N_1} & \dots & \mathcal{G}_0(k_2)U_{[(0, \frac{1}{2})\frac{1}{2}, 2], [(4, \frac{1}{2})\frac{7}{2}, 2]}^{\frac{3+}{2}, N_2N_2} \\ \dots & \dots & \dots & \dots & \dots \\ \mathcal{G}_4(k_2)U_{[(4, \frac{1}{2})\frac{7}{2}, 2], [(2, \frac{1}{2})\frac{3}{2}, 0]}^{\frac{3+}{2}, N_20} & \mathcal{G}_4(k_2)U_{[(4, \frac{1}{2})\frac{7}{2}, 2], [(1, \frac{1}{2})\frac{1}{2}, 1]}^{\frac{3+}{2}, N_2N_1} & \mathcal{G}_4(k_2)U_{[(4, \frac{1}{2})\frac{7}{2}, 2], [(1, \frac{1}{2})\frac{3}{2}, 1]}^{\frac{3+}{2}, N_2N_1} & \dots & \mathcal{G}_4(k_2)U_{[(4, \frac{1}{2})\frac{7}{2}, 2], [(4, \frac{1}{2})\frac{7}{2}, 2]}^{\frac{3+}{2}, N_2N_2} \end{pmatrix}^{-1} \begin{pmatrix} \overline{F_2^0} \\ \overline{k_i} \\ 0 \\ 0 \\ 0 \\ 0 \\ \dots \\ 0 \end{pmatrix} \quad (5.2.7)$$

The consequence of having such large matrix equations to solve is that time cost can become prohibitive. In order to tackle this issue, ECANOL can use routines of the LAPACK library and we wrote the code so that including the use of SCALAPACK is possible. The code can, in principle, be adapted to supercomputers. For the moment, ECANOL contains one matrix inversion routine written by our collaborator that can be used directly (without any library), one matrix inversion routine that uses the LAPACK library and one routine that, instead of compute the matrix inverse, solves the linear system of equations which consumes much less computation time. This later choice is thus the default option.

Once the linear system is solved, the solution wave functions are then used to compute the S matrix following equation (2.5.16). The T matrix and phase shifts are also calculated following:

$$\begin{aligned} T &= \frac{S - 1}{2i} \\ \delta &= \frac{\ln(S)}{2i} \end{aligned} \tag{5.2.8}$$

which can be compared to values given by the codes ECIS-06 and DWBA98. Finally, the total, elastic and reaction cross sections are computed using relations:

$$\begin{aligned} \sigma_{\text{total}} &= \frac{\pi}{k_0^2} \sum_{Ij'l'jl} (2I + 1) (1 - \text{Re}(S_{[(l'\frac{1}{2})j', J_0][(l\frac{1}{2})j, J_0]}^I)) \\ \sigma_{\text{elastic}} &= \frac{\pi}{k_0^2} \sum_{Ij'l'jl} \frac{2I + 1}{2} |1 - S_{[(l'\frac{1}{2})j', J_0][(l\frac{1}{2})j, J_0]}^I|^2 \\ \sigma_{\text{reaction}} &= \frac{\pi}{k_0^2} \sum_{Ij'l'jl} \frac{2I + 1}{2} (1 - |S_{[(l'\frac{1}{2})j', J_0][(l\frac{1}{2})j, J_0]}^I|^2) \end{aligned} \tag{5.2.9}$$

with I the total angular momentum, S the scattering matrix, k_0 the wave number of the elastic channel. These are Blatt-Biedenharn [100] factors that can be found in every textbook about nuclear reactions. And after these observables are computed, the angular distributions are computed using formulae (2.5.14) and (2.5.15). Moreover, we have written our own routines for the computation of Legendre polynomials and spherical harmonics. Clebsch-Gordan coefficients appearing in equation (2.5.14) are computed with the C++ routine we mentioned earlier. The treatment of the Coulomb part of the nucleon-nucleus potential is a critical point and is not straightforward when the nucleus is deformed. We mentioned in section 3.3 that it is possible to separate a long-range, deformed Coulomb potential into a short range deformed part and a long-range spherical part as shown through equations (3.3.1), (3.3.2), (3.3.3) and (3.3.5). ECANOL inherited this feature from HYDRA, the code written by Arellano, which makes it suitable also for the study of proton-induced reactions on deformed nuclei with (for the moment) a spherical Coulomb field.

As required in the specifications for the code, ECANOL follows a simple series of equations and can be read directly in parallel with its user's manual. But despite the apparent simplicity, the physics involved in the program are not trivial and the validation of such a code required a lot of careful verifications and comparisons with the codes ECIS-06 and DWBA98. We present next the validation process we followed for ECANOL in the case of DWBA and CC calculations.

5.3 Validation of ECANOL

It was not possible to do a direct validation of ECANOL in the CC framework using nonlocal potentials because we did not have the tools required for this: nonlocal coupling potentials for inelastic channels and a CC code for nonlocal potentials. So instead we validated our code step-by-step. First, we validated elastic scattering: in the case of a local potential parameterized as a complex Woods-Saxon form, we calculated and validated the S matrix, angular distribution and total cross section by comparison to the results yielded by the ECIS-06 code.

For a microscopic nonlocal potential, we first compared the potential obtained from our code MINOLOP to the one extracted from the DWBA98 code. Then, we compared the T matrix elements and the cross sections calculated by ECANOL to those computed with the DWBA98 code.

The case of inelastic scattering was not as straightforward as the elastic scattering case, partly because we couldn't extract the nonlocal part of transition potentials computed by the code DWBA98. First, we validated our calculations in the case of a macroscopic, local potential by comparing our results to the code ECIS-06, for both CC and DWBA calculations.

For microscopic transition potentials, we were able to compare the direct part of these potentials calculated by MINOLOP to that extracted from the DWBA98 code, in the case of a transition from the ground state to an excited state. We then compared the scattering observables calculated by ECANOL to those computed with DWBA98. We then fitted the parameters for a macroscopic model so that it reproduces approximately the direct part of our microscopic transition potentials, and compared the cross sections calculated by ECANOL in the CC framework (using the microscopic potentials) to those calculated by ECIS-06 using the fitted macroscopic potentials.

Finally, we compared angular distributions for inelastic scattering calculated by ECANOL (using microscopic nonlocal potentials) to the results yielded by the DWBA98 code.

Because of the structure of the matrix equation displayed on p 35, which is solved by the code ECANOL, it is possible to do a full CC calculation by considering all the coupling potentials, or to neglect the terms that are above the diagonal part (the top-right part of the matrix) which leads to an approximate calculation that differs little from the usual DWBA. We validated ECANOL and the microscopic potentials for inelastic scattering in the limit of the DWBA, but we estimated that this validation also stands for a CC calculation. Furthermore, we have checked in ECANOL that when the coupling potentials are small, the DWBA calculation gives results that converge to those done in the CC framework.

In the following, we give details regarding several aspects of the validations we just described.

5.3.1 The vibrational model

We derive here formulae for potentials that we used for our comparisons to ECIS-06 in the case of elastic and inelastic scattering with local potentials. Details concerning the derivation of the vibrational model can be found in references [101] and [102]. Conceptually, the vibrational model is a macroscopic description of some nuclear collective excitations

that make the nucleus “vibrate” (in a classical mechanics point of view). The nucleus in the ground state is described by a liquid drop in its equilibrium shape, and can thus be described in terms of macroscopic quantities such as incompressibility, surface tension and so on. Its excited states can be compression modes or surface vibration modes. In the case of surface vibrations, the model assumes that the surface of the nucleus oscillates around a mean, spherical (or deformed) shape in a small-amplitude harmonic vibration. From this hypothesis, the surface of the nucleus can be expanded in terms of spherical harmonics and a nuclear density (and therefore a nuclear potential) can be derived from these simple assumptions.

The real part of the optical potential is assumed to follow the shape of the nuclear density of the target in its ground state, which is approximated to a simple Woods-Saxon form. In radial coordinates this means that the real part of the optical potential takes the form (assuming a local potential):

$$U_{\text{optical}}(r) = \frac{V}{1 + e^{\frac{r-R_0A^{\frac{1}{3}}}{a}}} \quad (5.3.1)$$

with V the depth of the potential, R_0 is the mean radius parameter and A the number of nucleons of the target, and finally a the surface thickness. The surface vibrations of the nucleus is characterized by a deformation parameter β_J associated to the amplitude of the vibrations. J is the total spin of the excited state and can be directly associated to the multipolarity of the phonon. With these labels the radial form factor of a transition potential reads:

$$U_{\text{transition}}^J(r) = \frac{i^{-J}\beta_J R_0 A^{\frac{1}{3}}}{\hat{J}} \frac{dU_{\text{optical}}(r)}{dr} = -\frac{i^{-J}\beta_J R_0 A^{\frac{1}{3}}}{\hat{J}} \frac{V e^{\frac{r-R_0A^{\frac{1}{3}}}{a}}}{a(1 + e^{\frac{r-R_0A^{\frac{1}{3}}}{a}})^2} \quad (5.3.2)$$

Following the coupling scheme of equation (2.5.1), we use the macroscopic parameterizations to build potentials for CC calculations as defined in (3.2.3), taking the ground state of the nucleus $|\psi_0 \in 00+\rangle$ and one excited state $|\psi_N \in J_N M_N \Pi_N\rangle$. Following the uncoupling we have shown in section 4.5 for the optical potential of a nucleus with a 0^+ ground state, we can show that with the macroscopic parameterization the optical potential in its coupled form reads:

$$U_{[(\frac{1}{2})j,0^+],[(\frac{1}{2})j,0^+]}^{I,00}(r) = U_{\text{optical}}(r) = \frac{V}{1 + e^{\frac{r-R_0A^{\frac{1}{3}}}{a}}} \quad (5.3.3)$$

For simplicity, we assume that potentials coupling an excited state with itself would be approximated by the optical potential taken at the energy of the outgoing nucleon, with a different set of parameters for the Woods-Saxon density distribution. Furthermore, we take only diagonal terms and neglect off-diagonal terms. In résumé:

$$\begin{aligned} U_{[(\frac{1}{2})j, J_N^{\Pi_N}], [(\frac{1}{2})j, J_N^{\Pi_N}]}^{I, NN}(r) &= U_{[(\frac{1}{2})j, 0^+], [(\frac{1}{2})j, 0^+]}^{I, 00}(r) = U'_{\text{optical}}(r) = \frac{V'}{1 + e^{\frac{r-R'_0A^{\frac{1}{3}}}{a}}} \\ U_{[(\frac{1}{2})j', J_N^{\Pi_N}], [(\frac{1}{2})j, J_N^{\Pi_N}]}^{I, NN}(r) &= 0 \end{aligned} \quad (5.3.4)$$

Of course, we use the same potentials and approximations in ECIS-06. The hypotheses of the vibrational model intervene within our modeling in the derivation of transition potentials. The deformation parameter for this excitation is β_J . Let us derive matrix elements for the transition from this $|N\rangle$ state to the ground state 0^+ of our target nucleus. After simplifying

the first Clebsch-Gordan coefficient of the uncoupling, we obtain

$$U_{[(l'\frac{1}{2})j',0^+],[(l\frac{1}{2})j,J_N^{\Pi N}]}^{I,0N}(r) = \sum_{mM_N} (-)^{2j'+j-J_N+3m'} \widehat{j} \begin{pmatrix} j & J_N & j' \\ m & M_N & -m' \end{pmatrix} \langle j'm' | \langle 00 | U_{\text{transition}}^{J_N}(r) | J_N M_N \rangle | jm \rangle \quad (5.3.5)$$

We need to calculate now $\langle j'm' | \langle 00 | U_{\text{transition}}^{J_N}(r) | J_N M_N \rangle | jm \rangle$:

$$\begin{aligned} \langle j'm' | \langle 00 | U_{\text{transition}}^{J_N}(r) | J_N M_N \rangle | jm \rangle &= U_{\text{transition}}^{J_N}(r) i^{l-l'} \langle \frac{1}{2} l' j' | Y_{M_N}^{J_N}(\theta, \varphi) | \frac{1}{2} l j \rangle \\ &= U_{\text{transition}}^{J_N}(r) i^{l-l'} (-)^{l'+l+1-j'-j} \langle l' \frac{1}{2} j' | Y_{M_N}^{J_N}(\theta, \varphi) | l \frac{1}{2} j \rangle \\ &= U_{\text{transition}}^{J_N}(r) i^{l-l'} (-)^{l'+l+1-j'-j} (-)^{j'-m'} \begin{pmatrix} j' & J_N & j \\ -m' & M_N & m \end{pmatrix} \\ &\quad \langle j' || Y^{J_N} || j \rangle \\ &= U_{\text{transition}}^{J_N}(r) i^{l-l'} (-)^{l'+l+1-j'-j} (-)^{2j'+j+J_N-m'} \\ &\quad \begin{pmatrix} j' & j & J_N \\ -m' & m & M_N \end{pmatrix} \langle j' || Y^{J_N} || j \rangle \end{aligned}$$

in which we used the Wigner-Eckart theorem (F.0.2). Using the formula for spherical harmonic tensor reduced matrix elements (D.1.4), we obtain:

$$\begin{aligned} \langle j'm' | \langle 00 | U_{\text{transition}}^{J_N}(r) | J_N M_N \rangle | jm \rangle &= U_{\text{transition}}^{J_N}(r) i^{l-l'} (-)^{l'+l+1+j'+J-m'} \begin{pmatrix} j' & j & J_N \\ -m' & m & M_N \end{pmatrix} \\ &\quad (-)^{j'-\frac{1}{2}} \frac{\widehat{j'} \widehat{J_N} \widehat{j}}{\sqrt{4\pi}} \begin{pmatrix} j' & J_N & j \\ -\frac{1}{2} & 0 & \frac{1}{2} \end{pmatrix} \frac{1 + (-)^{l'+l+J_N}}{2} \\ &= \frac{\beta_{J_N} R_0 A^{\frac{1}{3}}}{\widehat{J_N}} \frac{dU_{\text{optical}}(r)}{dr} i^{l-l'-J_N} (-)^{l'+l+\frac{1}{2}+2j'+J_N-m'} \\ &\quad \frac{\widehat{j'} \widehat{J_N} \widehat{j}}{\sqrt{4\pi}} \begin{pmatrix} j' & j & J_N \\ -m' & m & M_N \end{pmatrix} \begin{pmatrix} j' & J_N & j \\ -\frac{1}{2} & 0 & \frac{1}{2} \end{pmatrix} \frac{1 + (-)^{l'+l+J_N}}{2} \end{aligned}$$

We insert this result in equation (5.3.5) and reduce the formula:

$$\begin{aligned} U_{[(l'\frac{1}{2})j',0^+],[(l\frac{1}{2})j,J_N^{\Pi N}]}^{I,0N}(r) &= \sum_{mM} (-)^{2j'+j-J_N+3m'} \widehat{j} \begin{pmatrix} j & J_N & j' \\ m & M_N & -m' \end{pmatrix} \frac{\beta_{J_N} R_0 A^{\frac{1}{3}}}{\widehat{J_N}} \frac{dU_{\text{optical}}(r)}{dr} i^{l-l'-J_N} \\ &\quad (-)^{l'+l+\frac{1}{2}+2j'+J_N-m'} \frac{\widehat{j'} \widehat{J_N} \widehat{j}}{\sqrt{4\pi}} \begin{pmatrix} j' & j & J_N \\ -m' & m & M_N \end{pmatrix} \begin{pmatrix} j' & J_N & j \\ -\frac{1}{2} & 0 & \frac{1}{2} \end{pmatrix} \\ &\quad \frac{1 + (-)^{l'+l+J_N}}{2} \\ &= \sum_{mM} (-)^{4j'+j+2m'+l'+l+\frac{1}{2}} \widehat{j}^2 \begin{pmatrix} j & J_N & j' \\ m & M_N & -m' \end{pmatrix}^2 \beta_{J_N} R_0 A^{\frac{1}{3}} \frac{dU_{\text{optical}}(r)}{dr} \\ &\quad i^{l-l'-J_N} \frac{\widehat{j}}{\sqrt{4\pi}} \begin{pmatrix} j' & J_N & j \\ -\frac{1}{2} & 0 & \frac{1}{2} \end{pmatrix} \frac{1 + (-)^{l'+l+J_N}}{2} \\ &= \sum_{mM} (-)^{2j'+j+l'+l+\frac{1}{2}} i^{l-l'-J_N} \widehat{j}^2 \begin{pmatrix} j & J_N & j' \\ m & M_N & -m' \end{pmatrix}^2 \beta_{J_N} R_0 A^{\frac{1}{3}} \frac{dU_{\text{optical}}(r)}{dr} \\ &\quad \frac{\widehat{j}}{\sqrt{4\pi}} \begin{pmatrix} j' & J_N & j \\ -\frac{1}{2} & 0 & \frac{1}{2} \end{pmatrix} \frac{1 + (-)^{l'+l+J_N}}{2} \end{aligned}$$

Finally, we apply the closure relation of Wigner 3J coefficients to simplify the formula of the transition potential derived with the vibrational model:

$$U_{[(l'\frac{1}{2})j',0^+],[(l\frac{1}{2})j,J_N^{\Pi N}]}^{I,0N}(r) = (-)^{j-\frac{1}{2}+l'+l+\frac{l-l'-J_N}{2}} \frac{\beta_{J_N} R_0 A^{\frac{1}{3}} \widehat{j}}{\sqrt{4\pi}} \frac{dU_{\text{optical}}(r)}{dr} \begin{pmatrix} j' & J_N & j \\ -\frac{1}{2} & 0 & \frac{1}{2} \end{pmatrix} \frac{1+(-)^{l'+l+J_N}}{2} \quad (5.3.6)$$

Using the same techniques, we obtain the potential for the inverse transition:

$$U_{[(l'\frac{1}{2})j',J_N^{\Pi N}],[(l\frac{1}{2})j,0^+]}^{I,0N}(r) = (-)^{j'-\frac{1}{2}+l'+l+\frac{l-l'-J_N}{2}} \frac{\beta_{J_N} R_0 A^{\frac{1}{3}} \widehat{j}}{\sqrt{4\pi}} \frac{dU_{\text{optical}}(r)}{dr} \begin{pmatrix} j' & J_N & j \\ -\frac{1}{2} & 0 & \frac{1}{2} \end{pmatrix} \frac{1+(-)^{l'+l+J_N}}{2} \quad (5.3.7)$$

We have included in ECANOL routines that compute these simple formulae so that the central part of potentials derived with the vibrational model can be used without giving any file to the program. Parameters (volume and surface depths V , thickness a , mean radius R_0 , deformation parameter β_J are to be given in the input file of ECANOL.

5.3.2 Validation of ECANOL for local potentials by comparison to ECIS-06

Within CC and DWBA frameworks, we computed cross sections and angular distributions for neutron induced elastic and inelastic scattering to one excited state on ^{208}Pb with both ECANOL and ECIS-06 and compared the results of the two codes. We imposed for both codes the same set of parameters for the model and studied, first, the convergence of ECIS-06, our purpose being to define a good reference. In order to do so, we had to define a maximum radius and a step size (thus, a meshing of the space). We began by using a very small step size $h = 0.01$ fm and varying the maximum radius of the calculation. ^{208}Pb has a mean radius of about 8 fm, so we expected to have a good convergence of the computation for maximum radii above 15 fm. Our results are gathered on figure 5.3. The results displayed correspond to a CC calculation. The same calculations done in DWBA converge similarly so we do not show them.

For a maximum radius of 10 fm, we see that the computation is not enough converged, because the matching of the computed wave function to the asymptotic solution is too close to the area of interaction. Therefore the hypothesis that led to equation (2.4.9) is no longer valid and this explains the insufficient convergence of the calculation. When we set the maximum radius to 15 fm, we obtain a much better convergence, with an average relative difference of about 10^{-6} . This kind of precision is enough to have a good confidence in the convergence of the calculation and can make a good comparison basis to validate ECANOL, but we see that for a maximum radius of 20 fm, the relative difference to the reference computation is close to the order of magnitude of the computer's precision. The calculation with a maximum radius of 20 fm does not - within the limits of our test - cost much more time than in the 15 fm case. Therefore, we have chosen to do our validation of ECANOL by fixing the maximum radius at 20 fm.

Secondly, we needed to see how the convergence of the calculation evolves when the step size is modified. In the notice of ECIS-06, it is indicated that the code computes angular distribution with an error of about h^4 , h being the step size. So we made a series of calculations with the same input as before, and varying the step size. Our results are drawn on figure 5.4.

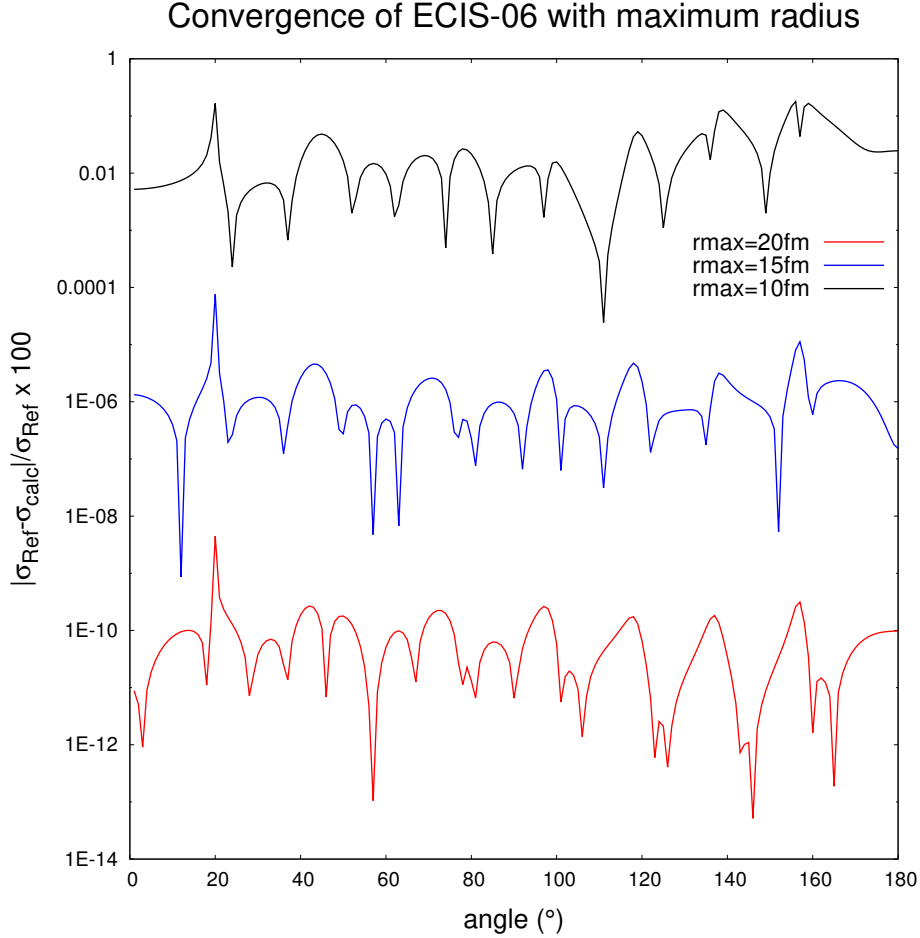


Figure 5.3: Relative difference between the angular distribution of a (n,n) reaction on ^{208}Pb computed by ECIS-06 with a given maximum radius r_{max} , and the reference with $r_{\text{max}}=25$ fm. The incident energy is 40 MeV.

In the case where $h = 0.5$ fm, the average relative difference to the reference calculation is around 10^{-2} which is close to the average value of $h^4 = 0.0625$ one would expect. Experimental cross sections and angular distributions are rarely given with a precision of 5% so, in principle, a step size of 0.5 fm could be used for practical calculations. But we see that with $h = 0.2$ fm, which does not imply a much bigger time cost when only 1 excited state is considered, the average precision is improved by a factor 10 and the relative difference to the reference calculation never reaches 1% which means this value is clearly satisfactory for practical computations. The case where $h = 0.05$ fm is interesting to see because the average relative difference to the reference calculation is very close to its theoretical value, $h^4 = 6.25 \times 10^{-6}$. But this precision requires too much computation time to make large scale studies like an application we will detail later. Thus, a good value for the step size with ECIS-06 is 0.2 fm. We would like to mention here that there are no such recommendations in the notice of ECIS-06 or other versions of this code. This work done on an already existing and widely used code as ECIS-06 was necessary to us, for it helped us define a good reference to validate our new code ECANOL, and the recommendations we follow in this Ph.D. work are also valid for any other study involving the use of Raynal's code.

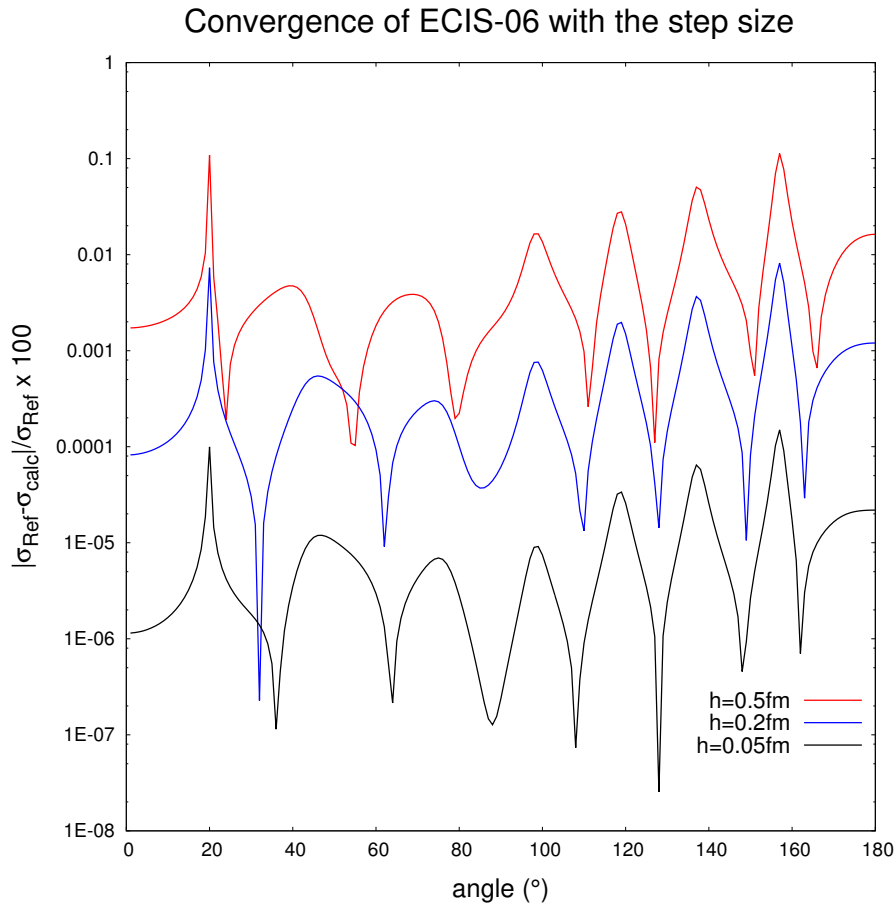


Figure 5.4: Relative difference between the angular distribution of a (n,n) reaction on ^{208}Pb computed by ECIS-06 with $r_{\text{max}}=20$ fm, for various values of the step size. The reference calculation is with $h=0.01$ fm, and the incident energy is 40 MeV.

The third and last step in the validation of ECANOL for local, macroscopic potentials is to compute cross sections and angular distributions with it and compare the results to those obtained with ECIS-06. ECANOL uses the same integration method for equation (3.3.7) as that of ECIS-06 but the method to solve the linear system of equations is different. However, the results of the calculations with ECANOL are very similar to those done with ECIS-06 as shown on figure 5.5. When the step size is equal to 0.5 fm, the average precision is consistent with the theoretical value. The large first peak is located at a minimum of the angular distribution, and the cross section at this angle is very low so the large relative difference between the two code here should not be a big concern.

But if we want to have a computation with a precision always better than 1%, without being too costly in terms of computation time, then again a step size of 0.2 fm seems to be reasonable. It is interesting to notice again here that what we observed in ECIS regarding the precision of the calculation with $h = 0.5$ fm is also true for a calculation done with ECANOL. The two codes use quite different methods to solve the CC equations (in ECIS we used the iterative calculation based on the modified Numerov method, while in ECANOL we solve a linear system) ; their main common point is the integration method for equation (3.3.7) which shows this particular point in the numerical calculation is critical.

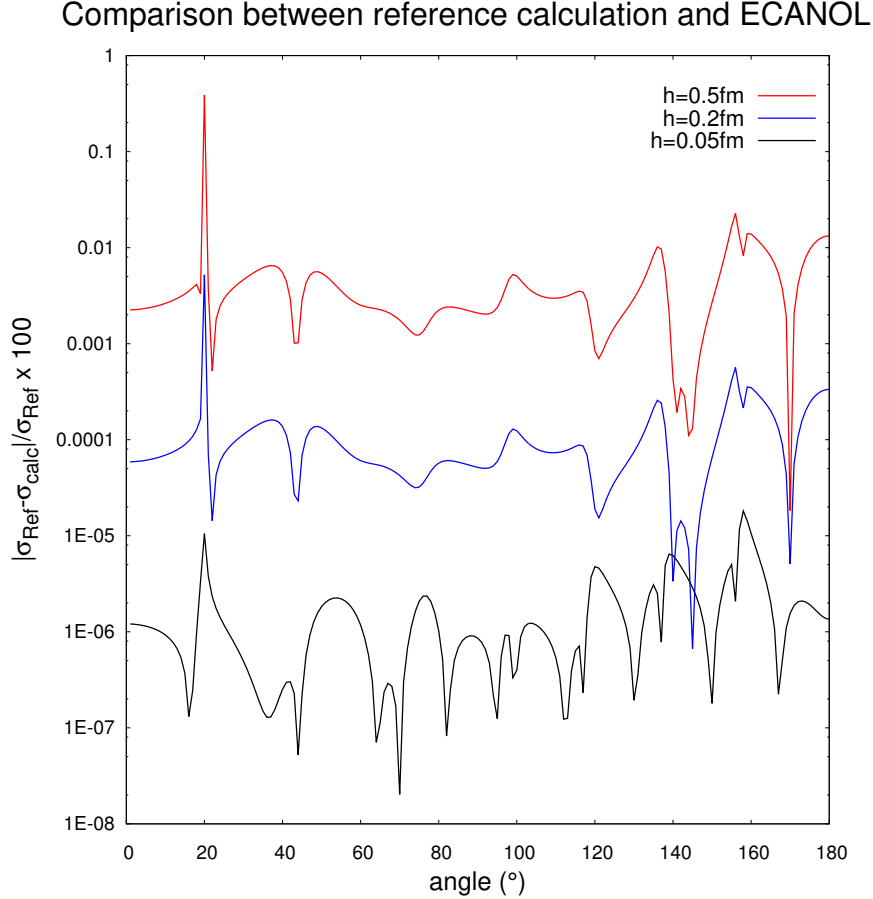


Figure 5.5: Relative difference between the reference angular distribution of a (n,n) reaction on ^{208}Pb computed by ECIS-06 with $r_{\text{max}}=20\text{fm}$ and $h=0.01\text{fm}$, and ECANOL calculations for various step sizes. The incident energy is 40 MeV.

After establishing properly a reference calculation done with ECIS-06, we have used it to validate ECANOL for elastic and inelastic scattering with local potentials in both the DWBA and the CC frameworks. The next step was to validate ECANOL in the case of elastic scattering with nonlocal potentials, then in the case of inelastic scattering also with nonlocal potentials.

5.3.3 Validation of both ECANOL and MINOLOP for nonlocal potentials by comparison to the DWBA98 code

In order to validate our derivations and the MINOLOP code, we have extracted from the DWBA98 code both the direct and the exchange terms of the optical potential it computes, which makes a very good qualification basis. On figure 5.6, an example is given of an optical potential computed with MINOLOP and compared to what we've extracted from DWBA98. The target nucleus is ^{208}Pb , and only the central part of the NN effective interaction was used for this calculation. On the up left panel, a comparison of the real part of the direct component of the optical potential computed by both codes is shown. On the up right panel, the same comparison is done for the imaginary part of the direct component of the optical potential. On the bottom left panel, we plotted the real part of the nonlocal term of the

optical potential and on the right panel we plotted its imaginary part. In both cases, we fixed the value of the radius $r = 5$ fm and we plotted the curves as functions of r' .

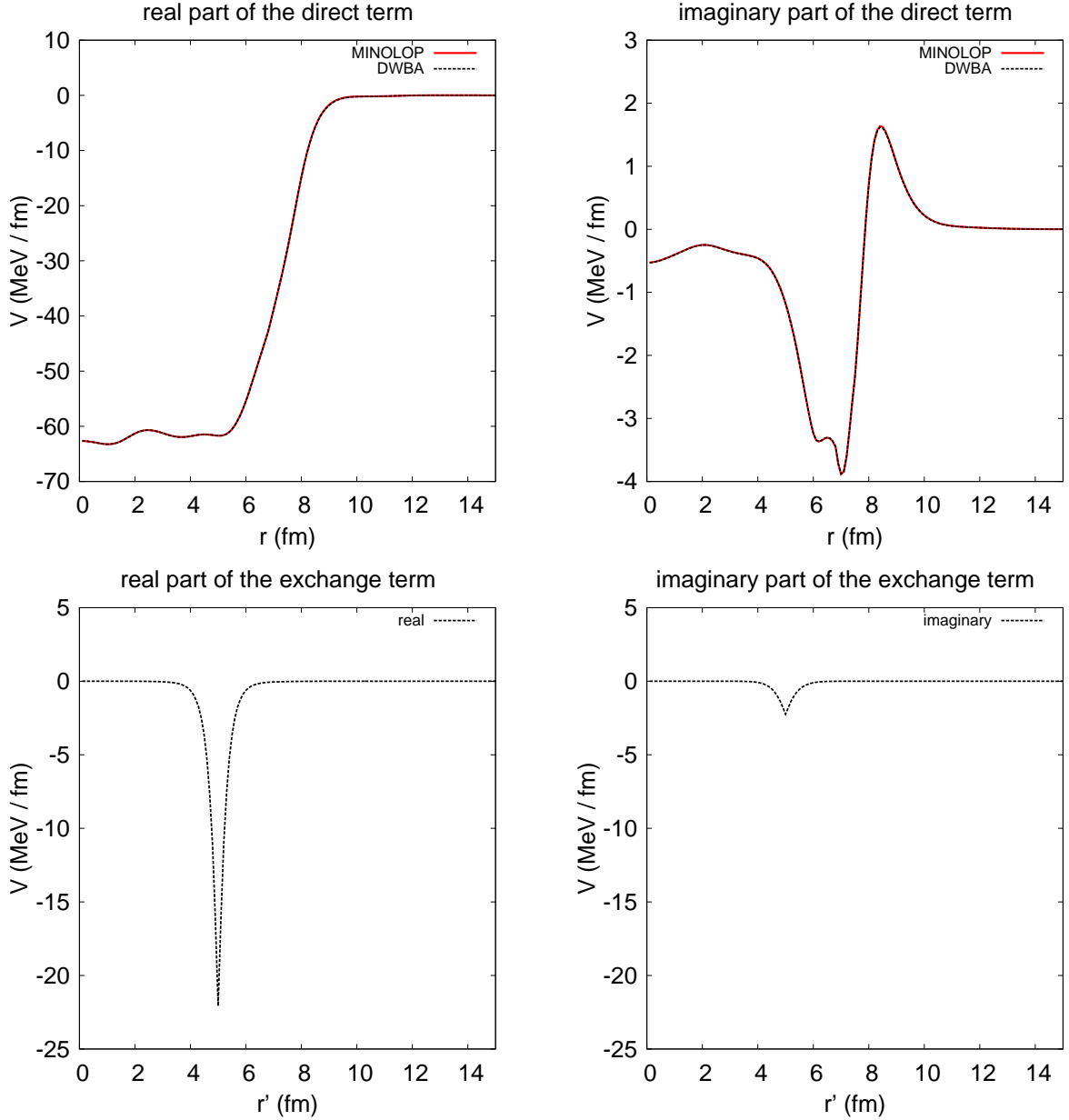


Figure 5.6: Plot of the optical potential for the reaction (n,n) on ^{208}Pb at an incident energy of 40 MeV in the lab frame, as computed by MINOLOP code. On the upper panels for the direct term, the same calculation done with DWBA code is displayed in red for comparison. The exchange term in the bottom panels is for $r = 5$ fm and for partial waves $\{j,l\} = \{\frac{3}{2}, 1\}$

The relative difference between the potentials computed by the two codes is of the order of the numerical precision of the computer (10^{-13}) for both the direct and the exchange part. Thanks to this comparison, it was possible to validate quantitatively our code MINOLOP in the case of the optical potential for a target nucleus with a 0^+ ground state. Therefore, we were able to use this optical potential in ECANOL to validate it for elastic scattering with

nonlocal potentials. We made calculations for elastic scattering of a neutron on ^{208}Pb and on ^{90}Zr at different incident energies and compared our results with DWBA98. An example is shown on figure 5.7: we computed the elastic scattering of a neutron with 40 MeV of incident energy on a ^{90}Zr target in its ground state, using the microscopic nonlocal optical potential calculated by MINOLOP. The agreement between the two codes is excellent: less than 0.1% relative difference. The average relative difference is less than 0.02%. This comparison validates ECANOL for nucleon-nucleus elastic scattering with nonlocal potentials.

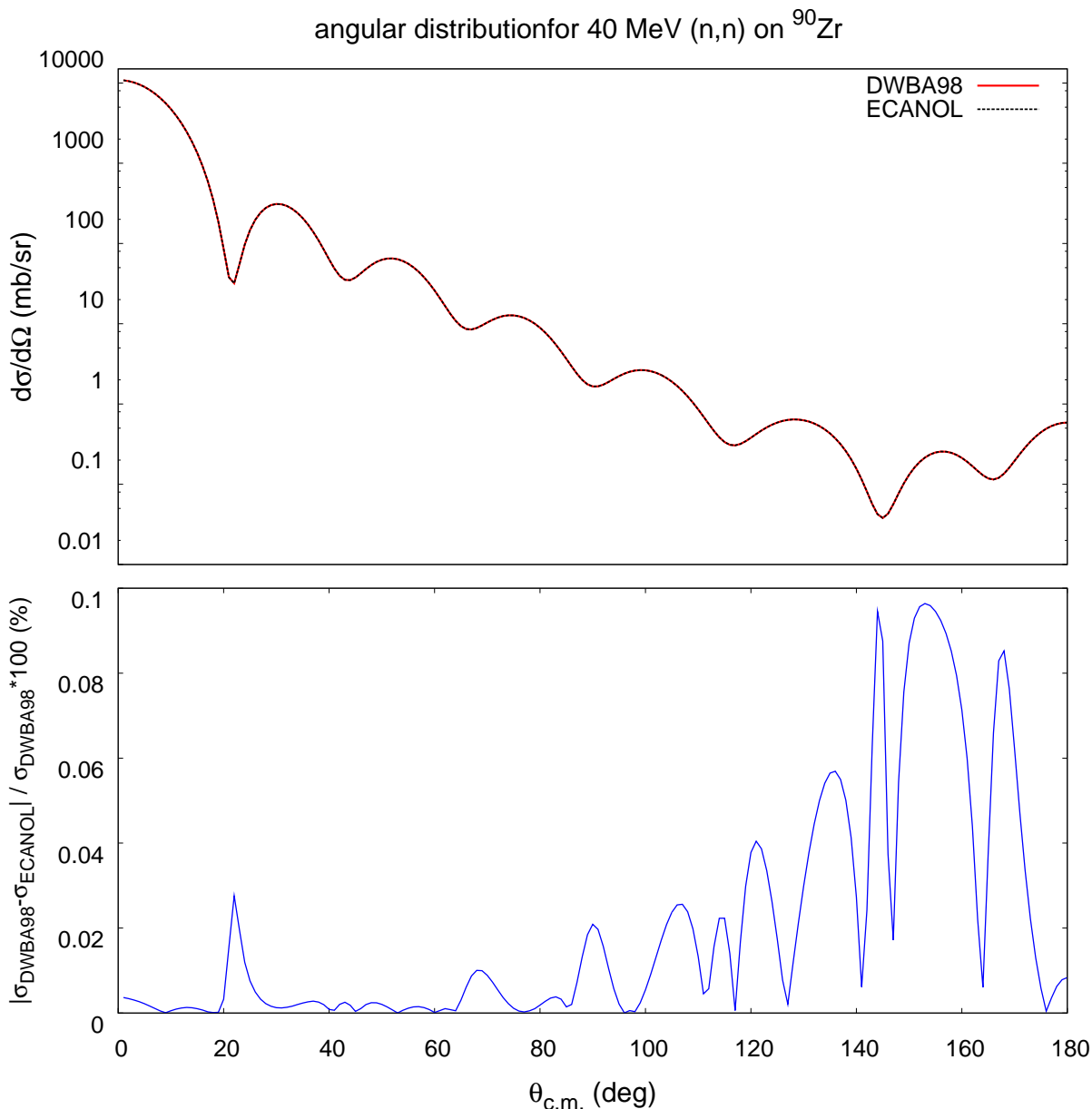


Figure 5.7: Angular distribution and relative difference between the computation done by DWBA98 and our codes for neutron elastic scattering on ^{90}Zr . The maximum radius and the step size used in both codes are $r_{\text{max}}=15$ fm and $h=0.2$ fm.

In the case of inelastic scattering we were unable to extract the nonlocal transition potentials from DWBA98, therefore we could not validate nonlocal potentials obtained with MINOLOP by direct comparison. But we managed to extract from the code DWBA98 the direct part of potentials for a transition from the ground state to an excited state. Formally, by using formulae (4.6.7) and (4.6.12), we can replace $|N_i \in J_i \Pi_i M_i\rangle$ by the ground state $|0^+\rangle$ and use the results given in (4.4.22) to derive the formulae of the transition potentials. We have done this work, and we summarize the result as:

$$\begin{aligned}
 U_{[(l'\frac{1}{2})j',J_f],[(l\frac{1}{2})j,0]}^{I,f0}(r,r')_{\text{direct}} &= \sum_{\bar{\alpha}\bar{\beta}J'k} (-)^{j'-j_\alpha-J'-1} \begin{Bmatrix} j & j' & J_f \\ j_\alpha & j_\beta & J' \end{Bmatrix} i^{l_\beta-l_\alpha+l-l'} (j' j_\alpha J' | V_{\text{eff}}^k | j j_\beta J') \\
 &\quad Z_{\alpha\beta}^{N_f} \frac{\widehat{J}_f \widehat{J}'^2}{\widehat{j}} \frac{\delta(r-r')}{rr'} \int \phi_{n_\alpha j_\alpha l_\alpha}(r_2) V_{\text{eff}}^k(r, r_2) \phi_\beta(r_2) r_2^2 dr_2 \\
 U_{[(l'\frac{1}{2})j',J_f],[(l\frac{1}{2})j,0]}^{I,f0}(r,r')_{\text{exchange}} &= \sum_{\bar{\alpha}\bar{\beta}J'k} (-)^{j'+j-j_\alpha-j_\beta} \begin{Bmatrix} j & j' & J_f \\ j_\alpha & j_\beta & J' \end{Bmatrix} i^{l_\beta-l_\alpha+l-l'} (j' j_\alpha J' | V_{\text{eff}}^k | j_\beta j J') \\
 &\quad Z_{\alpha\beta}^{N_f} \frac{\widehat{J}_f \widehat{J}'^2}{\widehat{j}} \phi_{n_\alpha j_\alpha l_\alpha}(r') V_{\text{eff}}^k(r, r') \phi_{n_\beta j_\beta l_\beta}(r)
 \end{aligned} \tag{5.3.8}$$

So it was possible to validate (as a first step) the direct term of microscopic nonlocal potentials for inelastic scattering computed by MINOLOP by comparison to the DWBA98 code. Then, we were able to validate inelastic scattering with these potentials. We put the direct term of these potentials calculated with MINOLOP and used it in ECANOL. We then compared our result to the same calculation made with DWBA98. This comparison yields similar results (for the angular distribution) to the elastic scattering case displayed on figure 5.7. But it was possible to push further the validation by using the work done on ECIS-06: we could fit macroscopic parameters of the vibrational model so as to reproduce a part of the direct term of potentials computed by MINOLOP, and then compare predictions of ECANOL and ECIS-06. We show next how the formulae for microscopic and macroscopic potentials can be compared and describe the result of our comparison.

Starting from equation (5.3.8), we insert the geometric matrix elements for a central, spin independent interaction that we derived in Appendix D.1, use the Racah algebra to simplify the formula and write it in a such a way that we will be able to compare it with macroscopic transition potentials and identify transition densities. First, we insert (D.1.6) in the direct part given in equation (5.3.8):

$$\begin{aligned}
 U_{[(l'\frac{1}{2})j',J^\Pi],[(l\frac{1}{2})j,0^+]}^{I,N0}(r,r')_{\text{direct}} &= \sum_{\bar{\alpha}\bar{\beta}J'k} (-)^{j'-j_\alpha-J'-1} \begin{Bmatrix} j & j' & J \\ j_\alpha & j_\beta & J' \end{Bmatrix} i^{l_\beta-l_\alpha+l-l'} Z_{\alpha\beta}^N \frac{\widehat{j}' \widehat{j} \widehat{j}_\alpha \widehat{j}_\beta \widehat{J} \widehat{J}'^2}{\widehat{j}} \\
 &\quad (-)^{j_\alpha+2j+j_\beta+J'-l'-l-l_\alpha-l_\beta-1} \begin{Bmatrix} j' & j_\alpha & J' \\ j_\beta & j & k \end{Bmatrix} \begin{pmatrix} j' & k & j \\ -\frac{1}{2} & 0 & \frac{1}{2} \end{pmatrix} \\
 &\quad \begin{pmatrix} j_\alpha & k & j_\beta \\ -\frac{1}{2} & 0 & \frac{1}{2} \end{pmatrix} \frac{1 + (-)^{l'+l+k}}{2} \frac{1 + (-)^{l_\alpha+l_\beta+k}}{2} \frac{\delta(r-r')}{rr'} \\
 &\quad \int \phi_{n_\alpha j_\alpha l_\alpha}(r_2) V_{\text{eff}}^k(r, r_2) \phi_{n_\beta j_\beta l_\beta}(r_2) r_2^2 dr_2
 \end{aligned}$$

$$\begin{aligned}
 U_{[(l'\frac{1}{2})j',J^{\text{II}}],[(l\frac{1}{2})j,0^+]}^{I,N0}(r,r')_{\text{direct}} &= \sum_{\bar{\alpha}\bar{\beta}J'k} (-)^{j'+2j+j\beta-l'-l-l_{\alpha}-l_{\beta}j'l_{\beta}-l_{\alpha}+l-l'} Z_{\alpha\beta}^N \widehat{J}'^2 \widehat{j}' \widehat{j}_{\alpha} \widehat{j}_{\beta} \widehat{J} \\
 &\quad \left\{ \begin{matrix} j & j' & J \\ j_{\alpha} & j_{\beta} & J' \end{matrix} \right\} \left\{ \begin{matrix} j & j' & k \\ j_{\alpha} & j_{\beta} & J' \end{matrix} \right\} \begin{pmatrix} j' & k & j \\ -\frac{1}{2} & 0 & \frac{1}{2} \end{pmatrix} \begin{pmatrix} j_{\alpha} & k & j_{\beta} \\ -\frac{1}{2} & 0 & \frac{1}{2} \end{pmatrix} \\
 &\quad \frac{1 + (-)^{l'+l+k}}{2} \frac{1 + (-)^{l_{\alpha}+l_{\beta}+k}}{2} \frac{\delta(r-r')}{rr'} \\
 &\quad \int \phi_{n_{\alpha}j_{\alpha}l_{\alpha}}(r_2) V_{\text{eff}}^k(r, r_2) \phi_{n_{\beta}j_{\beta}l_{\beta}}(r_2) r_2^2 dr_2
 \end{aligned}$$

in which we used the symmetries of Wigner 6J coefficients. We use the closure relation on these coefficients (A.0.14) to simplify the formula:

$$\begin{aligned}
 U_{[(l'\frac{1}{2})j',J^{\text{II}}],[(l\frac{1}{2})j,0^+]}^{I,N0}(r,r')_{\text{direct}} &= \sum_{\bar{\alpha}\bar{\beta}} (-)^{j'+2j+j\beta-l'-l-l_{\alpha}-l_{\beta}j'l_{\beta}-l_{\alpha}+l-l'} \frac{Z_{\alpha\beta}^N \widehat{J}' \widehat{j}_{\alpha} \widehat{j}_{\beta}}{\widehat{J}} \begin{pmatrix} j' & J & j \\ -\frac{1}{2} & 0 & \frac{1}{2} \end{pmatrix} \\
 &\quad \begin{pmatrix} j_{\alpha} & J & j_{\beta} \\ -\frac{1}{2} & 0 & \frac{1}{2} \end{pmatrix} \frac{1 + (-)^{l'+l+J}}{2} \frac{1 + (-)^{l_{\alpha}+l_{\beta}+J}}{2} \frac{\delta(r-r')}{rr'} \\
 &\quad \int \phi_{n_{\alpha}j_{\alpha}l_{\alpha}}(r_2) V_{\text{eff}}^J(r, r_2) \phi_{n_{\beta}j_{\beta}l_{\beta}}(r_2) r_2^2 dr_2
 \end{aligned}$$

and we reorder this expression so as to separate terms that depend exclusively on the target's structure from other geometric terms:

$$\begin{aligned}
 U_{[(l'\frac{1}{2})j',J^{\text{II}}],[(l\frac{1}{2})j,0^+]}^{I,N0}(r,r')_{\text{direct}} &= (-)^{j'+\frac{1}{2}-l'-l+\frac{l-l'}{2}} \widehat{j}' \begin{pmatrix} j' & J & j \\ -\frac{1}{2} & 0 & \frac{1}{2} \end{pmatrix} \frac{1 + (-)^{l'+l+J}}{2} \times \\
 &\quad \sum_{\bar{\alpha}\bar{\beta}} (-)^{j_{\beta}+\frac{1}{2}-l_{\alpha}-l_{\beta}+\frac{l_{\beta}-l_{\alpha}}{2}} \frac{Z_{\alpha\beta}^N \widehat{j}_{\alpha} \widehat{j}_{\beta}}{\widehat{J}} \begin{pmatrix} j_{\alpha} & J & j_{\beta} \\ -\frac{1}{2} & 0 & \frac{1}{2} \end{pmatrix} \frac{1 + (-)^{l_{\alpha}+l_{\beta}+J}}{2} \\
 &\quad \frac{\delta(r-r')}{rr'} \int \phi_{n_{\alpha}j_{\alpha}l_{\alpha}}(r_2) V_{\text{eff}}^J(r, r_2) \phi_{n_{\beta}j_{\beta}l_{\beta}}(r_2) r_2^2 dr_2
 \end{aligned}$$

which can also be written as:

$$\begin{aligned}
 U_{[(l'\frac{1}{2})j',J^{\text{II}}],[(l\frac{1}{2})j,0^+]}^{I,N0}(r,r')_{\text{direct}} &= (-)^{j'+\frac{1}{2}-l'-l+\frac{l-l'-J}{2}} \widehat{j}' \begin{pmatrix} j' & J & j \\ -\frac{1}{2} & 0 & \frac{1}{2} \end{pmatrix} \frac{1 + (-)^{l'+l+J}}{2} \times \\
 &\quad \sum_{\bar{\alpha}\bar{\beta}} (-)^{j_{\beta}+\frac{1}{2}-l_{\alpha}-l_{\beta}+\frac{l_{\beta}-l_{\alpha}+J}{2}} \frac{Z_{\alpha\beta}^N \widehat{j}_{\alpha} \widehat{j}_{\beta}}{\widehat{J}} \begin{pmatrix} j_{\alpha} & J & j_{\beta} \\ -\frac{1}{2} & 0 & \frac{1}{2} \end{pmatrix} \frac{1 + (-)^{l_{\alpha}+l_{\beta}+J}}{2} \\
 &\quad \frac{\delta(r-r')}{rr'} \int \phi_{n_{\alpha}j_{\alpha}l_{\alpha}}(r_2) V_{\text{eff}}^J(r, r_2) \phi_{n_{\beta}j_{\beta}l_{\beta}}(r_2) r_2^2 dr_2
 \end{aligned} \tag{5.3.9}$$

and if we do the same manipulation for equation (5.3.7), that is, for the potential derived with the vibrational model we obtain:

$$\begin{aligned}
 U_{[(l'\frac{1}{2})j',J^{\text{II}}],[(l\frac{1}{2})j,0^+]}^{I,N0}(r) &= (-)^{j'-\frac{1}{2}+l'+l+\frac{l-l'-J}{2}} \widehat{j}' \begin{pmatrix} j' & J & j \\ -\frac{1}{2} & 0 & \frac{1}{2} \end{pmatrix} \frac{1 + (-)^{l'+l+J}}{2} \times \\
 &\quad \frac{\beta_J R_0 A^{\frac{1}{3}}}{\sqrt{4\pi}} \frac{V e^{-\frac{r-R_0 A^{\frac{1}{3}}}{a}}}{a(1 + e^{-\frac{r-R_0 A^{\frac{1}{3}}}{a}})^2}
 \end{aligned} \tag{5.3.10}$$

The comparison of these two formulae shows that there is a direct link that can be made between the macroscopic, vibrational model and a microscopic model. We fitted parameters of the vibrational model so as to reproduce approximately the microscopic potential obtained with the RPA and use this fitted potential in ECIS-06 so as to compute cross sections. We compared the angular distributions computed by each code. Despite a crude fitting procedure, the results yielded by both codes were remarkably close: the relative error is around a few percents which completes the validation of MINOLOP for local, microscopic transition potentials.

The last step is the validation of MINOLOP for the exchange term of coupling potentials and ECANOL for inelastic scattering with nonlocal potentials. Since we did not have a basis to validate the nonlocal part of potentials computed with MINOLOP, we had to validate simultaneously potentials and ECANOL. We made a calculation for the first 5^- state in ^{90}Zr at 40 MeV of incident energy with the full central part of the nonlocal coupling potential. The comparison to DWBA98 is presented on figure 5.8. Both calculations are close, the shapes are identical as well as amplitudes. At very forward angles, there is a big discrepancy that is not understood yet. In average, the relative error between the two calculations is 3.7% which is acceptable, so finally both MINOLOP and ECANOL are validated for elastic and inelastic scattering with nonlocal potentials in the DWBA limit. In practice, the only difference between a CC and a DWBA calculation for our codes lies in ECANOL: instead of filling all terms of the matrix in equations like (5.2.7), only the diagonal and the bottom left are filled while the top right terms are put to zero. Therefore, the treatment done in ECANOL is exactly the same in CC and in DWBA so now that the code is validated for DWBA it is also validated for CC calculations.

MINOLOP is a new tool to calculate microscopic nonlocal potentials for nucleon-nucleus scattering, and ECANOL is a new code to study direct reactions with nonlocal potentials within the CC as well as the DWBA frameworks. These codes are ready for practical calculations, but their time consumption can still be improved. We give now some indicative values of the time cost for typical calculations made on ^{90}Zr that can be done with them. A single processor Intel[®] Xeon[®] E3-1220 with a frequency of 3.10GHz was used for our tests. In our calculations, the maximum total orbital angular momentum considered is $L_{\text{max}} = 30$ (which means we consider 61 partial waves), the multipole expansion of the Melbourne G matrix is stopped for a maximum pole $k_{\text{max}} = 40$, the maximum radius is $r_{\text{max}} = 15$ fm, the step size is $h = 0.2$ fm.

As for ECANOL, with the same parameters for the calculation, it takes 0.9s to compute elastic scattering, 30s to compute inelastic scattering with only the 5^- excited state, and 120s when considering both the 5^- and the 7^- states. While these time costs are small enough to allow practical applications, it is still possible to speed up the codes to make them even more efficient.

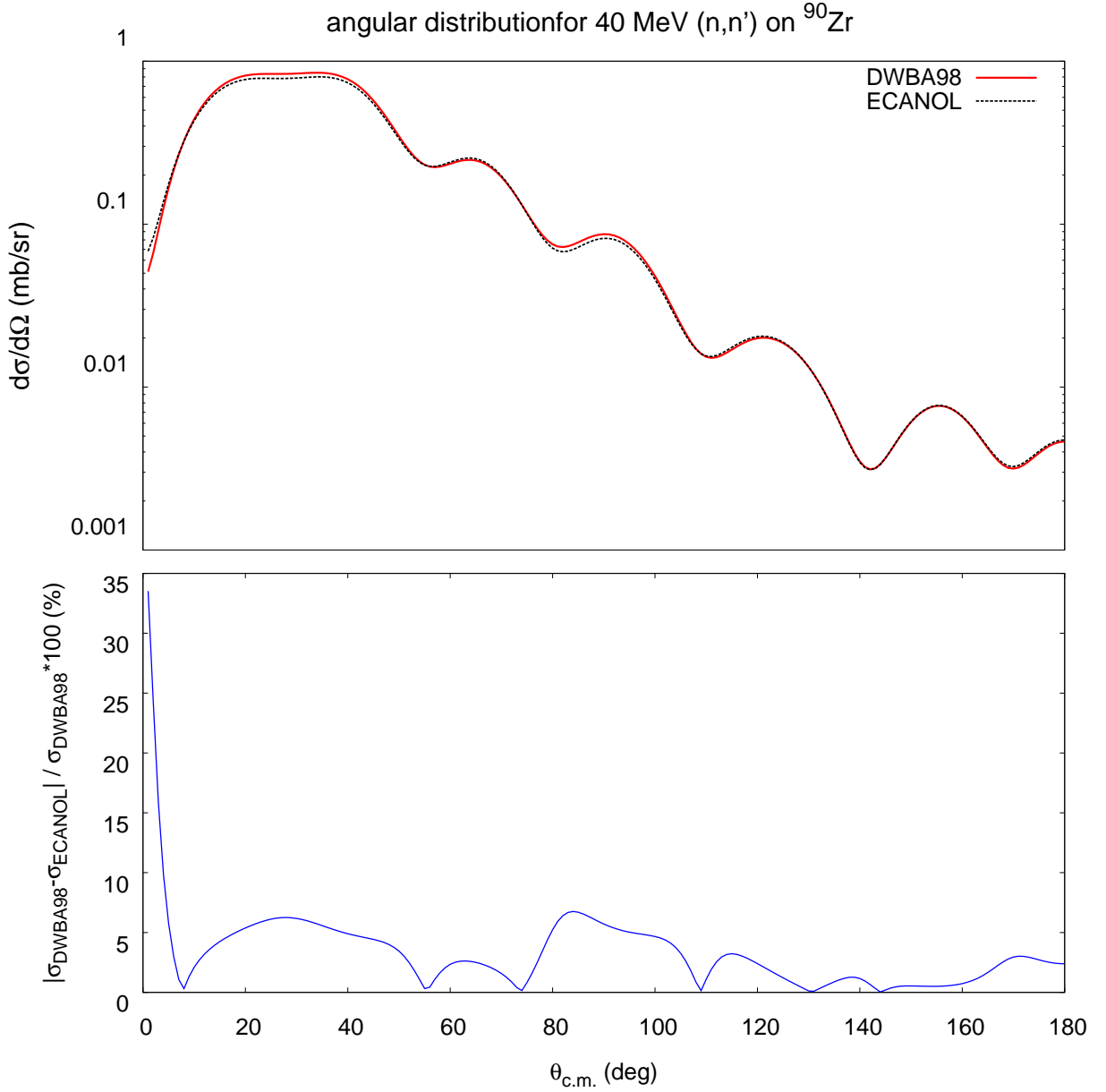


Figure 5.8: Angular distribution for (n,n') to the first 5^- state of ^{90}Zr at incident energy of 40 MeV.

element	model	number of elements	time cost
$\langle \psi_{GS} \widehat{V}_{\text{eff}} \psi_{GS} \rangle$	HF	21	1.7 s
	RPA	1022	6.7 s
$\langle \psi_{5^-} \widehat{V}_{\text{eff}} \psi_{GS} \rangle$	RPA	452	26 s
$\langle \psi_{7^-} \widehat{V}_{\text{eff}} \psi_{5^-} \rangle$	RPA	456	110 s

Table 5.1: Table describing the time cost of MINOLOP to compute the central part of microscopic nonlocal potentials.

Chapter 6

Applications

One interesting application that can demonstrate the robustness of the tools we have developed is the study of preequilibrium emission due to 2-step processes. In the present chapter, we give an overview of our microscopic modeling of preequilibrium mechanisms.

We briefly describe the multistep direct process, and we describe one particular study - led within the multistep direct process framework - in which a single, coherent, microscopic description of both direct inelastic scattering and preequilibrium emission is achieved.

We explain then how to include 2-step processes in the preequilibrium calculation, and give in detail the approximation scheme that can be used for it. We demonstrate with practical calculations (in the case when we use the RPA to describe the target's structure) the validity of one particular approximation that is related to interference effects. Next, we present our calculations for preequilibrium emission using collective states predicted by the RPA. We describe how the number of states associated to 2-step processes compares to the number of states for 1-step processes. We compare their contributions to the angular distribution for direct inelastic scattering in a specific case, and finally we show the effect of the explicit treatment of 2-step processes within our approximation scheme by displaying our results of preequilibrium calculations.

We derive coupling densities in the case of uncorrelated particle-hole excitations. We discriminate cases where particle states and hole states are all different from other cases, and show through practical calculations that the approximation on interference effects holds also in this case. We count the number of 1p1h and 2p2h states and compare it to the number of 1 and 2-phonon states in the case of an RPA description of the target. Finally, we compare the results yielded by the preequilibrium calculation with RPA 2-phonon states and with uncorrelated 2p2h states. We describe how the collectivity increases the cross section in the case of 2-phonon states, then we discuss the quasi-boson approximation that may artificially increase the cross section.

6.1 Preequilibrium stage of a nuclear reaction

6.1.1 Multistep Direct and Multistep Compound processes

In the introduction of this work, we mentioned a stage of a nucleon-nucleus reaction during which the projectile shares enough of its energy and angular momentum with a few nucleons of the target so that excitations lying in the continuum can be reached, leading to the possibility to emit particles with a continuous energy spectrum. This stage of a nuclear reaction is usually called the preequilibrium. While the direct and the compound parts of a nuclear reaction have been theorized for a long time (Niels Bohr formulated his idea of a compound nucleus in 1936 [103] and the Feshbach formalism for the generalized optical model was proposed in 1958 [17]), the description of preequilibrium mechanisms started only in the 1960s with the phenomenological model of the excitons of Griffin [104, 105]. The basic idea of this model is that the projectile creates step-by-step new particle-hole excitations (\equiv excitons) in the total system, and loses energy and angular momentum during each creation. A statistical treatment is applied to the equation that rules the creation and annihilation of excitons. This intuitive modeling of preequilibrium has been used successfully in many analyzes and has been extended and refined until quite recently [106]. An important quantity involved in this model is the residual effective interaction M^2 for intranuclear scattering leading to creation or annihilation of excitons. Parameterizations of this quantity have been proposed [107] but lack a microscopic equivalent formulation and rely on fitting to experimental data.

First microscopic descriptions of the preequilibrium were proposed in the late 1970s and in the 1980s [108–110] ; a review, comparison and analysis of the some of the most renown microscopic models is given in references [95] and [111]. All these models, based on a fully quantum-mechanical approach, involve approximations of the Born series for the transition amplitude from an initial state $|i\rangle$ to a final state $|f\rangle$ [72]:

$$T^{i \rightarrow f} = \langle f | \widehat{V}_{\text{eff}} \sum_{n=0}^{\infty} \left(\frac{1}{H - E + i\epsilon} \widehat{V}_{\text{eff}} \right)^n | i \rangle \quad (6.1.1)$$

in which $T^{i \rightarrow f}$ is the transition amplitude, \widehat{V}_{eff} is the 2-body effective interaction, H is the unperturbed Hamiltonian of the system {projectile+ target} and E the total energy of this system. The n^{th} term of this expansion corresponds to a preequilibrium process made of n steps, called “Multistep”. The initial state is made of the target in its ground state and one particle lying in the continuum (the projectile). During each step, the projectile exchanges energy and angular momentum with the target. If, during the n steps of the reaction, the projectile remains in the continuum, we call the the process “Multistep Direct” (MSD). MSD processes can also be initiated by charge exchange reactions, which we do not consider here. If instead of staying in the continuum, the projectile is captured by the target, then we call the process “Multistep Compound” (MSC). For incident energies above 30 MeV, the MSD process is predominant because, schematically, the projectile needs to lose a lot of energy in order to be captured and is more likely to be ejected by the target rather than absorbed. All our applications concern MSD processes, and in particular 1-step and 2-step cases.

6.1.2 Microscopic formulation of MSD processes

In the case of a MSD reaction, the projectile can be inelastically scattered from an initial state to a final state. We denote as $|\chi_{k_i}^+\rangle$ the distorted wave in the entrance channel and $|\chi_{k_f}^-\rangle$ the distorted wave in the exit channel. During the reaction the target undergoes a transition from its ground state $|\psi_i\rangle$ to a final state $|\psi_f\rangle$. The transition amplitude that corresponds to this situation can be written (using the Born expansion):

$$T^{i\rightarrow f} = \langle \chi_{k_f}^-, \psi_f | \sum_{n=1}^{\infty} V(GV)^{n-1} | \chi_{k_i}^+, \psi_i \rangle = \sum_{n=1}^{\infty} T_n^{i\rightarrow f} \quad (6.1.2)$$

where the operator $G = \frac{1}{H - E + i\epsilon}$ is the propagator for the system {projectile + target} at each step, $T_n^{i\rightarrow f}$ is the n^{th} term of the Born expansion for the transition amplitude:

$$T_n^{i\rightarrow f} = \langle \chi_{k_f}^-, \psi_f | V(GV)^{n-1} | \chi_{k_i}^+, \psi_i \rangle \quad (6.1.3)$$

and the double differential cross section for this reaction reads:

$$\frac{d^2\sigma(\vec{k}_i, \vec{k}_f)}{d\Omega_f dE_{k_f}} = \frac{\mu^2}{(2\pi\hbar^2)^2} \frac{k_f}{k_i} \sum_{\psi_N} |T^{i\rightarrow f}|^2 \delta(E_{k_i} - E_{k_f} - E_N) \quad (6.1.4)$$

with μ the reduced mass of the system, E_{k_i} the projectile's kinetic energy in the center of mass frame, E_{k_f} its outgoing energy, $|\psi_N\rangle$ an excited state of the target associated to an excitation energy E_N . Now, if we introduce the Born expansion for the transition amplitude in equation (6.1.4) and truncate it to the first order (which means we take into account only 1-step processes), then the double differential cross section reads:

$$\begin{aligned} \frac{d^2\sigma(\vec{k}_i, \vec{k}_f)}{d\Omega_f dE_{k_f}} &= \frac{\mu^2}{(2\pi\hbar^2)^2} \frac{k_f}{k_i} \sum_{\psi_N} |T_1^{i\rightarrow f}|^2 \delta(E_{k_i} - E_{k_f} - E_N) \\ &= \frac{\mu^2}{(2\pi\hbar^2)^2} \frac{k_f}{k_i} \sum_{\psi_N} |\langle \chi_{k_f}^-, \psi_N | V | \chi_{k_i}^+, \psi_i \rangle|^2 \delta(E_{k_i} - E_{k_f} - E_N) \end{aligned} \quad (6.1.5)$$

in which we kept $T_1^{i\rightarrow f}$ the term with $n = 1$ of equation (6.1.3). This second form exhibits a particular feature: when we consider only 1-step processes, then the double differential cross section is simply related to the DWBA transition amplitude for direct inelastic scattering as defined in equation (5.2.1).

Similarly, we can truncate the Born expansion for the transition amplitude to the second order (and thus include also 2-step processes). The double differential cross section reads in this case:

$$\frac{d^2\sigma(\vec{k}_i, \vec{k}_f)}{d\Omega_f dE_{k_f}} = \frac{\mu^2}{(2\pi\hbar^2)^2} \frac{k_f}{k_i} \sum_{\psi_N} \left(|T_1^{i\rightarrow f}|^2 + |T_2^{i\rightarrow f}|^2 + 2\text{Re}(T_1^{i\rightarrow f*} T_2^{i\rightarrow f}) \right) \delta(E_{k_i} - E_{k_f} - E_N) \quad (6.1.6)$$

In this formula, $T_2^{i\rightarrow f}$ is the second term in the Born expansion of the transition amplitude. It takes into account all 2-step processes. The last term $2\text{Re}(T_1^{i\rightarrow f*} T_2^{i\rightarrow f})$ is a cross terms that embodies the interference between 1-step and 2-step processes. The explicit form for $T_2^{i\rightarrow f}$ reads:

$$T_2^{i\rightarrow f} = \langle \chi_{k_f}^-, \psi_f | VGV | \chi_{k_i}^+, \psi_i \rangle \quad (6.1.7)$$

Let us introduce some notions and approximations that can be found in MSD models. In the expression of $T^{i \rightarrow f}$, the propagator G reads formally:

$$G = \frac{1}{E - H + i\epsilon} = \frac{1}{E - H_A - T - U + i\epsilon} \quad (6.1.8)$$

in which H_A is the Hamiltonian of the target nucleus, T is the kinetic operator for the projectile-target relative motion and U is the potential of interaction between the projectile and the target. The Hamiltonian of the target can be decomposed as:

$$H_A = H_0 + H_1 \quad (6.1.9)$$

where H_0 is the main part of the target's Hamiltonian and H_1 is the residual part. In most MSD models, H_0 is taken to be some shell model Hamiltonian, in which case its eigenstates are particle-hole states. The residual Hamiltonian H_1 causes configuration mixing and the eigenstate $|\psi_N\rangle$ of H_A can be written as:

$$|\psi_N\rangle = \sum_{ph} \lambda_{1p1h}^N |1p1h\rangle + \lambda_{2p2h}^N |2p2h\rangle + \dots \quad (6.1.10)$$

$$|\psi_N\rangle = \sum \lambda_{1\text{phonon}}^N |1\text{phonon}\rangle + \lambda_{2\text{phonon}}^N |2\text{phonon}\rangle + \dots \quad (6.1.11)$$

with λ_{ph}^N the coefficients for each particle-hole state. In order to obtain expressions for the double differential cross section that can easily be computed, some statistical assumptions are made. The first assumption, called the "leading particle statistics" scheme, is based on the idea that in a given interval of energy, the effective interaction can connect the initial system to many states and the corresponding matrix elements vary widely in both amplitude and sign. The other scheme, called "residual system statistics", assumes a random configuration mixing and leads to different consequences on the formula of the transition amplitude. Both schemes involve some energy averaging, and a review with details on the approximations within these two schemes is given in reference [112].

In our case, we will adopt the residual system statistics and H_0 will be taken whether as the HF Hamiltonian or the RPA Hamiltonian. In the RPA case, the Hamiltonian reads:

$$H_{RPA} = E_{\tilde{0}} + \sum_N E_N^* \Theta_N^\dagger \Theta_N \quad (6.1.12)$$

Eigenstates of this Hamiltonian satisfy the relation (in the case of 1 and 2-phonon states):

$$\begin{aligned} H_{RPA} \Theta_{N_1}^\dagger |\tilde{0}\rangle &= (E_{\tilde{0}} + E_{N_1}^*) \Theta_{N_1}^\dagger |\tilde{0}\rangle \quad (1 \text{ phonon case}) \\ H_{RPA} \Theta_{N_1}^\dagger \Theta_{N_2}^\dagger |\tilde{0}\rangle &= (E_{\tilde{0}} + E_{N_1}^* + E_{N_2}^*) \Theta_{N_1}^\dagger \Theta_{N_2}^\dagger |\tilde{0}\rangle \quad (2 \text{ phonon case}) \end{aligned} \quad (6.1.13)$$

This can be found within the QBA by using the relations (4.4.27). In the case of a 1-step process, if we use the residual system statistics on the final state, then we can use (6.1.10) (and its equivalent formulation for RPA states). For uncorrelated 1p1h states, the double differential cross section reads:

$$\begin{aligned} \frac{d^2\sigma(\vec{k}_i, \vec{k}_f)}{d\Omega_f dE_{k_f}} &= \frac{\mu^2}{(2\pi\hbar^2)^2} \frac{k_f}{k_i} \sum_{\psi_N} |T_1^{i \rightarrow f}|^2 \delta(E_{k_i} - E_{k_f} - E_N) \\ &= \frac{\mu^2}{(2\pi\hbar^2)^2} \frac{k_f}{k_i} \sum_{\psi_N} \delta(E_{k_i} - E_{k_f} - E_N) \\ &\quad \sum_{ph, p'h'} \lambda_{ph}^N \lambda_{p'h'}^N \langle \chi_{k_f}^-, ph | V | HF, \chi_{k_i}^+ \rangle^* \langle \chi_{k_f}^-, p'h' | V | HF, \chi_{k_i}^+ \rangle \end{aligned} \quad (6.1.14)$$

The sum over ψ_N with the δ function inside is equivalent to an energy averaged sum: an integral over an interval ΔE centered at E_N and divided by ΔE . Furthermore, since in the residual system statistics the coefficients λ_{ph}^N for the final state are random, we have:

$$\sum_{\psi_N} \lambda_{ph}^N \lambda_{p'h'}^N \delta(E_{k_i} - E_{k_f} - E_N) = \delta_{pp'h'h'} \rho_{ph}(E_{k_i} - E_{k_f}) \quad (6.1.15)$$

in which we have introduced the energy dependent density of 1p1h states ρ_{ph} . Finally, we can rewrite the double differential cross section for a 1-step process as:

$$\begin{aligned} \frac{d^2\sigma(\vec{k}_i, \vec{k}_f)}{d\Omega_f dE_{k_f}} &= \frac{\mu^2}{(2\pi\hbar^2)^2} \frac{k_f}{k_i} \sum_{\psi_N} |T_1^{i \rightarrow f}|^2 \delta(E_{k_i} - E_{k_f} - E_N) \\ &= \frac{\mu^2}{(2\pi\hbar^2)^2} \frac{k_f}{k_i} \sum_{ph} \rho_{ph}(E_{k_i} - E_{k_f}) |\langle \chi_{k_f}^-, ph | V | HF, \chi_{k_i}^+ \rangle|^2 \\ &= \sum_{ph} \rho_{ph}(E_{k_i} - E_{k_N}) \frac{d\sigma(\vec{k}_i, \vec{k}_N)}{d\Omega_f} \end{aligned} \quad (6.1.16)$$

Therefore, the double differential cross section can be linked to the angular distribution. This discussion can easily be extended to the case of 2-step processes.

In this case, the transition amplitude is that of equation (6.1.7). If we introduce a closure relation (using a basis made of the state vectors of the target) on each side of the propagator, the following term appears in the transition amplitude:

$$\langle \psi_{N'} | \frac{1}{E - H_0 - H_1 - U - T + i\epsilon} | \psi_N \rangle \quad (6.1.17)$$

in which $\psi_{N'}$ and ψ_N are intermediate states. Since in the first step, we use a 2-body interaction and the QBA (for RPA states), only the 1-phonon (resp. 1p1h) components of the intermediate state remain. At each step of a preequilibrium reaction, it is possible to assume that the configuration mixing caused by H_1 is slower or faster than the process of excitation of the target, and this is called in the first case the sudden approximation and in the later case the adiabatic approximation. If we use the sudden approximation on intermediate states, then there is no configuration mixing of 1-phonon (resp. 1p1h) states and the intermediate state consists of one single 1-phonon state (resp. 1p1h state), and it is the same on each side of the propagator which yields:

$$\frac{1}{E - U - T - E_N + i\epsilon} \delta_{\psi_N \psi_{N'}} \quad (6.1.18)$$

One interesting consequence on the propagator is that now, it can be written as:

$$G = \sum_{\psi_N} \int \frac{|\chi_{\vec{k}}^+, \psi_N\rangle \langle \widehat{\chi}_{\vec{k}}^+, \psi_N|}{E - E_k - E_N + i\epsilon} \frac{d\vec{k}}{(2\pi)^3} \quad (6.1.19)$$

where \vec{k} is the wave vector in the space of the projectile, $|\chi_{\vec{k}}^+\rangle$ is the eigenvector of the projectile's Hamiltonian $H_p = U + T$ associated to the eigenvalue \vec{k} , $|\widehat{\chi}_{\vec{k}}^+\rangle$ is the eigenvector of the hermitian conjugate H_p^\dagger of the projectile's Hamiltonian, associated to the eigenvalue

\vec{k} with the property $\langle \chi_{\vec{k}}^{\pm} | \widetilde{\chi}_{\vec{k}'}^{\pm} \rangle = \delta(\vec{k} - \vec{k}')$. Next, we use the residual system statistics on the final state and, following the same reasoning as in the case of the 1-step process, we deduce from our use of the QBA and of a 2-body interaction that only matrix elements connecting the intermediate state to the 2-phonon (resp. 2p2h) component of the final states remain, and the double differential cross section can be linked to their angular distribution and an energy dependent density of 2-phonon (resp 2p2h) states. The energy dependent density of final states is parameterized, in our case, as a Lorentzian distribution:

$$\rho_N(E) = \frac{1}{\pi} \frac{\Gamma_N}{(E - E_N)^2 + \left(\frac{\Gamma_N}{2}\right)^2} \quad (6.1.20)$$

in which N labels the final state, E_N its energy and Γ_N the width associated to this state. It is worth noticing that a similar formula can be obtained: in equation (6.1.5), the δ function is obtained assuming we know exactly eigenvalues and eigenstates of the target's Hamiltonian. Also in this case, the final states are a combination of RPA (or HF) states. However, these nuclear structure descriptions are only approximate calculations. But it is possible to show (when using RPA states) that we can do a calculation that takes into account implicitly the correlations we neglect (2p2h, 3p3h ...), provided we modify the eigenenergies E_N of RPA states by $E_{N'} = E_N + i\frac{\Gamma_N}{2}$, in which Γ_N is a damping width that implies the target's state $|\psi_N\rangle$ has a finite lifetime because it is not an exact eigenstate of the total Hamiltonian of the target.

In our calculations of 2-step processes, we also make use of the on-shell approximation - which amounts to a conservation of energy - to simplify the propagator:

$$\frac{1}{E - E_k - E_N + i\epsilon} \approx -i\pi\delta(E - E_k - E_N) \quad (6.1.21)$$

In the following sections, we further describe the approximation scheme we adopted for our practical calculations. The main purpose of this study is to evaluate the effect of considering collective excitations within the 2-step direct process. Our approach is very close to the one adopted by Kawano *et al.* [113] to calculate the contribution of the 2-step processes within the Nishioka-Weidenmuller-Yoshida model [110]. We adopt the never-come-back approximation (which will be described later), we use a 2-body effective interaction, the main part H_0 of the target's Hamiltonian is taken to be the RPA (and afterwards the HF) Hamiltonian and we use the QBA in the calculation of RPA states. For two step direct processes, we use the sudden approximation in the intermediate step and the residual system statistics for the last step. Finally, we adopt the on-shell approximation in our calculations (A-0). The double differential cross section for 2-step processes with these approximations reads:

$$\frac{d^2\sigma(\vec{k}_i, \vec{k}_f)}{d\Omega_f dE_{k_f}} = \frac{\mu^2}{(2\pi\hbar^2)^2} \frac{k_f}{k_i} \sum_{\alpha} \rho_{2\alpha}(E_{k_i} - E_{k_f}) \left| \sum_{\beta} \langle \widetilde{\chi}_{\vec{k}_f}^-, \psi_{\alpha} | V | \psi_{\beta} \rangle \langle \psi_{\beta} | V | \chi_{\vec{k}_i}^+, \psi_i \rangle \delta(E - E_k - E_{\beta}) \right|^2 \pi^2 \quad (6.1.22)$$

where $\rho_{2\alpha}$ is the density of 2-phonon (resp. 2p2h) states parameterized as in equation (6.1.20), α is a label for coupling 2-phonon (resp. 2p2h) states, β is a label for coupling

1-phonon (resp. 1p1h) states, ψ_α and ψ_β denote these 1 and 2 phonon (resp. 1p1h and 2p2h) states. Moreover, we consider the contribution to 2-step processes that comes, on one hand from collective states (phonons) energetically accessible, and on the other hand from uncorrelated 2p2h states energetically accessible.

6.1.3 Practical calculation for MSD processes

Each MSD model is based on some approximation to compute the transition amplitude, and the difference in the choice of approximations leads to a different modeling of the physics. Moreover, in these microscopic modelings the description of direct inelastic scattering to discrete states and giant resonances is done with a model that is distinct from the preequilibrium model (the only exception being the Tamura Udagawa Lenske model [109]). Usually, the direct inelastic scattering to discrete states with low excitation energy and strong collectivity is computed within the optical model framework, using a macroscopic, phenomenological description of excitations such as the vibrational model and experimental deformation parameters. The quantitative description of systems for which experimental data are available is excellent with this modeling, but is very difficult to extend to systems for which little to no experimental data exist. One possible way of tackling this difficulty is to use inputs (such as ground state and transition densities) obtained with an accurate nuclear structure model. For example, target excitations described with the RPA were used to calculate for 6 to 20 MeV incident neutrons, the (n,xn) direct emission component on ^{90}Zr and ^{208}Pb [114], and in another study inputs from the Quasi-particle Random Phase Approximation (QRPA) were used to describe (n,xn) reactions on ^{238}U with a semi-microscopic modeling of the optical and transition potentials [26].

Recently efforts have been put in describing on an equal footing direct inelastic scattering to discrete states and preequilibrium emission in a fully quantum mechanical, microscopic framework [23, 64, 79]. In these works, the Melbourne G matrix and RPA wave functions are used to compute direct elastic and inelastic scattering observables for doubly closed shell nuclei like ^{90}Zr and ^{208}Pb . Discrete excited states as well as states lying in the continuum are included, considering all 1-step process (all 1-boson excitations) that are accessible. Both natural and unnatural parities as predicted by the RPA (implemented with the Gogny D1S interaction) are treated. Raynal's code DWBA98 is used to compute cross sections, thus allowing for an explicit treatment of knock-out exchange without a localization procedure. An example of the results obtained in this study is shown on figure 6.1. The left panel of this plot displays the cross section as a function of the outgoing proton energy at the emission angle $\theta_{\text{c.m.}} = 69^\circ$, and the right panel shows angular distributions at various outgoing energies. Since only 1-step processes are considered in this study, it is to be expected that only the higher outgoing energy part of the emitted nucleon spectrum and the forward angular distribution can be accurately reproduced by the calculation. This is indeed the case: the energy spectrum is well reproduced for excitation energies up to about 15 MeV but the angular distribution is underestimated at backward angles.

While discrepancies between experimental data and calculations exist, the overall agreement remains satisfactory considering the fact that the entire calculation is parameter-free. Such encouraging results can be improved by several means (see reference [79]), including the treatment of more complex excitations of the target that would allow for the inclusion of 2-step processes.

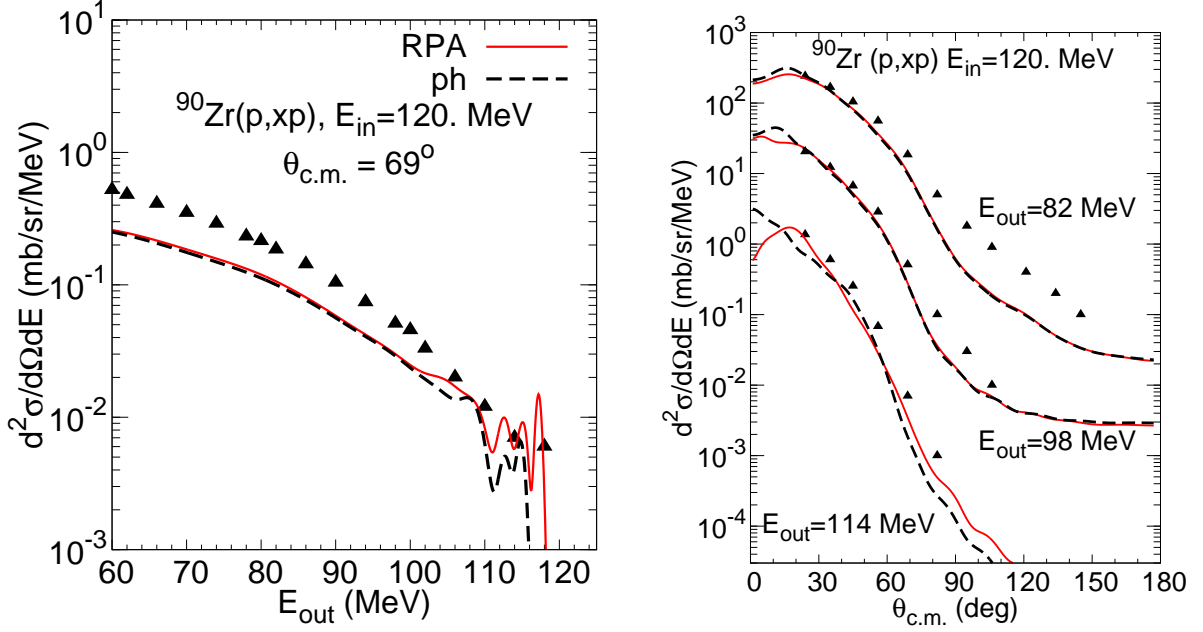


Figure 6.1: Double differential cross sections for (p,xp) off ^{90}Zr at 120 MeV of incident energy. RPA calculations are displayed as full red curves, uncorrelated particle-hole calculations as black dashed curves. Experimental data from references [2] and [3] are depicted as symbols.

Our goal was initially to extend this calculation - using the tools ECANOL and MINOPOP that we have developed - to the 2-step cross section (in the limit of $A=0$). A key ingredient of the previously calculated 1-step cross section is the use of a realistic interaction, the Melbourne G matrix. Associated to a description of the target's excited states done with the RPA, it leads to a very good determination of the continuum emission at angles and energies where higher step process contributions are believed to be negligible. A particular achievement of the study on 1-step contributions is that no adjustment of the interaction was required to reproduce the magnitudes and shapes of the cross sections as displayed on figure 6.1. Another point of importance is that no localization procedure was done on the potentials, therefore this calculation is free of any problem that could be related to the Perey effect.

We couldn't achieve a full determination of the second order contributions to the cross section with the same ingredients, because the number of 2-phonon (or similarly of 2p2h) becomes very large as the excitation energy grows. Even if such a calculation is accessible considering the available computing power, we have chosen to first analyze some features of the calculation for 2-step processes, such as interference effects in the intermediate state when the final states are made of 2p2h excitations on a HF ground state, or 2-phonon excitations on the RPA ground state. This first calculation allows for an evaluation of the impact of collectivity in a 2-step process. We also discuss the issue of the QBA in this study. In order to establish a reliable set of approximations that can be used to perform a complete calculation for 2-step processes with a microscopic description of the target's states and a realistic 2-body interaction, the study we present here constitutes a necessary step.

6.2 Extending preequilibrium calculations by including 2-step processes

6.2.1 Scheme of approximations

If we consider that final states are made of 1p1h and 2p2h excitations over the HF ground state, then the 1-step process can only lead to 1p1h states since we use a 2-body interaction. As for 2-step processes, if we start from a 1p1h state after the first step, then the return to the ground state should not be included because it is already accounted for in the calculation of elastic scattering. Namely, elastic scattering observables are well accounted for in studies based on the nonlocal optical potentials $\langle \psi_{\tilde{0}} | \widehat{V}_{\text{eff}} | \psi_{\tilde{0}} \rangle$, where \widehat{V}_{eff} is the Melbourne G matrix and $\psi_{\tilde{0}}$ the RPA correlated ground state (see [23, 79, 95]). We also use another approximation, which is usually applied in MSD theories, the never-come-back approximation (labeled A-2): at each step of the reaction, the process leading to the creation of a new pair particle-hole strongly dominates - because of the relative sizes of accessible phase spaces - over the processes of particle-hole scattering and annihilation. Consequently, the 2-step process can only lead to 2p2h excitations. Thus, within this approximation scheme, the 1-step and the 2-step processes lead to distinct final states, and there is no cross term $2\text{Re}(T_1^{i \rightarrow f*} T_2^{i \rightarrow f})$ in equation (6.1.6).

This discussion can easily be extended to the case of 1 and 2-phonon states within the QBA: the first step can only connect the correlated ground state to 1-phonon state, which means we neglect terms coming from equation (4.4.28) that populate a 2-phonon state in a 1-step process (we label this approximation A-1). Also, the second step leading back to the ground state should be excluded as its contribution to elastic scattering is already accounted for in the effective interaction. Approximation A-2 can also be used in the present case. Thus, in this approximation scheme, a 2-step process only connects the ground state to a 2-phonon state.

Now, if we consider the on shell approximation A-0, which implies energy conservation at each step, The second term of the Born expansion for the transition amplitude reduces to:

$$T_2^{i \rightarrow f} = \sum_N \langle \chi_{k_f}^-, \psi_f | V | \chi_k^+, \psi_N \rangle \langle \widehat{\chi}_k^+, \psi_N | V | \chi_{k_i}^+, \psi_i \rangle \delta(E - E_k - E_N) \quad (6.2.1)$$

This approximation was used in the Feshbach-Kerman-Koonin model [108] for preequilibrium. We will not discuss its validity in the present work.

The combination of A-0, A-1, and A-2 can be summarized by using the following labeling: let us denote the ground state of the target nucleus by $|\tilde{0}\rangle$. Let $\Theta_{N,J}^\dagger$ be an operator that creates - by a 1-step process - an excited state $|N\rangle$ with total spin J . We consider a first excited state $|N_1\rangle = \Theta_{N_1,J_1}^\dagger |\tilde{0}\rangle$, and another one $|N_2\rangle = \Theta_{N_2,J_2}^\dagger |\tilde{0}\rangle$. Finally, we label by $|N_3\rangle$ the excited state that comes from the combination of $|N_1\rangle$ and $|N_2\rangle$. Figure 6.2 summarizes (partly) our scheme of approximation.

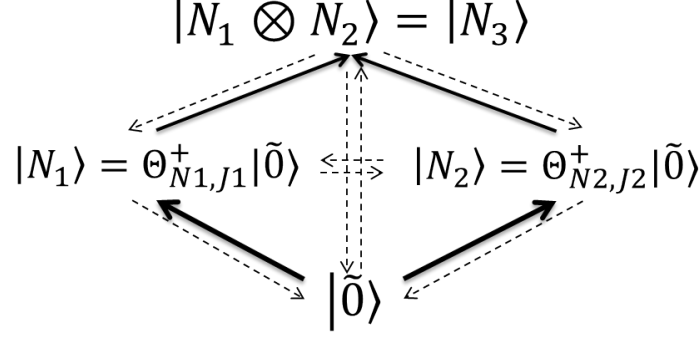


Figure 6.2: Schematic depiction of the couplings leading to an excitation for a 2-step process from excitations of 1-step processes. The full arrows are potentials that are calculated explicitly and included in our calculations, and the dashed arrows represent potentials that are neglected.

6.2.2 Illustration through an example

We can further illustrate the situation through a practical example. We take an even-even target with a 0^+ ground state, $|N_1\rangle = |5^- \rangle$ and $|N_2\rangle = |3^- \rangle$. In this case, possible values for the total spin of $|N_3\rangle$ range from 2 to 8, and its parity must be positive. Let us consider here only one value: $|N_3\rangle = |2^+ \rangle$. The matrix equation when no approximation is done reads (for our example):

$$D \begin{pmatrix} \phi_{GS}^{0^+} \\ \phi^{5^-} \\ \phi^{3^-} \\ \phi_{[5^- \otimes 3^-]}^{2^+} \end{pmatrix} = \begin{pmatrix} U^{0^+0^+} & U^{0^+5^-} & U^{0^+3^-} & U^{0^+2^+} \\ U^{5^-0^+} & U^{5^-5^-} & U^{5^-3^-} & U^{5^-2^+} \\ U^{3^-0^+} & U^{3^-5^-} & U^{3^-3^-} & U^{3^-2^+} \\ U^{2^+0^+} & U^{2^+5^-} & U^{2^+3^-} & U^{2^+2^+} \end{pmatrix} \begin{pmatrix} \phi_{GS}^{0^+} \\ \phi^{5^-} \\ \phi^{3^-} \\ \phi_{[5^- \otimes 3^-]}^{2^+} \end{pmatrix} \quad (6.2.2)$$

in which we labeled as D the matrix containing the differential operators D_i introduced in chapter 3.3, and the coupling potentials between channels I and J as U^{IJ} . We will now rewrite this matrix equation after each approximation to make their effect appear clearly. First, the coupling of the 2-phonon state with the ground state vanishes because of A-1. The matrix equation reads:

$$D \begin{pmatrix} \phi_{GS}^{0^+} \\ \phi^{5^-} \\ \phi^{3^-} \\ \phi_{[5^- \otimes 3^-]}^{2^+} \end{pmatrix} = \begin{pmatrix} U^{0^+0^+} & U^{0^+5^-} & U^{0^+3^-} & 0 \\ U^{5^-0^+} & U^{5^-5^-} & U^{5^-3^-} & U^{5^-2^+} \\ U^{3^-0^+} & U^{3^-5^-} & U^{3^-3^-} & U^{3^-2^+} \\ 0 & U^{2^+5^-} & U^{2^+3^-} & U^{2^+2^+} \end{pmatrix} \begin{pmatrix} \phi_{GS}^{0^+} \\ \phi^{5^-} \\ \phi^{3^-} \\ \phi_{[5^- \otimes 3^-]}^{2^+} \end{pmatrix} \quad (6.2.3)$$

Then we apply approximation A-2, which leads to the matrix equation associated to the situation depicted on figure 6.2:

$$D \begin{pmatrix} \phi_{GS}^{0^+} \\ \phi^{5^-} \\ \phi^{3^-} \\ \phi_{[5^- \otimes 3^-]}^{2^+} \end{pmatrix} = \begin{pmatrix} U^{0^+0^+} & 0 & 0 & 0 \\ U^{5^-0^+} & U^{5^-5^-} & 0 & 0 \\ U^{3^-0^+} & 0 & U^{3^-3^-} & 0 \\ 0 & U^{2^+5^-} & U^{2^+3^-} & U^{2^+2^+} \end{pmatrix} \begin{pmatrix} \phi_{GS}^{0^+} \\ \phi^{5^-} \\ \phi^{3^-} \\ \phi_{[5^- \otimes 3^-]}^{2^+} \end{pmatrix} \quad (6.2.4)$$

Finally we can assume that, in order to reach the 2p2h state, we can whether step by the 3^- state or the 5^- but not both at the same time, meaning we neglect interference effects

between the two paths (approximation A-3). If we step only by the 5^- state, the matrix equation with this approximation reads:

$$D \begin{pmatrix} \phi_{GS}^{0+} \\ \phi^{5-} \\ \phi^{3-} \\ \phi_{[5^- \otimes 3^-]}^{2+} \end{pmatrix} = \begin{pmatrix} U^{0+0+} & 0 & 0 & 0 \\ U^{5^-0+} & U^{5^-5^-} & 0 & 0 \\ U^{3^-0+} & 0 & U^{3^-3^-} & 0 \\ 0 & U^{2+5^-} & 0 & U^{2+2+} \end{pmatrix} \begin{pmatrix} \phi_{GS}^{0+} \\ \phi^{5-} \\ \phi^{3-} \\ \phi_{[5^- \otimes 3^-]}^{2+} \end{pmatrix} \quad (6.2.5)$$

6.3 Contribution of 2-phonon states to preequilibrium emission

6.3.1 Interference terms

To check the validity of approximation A-3, we made a calculation of the direct inelastic scattering associated to the first 5^- and 3^- 1-phonon states in ^{90}Zr , and the 2-phonon states of natural parity that can be built from them (this corresponds to the example given in the previous subsection). We plotted our results for the 2^+ and 4^+ 2-phonon states on figure 6.3 (the results for the 6^+ and the 8^+ are similar so we do not show them).

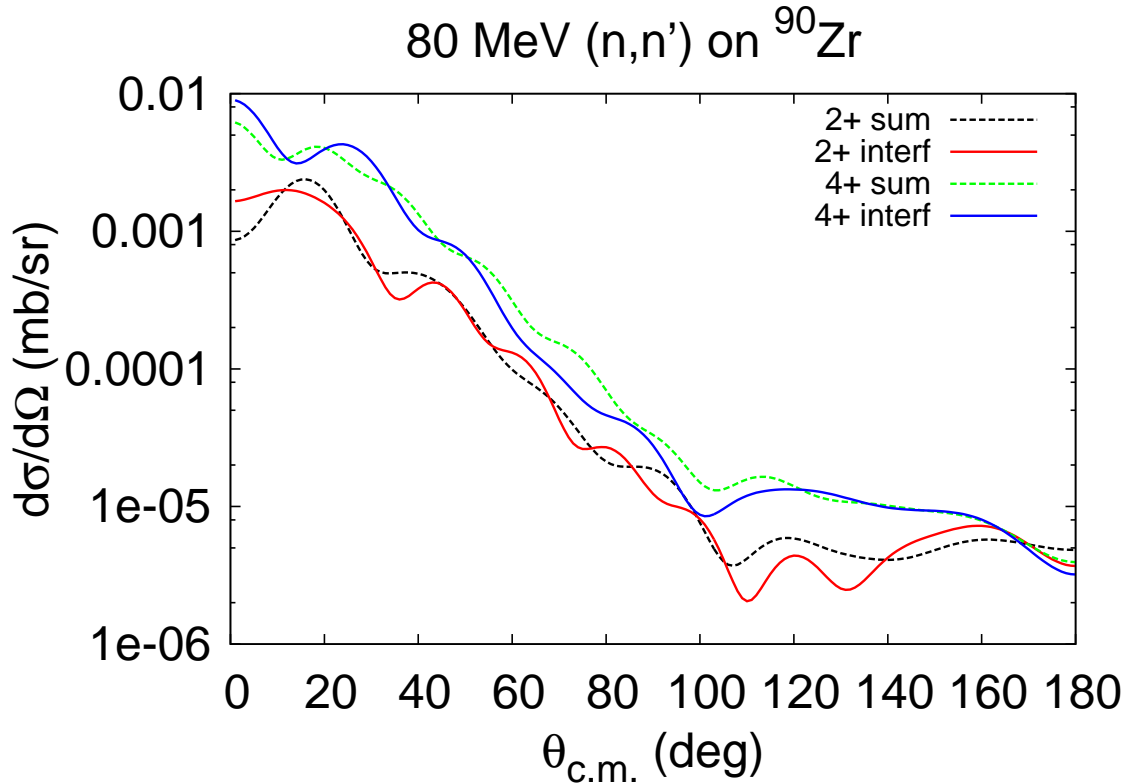


Figure 6.3: Angular distribution to 2-phonon states built by coupling the first, 1-phonon 3^- and 5^- states in ^{90}Zr for an incident neutron. Dotted lines are for the sum of the separate contributions from both 1-phonon states (when A-3 is used), and full curves are for calculations that include interference terms (when A-3 is not used).

In both cases, the shape of the angular distribution is locally changed but the global shape and magnitude remain quite comparable. The relative difference of the integrated cross section for the 2^+ is about 2.5% and is under 10 % for the other cases, except in the case of the 4^+ for which it reaches 14%. Since a sum over a large number of states is involved in our calculation for the preequilibrium emission cross section, these differences may well cancel because of averaging effects. These elements give us a satisfying confidence in using approximation A-3.

6.3.2 Counting of 2-phonon states

We present here our counting of 2-phonon states in ^{90}Zr , a comparison between the number of 1-phonon and 2-phonon states with increasing excitation energy, and a comparison of their contribution to the preequilibrium cross section.

Starting from all 1-phonon states predicted by RPA calculations implemented with the Gogny D1S force (4.4.22) in ^{90}Zr , we extracted the states of natural parity and we built from them all 2-phonon states (4.4.33) with natural parity. We enumerated the number of states, considering an excitation energy beam of 0.5 MeV, for both 1 and 2-phonon states and plotted the result on figure 6.4.

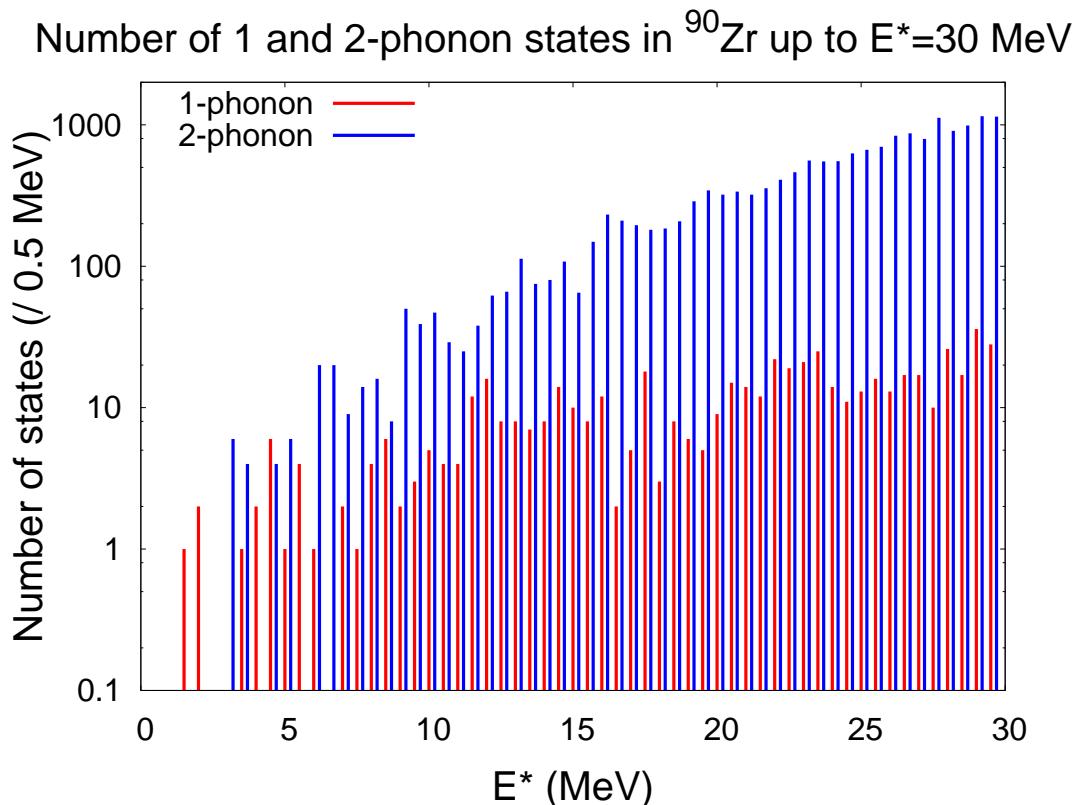


Figure 6.4: Comparison between the number of 1 and 2-phonon states in ^{90}Zr for excitation energies below 30 MeV. The red bars are for 1-phonon states and the black bars are for 2-phonon states. Each bar corresponds to the counting of all states in an energy bin of 0.5 MeV

Above 5 MeV of excitation energy, the number of 2-phonon states is quite larger than the number of 1-phonon states. But for excitation energies above 20 MeV the number of 2-phonon states is about 10 times greater than that of the 1-phonon. As the excitation energy increases, the difference between the number of 1 and 2-phonon states becomes bigger and bigger. This means that the contribution of 2-phonon states to the preequilibrium emission can be significant if the cross section for these states is large enough.

We investigated this point by doing a calculation of the direct inelastic scattering associated to the first 5^- and 3^- 1-phonon states in ^{90}Zr , and the 2-phonon states of natural parity that can be built from them: 2^+ , 4^+ , 6^+ and 8^+ . We did the calculations in the limit of approximation A-3 by considering first that 2-phonon states are populated from the 3^- (figure 6.5), then from the 5^- (figure 6.6). At small angles, the magnitude of the angular distribution to 2-phonon states appears to be about 1 or 2 orders of magnitude smaller than for 1-phonon states but becomes comparable at larger angles. This means that the contribution of 2-phonon states should significantly impact the calculation of preequilibrium emission, especially at backward angles, as expected.

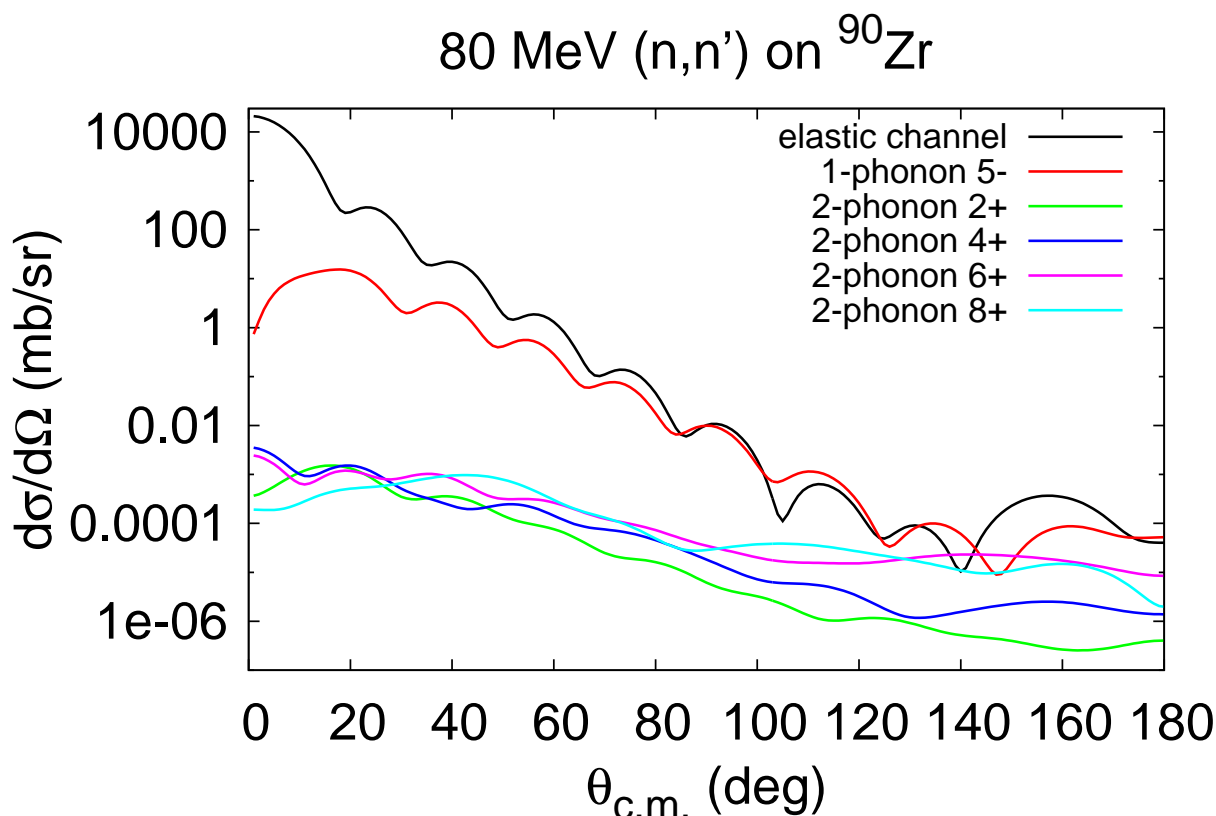


Figure 6.5: Angular distribution to 2-phonon states built by coupling the first, 1-phonon 3^- state and 5^- state in ^{90}Zr for an incident neutron. Here, 2-phonon states are populated exclusively from the 1-phonon 3^- state.

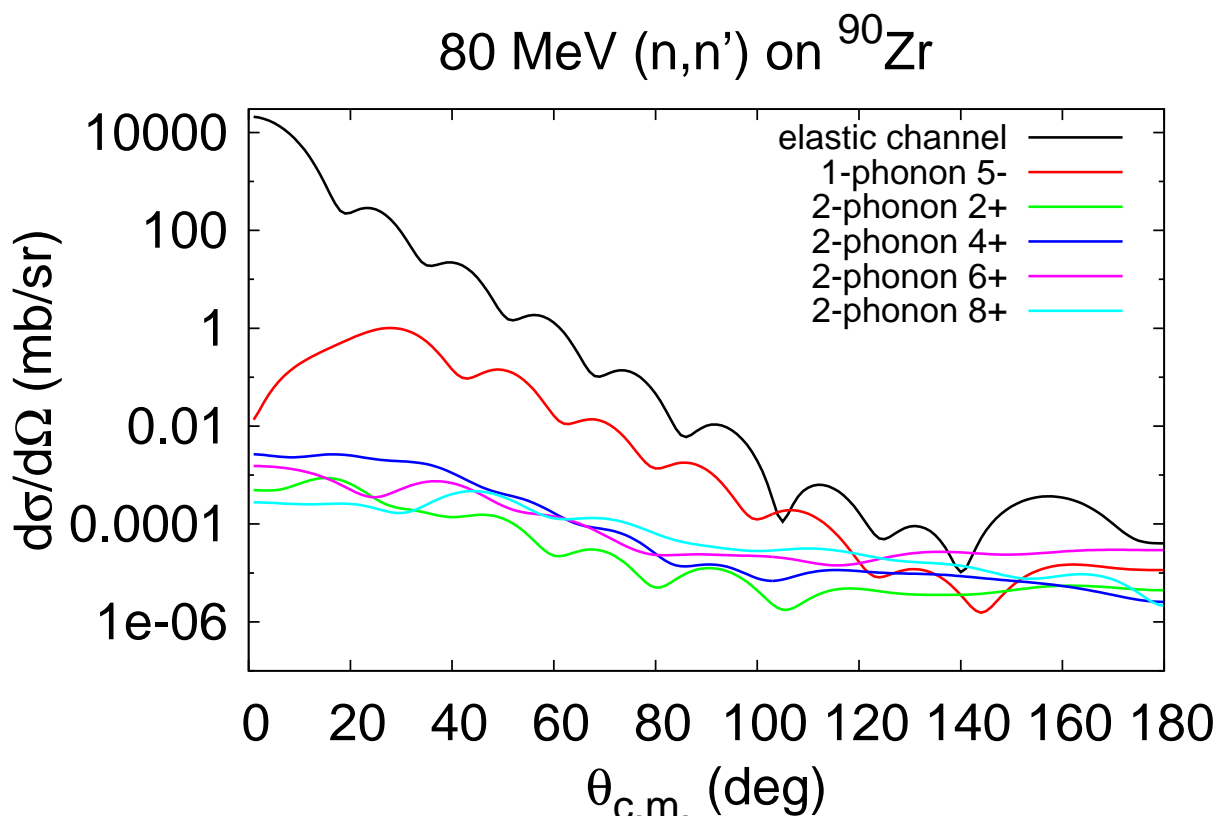


Figure 6.6: Angular distribution to 2-phonon states built by coupling the first, 1-phonon 3^- state and 5^- state in ^{90}Zr for an incident neutron. Here, 2-phonon states are populated exclusively from the 1-phonon 5^- state.

The central part of our nonlocal potentials allows unnatural parity transitions, but its contribution is negligible compared to that of the 2-body spin orbit and tensor terms. In our calculation, we only considered states with natural parity because MINOLOP had been validated - at the time of the calculation - only for the central term. For excitation energies up to 30 MeV, this still corresponds to more than 16,000 2-phonon states in ^{90}Zr . This huge number has a dramatic impact on the computation time: the results presented on figure 6.6 took approximately 8 minutes of computation time (including the calculation of 1-body transition densities for the 2-phonon state, the calculation by MINOLOP of all the potentials in equation (6.2.4) and the calculation of observables by ECANOL). The higher the spin of the 2-phonon state, the longer the calculation takes because it involves more couplings. We made calculations similar to that presented on figure 6.6 for all 1 and 2-phonon states up to 14 MeV of excitation energy and computed the integrated cross section for each 2-phonon state. We then discriminated the results in terms of the spin of the 2-phonon states to see how much they contribute to the total cross section coming from 2-phonon excitations. This work is summarized on figure 6.7:

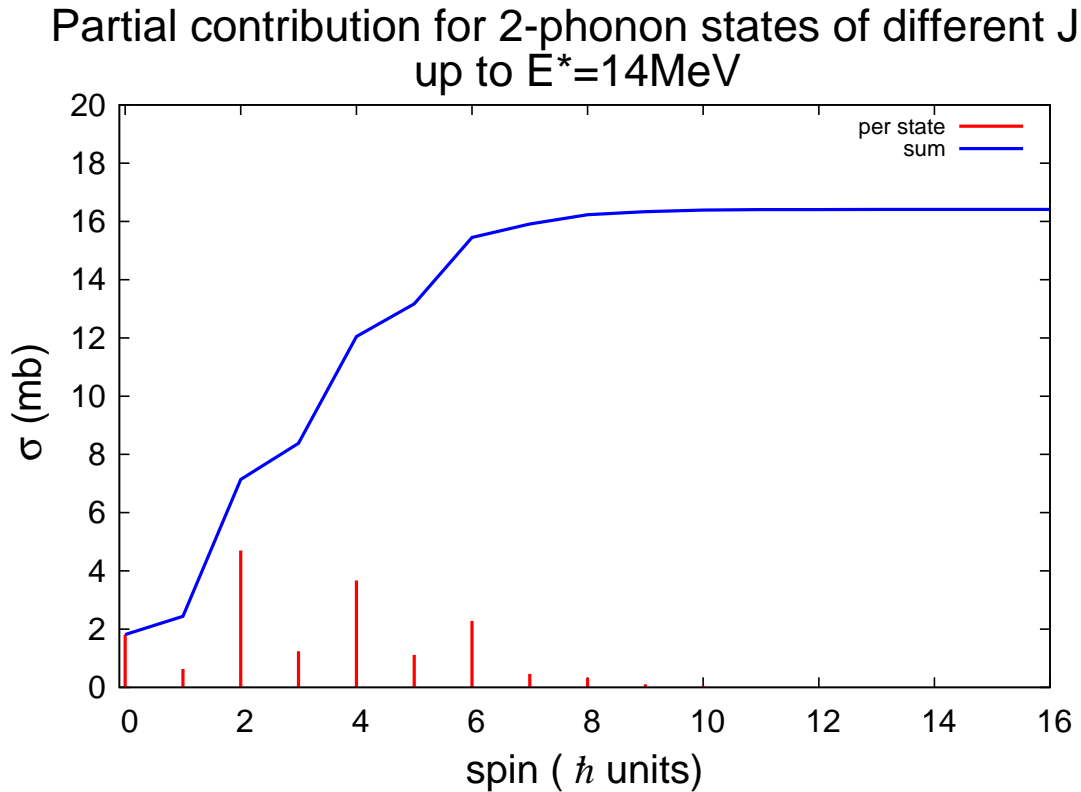


Figure 6.7: Contribution of 2-phonon states (discriminated in terms of their spin) to the total inelastic cross section to 2-phonons up to $E^*=14$ MeV. The red bars correspond to the total cross section of 2-phonon states with a given spin, and the blue curve is the cumulative sum of their contributions.

We can see that excitations with a spin higher than $8\hbar$ contribute for less than 0.5% and, on the other hand, they require much more computation time than states with a smaller spin. Therefore, we chose not to consider 2-phonon excitations with a spin higher than $8\hbar$ in our calculation which reduced the number of states to consider by approximately 12 %.

6.3.3 Results for 2-phonon states

The calculation we have done can be summarized with the following features:

- We consider a neutron induced reaction on ^{90}Zr . The projectile's kinetic energy is 80 MeV.
- All 1-phonon and 2-phonon states of natural parity with excitation energy under 20 MeV are included. 2-phonon states with a spin higher than $8\hbar$ are neglected. This represents 205 1-phonon states and about 3,000 2-phonon states.
- Only the central term of the Melbourne G matrix is used to compute potentials.
- The structure of ^{90}Zr is described with the RPA implemented with the Gogny force in its D1S parameterization.
- Approximations A-0 to A-3 are used in this calculation.

The angular distributions for low excitation energies (6, 9 and 12 MeV) and particle emission spectra are gathered on figures 6.8 and 6.9. On figure 6.8, we see that for emission angles lower than 60° the contribution of 2-phonon excitations is negligible compared to that of 1-phonon states. Between 60° and about 120° , the 1-phonon contribution is still larger than the 2-phonon contribution, but it is becoming important to consider 2-phonon excitations. Above 120° the 2-phonon contribution is the most important one. It is interesting to see with this plot that even for low excitation energies the contribution of 2-phonon states is important and even necessary at backward angles.

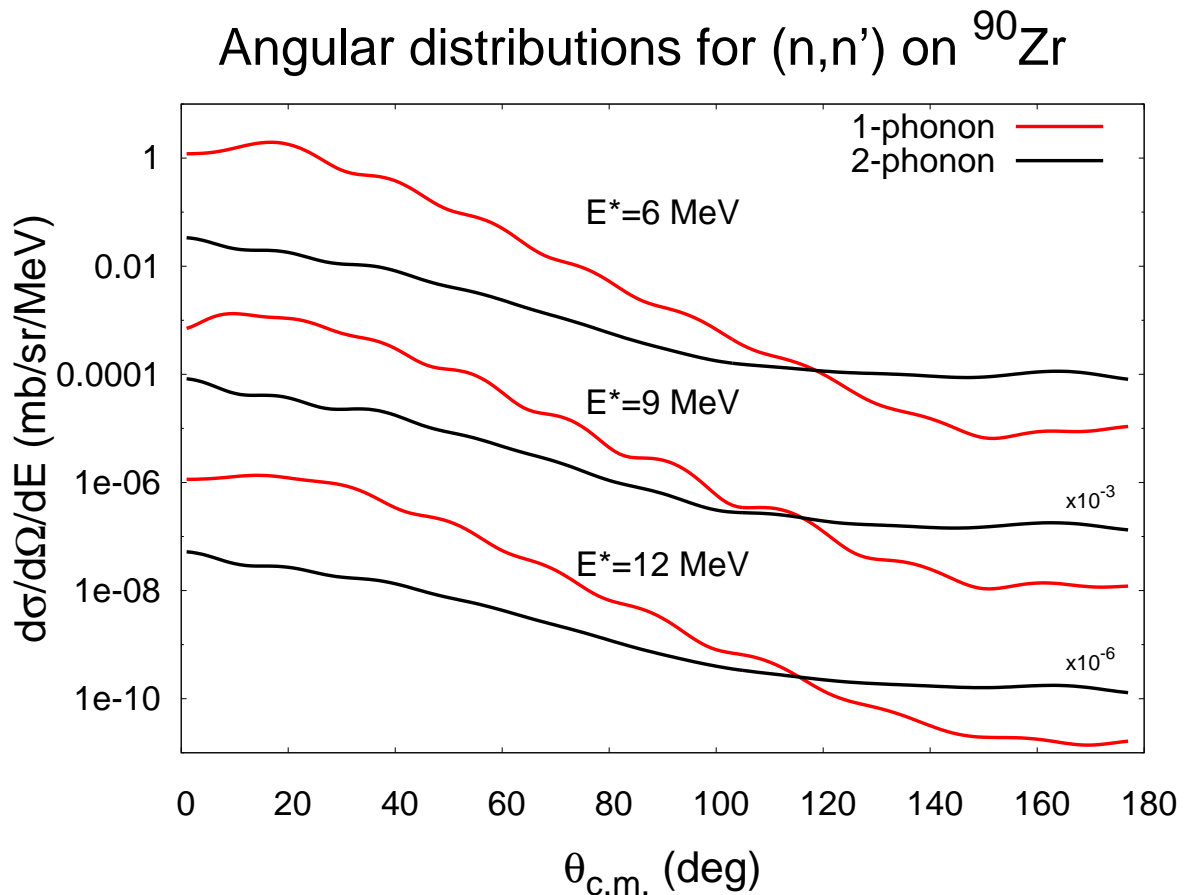


Figure 6.8: Double differential cross section as a function of the angle of emission for a (n,n') reaction with an incident energy of 80 MeV on ^{90}Zr . The black curves are the contribution from 2-phonon states up to 20 MeV of excitation energy, the red curves are the contributions from 1-phonon states up to 20 MeV of excitation energy. Results are displayed for the three outgoing energies $E_{\text{out}} = 74, 71, 68$ MeV, which correspond to excitation energies of 6, 9 and 12 MeV.

Similarly, the energy spectrum plotted on figure 6.9 shows that at low emission angle ($<90^\circ$) the 2-phonon contribution is negligible, while at medium and high emission angles their contribution is important and even dominant for angles above 120° . As the excitation energy increases, the difference between the number of 1-phonon states and 2-phonon states becomes larger and larger (see figure 6.4), so the trends we observe for excitations energies below 15 MeV are likely to be even more pronounced at higher excitations energies. The lacking contributions at emission energies below 105 MeV that we observe on figure 6.1 may well come from 2-phonon excitations, according to this.

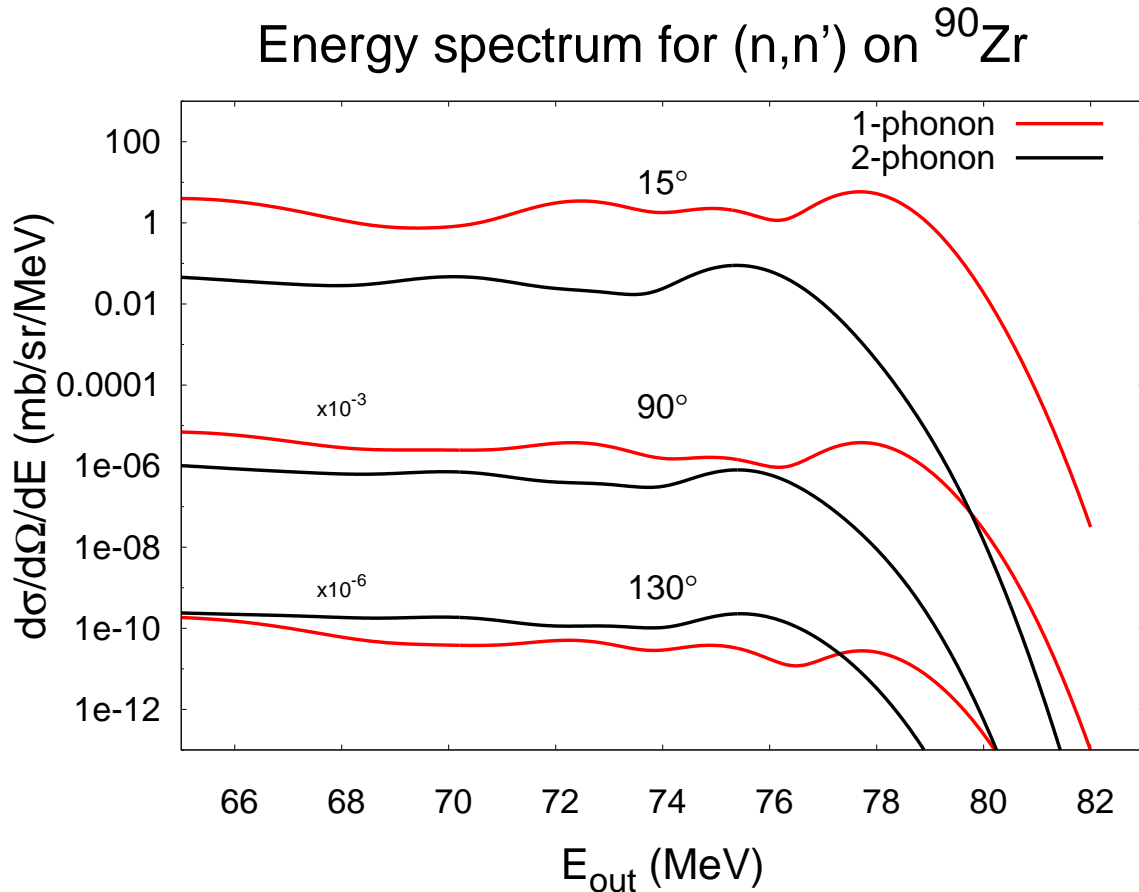


Figure 6.9: Double differential cross section as a function of the emission energy for a (n,n') reaction with an incident energy of 80 MeV on ^{90}Zr . The black curves are the contribution from 2-phonon states up to 20 MeV of excitation energy, the red curves are the contributions from 1-phonon states up to 20 MeV of excitation energy. We display results for emission angles $\theta = 15, 90, 130^\circ$ in the center of mass frame.

In order to establish the impact of using the RPA theory in MSD calculations, we compare in the next section these results to a calculation implying uncorrelated 1p1h and 2p2h excitations. Then, one drawback of the present RPA approach that could artificially increase the 2-step cross section, the QBA, is discussed.

6.4 Contribution of uncorrelated 2p2h states to the preequilibrium emission

In this section, we derive formulae for reduced matrix elements of 1-body coupling densities between the HF ground state and a 1p1h excited state, and between the 1p1h state and an uncorrelated 2p2h state. Then, we compare (like in the case of calculations with RPA states) the number of 1p1h and 2p2h states up to 30 MeV of excitation energy, and then we describe some approximations we use for preequilibrium calculations and show their validity through an example. Finally, we present our results for preequilibrium emission cross section and compare them to those displayed on figures 6.8 and 6.9.

6.4.1 Derivation of reduced matrix elements for 1-body densities

Let $|N \in J_N M_N \Pi_N\rangle$ be an uncorrelated 1p1h excitation built on the HF ground state. By analogy to formulae (4.4.7) and (4.4.10), we can write this state as:

$$|N\rangle = [a_p^\dagger \otimes a_{\tilde{h}}]_{M_N}^{J_N} |\text{HF}\rangle \quad (6.4.1)$$

The transition density's reduced matrix elements coupling the HF ground state to this excited state is:

$$\rho_{\alpha\beta}^{HF \rightarrow N, J} = \frac{\langle N | [a_\alpha^\dagger \otimes a_{\tilde{\beta}}]_M^J |\text{HF}\rangle}{\langle 00JM | J_N M_N \rangle \widehat{J}_N^{-1}} = \widehat{J}_N \langle N | [a_\alpha^\dagger \otimes a_{\tilde{\beta}}]_{M_N}^{J_N} |\text{HF}\rangle \quad (6.4.2)$$

Expanding the two tensor products of this density generates a pair of Clebsch-Gordan coefficients and a contraction of creation and annihilation operators between two HF states. The evaluation of these terms is straightforward and leads to the result:

$$\rho_{\alpha\beta}^{HF \rightarrow N, J} = \widehat{J}_N \delta_{\alpha p} \delta_{\beta h} \delta_{J_N J} \quad (6.4.3)$$

Our purpose here is to derive a formula for the transition density's reduced matrix elements of equation (4.1.6) in the particular case when $|N_1\rangle$ is an uncorrelated 1p1h excited state and $|N_3\rangle$ is an uncorrelated 2p2h excited state. We define uncorrelated 1p1h excited states by:

$$|N_1\rangle = [a_{p_1}^\dagger \otimes a_{\tilde{h}_1}]_{M_1}^{J_1} |\text{HF}\rangle = \sum_{\substack{m_{p_1} \\ m_{h_1}}} (-)^{j_{h_1} - m_{h_1}} \langle j_{p_1} m_{p_1} j_{h_1} - m_{h_1} | J_1 M_1 \rangle a_{p_1}^\dagger a_{h_1} |\text{HF}\rangle \quad (6.4.4)$$

In order to construct an uncorrelated 2p2h state, we consider another 1p1h state:

$$|N_2\rangle = [a_{p_2}^\dagger \otimes a_{\tilde{h}_2}]_{M_2}^{J_2} |\text{HF}\rangle \quad (6.4.5)$$

and from this, the uncorrelated 2p2h state reads:

$$\begin{aligned} |N_3\rangle &= |N_2 \otimes N_1\rangle = N \left[[a_{p_2}^\dagger \otimes a_{\tilde{h}_2}]_{M_2}^{J_2} \otimes [a_{p_1}^\dagger \otimes a_{\tilde{h}_1}]_{M_1}^{J_1} \right]_{M_3}^{J_3} |\text{HF}\rangle \\ &= N \sum_{\substack{m_{p_1} m_{h_1} \\ m_{p_2} m_{h_2} \\ M_1 M_2}} (-)^{j_{h_1} + j_{h_2} - m_{h_1} - m_{h_2}} \langle j_{p_1} m_{p_1} j_{h_1} - m_{h_1} | J_1 M_1 \rangle \langle j_{p_2} m_{p_2} j_{h_2} - m_{h_2} | J_2 M_2 \rangle \\ &\quad \langle J_2 M_2 J_1 M_1 | J_3 M_3 \rangle a_{p_2}^\dagger a_{h_2} a_{p_1}^\dagger a_{h_1} |\text{HF}\rangle \end{aligned} \quad (6.4.6)$$

where N is a normalization factor. A difference can be made between the case when $p_1 \neq p_2$ and $h_1 \neq h_2$, and other cases.

6.4.1.1 Case when $p_1 \neq p_2$ and $h_1 \neq h_2$

When the particle states are different as well as the hole states, the calculation of the normalization factor reads:

$$\begin{aligned} \langle N_3 | N_3 \rangle = & |N|^2 \sum_{\text{all } m_i} (-)^{2j_{h_1} + 2j_{h_2} - m_{h_1} - m_{h_2} - m'_{h_1} - m'_{h_2}} \langle j_{p_1} m'_{p_1} j_{h_1} - m'_{h_1} | J_1 M'_1 \rangle \langle j_{p_2} m'_{p_2} j_{h_2} - m'_{h_2} | J_2 M'_2 \rangle \\ & \langle J_2 M'_2 J_1 M'_1 | J_3 M_3 \rangle \langle j_{p_1} m_{p_1} j_{h_1} - m_{h_1} | J_1 M_1 \rangle \langle j_{p_2} m_{p_2} j_{h_2} - m_{h_2} | J_2 M_2 \rangle \\ & \langle J_2 M_2 J_1 M_1 | J_3 M_3 \rangle \langle \text{HF} | a_{h'_1}^\dagger a_{p'_1}^\dagger a_{h'_2}^\dagger a_{p'_2}^\dagger a_{h_2} a_{p_1} | \text{HF} \rangle \end{aligned}$$

By using the Wick theorem, we can expand the contraction of creation and annihilation operators as:

$$\begin{aligned} \langle \text{HF} | a_{h'_1}^\dagger a_{p'_1}^\dagger a_{h'_2}^\dagger a_{p'_2}^\dagger a_{h_2} a_{p_1} | \text{HF} \rangle = & \langle \text{HF} | a_{h'_1}^\dagger a_{h_2} | \text{HF} \rangle \langle \text{HF} | a_{p'_1}^\dagger a_{p'_2} | \text{HF} \rangle \langle \text{HF} | a_{h'_2}^\dagger a_{h_1} | \text{HF} \rangle \\ & \langle \text{HF} | a_{p'_2}^\dagger a_{p_1} | \text{HF} \rangle \\ & - \langle \text{HF} | a_{h'_1}^\dagger a_{h_2} | \text{HF} \rangle \langle \text{HF} | a_{p'_1}^\dagger a_{p_1} | \text{HF} \rangle \langle \text{HF} | a_{h'_2}^\dagger a_{h_1} | \text{HF} \rangle \\ & \langle \text{HF} | a_{p'_2}^\dagger a_{p_2} | \text{HF} \rangle \\ & - \langle \text{HF} | a_{h'_1}^\dagger a_{h_1} | \text{HF} \rangle \langle \text{HF} | a_{p'_1}^\dagger a_{p'_2} | \text{HF} \rangle \langle \text{HF} | a_{h'_2}^\dagger a_{h_2} | \text{HF} \rangle \\ & \langle \text{HF} | a_{p'_2}^\dagger a_{p_1} | \text{HF} \rangle \\ & + \langle \text{HF} | a_{h'_1}^\dagger a_{h_1} | \text{HF} \rangle \langle \text{HF} | a_{p'_1}^\dagger a_{p_1} | \text{HF} \rangle \langle \text{HF} | a_{h'_2}^\dagger a_{h_2} | \text{HF} \rangle \\ & \langle \text{HF} | a_{p'_2}^\dagger a_{p_2} | \text{HF} \rangle \end{aligned}$$

and by using the properties of HF single particle states we can reduce this formula to:

$$\langle \text{HF} | a_{h'_1}^\dagger a_{p'_1}^\dagger a_{h'_2}^\dagger a_{p'_2}^\dagger a_{h_2} a_{p_1} | \text{HF} \rangle = \delta_{h'_1 h_1} \delta_{p'_1 p_1} \delta_{h'_2 h_2} \delta_{p'_2 p_2} \quad (6.4.7)$$

We insert this result in the normalization factor's formula:

$$\begin{aligned} 1 = \langle N_3 | N_3 \rangle = & |N|^2 \sum_{\text{all } m_i} (-)^{2j_{h_1} + 2j_{h_2} - 2m_{h_1} - 2m_{h_2}} \langle j_{p_1} m_{p_1} j_{h_1} - m_{h_1} | J_1 M'_1 \rangle \langle j_{p_2} m_{p_2} j_{h_2} - m_{h_2} | J_2 M'_2 \rangle \\ & \langle J_2 M'_2 J_1 M'_1 | J_3 M_3 \rangle \langle j_{p_1} m_{p_1} j_{h_1} - m_{h_1} | J_1 M_1 \rangle \langle j_{p_2} m_{p_2} j_{h_2} - m_{h_2} | J_2 M_2 \rangle \\ & \langle J_2 M_2 J_1 M_1 | J_3 M_3 \rangle \delta_{h'_1 h_1} \delta_{p'_1 p_1} \delta_{h'_2 h_2} \delta_{p'_2 p_2} \\ = & |N|^2 \sum_{\text{all } m_i} \langle j_{p_1} m_{p_1} j_{h_1} - m_{h_1} | J_1 M_1 \rangle^2 \langle j_{p_2} m_{p_2} j_{h_2} - m_{h_2} | J_2 M_2 \rangle^2 \\ & \langle J_2 M_2 J_1 M_1 | J_3 M_3 \rangle^2 \delta_{M'_1 M_1} \delta_{M'_2 M_2} \\ = & |N|^2 \end{aligned}$$

where we used (A.0.10) the closure relation of Wigner 3J coefficients associated to Clebsch-Gordan coefficients. So the normalization factor is $e^{i\theta}$, $\theta \in \mathbb{R}$, and we choose the $N = 1$ value. Now, we can calculate the reduced matrix elements of transition density from an uncorrelated 1p1h state to a similar 2p2h state in the particular case where $p_1 \neq p_2$ and $h_1 \neq h_2$. In the following derivation, the initial 1p1h state on which we construct the 2p2h state will be labeled with an i to make it easily distinguished. Using equations (6.4.4) to (6.4.7), we write the reduced matrix elements of the 1-body coupling density as:

$$\begin{aligned} \rho_{\alpha\beta}^{N_i \rightarrow N_3, J} = & \sum_{\text{all } m_i} (-)^{j_{h_1} + j_{h_i} + j_{h_2} + j_\beta - m_{h_1} - m_{h_i} - m_{h_2} - m_\beta} \langle j_{p_1} m_{p_1} j_{h_1} - m_{h_1} | J_1 M_1 \rangle \\ & \langle j_{p_2} m_{p_2} j_{h_2} - m_{h_2} | J_2 M_2 \rangle \langle J_2 M_2 J_1 M_1 | J_3 M_3 \rangle \langle j_{p_i} m_{p_i} j_{h_i} - m_{h_i} | J_i M_i \rangle \\ & \frac{\langle j_\alpha m_\alpha j_\beta - m_\beta | J M \rangle}{\langle J_i M_i J M | J_3 M_3 \rangle \widehat{J}_3^{-1}} \langle \text{HF} | a_{h_1}^\dagger a_{p_1}^\dagger a_{h_2}^\dagger a_{p_2}^\dagger a_\alpha a_\beta a_{p_i}^\dagger a_{h_i} | \text{HF} \rangle \end{aligned}$$

$$\begin{aligned} \rho_{\alpha\beta}^{N_i \rightarrow N_3, J} = & \sum_{\text{all } m_i} (-)^{j_{h_1} + j_{h_i} + j_{h_2} + j_{\beta} - m_{h_1} - m_{h_i} - m_{h_2} - m_{\beta}} \frac{\langle \text{HF} | a_{h_1}^{\dagger} a_{p_1} a_{h_2}^{\dagger} a_{p_2} a_{\alpha}^{\dagger} a_{\beta} a_{p_i}^{\dagger} a_{h_i} | \text{HF} \rangle}{\langle J_i M_i J M | J_3 M_3 \rangle \widehat{J}_3^{-1}} \\ & (-)^{j_{p_1} - j_{h_1} + M_1 + j_{p_2} - j_{h_2} + M_2 + J_2 - J_1 + M_3 + j_{p_i} - j_{h_i} + M_i + j_{\alpha} - j_{\beta} + M} \\ & \widehat{J}_1 \widehat{J}_i \widehat{J}_2 \widehat{J}_3 \widehat{J} \begin{pmatrix} j_{p_1} & j_{h_1} & J_1 \\ m_{p_1} & -m_{h_1} & -M_1 \end{pmatrix} \begin{pmatrix} j_{p_2} & j_{h_2} & J_2 \\ m_{p_2} & -m_{h_2} & -M_2 \end{pmatrix} \\ & \begin{pmatrix} J_2 & J_1 & J_3 \\ M_2 & M_1 & -M_3 \end{pmatrix} \begin{pmatrix} j_{p_i} & j_{h_i} & J_i \\ m_{p_i} & -m_{h_i} & -M_i \end{pmatrix} \begin{pmatrix} j_{\alpha} & j_{\beta} & J \\ m_{\alpha} & -m_{\beta} & -M \end{pmatrix} \end{aligned}$$

So we have, after gathering the phases:

$$\begin{aligned} \rho_{\alpha\beta}^{N_i \rightarrow N_3, J} = & \sum_{\text{all } m_i} (-)^{j_{p_1} + j_{p_i} + j_{p_2} + j_{\alpha} + J_2 - J_1 + M_1 + M_i + M_2 + M_3 + M - m_{h_1} - m_{h_i} - m_{h_2} - m_{\beta}} \widehat{J}_1 \widehat{J}_i \widehat{J}_2 \widehat{J}_3 \widehat{J} \\ & \begin{pmatrix} j_{p_1} & j_{h_1} & J_1 \\ m_{p_1} & -m_{h_1} & -M_1 \end{pmatrix} \begin{pmatrix} j_{p_2} & j_{h_2} & J_2 \\ m_{p_2} & -m_{h_2} & -M_2 \end{pmatrix} \begin{pmatrix} J_2 & J_1 & J_3 \\ M_2 & M_1 & -M_3 \end{pmatrix} \\ & \begin{pmatrix} j_{p_i} & j_{h_i} & J_i \\ m_{p_i} & -m_{h_i} & -M_i \end{pmatrix} \begin{pmatrix} j_{\alpha} & j_{\beta} & J \\ m_{\alpha} & -m_{\beta} & -M \end{pmatrix} \\ & \frac{\langle \text{HF} | a_{h_1}^{\dagger} a_{p_1} a_{h_2}^{\dagger} a_{p_2} a_{\alpha}^{\dagger} a_{\beta} a_{p_i}^{\dagger} a_{h_i} | \text{HF} \rangle}{\langle J_i M_i J M | J_3 M_3 \rangle \widehat{J}_3^{-1}} \end{aligned} \quad (6.4.8)$$

Now, we need to calculate the contraction of creation and annihilation operators on the HF ground state. Using the anti-commutation relations of equation (4.4.2), we can show that:

$$\begin{aligned} \langle \text{HF} | a_{h_1}^{\dagger} a_{p_1} a_{h_2}^{\dagger} a_{p_2} a_{\alpha}^{\dagger} a_{\beta} a_{p_i}^{\dagger} a_{h_i} | \text{HF} \rangle = & \delta_{p_2\alpha} \delta_{h_2\beta} \delta_{p_1 p_i} \delta_{h_1 h_i} - \delta_{p_2\alpha} \delta_{h_2 h_i} \delta_{h_1 \beta} \delta_{p_1 p_i} - \\ & \delta_{p_2 p_i} \delta_{p_1 \alpha} \delta_{h_1 h_i} \delta_{h_2 \beta} + \delta_{p_2 p_i} \delta_{h_2 h_i} \delta_{p_1 \alpha} \delta_{h_1 \beta} \\ = & \rho_1 - \rho_2 - \rho_3 + \rho_4 \end{aligned} \quad (6.4.9)$$

Four terms appear in this sum, and each of them corresponds to a given starting state: ρ_1 represents the situation in which the initial state is $|N_1\rangle$ and the particle-hole pair embodied by $|N_2\rangle$ is built upon $|N_1\rangle$. ρ_4 is the inverse situation: the initial state is $|N_2\rangle$ and the pair $|N_1\rangle$ is built upon it. ρ_2 and ρ_3 are cases in which the initial state is a combination of the hole state of $|N_2\rangle$ (resp. $|N_1\rangle$) and the particle state of $|N_1\rangle$ (resp. $|N_2\rangle$). We give the derivation of $\rho_{\alpha\beta}^{N_i \rightarrow N_3, J}$ in appendix E for each term, and write the results here:

$$\begin{aligned} \rho_1 \rightarrow \rho_{p_2 h_2}^{N_i \rightarrow N_3, J} = & (-)^{J_1 - J_2 + J_3} \widehat{J}_3 \delta_{J J_2} \\ \rho_2 \rightarrow \rho_{p_1 h_2}^{N_i \rightarrow N_3, J} = & (-)^{J_2 - J_i + j_{p_1} + 2j_{h_1} + j_{p_2}} \widehat{J}_1 \widehat{J}_i \widehat{J}_2 \widehat{J}_3 \widehat{J} \begin{Bmatrix} J_i & J & J_3 \\ j_{h_2} & j_{p_2} & J_2 \\ j_{p_1} & j_{h_1} & J_1 \end{Bmatrix} \\ \rho_3 \rightarrow \rho_{p_2 h_1}^{N_i \rightarrow N_3, J} = & (-)^{J - J_3} (-)^{J_2 + j_{p_1} + 2j_{h_1} + j_{p_2}} \widehat{J}_1 \widehat{J}_i \widehat{J}_2 \widehat{J}_3 \widehat{J} \begin{Bmatrix} J & J_i & J_3 \\ j_{h_2} & j_{p_2} & J_2 \\ j_{p_1} & j_{h_1} & J_1 \end{Bmatrix} \\ \rho_4 \rightarrow \rho_{p_1 h_1}^{N_2 \rightarrow N_3, J} = & \widehat{J}_3 \delta_{J J_1} \end{aligned} \quad (6.4.10)$$

6.4.1.2 Other cases

When the two particles (or the two holes, or the two particles and the two holes) have the same quantum numbers (except the projection of their total angular momentum m_p), we

can use another coupling scheme for the final state that will help us simplify the formulae we want to derive. This choice of a new coupling scheme is motivated by the derivations done by Kawano *et al.* [113] and by Boeker [115]. Instead of coupling pairs of particle-hole, we recouple the particles (resp. the holes) together:

$$|N_3\rangle = N \left[[a_{p_1} \otimes a_{p_2}]_{M_p}^{J_p} \otimes [a_{h_1}^\dagger \otimes a_{h_2}^\dagger]_{M_h}^{J_h} \right]_{M_3}^{J_3} |\text{HF}\rangle \quad (6.4.11)$$

The states built with this coupling scheme are orthogonal to those used in the previous subsection for $p_1 \neq p_2$ and $h_1 \neq h_2$. The evaluation of the normalization factor N can be done exactly like in the previous case, by first uncoupling the states:

$$\begin{aligned} 1 = \langle N_3 | N_3 \rangle = |N|^2 \sum (-)^{2j_{h_1} + 2j_{h_2} - m_{h_1} - m_{h_2} - m'_{h_1} - m'_{h_2}} & \langle j_{p_2} m'_{p_2} j_{p_1} - m'_{p_1} | J_p M'_p \rangle \langle j_{h_2} m'_{h_2} j_{h_1} - m'_{h_1} | J_h M'_h \rangle \\ & \langle J_h M'_h J_p M'_p | J_3 M_3 \rangle \langle j_{p_1} m_{p_1} j_{p_2} - m_{p_2} | J_p M_p \rangle \langle j_{h_1} m_{h_1} j_{h_2} - m_{h_2} | J_h M_h \rangle \\ & \langle J_h M_h J_p M_p | J_3 M_3 \rangle \langle \text{HF} | a_{h_2}^\dagger a_{h_1}^\dagger a_{p_2} a_{p_1} a_{p_1}^\dagger a_{p_2}^\dagger a_{h_1} a_{h_2} | \text{HF} \rangle \end{aligned} \quad (6.4.12)$$

and then using the Wick theorem:

$$\begin{aligned} \langle \text{HF} | a_{h_2}^\dagger a_{h_1}^\dagger a_{p_2} a_{p_1} a_{p_1}^\dagger a_{p_2}^\dagger a_{h_1} a_{h_2} | \text{HF} \rangle &= \delta_{h_2' h_2} \delta_{h_1' h_1} \delta_{p_2' p_2} \delta_{p_1' p_1} - \delta_{h_2' h_1} \delta_{h_1' h_2} \delta_{p_2' p_2} \delta_{p_1' p_1} \\ &\quad - \delta_{h_2' h_2} \delta_{h_1' h_1} \delta_{p_2' p_1} \delta_{p_1' p_2} + \delta_{h_2' h_1} \delta_{h_1' h_2} \delta_{p_2' p_1} \delta_{p_1' p_2} \\ &= \rho_1 - \rho_2 - \rho_3 + \rho_4 \end{aligned} \quad (6.4.13)$$

We consider here three cases:

- $p_1 = p_2$ and $h_1 = h_2$
- $p_1 = p_2$ and $h_1 \neq h_2$
- $p_1 \neq p_2$ and $h_1 = h_2$

In the case of $p_1 \neq p_2$ and $h_1 = h_2$, only two terms ρ_1 and ρ_2 subsist in (6.4.13). When we calculate the norm in this case, the following factor appears:

$$\langle j_{h_1} m_{h_1} j_{h_1} - m_{h_2} | J_h M_h \rangle - \langle j_{h_1} m_{h_2} j_{h_1} - m_{h_1} | J_h M_h \rangle$$

and with the property (A.0.2) of Clebsch-Gordan coefficients, we can rewrite this factor as:

$$\langle j_{h_1} m_{h_1} j_{h_1} - m_{h_2} | J_h M_h \rangle (1 - (-)^{2j_{h_1} + J_h})$$

Then, the sums over projections of angular momenta reduces thanks to (A.0.10) and (A.0.11) and we finally get:

$$|N|^2 = 1 + (-)^{J_h}$$

The demonstration is similar for the two other cases, and finally the normalized state reads:

$$|N_3\rangle = \frac{\sqrt{(1 + (-)^{J_p} \delta_{p_1 p_2})(1 + (-)^{J_h} \delta_{h_1 h_2})}}{(1 + \delta_{p_1 p_2})(1 + \delta_{h_1 h_2})} \left[[a_{p_1}^\dagger \otimes a_{p_2}^\dagger]^{J_p} \otimes [a_{h_1} \otimes a_{h_2}]^{J_h} \right]_{M_3}^{J_3} |\text{HF}\rangle \quad (6.4.14)$$

The derivation of the reduced matrix elements for the transition density from the initial state $|N_1\rangle$ defined in equation (6.4.4) to $|N_3\rangle$ in the new coupling scheme can be done by using the same derivation method that we used previously. But there is another method,

which we describe here in the case when the initial state is $|N_1\rangle$. We need to calculate (we omit the normalization factor for now):

$$\rho_{p_2 h_2}^{N_1 \rightarrow N_3, J} = \frac{\widehat{J}_3}{\langle J_1 M_1 J M | J_3 M_3 \rangle} \langle HF | \left[[a_{p_1}^\dagger \otimes a_{p_2}^\dagger]^{J_p} \otimes [a_{h_1} \otimes a_{h_2}]^{J_h} \right]_{M_3}^{J_3} \left[a_{p_2}^\dagger \otimes a_{h_2} \right]_M^J \left[a_{p_1}^\dagger \otimes a_{h_1} \right]_{M_1}^{J_1} |HF\rangle \quad (6.4.15)$$

Instead of uncoupling all the terms, we can recouple J_1 and J to J_3 which yields:

$$\rho_{p_2 h_2}^{N_1 \rightarrow N_3, J} = \widehat{J}_3 (-)^{J_1 + J - J_3} \langle HF | \left[[a_{p_1}^\dagger \otimes a_{p_2}^\dagger]^{J_p} \otimes [a_{h_1} \otimes a_{h_2}]^{J_h} \right]_{M_3}^{J_3} \left[[a_{p_2}^\dagger \otimes a_{h_2}]^J \otimes [a_{p_1}^\dagger \otimes a_{h_1}]^{J_1} \right]_{M_3}^{J_3} |HF\rangle \quad (6.4.16)$$

and then we can use the definition of the Wigner 9J symbols:

$$\left[[a_{p_2}^\dagger \otimes a_{h_2}]^J \otimes [a_{p_1}^\dagger \otimes a_{h_1}]^{J_1} \right]_{M_3}^{J_3} |HF\rangle = \sum_{J_p J_h} \widehat{J}_1 \widehat{J}_2 \widehat{J}_p \widehat{J}_h \begin{Bmatrix} j_{p_2} & j_{h_2} & J \\ j_{p_1} & j_{h_1} & J_1 \\ J_p & J_h & J_3 \end{Bmatrix} \left[[a_{p_2}^\dagger \otimes a_{p_1}^\dagger]^{J_p} \otimes [a_{h_2} \otimes a_{h_1}]^{J_h} \right]_{M_3}^{J_3} |HF\rangle \quad (6.4.17)$$

in order to correspond to the bra of equation (6.4.16), we must exchange the position of p_1 with that of p_2 and the position of h_1 with that of h_2 . This introduces two phases. Finally, when we insert this result in equation (6.4.16), we can simplify the global phase by inverting the positions of the two first rows in the Wigner 9J coefficient:

$$\rho_{p_2 h_2}^{N_1 \rightarrow N_3, J} = \widehat{J}_3 \widehat{J}_1 \widehat{J}_2 \widehat{J}_p \widehat{J}_h \begin{Bmatrix} j_{p_1} & j_{h_1} & J_1 \\ j_{p_2} & j_{h_2} & J \\ J_p & J_h & J_3 \end{Bmatrix} \quad (6.4.18)$$

The derivation is similar when for another initial state is $|N_i\rangle$ and the result differs simply by a phase $(-)^{J_i + J - J_3}$. The last step is to take into account the normalization factor, so we write the result in each case:

$$p_1 = p_2, h_1 = h_2 \rightarrow \rho_{p_1 h_1}^{N_1 \rightarrow N_3, J} = (1 + (-)^{J_p})(1 + (-)^{J_h}) \widehat{J}_1 \widehat{J}_2 \widehat{J}_3 \widehat{J}_p \widehat{J}_h \begin{Bmatrix} j_{p_1} & j_{h_1} & J_1 \\ j_{p_1} & j_{h_1} & J \\ J_p & J_h & J_3 \end{Bmatrix} \quad (6.4.19)$$

$$p_1 = p_2, h_1 \neq h_2 \rightarrow \rho_{p_1 h_1}^{N_1 \rightarrow N_3, J} = (1 + (-)^{J_p}) \widehat{J}_1 \widehat{J}_2 \widehat{J}_3 \widehat{J}_p \widehat{J}_h \begin{Bmatrix} j_{p_1} & j_{h_1} & J_1 \\ j_{p_1} & j_{h_2} & J \\ J_p & J_h & J_3 \end{Bmatrix} \quad (6.4.20)$$

$$\rho_{p_1 h_2}^{N_i \rightarrow N_3, J} = (1 + (-)^{J_p}) (-)^{J_i + J - J_3} \widehat{J}_i \widehat{J}_2 \widehat{J}_3 \widehat{J}_p \widehat{J}_h \begin{Bmatrix} j_{p_1} & j_{h_1} & J_i \\ j_{p_1} & j_{h_2} & J \\ J_p & J_h & J_3 \end{Bmatrix}$$

$$p_1 \neq p_2, h_1 = h_2 \rightarrow \rho_{p_1 h_1}^{N_1 \rightarrow N_3, J} = (1 + (-)^{J_h}) \widehat{J}_1 \widehat{J}_2 \widehat{J}_3 \widehat{J}_p \widehat{J}_h \begin{Bmatrix} j_{p_1} & j_{h_1} & J_1 \\ j_{p_2} & j_{h_1} & J \\ J_p & J_h & J_3 \end{Bmatrix} \quad (6.4.21)$$

$$\rho_{p_2 h_1}^{N_i \rightarrow N_3, J} = (1 + (-)^{J_p}) (-)^{J_i + J - J_3} \widehat{J}_i \widehat{J}_2 \widehat{J}_3 \widehat{J}_p \widehat{J}_h \begin{Bmatrix} j_{p_1} & j_{h_1} & J_i \\ j_{p_2} & j_{h_2} & J \\ J_p & J_h & J_3 \end{Bmatrix}$$

6.4.2 Counting of 2p2h states

We enumerated in ^{90}Zr all 1p1h and 2p2h states with natural parity up to 30 MeV of excitation energy, and we plotted the result on figure 6.10. This plot is to be compared to figure 6.4, which displays the same counting but for 1 and 2-phonon states. The same kind of differences between the number of 1p1h and 2p2h states, and between the number of 1-phonon and 2-phonon states is observed. We notice here that for excitation energies below 10 MeV, the number of collective states (phonons) is larger than the number of particle-hole states.

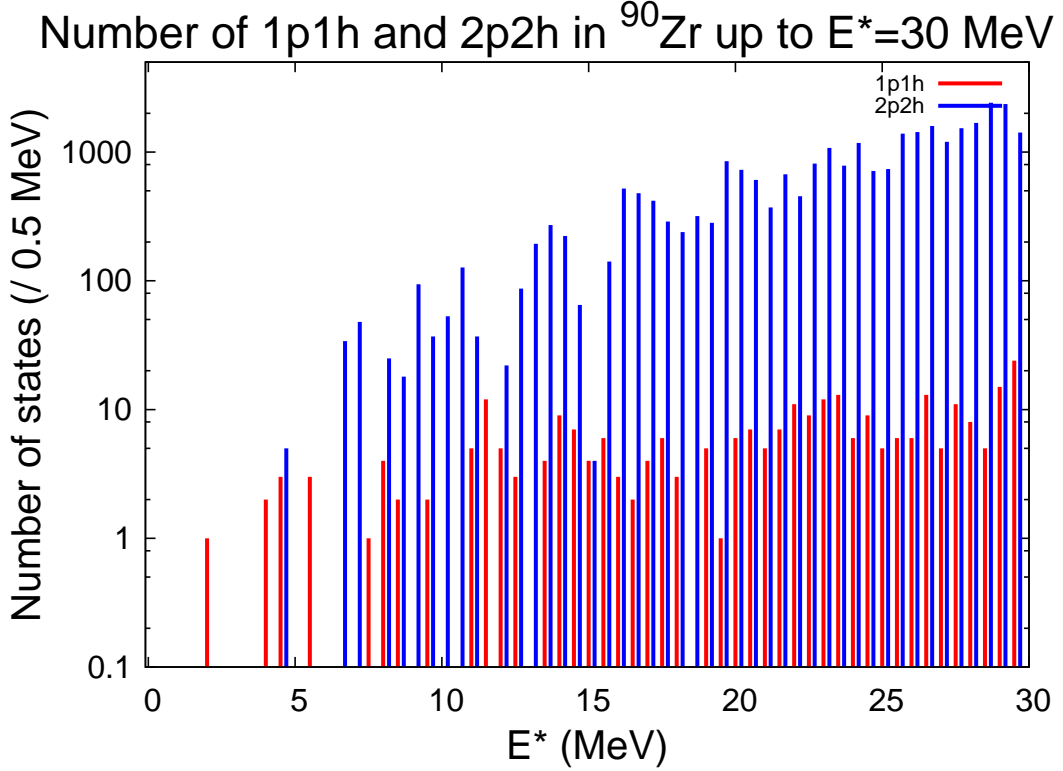


Figure 6.10: Comparison between the number of 1p1h and 2p2h states in ^{90}Zr for excitation energies below 30 MeV. The red bars correspond to the counting of all 1p1h states and the black bars are for the counting of all 2p2h states, in both cases for an energy bin of 0.5 MeV.

We investigated the effect of approximation A-3 in the case of particle-hole excitations. The calculation is done in the same spirit as that of Kawano *et al.* [113]. 1p1h states are defined by the set of quantum numbers $\{n_p, j_p, l_p, n_h, j_h, l_h, J\}$, while 2p2h states are defined by $\{n_{p_1}, j_{p_1}, l_{p_1}, n_{h_1}, j_{h_1}, l_{h_1}, J_1, n_{p_2}, j_{p_2}, l_{p_2}, n_{h_2}, j_{h_2}, l_{h_2}, J_2, J_3\}$. It is to be noticed that states with various $\{J_1, J_2, J_3\}$ numbers can have the same excitation energy but still need to be considered as different states, because the residual interaction beyond the mean-field level shall lift the degeneracy. So, we took a pair 1p1h coupled to 3^- , another pair coupled to 5^- and we formed the 2p2h states with spin and parity 2^+ , 4^+ , 6^+ and 8^+ . Given the result of equation (6.4.9), we need to consider (using equations (6.4.19) to (6.4.21)) all initial and intermediate states that can be formed by the four possible orderings of the particles and holes. In the present calculation, the initial states we have to consider are (keeping only states with natural parity):

- $\left[a_{p_1}^\dagger \otimes a_{\tilde{h}_1} \right]^{3^-}$, $\left[a_{p_2}^\dagger \otimes a_{\tilde{h}_2} \right]^{5^-}$
- $\left[a_{p_1}^\dagger \otimes a_{\tilde{h}_2} \right]^{1^-}$, $\left[a_{p_1}^\dagger \otimes a_{\tilde{h}_2} \right]^{3^-}$, $\left[a_{p_2}^\dagger \otimes a_{\tilde{h}_1} \right]^{3^-}$

We made a coherent calculation (without A-3) and compared it to the sum of incoherent calculations (with A-3). The result is displayed on figure 6.11 for the 2^+ (other cases show the same tendencies so we do not show them). We see that the angular distribution obtained with the incoherent sum is close to the prediction done with a coherent calculation, the situation is similar to the case displayed on figure 6.3 for collective states. This means that we can use approximation A-3 with confidence in the present case too.

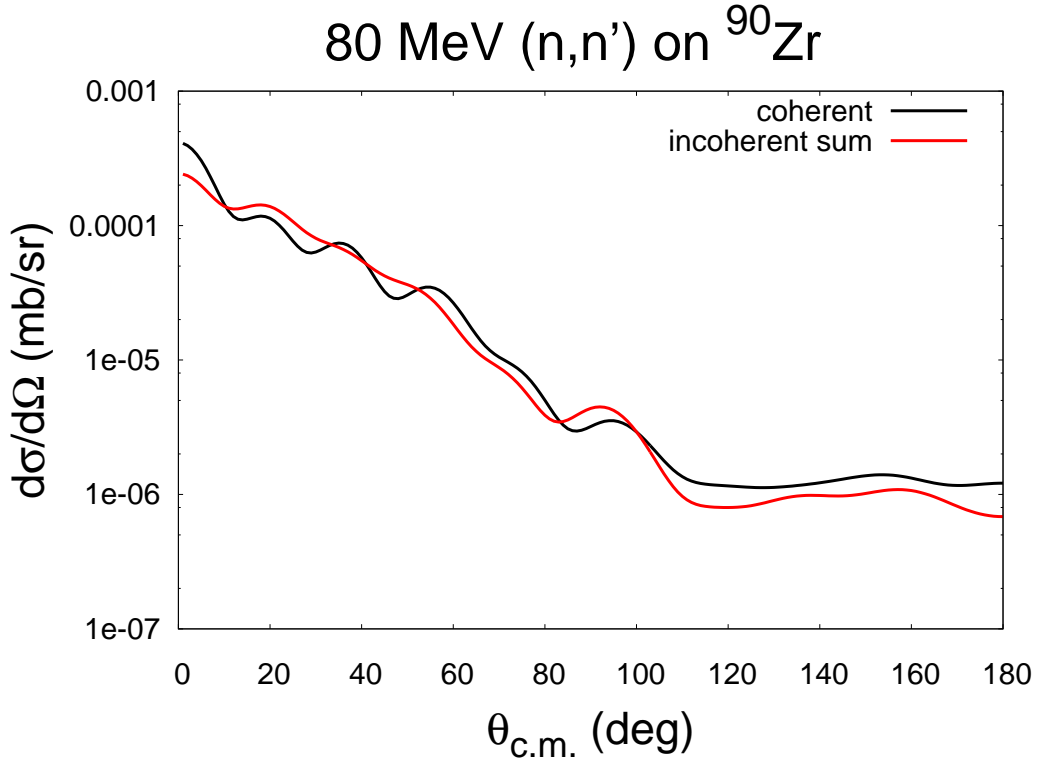


Figure 6.11: Comparison between the angular distribution obtained in a coherent calculation, and the sum of contributions coming from incoherent calculations. The red curve is for the incoherent sum, and the black curve for the coherent calculation.

Therefore, we made a calculation of the preequilibrium emission cross section in ^{90}Zr for an incident neutron with 80 MeV of kinetic energy. In this calculation, we considered the contribution of all 2p2h states with an excitation energy below 16 MeV, with natural parity and with a total spin $J \leq 8\hbar$ (to be consistent with the calculation done in the case of 2-phonon states). We used approximations A-0 to A-3, and only the central part of the Melbourne G matrix.

6.5 Comparison between the contributions of 2-phonon and 2p2h states

On figure 6.12, we display the angular distribution computed when considering collective states and when considering uncorrelated 2p2h states, for several bins in excitation energy.

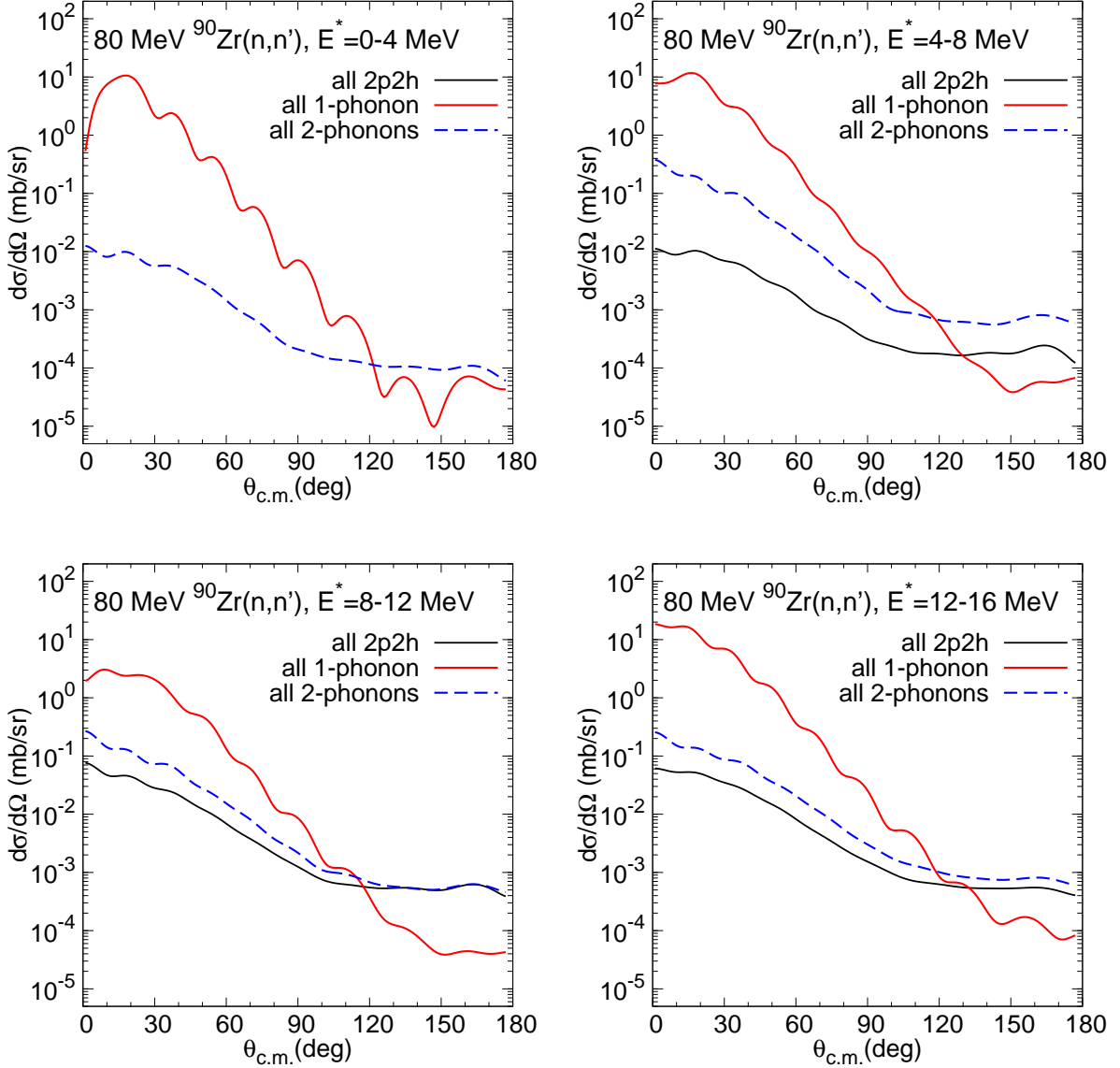


Figure 6.12: Comparison between the angular distribution obtained in a coherent calculation for 1 (red curves) and 2-phonon states (blue curves), and the sum of contributions coming from incoherent calculations of uncorrelated 2p2h (black curves) states. Each panel displays the angular distribution for preequilibrium emission due to states in a given energy bin. The upper left panel is for states with excitation energy between 0 and 4 MeV, the upper right for excitation energies between 4 and 8 MeV, the bottom left for excitation energies between 8 and 12 MeV, and the bottom right for excitation energies between 12 and 16 MeV.

Between 0 and 4 MeV of excitation energy, our calculation in ^{90}Zr (with the Gogny force D1S) yields no 2p2h state, but several 1 and 2-phonon states. Therefore, there is no contribution to the preequilibrium cross section coming from 2p2h states in this energy interval, but such is not the case for collective states. We observe that at backward angles, the contribution coming from 2-phonon states is larger than the contribution of 1-phonon states, which is consistent with the results displayed on figure 6.9.

Between 4 and 8 MeV of excitation energy, some 2p2h states are predicted but the number of 2-phonon states is still much larger, and consequently the angular distribution predicted when considering collective states is much larger. However, we notice an interesting feature: the difference between the cross section obtained with 2-phonon states and 2p2h states is larger at forward emission angles, and is almost constant for emission angles above 90° . At backward angles, both 2p2h and 2-phonon calculations yield a larger cross section than 1-phonon states.

Between 8 and 12 MeV of excitation energy, the number of 2p2h states is about 4 times larger than the number of 2-phonon states, but we still see that the 2-phonon contribution is larger than that of the 2p2h at forward angles. On the other hand, at backward angles, the two contributions are very close, and are quite larger than 1-phonon contributions.

Between 12 and 16 MeV of excitation energy, the numbers of 2p2h states and 2-phonon states are approximately comparable. The angular distribution predicted by each calculation presents similar discrepancies as those observed at lower excitation energies : at forward angles the 2-phonon calculation yields a larger cross section, and at backward angles this difference becomes smaller.

On figure 6.13, we display the angular distribution due to 1-phonon states, 2-phonon states and 2p2h states for all excitation energies between 0 and 16 MeV. The same trends are observed: at forward angles, the 1-phonon is clearly dominant, the 2-phonon contribution is larger than that of the 2p2h. As the emission angle increases, the contributions of 2-phonon states and 2p2h states gets closer and closer, and both become larger than the 1-phonon contribution for emission angles above 120° .

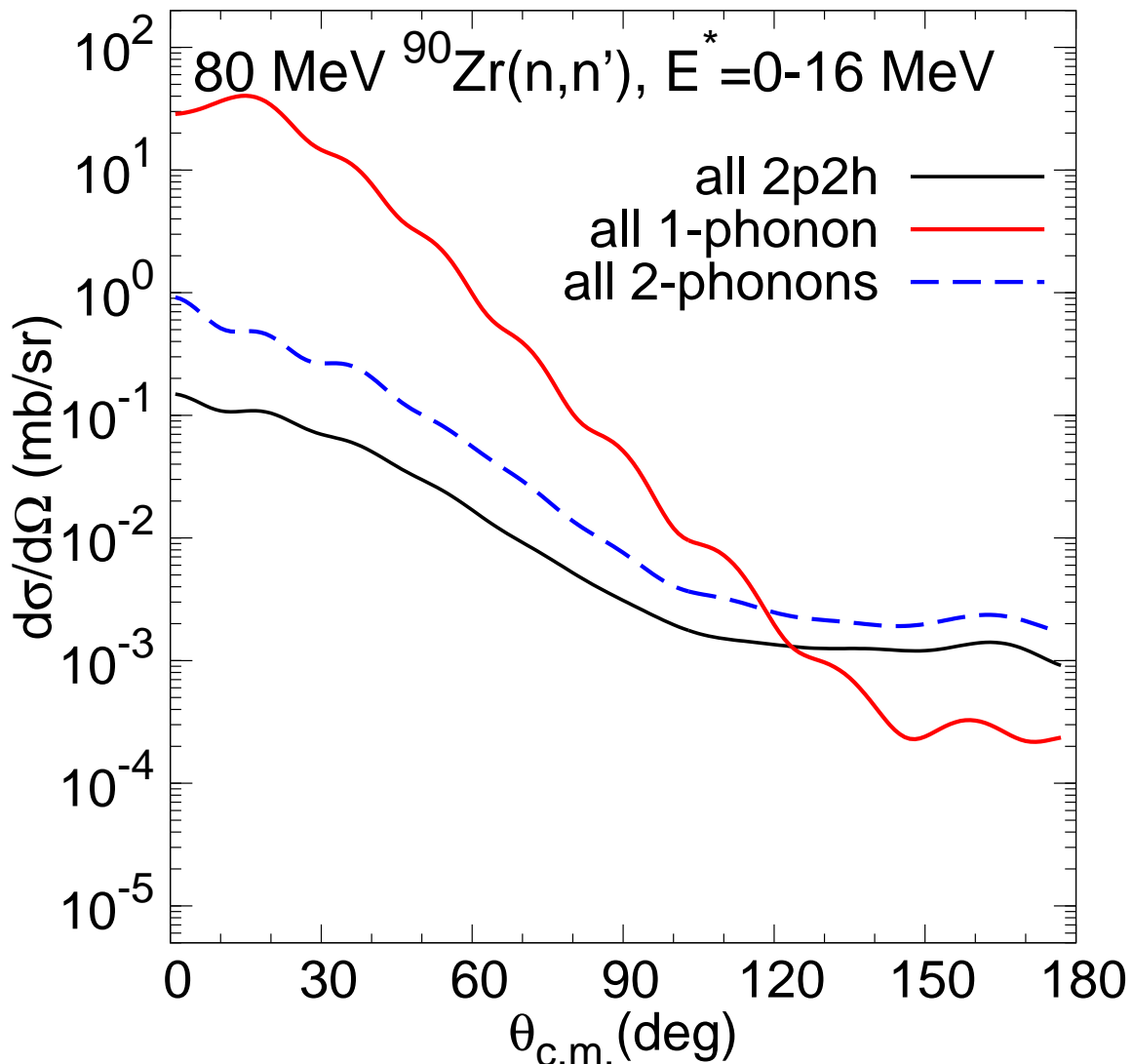


Figure 6.13: Comparison between the angular distribution obtained in a coherent calculation for 1 (red curves) and 2-phonon states (blue curves), and the sum of contributions coming from incoherent calculations of uncorrelated 2p2h (black curves) states. The excitation energies considered in this calculation range from 0 to 16 MeV.

At forward angles, the contributions to the cross section that come from states with low excitation energy and spin are dominant. We noticed in the counting of 2-phonon and 2p2h states that for low excitation energy there were more 2-phonon states, which is one source for the difference observed at forward angles. Another source is the impact of collectivity in a 2-step process. The last source we mention comes from using the QBA that we discuss in the next paragraph.

6.5.1 Violation of the Pauli exclusion principle due to the QBA

In section 4.5 we gave a microscopic description of a nucleus both at the mean field level (HF) and beyond (RPA). In our description of the RPA theory, we introduced the amplitudes X_{ph}^N and Y_{ph}^N . We can write for these amplitudes (using their definition and (4.4.7)):

$$X_{ph}^N = \langle \psi_N | a_p^\dagger a_h | \psi_0 \rangle = \langle \psi_0 | \Theta_N a_p^\dagger a_h | \psi_0 \rangle = \langle \psi_0 | [\Theta_N, a_p^\dagger a_h] | \psi_0 \rangle \quad (6.5.1)$$

$$Y_{ph}^N = \langle \psi_N | a_h^\dagger a_p | \psi_0 \rangle = \langle \psi_0 | \Theta_N a_h^\dagger a_p | \psi_0 \rangle = \langle \psi_0 | [\Theta_N, a_h^\dagger a_p] | \psi_0 \rangle$$

The calculation of these elements leads, using (4.4.8), to the evaluation of commutators of the form:

$$[a_h^\dagger a_p, a_{p'}^\dagger a_{h'}] = \delta_{hh'} \delta_{pp'} - \delta_{pp'} a_{h'} a_h^\dagger - \delta_{hh'} a_p a_{p'}^\dagger \quad (6.5.2)$$

The quasi-boson approximation assumes that the correlated ground state of the nucleus $|\psi_0\rangle$ is very close to the HF ground state $|\psi_{HF}\rangle$, which leads for these commutators to:

$$\langle \psi_0 | [a_h^\dagger a_p, a_{p'}^\dagger a_{h'}] | \psi_0 \rangle \approx \langle \psi_{HF} | [a_h^\dagger a_p, a_{p'}^\dagger a_{h'}] | \psi_{HF} \rangle = \delta_{hh'} \delta_{pp'} \quad (6.5.3)$$

Equation (6.5.3) violates the Pauli exclusion principle because terms coming from the commutator are neglected. Realistic calculations made with the RPA implemented with the Gogny D1S force [23, 43, 44, 64, 79] proved that this approximation holds in the case of 1-phonon states. However, we don't know the quality of this approximation in the case of 2-phonon states. The calculation we have done doesn't allow us to distinguish between the effects coming from the collectivity and from those that are due to the QBA. Therefore, it would be interesting to lift the QBA in the future.

One possible way would be to calculate the reduced matrix elements of the 1-body density provided in equation (4.4.33), but without relying on the QBA which means using the exact commutators given in equation (6.5.2). Another method would be to use nuclear structure information obtained with the second RPA, that mixes coherently ph, hp, phhp, phph and hphp components without using the QBA [116, 117]. However, a very large number of states for 1-step and 2-step processes will have to be considered which may render a practical calculation very heavy, so an initial study of randomness effects of components and cancellation through energy averaging should be considered first. We have shown with our approach that a first calculation for a large number of states was possible, so an exact calculation (with all the terms of the Melbourne G matrix) with and without considering randomness is feasible and can yield good insight on its effects. This would help in devising a relevant set of approximations for a complete MSD calculation at second (and then higher) order.

Chapter 7

Conclusion

Through this Ph.D. work, we have derived within a unique, consistent framework the coupled equations for the study of nucleon-nucleus elastic and inelastic scattering, and associated formulae for the computation of microscopic, nonlocal potentials using the nuclear matter approach. Basing ourselves on these equations and the HYDRA code provided to us by Arellano, we wrote two codes: the ECANOL program that solves CC equations using nonlocal potentials as input, and the MINOLOP code that computes microscopic nonlocal potentials within the nuclear matter framework. We made a first application using these new tools to improve the microscopic modeling of preequilibrium emissions by considering 2-step processes.

Within the nuclear matter approach, we use the Melbourne G matrix as effective NN interaction. We fold it to nuclear structure inputs under the form of 1-body densities obtained with the RPA implemented with the Gogny D1S force and single particle wave functions on a large basis computed with the D1S force as well. We thus obtain microscopic, parameter free, nonlocal potentials to study both elastic and inelastic scattering of a nucleon on a target nucleus.

We have derived all our equations in a unique angular momentum coupling scheme, starting from the time independent Schrödinger equation, to formulae for coupling potentials. Each obtained formula can be included in a computation code straightforwardly. Especially, we remained very general in our derivations for the nucleon-nucleus scattering problem, and also for coupling potentials. Consequently, the formulae we give hold for any local, finite range 2-body NN interaction with central, spin-orbit and tensor terms ; the one part that is specific in our study and that may require to be changed (depending on the NN interaction of choice) would be the radial form factors which are Yukawas in our case, and which are not difficult to change in our code. Again, we tried to derive and give the geometric matrix elements for each component of the Melbourne G matrix in a way that is as easy to code as possible.

Using this feature, we have written the MINOLOP code. We have presented how the inputs required by the code should be given and how we have validated central potentials computed with MINOLOP by comparing its calculation of the optical potential, the direct part of transition potentials and scattering observables to the same quantities computed by the ECIS-06 and the DWBA98 codes.

Similarly, we wrote the ECANOL code for the resolution of CC equations using nonlocal potentials as input and treating the nonlocality explicitly, without any localization procedure. This code can compute total, elastic and reaction cross sections, the angular distribution and the transferred momentum for nucleon-nucleus scattering reactions. Extending the code so as to calculate spin observables can be done easily by using the S matrix of equation (2.5.16). Using an example, we presented how ECANOL solves the scattering problem using a method - based on linear algebra - developed by Arellano, and extended by our means. We show our validation process first for elastic scattering by comparison to the DWBA98 code. Then, we briefly derived formulae for macroscopic potentials that we used to validate ECANOL by comparison to ECIS-06 ; we used the vibrational model to obtain transition potentials. We show that the agreement between ECANOL and ECIS-06 is satisfactory. We also studied the convergence of both codes as a function of the cutoff radius and of the mesh step size. We found that using a cutoff radius that is much bigger (at least by a factor 2) than the radius of the target nucleus is necessary to obtain a good convergence. We found that for ECIS-06 as well as for ECANOL, a reasonable step size that ensures a good convergence and that is not too costly in computational time is $h = 0.2fm$. Finally, we presented our validation of both ECANOL and MINOLOP for nonlocal potentials in the case of inelastic scattering.

We used our new tools ECANOL and MINOLOP to study the microscopic modeling of preequilibrium emissions. In the multistep direct process, we studied the inclusion of 2-step processes by considering 2-phonon states with natural parity obtained with the RPA from 1-phonon states (also obtained with the RPA and of natural parity), and we made another calculation of the 2-step processes by considering uncorrelated 2p2h excitations. Our results show the combined effects of the collectivity and of the QBA on the prediction of preequilibrium emission observables. Their impact is strong at forward angles, but almost negligible at backward angles. We propose ways to refine our calculation by removing the QBA, and explain the strength of our approach based on tools we developed during this thesis. One possible extension of these tools for preequilibrium calculations would be, rather than solving the whole linear system, to uncouple the system by first calculating the wave function in the elastic channel, use it as a source term for states associated to 1-step processes (1-phonon or 1p1h states), then by calculating the wave function for these same states and use the solutions as source terms for states associated to 2-step processes. This simplification is equivalent to an explicit calculation of the second order term in the Born expansion of the transition amplitude, and is closely related to the approach adopted by Kawano *et al.* [113]. The calculation we made for this work can be used to validate such an extension of our codes.

Through this application, we have demonstrated that ECANOL and MINOLOP are powerful tools to lead microscopic investigations on nucleon-nucleus direct reactions. But for now, MINOLOP is limited to the central part of a microscopic potential. Therefore, the implementation and the validation of the spin orbit and tensor terms of the interaction will have to be done in order to obtain potentials that can be used in studies involving comparisons to experimental data. Besides, we made our tests only with neutrons as projectiles, so in order to be able to study proton-nucleus reactions it will be necessary to add the 2-body Coulomb interaction in the determination of the potentials in MINOLOP. In principle, the treatment of a Coulomb potential in ECANOL is already validated because it was directly inherited from HYDRA, the code written and used by Arellano [62]. But it

was done with local, point-like Coulomb potentials so it will be necessary to validate this part too in ECANOL.

For the cases we have studied here, the time consumption of our codes presented at the end of chapter 5 was not too strongly limiting. But they can still be optimized and especially, they can be parallelized. We have designed MINOLOP and ECANOL in such a way that it should be straightforward to parallelize them and put them on modern supercomputers, which would open the way to very large scale studies. Moreover, the use of Lagrange mesh - which can considerably reduce the number of points required in the radial mesh - could be another very interesting improvement for the computation cost and, now that there exists a CC code for nonlocal potentials that uses the Lagrange mesh [58], we would have a reference for validations.

One particular application of interest would be the study in a fully microscopic framework of the rotational band of ^{238}U . In 2015, Dupuis *et al.* studied in a semi-microscopic framework the scattering of nucleons off ^{238}U [26]. Using the Jeukenne Lejeune Mahaux (JLM) folding model, and nuclear densities obtained with the Hartree-Fock-Bogoliubov and the Quasi particle Random Phase Approximation (QRPA) implemented with the Gogny D1S force, they studied and successfully described (n,n) and (n,n') reactions on ^{238}U for incident energies below 30 MeV. But some effects, including the nonlocality, were only partly taken into account because the potential they used were local. With the tools we have developed (once completed), it would be possible to study the same kind of reactions for incident energies above 40 MeV. One state of an axially deformed target nucleus can be taken as (in the intrinsic frame of the nucleus):

$$|\alpha K^\Pi\rangle \quad (7.0.1)$$

with α internal variables of the state, K the projection of the state's spin on the symmetry axis and Π its parity. In the particular case of ^{238}U , because it is an even-even nucleus, its ground state in the intrinsic frame can be shown to be $|\alpha 0^+\rangle$. We can build states in the lab frame by using the relation:

$$|\alpha J M K^\Pi = 0^+\rangle = \sqrt{\frac{2J+1}{8\pi^2}} \int \mathcal{D}_{M0}^{J*}(\Omega) R(\Omega) |\alpha 0^+\rangle d\Omega \quad (7.0.2)$$

with \mathcal{D}_{M0}^{J*} the Wigner rotation matrix elements and $R(\Omega)$ the rotation operator. From the $|\alpha 0^+\rangle$ ground state in the intrinsic frame, the rotational band made of $J^\Pi = 0^+, 2^+, 4^+ \dots$ is constructed. To study this band, we need to solve the system of coupled equations that links these states together. In particular, we need to compute the coupling potentials that appear in these equations. To do this in practice with our new tools, we will need to calculate terms that read:

$$\langle J_f M_f 0^+ | \widehat{V}_{\text{eff}} | J_i M_i 0^+ \rangle \quad (7.0.3)$$

Using (7.0.2), we can expand (7.0.3) and reach a form suitable for practical calculations with MINOLOP, if we choose to use the Melbourne G matrix as effective interaction and the results of QRPA calculations for 1-body densities done for example in Bruyères-le-Châtel [118, 119]. We could even consider cases in which we would study the coupling between the states of the rotational band formed by the ground state $|\alpha 0^+\rangle$ of ^{238}U , and the states in the band formed by an excited state in the intrinsic frame $|\alpha K^\Pi\rangle$. For such states, equation (7.0.2) is modified to (for $K > 0$):

$$|\alpha J M K^\Pi\rangle = \sqrt{\frac{2J+1}{16\pi^2}} \int \mathcal{D}_{MK}^{J*}(\Omega) R(\Omega) |\alpha K^\Pi\rangle d\Omega + (-)^{J+K} \mathcal{D}_{M-K}^{J*}(\Omega) R(\Omega) |\overline{\alpha K^\Pi}\rangle \quad (7.0.4)$$

with $|\overline{\alpha K^{\Pi}}\rangle$ the rotated state with negative spin projection on the quantization axis. For excited states with $K = 0$, the definition (7.0.2) still holds. Making such a study would constitute another step forward towards a fully microscopic study of nucleon direct elastic and direct inelastic scattering on ^{238}U and could help in a better modeling of these reactions which are, up to this day, not well enough described for applications like light water reactors [120, 121]. Some extension to our code MINOLOP would have to be done in order to generate potentials for such calculations, but ECANOL is ready for this kind of studies (provided the projectile is a neutron).

Another interesting application that can be done with our new codes is the investigation of nonlocal effects in CC equations. Most studies that use nonlocal potentials are done within the DWBA framework [23, 57, 63] and nucleon-nucleus direct inelastic scattering has yet to be studied with nonlocal potentials in the CC framework. In particular, we know the Perey effect in the case of inelastic scattering within the DWBA framework [24] but little is known about the effect of using local equivalent potentials in CC calculations. With our tools, it is possible to describe direct elastic and direct inelastic scattering of a nucleon off a target nucleus with microscopic nonlocal potentials, and then use macroscopic models to derive phenomenological potentials, fit their parameters so as to reproduce the scattering matrix obtained with our local potentials in the CC framework, and finally compare the solution wave functions computed by each method. The Perey effect was discovered using such a procedure but in the limit of elastic and inelastic scattering within the DWBA, we propose to extend the study to CC calculations with MINOLOP and ECANOL.

The nonlocality of potentials that are used in the GOM is difficult to interpret, and studies comparing the nonlocality of potentials derived with various methods are under way [122]. They show that even in the elastic scattering limit, the nonlocality of potentials obtained with Chiral interactions, realistic NN free interactions, the nuclear structure method and the nonlocality of the Perey-Buck are very different but lead to predictions of scattering observables that are remarkably similar qualitatively and quantitatively. With ECANOL and MINOLOP, it will be possible to add another computation method for the potentials in the comparison, and investigate how the difference in the nonlocality impacts the prediction of inelastic scattering observables.

ECANOL was designed to study nucleon-nucleus scattering within the CC and DWBA frameworks without any restriction on the target nucleus, but it has been validated and used mainly with medium to heavy mass nuclei. On the contrary, the code written by Descouvemont [58] was used with light targets. It would be interesting to compare the predictions of the two codes, especially since they rely on very different approaches to solve the CC system.

Recently, lots of efforts have been put in the theoretical description of surrogate reactions [123, 124]. ECANOL could be extended so as to treat such reactions using the CC framework, and it could also be used to compare predictions from surrogate models with more classical ones.

Finally, once ECANOL is optimized enough, it will be possible to add it to nuclear reaction codes like TALYS [125] and use it for nuclear data evaluation, thus allowing for the use of nonlocal potentials in the creation and improvement of data libraries.

Appendix A

Wigner 3J, 6J and 9J symbols, Clebsch-Gordan coefficients

The Clebsch-Gordan coefficients are a formulation of the addition of two angular momenta j_1 and j_2 in terms of a third one J :

$$|j_1 j_2 JM\rangle = \sum_{m_1 m_2} \langle j_1 m_1 j_2 m_2 | JM \rangle |j_1 m_1\rangle |j_2 m_2\rangle \quad (\text{A.0.1})$$

In which m_1 (resp. m_2 and M) is the projection of j_1 (resp. j_2 and J) on the quantization axis. The Clebsch-Gordan coefficient $\langle j_1 m_1 j_2 m_2 | JM \rangle$ is a real number that vanishes unless $m_1 + m_2 = M$ and $|j_1 - j_2| \leq J \leq j_1 + j_2$, and it follows the symmetry:

$$\langle j_1 m_1 j_2 m_2 | JM \rangle = (-)^{j_1 + j_2 - J} \langle j_2 m_2 j_1 m_1 | JM \rangle \quad (\text{A.0.2})$$

Special cases for these coefficients are:

$$\langle j_1 m_1 j_2 m_2 | 00 \rangle = \frac{(-)^{j_1 - m_1}}{\widehat{j_1}} \delta_{j_1, j_2} \delta_{m_1, -m_2} \quad (\text{A.0.3})$$

$$\langle j_1 m_1 00 | JM \rangle = \delta_{j_1, J} \delta_{m_1, M} \quad (\text{A.0.4})$$

Wigner 3J symbols are related to Clebsch-Gordan coefficients by:

$$\langle j_1 m_1 j_2 m_2 | JM \rangle = (-)^{j_1 - j_2 + M} \widehat{J} \begin{pmatrix} j_1 & j_2 & J \\ m_1 & m_2 & -M \end{pmatrix} \quad (\text{A.0.5})$$

Symmetries of the Wigner 3J coefficients read:

$$\begin{pmatrix} j_1 & j_2 & j_3 \\ m_1 & m_2 & m_3 \end{pmatrix} = \begin{pmatrix} j_2 & j_3 & j_1 \\ m_2 & m_3 & m_1 \end{pmatrix} = \begin{pmatrix} j_3 & j_1 & j_2 \\ m_3 & m_1 & m_2 \end{pmatrix} \quad (\text{A.0.6})$$

The 3J coefficients are multiplied by the phase $(-)^{j_1 + j_2 + j_3}$ upon interchange of two adjacent columns:

$$\begin{pmatrix} j_1 & j_2 & j_3 \\ m_1 & m_2 & m_3 \end{pmatrix} = (-)^{j_1 + j_2 + j_3} \begin{pmatrix} j_2 & j_1 & j_3 \\ m_2 & m_1 & m_3 \end{pmatrix} \quad (\text{A.0.7})$$

They vanish unless $m_1 + m_2 + m_3 = 0$ and they also obey the relation:

$$\begin{pmatrix} j_1 & j_2 & j_3 \\ m_1 & m_2 & m_3 \end{pmatrix} = (-)^{j_1 + j_2 + j_3} \begin{pmatrix} j_1 & j_2 & j_3 \\ -m_1 & -m_2 & -m_3 \end{pmatrix} \quad (\text{A.0.8})$$

Special value of 3J coefficients associated to equation (A.0.3) is:

$$\begin{pmatrix} j_1 & j_2 & 0 \\ m_1 & m_2 & 0 \end{pmatrix} = \frac{(-)^{j_1-m_1}}{\widehat{j_1}} \delta_{j_1, j_2} \delta_{m_1, -m_2} \quad (\text{A.0.9})$$

Finally, Wigner 3J coefficients follow the closure relations:

$$\sum_{m_1 m_2} \widehat{J}^2 \begin{pmatrix} j_1 & j_2 & J \\ m_1 & m_2 & M \end{pmatrix} \begin{pmatrix} j_1 & j_2 & J' \\ m_1 & m_2 & M' \end{pmatrix} = \delta_{JJ'} \delta_{MM'} \quad (\text{A.0.10})$$

$$\sum_{JM} \widehat{J}^2 \begin{pmatrix} j_1 & j_2 & J \\ m_1 & m_2 & M \end{pmatrix} \begin{pmatrix} j_1 & j_2 & J \\ m'_1 & m'_2 & M \end{pmatrix} = \delta_{m_1 m'_1} \delta_{m_2 m'_2} \quad (\text{A.0.11})$$

The Wigner 6J symbols are related to the Racah W function, which is a formulation of the addition of three angular momenta. They can be written in terms of 3J coefficients as:

$$\left\{ \begin{matrix} j_1 & j_2 & j_3 \\ j_4 & j_5 & j_6 \end{matrix} \right\} = \sum_{\text{all } m_i} (-)^{j_4+j_5+j_6+m_1+m_2+m_3} \begin{pmatrix} j_1 & j_2 & j_3 \\ m_1 & m_2 & m_3 \end{pmatrix} \begin{pmatrix} j_1 & j_5 & j_6 \\ m_1 & m_5 & -m_6 \end{pmatrix} \begin{pmatrix} j_4 & j_2 & j_6 \\ -m_4 & m_2 & m_6 \end{pmatrix} \begin{pmatrix} j_4 & j_5 & j_3 \\ m_4 & -m_5 & m_3 \end{pmatrix} \quad (\text{A.0.12})$$

These symbols are symmetric under the exchange of two columns, and also under the interchange of upper and downer arguments of two columns. Another important relation between 6J and 3J coefficients is:

$$\sum_{\substack{m_4 \\ m_5 \\ m_6}} (-)^{j_4+j_5+j_6+m_4+m_5+m_6} \begin{pmatrix} j_4 & j_5 & j_3 \\ m_4 & -m_5 & m_3 \end{pmatrix} \begin{pmatrix} j_5 & j_6 & j_1 \\ m_5 & -m_6 & m_1 \end{pmatrix} \begin{pmatrix} j_6 & j_4 & j_2 \\ m_6 & -m_4 & m_2 \end{pmatrix} = \begin{pmatrix} j_1 & j_2 & j_3 \\ m_1 & m_2 & m_3 \end{pmatrix} \left\{ \begin{matrix} j_1 & j_2 & j_3 \\ j_4 & j_5 & j_6 \end{matrix} \right\} \quad (\text{A.0.13})$$

and finally, we give a closure relation for 6J symbols:

$$\sum_{j_3} \widehat{j_3}^2 \widehat{j_6}^2 \left\{ \begin{matrix} j_1 & j_2 & j_3 \\ j_4 & j_5 & j_6 \end{matrix} \right\} \left\{ \begin{matrix} j_1 & j_2 & j_3 \\ j_4 & j_5 & j_7 \end{matrix} \right\} = \delta_{j_6 j_7} \quad (\text{A.0.14})$$

We also mention the Wigner 9J coefficients, used for the recoupling of 4 angular momenta, which can be expressed as:

$$\left\{ \begin{matrix} j_1 & j_2 & j_3 \\ j_4 & j_5 & j_6 \\ j_7 & j_8 & j_9 \end{matrix} \right\} = \widehat{j_1}^2 \sum \begin{pmatrix} j_1 & j_2 & j_3 \\ m_1 & m_2 & m_3 \end{pmatrix} \begin{pmatrix} j_2 & j_5 & j_8 \\ m_2 & m_5 & m_8 \end{pmatrix} \begin{pmatrix} j_3 & j_6 & j_9 \\ m_3 & m_6 & m_9 \end{pmatrix} \begin{pmatrix} j_1 & j_4 & j_7 \\ m_1 & m_4 & m_7 \end{pmatrix} \begin{pmatrix} j_4 & j_5 & j_6 \\ m_4 & m_5 & m_6 \end{pmatrix} \begin{pmatrix} j_7 & j_8 & j_9 \\ m_7 & m_8 & m_9 \end{pmatrix} \quad (\text{A.0.15})$$

Where the sum runs over all projections except m_1 .

Appendix B

The Gogny D1S force

The Gogny energy density functional with the parameterization D1S reads:

$$\begin{aligned}
 V(\vec{r}, \vec{r}') = & \sum_{j=1}^2 e^{-\frac{|\vec{r}-\vec{r}'|^2}{\mu_j^2}} (W_j + B_j P_\sigma - H_j P_\tau - M_j P_\sigma P_\tau) && \text{(Central term)} \\
 & + t_3(1 + x_0 P_\sigma) \delta(\vec{r} - \vec{r}') \rho^\alpha \left(\frac{\vec{r} + \vec{r}'}{2} \right) && \text{(Density term)} \\
 & + iW_{ls} \nabla_{rr'} \delta(\vec{r} - \vec{r}') \wedge \nabla_{rr'} \cdot (\sigma + \sigma') && \text{(Spin - Orbit term)} \\
 & + (1 + 2\tau_{1z})(1 + 2\tau_{2z}) \frac{e^2}{|\vec{r} - \vec{r}'|} && \text{(Coulomb term)}
 \end{aligned} \tag{B.0.1}$$

The value for all the parameters of the D1S parameterization of the Gogny force are given in reference [93].

Appendix C

Slater expansion of a Yukawa form factor

Any interaction that is expressed as a function of $|\vec{r}_1 - \vec{r}_2|$ can be expanded on the Legendre polynomial basis:

$$V(|\vec{r}_1 - \vec{r}_2|) = V(\sqrt{r_1^2 + r_2^2 - 2r_1r_2 \cos \omega_{12}}) = \sum_{k=0}^{\infty} V_k(r_1, r_2) P_k(\cos \omega_{12}) \quad (\text{C.0.1})$$

and the inverse relation reads:

$$V_k(r_1, r_2) = \frac{2k+1}{2} \int_{-1}^{+1} V(|\vec{r}_1 - \vec{r}_2|) P_k(\cos \omega_{12}) d \cos \omega_{12} \quad (\text{C.0.2})$$

By inserting (C.0.2) in (C.0.1) we obtain:

$$V(|\vec{r}_1 - \vec{r}_2|) = \sum_k \frac{2k+1}{2} \int \left(V(|\vec{r}_1 - \vec{r}_2|) P_k(\cos \omega_{12}) d \cos \omega_{12} \right) P_k(\cos \omega_{12}) \quad (\text{C.0.3})$$

The Slater - or multipole - expansion of an interaction is obtained in practice by evaluating the integral term. The interaction we use in our study is the Melbourne G matrix, which is parameterized as a sum of Yukawas. Therefore, we will now proceed with the calculation of the integral, assuming a Yukawa form for V . We write V as:

$$V(|\vec{r}_1 - \vec{r}_2|) = \frac{e^{-\frac{|\vec{r}_1 - \vec{r}_2|}{\mu}}}{|\vec{r}_1 - \vec{r}_2|} \quad (\text{C.0.4})$$

with μ the range. We insert this expression in:

$$V(|\vec{r}_1 - \vec{r}_2|) = \sum_k \frac{2k+1}{2} \int \left(\frac{e^{-\frac{|\vec{r}_1 - \vec{r}_2|}{\mu}}}{|\vec{r}_1 - \vec{r}_2|} P_k(\cos \omega_{12}) d \cos \omega_{12} \right) P_k(\cos \omega_{12}) \quad (\text{C.0.5})$$

In order to calculate this integral, we do a changing in the variables:

$$w = \frac{|\vec{r}_1 - \vec{r}_2|}{\mu} \quad u = \frac{r_1 + r_2}{\mu} \quad v = \frac{r_1 - r_2}{\mu} \quad m = \sqrt{\frac{u^2 + v^2}{2}} \quad \kappa = \frac{u^2 - v^2}{u^2 + v^2} \quad (\text{C.0.6})$$

and we use these new variables to rewrite the integral of equation (C.0.5) as:

$$V(|\vec{r}_1 - \vec{r}_2|) = \sum_k \frac{2k+1}{2} \frac{4}{u^2 - v^2} \int_{|v|}^u \left[P_k \left(\frac{1 - w^2/m^2}{\kappa} \right) e^{-w} dw \right] P_k(\cos \omega_{12}) \quad (\text{C.0.7})$$

We can use the results derived by Watson [126] to express this integral in terms of modified Bessel functions of the first and second kinds:

$$\begin{aligned} V(|\vec{r}_1 - \vec{r}_2|) &= \sum_k (2k+1) \frac{K_{k+\frac{1}{2}}\left(\frac{r_1}{\mu}\right) I_{k+\frac{1}{2}}\left(\frac{r_2}{\mu}\right)}{\sqrt{r_1 r_2}} P_k(\cos \omega_{12}), & r_1 > r_2 \\ &= \sum_k V_k(r_1, r_2) P_k(\cos \omega_{12}) \\ &= \sum_k V_k(r_1, r_2) \overline{\overline{C}}_k(1) \cdot \overline{\overline{C}}_k(2) \\ &= \sum_k \frac{4\pi}{2k+1} V_k(r_1, r_2) \overline{\overline{Y}}_k(1) \cdot \overline{\overline{Y}}_k(2) \end{aligned} \quad (\text{C.0.8})$$

where we have used the addition theorem for normalized spherical harmonic tensors, and in which we use the notation $\overline{\overline{T}}$ to denote an irreducible spherical tensor operator (we use this notation henceforth). The great advantage given by this multipole expansion is that the interaction is now divided into a sum of a term that depends only on radial variables and one term that contains the geometric dependence of the interaction. Furthermore, this geometric dependence is expressed in terms of tensor operators for which powerful matrix elements evaluation technics exist. We use these technics in the next appendix to derive geometric terms for the operators that appear in the parameterization of the Melbourne G matrix.

Appendix D

Matrix elements

Eventhough the free NN interaction is not known exactly, many of its features have been established as early as in the 1950s. In particular, it contains a central, a spin-orbit and a tensor terms. The derivations of these terms are out of the scope of the present work, but it is interesting to note that formulae (4.3.5) and (4.3.6) can be obtained whether by using fundamental symmetries, or by starting from the meson-exchange picture of nuclear forces. Similarly, many existing NN effective interactions are made of a central, a spin-orbit and a tensor operators. Therefore, geometric matrix elements for each of these operators can be used for any interaction provided it has such operators. Blanchon *et al.* derived formulae for both the geometric matrix elements and the radial form factors of the potential computed from the Gogny D1S force [127]. We provide here all the details of these derivations with the same conventions and notations that we used in the rest of this manuscript, for the operators that intervene in the parameterization of the Melbourne G matrix. The work done here is also valid for any 2-body, finite range interaction with the same operators as presented hereafter.

D.1 Central terms

The central term of the Melbourne G matrix, which depends on the total spin and isospin, reads:

$$V_{\text{central}} = \sum_{S,T=0,1} V_{\text{central}}^{ST} P^S P^T \quad (\text{D.1.1})$$

which can be shown to be equivalent to:

$$V_{\text{central}} = (V_{\text{central}}^{00} + V_{\text{central}}^{01}) \left(1 - \frac{S^2}{2}\right) + (V_{\text{central}}^{10} + V_{\text{central}}^{11}) \frac{S^2}{2} \quad (\text{D.1.2})$$

so the central part of the effective interaction will have terms that depend on the total spin S and terms that don't depend on it. We shall derive formulae for both cases.

D.1.1 Central terms, spin independent

We use a scheme in which the two particles connected by the interaction are coupled to a total angular momentum J :

$$\begin{aligned}
 (jj_\alpha J | V_{\text{central}}(\vec{r}, \vec{r}') | j' j_\beta J) &= (jj_\alpha J | \sum_k V_k(r_1, r_2) \overline{C}_k(1) \cdot \overline{C}_k(2) | j' j_\beta J) \\
 &= \sum_k (-)^{j_\alpha + j' + J} \begin{Bmatrix} j & j_\alpha & J \\ j_\beta & j' & k \end{Bmatrix} \langle l \frac{1}{2} j | \overline{C}_k(1) | l' \frac{1}{2} j' \rangle \\
 &\quad \langle l_\alpha \frac{1}{2} j_\alpha | \overline{C}_k(2) | l_\beta \frac{1}{2} j_\beta \rangle
 \end{aligned} \tag{D.1.3}$$

Reduced matrix elements for tensor spherical harmonic operators have been derived by Talmi [80]:

$$\langle \frac{1}{2} l j | \overline{C}_k | \frac{1}{2} l' j' \rangle = (-)^{j - \frac{1}{2}} \widehat{j j'} \begin{pmatrix} j & k & j' \\ -\frac{1}{2} & 0 & \frac{1}{2} \end{pmatrix} \frac{1 + (-)^{l+l'+k}}{2} \tag{D.1.4}$$

This result is given assuming a coupling scheme $[s \otimes l]_m^j$ which is different from the coupling scheme we have used through all our derivations. Thus, we change the coupling order:

$$\begin{aligned}
 |j_1 j_2 J\rangle &= \sum_{m_1 m_2} \langle j_1 j_2 m_1 m_2 | J m \rangle |j_1 m_1\rangle |j_2 m_2\rangle \\
 &= \sum_{m_1 m_2} (-)^{j_1 - j_2 + m} \widehat{J} \begin{pmatrix} j_1 & j_2 & J \\ m_1 & m_2 & -m \end{pmatrix} |j_1 m_1\rangle |j_2 m_2\rangle \\
 &= \sum_{m_1 m_2} (-)^{j_1 - j_2 + m} \widehat{J} (-)^{j_1 + j_2 + J} \begin{pmatrix} j_2 & j_1 & J \\ m_2 & m_1 & -m \end{pmatrix} |j_1 m_1\rangle |j_2 m_2\rangle \\
 &= \sum_{m_1 m_2} (-)^{3j_1 - j_2 + J} \widehat{J} (-)^{j_2 - j_1 + m} \begin{pmatrix} j_2 & j_1 & J \\ m_2 & m_1 & -m \end{pmatrix} |j_1 m_1\rangle |j_2 m_2\rangle \\
 &= (-)^{3j_1 - j_2 + J} |j_2 j_1 J\rangle = (-)^{J - j_1 - j_2} |j_2 j_1 J\rangle
 \end{aligned}$$

which yields once inserted in (D.1.4):

$$\langle l \frac{1}{2} j | \overline{C}_k | l' \frac{1}{2} j' \rangle = (-)^{j - l - \frac{1}{2} + j' - l' - \frac{1}{2}} \langle \frac{1}{2} l j | \overline{C}_k | \frac{1}{2} l' j' \rangle = (-)^{j' - \frac{1}{2} - l - l'} \widehat{j j'} \begin{pmatrix} j & k & j' \\ -\frac{1}{2} & 0 & \frac{1}{2} \end{pmatrix} \frac{1 + (-)^{l+l'+k}}{2} \tag{D.1.5}$$

and finally we use this result in equation (D.1.2) which yields the general formula for geometric matrix elements of the central, spin-independent term of a finite-range 2-body interaction:

$$\boxed{
 \begin{aligned}
 (jj_\alpha J | V_{\text{central}}(\vec{r}, \vec{r}') | j' j_\beta J) &= \sum_k (-)^{j_\alpha + 2j' + j_\beta + J - l - l' - l_\alpha - l_\beta - 1} \widehat{j j'} \widehat{j_\alpha j_\beta} \begin{Bmatrix} j & j_\alpha & J \\ j_\beta & j' & k \end{Bmatrix} \\
 &\quad \begin{pmatrix} j & k & j' \\ -\frac{1}{2} & 0 & \frac{1}{2} \end{pmatrix} \begin{pmatrix} j_\alpha & k & j_\beta \\ -\frac{1}{2} & 0 & \frac{1}{2} \end{pmatrix} \frac{1 + (-)^{l+l'+k}}{2} \frac{1 + (-)^{l_\alpha + l_\beta + k}}{2}
 \end{aligned}
 } \tag{D.1.6}$$

D.1.2 Central terms, spin dependent

As shown on equation (D.1.2), the Melbourne G matrix contains terms which consist of a product of a spin-independent interaction times S^2 . Consequently, we will change the

coupling scheme from a JJ form to a Russel-Saunders (LS) form in which S^2 is diagonal. The transformation from a JJ to a LS coupling scheme reads:

$$|ll_\alpha jj_\alpha J\rangle = \sum_{LS} \widehat{j} \widehat{j}_\alpha \widehat{L} \widehat{S} \begin{Bmatrix} l & l_\alpha & L \\ \frac{1}{2} & \frac{1}{2} & S \\ j & j_\alpha & J \end{Bmatrix} |ll_\alpha LSJ\rangle \quad (\text{D.1.7})$$

which allows us to rewrite matrix elements as:

$$(jj_\alpha J | V_{\text{central}}(\vec{r}, \vec{r}') S^2 | j' j_\beta J) = \sum_{\substack{LS \\ L'S'}} \widehat{j} \widehat{j}_\alpha \widehat{L} \widehat{S} \widehat{j}' \widehat{j}'_\beta \widehat{L}' \widehat{S}' \begin{Bmatrix} l & l_\alpha & L \\ \frac{1}{2} & \frac{1}{2} & S \\ j & j_\alpha & J \end{Bmatrix} \begin{Bmatrix} l' & l_\beta & L' \\ \frac{1}{2} & \frac{1}{2} & S' \\ j' & j_\beta & J \end{Bmatrix} (ll_\alpha LSJ | V_{\text{central}}(\vec{r}, \vec{r}') S^2 | l' l_\beta L' S' J)$$

Moreover, the coupled state vector $|ll_\alpha LSJ\rangle$ can be written in an uncoupled form:

$$|ll_\alpha LSJ\rangle = \sum_{m_L m_S} \langle L S m_L m_S | J M \rangle |S m_S\rangle |ll_\alpha L m_L\rangle \quad (\text{D.1.8})$$

that can be used to write:

$$(jj_\alpha J | V_{\text{central}}(\vec{r}, \vec{r}') S^2 | j' j_\beta J) = \sum_{LSL'S'} \widehat{j} \widehat{j}_\alpha \widehat{L} \widehat{S} \widehat{j}' \widehat{j}'_\beta \widehat{L}' \widehat{S}' \begin{Bmatrix} l & l_\alpha & L \\ \frac{1}{2} & \frac{1}{2} & S \\ j & j_\alpha & J \end{Bmatrix} \begin{Bmatrix} l' & l_\beta & L' \\ \frac{1}{2} & \frac{1}{2} & S' \\ j' & j_\beta & J \end{Bmatrix} \sum_{\substack{m_L m_S \\ m_{L'} m_{S'}}} \langle L S m_L m_S | J M \rangle \langle L' S' m_{L'} m_{S'} | J M \rangle (S m_S | \langle ll_\alpha L m_L | V_{\text{central}}(\vec{r}, \vec{r}') S^2 | l' l_\beta L' m_{L'} \rangle | S' m_{S'})$$

We now expand the interaction on a spherical harmonic basis and separate spin independent part of the matrix elements from spin independent parts:

$$(jj_\alpha J | V_{\text{central}}(\vec{r}, \vec{r}') S^2 | j' j_\beta J) = \sum_{LSL'S'k} \widehat{j} \widehat{j}_\alpha \widehat{L} \widehat{S} \widehat{j}' \widehat{j}'_\beta \widehat{L}' \widehat{S}' \begin{Bmatrix} l & l_\alpha & L \\ \frac{1}{2} & \frac{1}{2} & S \\ j & j_\alpha & J \end{Bmatrix} \begin{Bmatrix} l' & l_\beta & L' \\ \frac{1}{2} & \frac{1}{2} & S' \\ j' & j_\beta & J \end{Bmatrix} \sum_{\substack{m_L m_S \\ m_{L'} m_{S'}}} \langle L S m_L m_S | J M \rangle \langle L' S' m_{L'} m_{S'} | J M \rangle \langle S m_S | S^2 | S' m_{S'} \rangle (ll_\alpha L m_L | V_k(r, r') \overline{\overline{C}}_k(1) \cdot \overline{\overline{C}}_k(2) | l' l_\beta L' m_{L'})$$

Using results from tensor algebra and reduced matrix elements calculations [80], we may write:

$$\langle S m_S | S^2 | S' m_{S'} \rangle = \delta_{SS'} \delta_{m_S m_{S'}} S(S+1)$$

$$\langle ll_\alpha L m_L | \overline{\overline{C}}_k(1) \cdot \overline{\overline{C}}_k(2) | l' l_\beta L' m_{L'} \rangle = \delta_{LL'} \delta_{m_L m_{L'}} (-)^{2l_\alpha + l + l' + L} \widehat{l} \widehat{l}' \widehat{l}_\alpha \widehat{l}_\beta \begin{Bmatrix} l & l_\alpha & L \\ l_\beta & l' & k \end{Bmatrix} \begin{pmatrix} l & k & l' \\ 0 & 0 & 0 \end{pmatrix} \begin{pmatrix} l_\alpha & k & l_\beta \\ 0 & 0 & 0 \end{pmatrix}$$

We insert these relations in the previous equation to obtain:

$$(jj_\alpha J | V_{\text{central}}(\vec{r}, \vec{r}') S^2 | j' j_\beta J) = \sum_{LSk} (-)^{2l_\alpha + l + l' + L} \widehat{j} \widehat{j}_\alpha \widehat{L}^2 \widehat{S}^2 \widehat{j}' \widehat{j}'_\beta \begin{Bmatrix} l & l_\alpha & L \\ \frac{1}{2} & \frac{1}{2} & S \\ j & j_\alpha & J \end{Bmatrix} \begin{Bmatrix} l' & l_\beta & L \\ \frac{1}{2} & \frac{1}{2} & S \\ j' & j_\beta & J \end{Bmatrix} \sum_{\substack{m_L \\ m_S}} \langle L S m_L m_S | J M \rangle \langle L S m_L m_S | J M \rangle S(S+1) \delta_{LL'} \delta_{m_L m_{L'}} \widehat{l} \widehat{l}' \widehat{l}_\alpha \widehat{l}_\beta \begin{Bmatrix} l & l_\alpha & L \\ l_\beta & l' & k \end{Bmatrix} \begin{pmatrix} l & k & l' \\ 0 & 0 & 0 \end{pmatrix} \begin{pmatrix} l_\alpha & k & l_\beta \\ 0 & 0 & 0 \end{pmatrix}$$

Using sum rules of the Clebsch-Gordan coefficients associated to equation (A.0.10), we can further simplify this relation and, finally, give the fully expanded geometric matrix elements of the spin-dependent central term of the interaction:

$$\begin{aligned}
 (jj_\alpha J|V_{\text{central}}(\vec{r}, \vec{r}')S^2|j'j_\beta J) = \sum_{LSk} (-)^{2l_\alpha+l+l'+L} \widehat{j} \widehat{j}_\alpha \widehat{j}' \widehat{j}_\beta \widehat{L}^2 \widehat{S}^2 S(S+1) \widehat{l} \widehat{l}' \widehat{l}_\alpha \widehat{l}_\beta \begin{Bmatrix} l & l_\alpha & L \\ \frac{1}{2} & \frac{1}{2} & S \\ j & j_\alpha & J \end{Bmatrix} \\
 \begin{Bmatrix} l' & l_\beta & L \\ \frac{1}{2} & \frac{1}{2} & S \\ j' & j_\beta & J \end{Bmatrix} \begin{Bmatrix} l & l_\alpha & L \\ l_\beta & l' & k \end{Bmatrix} \begin{pmatrix} l & k & l' \\ 0 & 0 & 0 \end{pmatrix} \begin{pmatrix} l_\alpha & k & l_\beta \\ 0 & 0 & 0 \end{pmatrix}
 \end{aligned}
 \tag{D.1.9}$$

D.2 Spin-orbit terms

While matrix elements for the central part of the Melbourne G matrix have been fully included and validated in MINOLOP, only the geometric matrix elements for the 2-body spin orbit term have been implemented and partly validated. We provide here the derivation of these terms. The orbital angular momentum part of the 2-body spin-orbit operator from equation (4.3.6) can be written as:

$$\begin{aligned}
 \vec{L}_{12} = \vec{L}_1 + \vec{L}_2 + \mathbf{i} \vec{n}_1 \wedge \vec{n}_2 \left(r_1 \frac{\partial}{\partial r_2} - r_2 \frac{\partial}{\partial r_1} \right) \\
 + \vec{n}_1 \wedge (\vec{n}_2 \wedge \vec{L}_2) \frac{r_1}{r_2} \\
 + \vec{n}_2 \wedge (\vec{n}_1 \wedge \vec{L}_1) \frac{r_2}{r_1}
 \end{aligned}
 \tag{D.2.1}$$

with $\vec{n}_i = \frac{\vec{r}_i}{|\vec{r}_i|}$. This forms a spin-orbit operator that is basically a sum of three independent terms:

- The usual 1-body operator $\vec{L} \cdot \vec{S}$
- A derivative term
- Two double vector products, which we choose to label X_{12} and X_{21} terms

We will now derive fully expanded expressions of their geometric matrix elements.

D.2.1 1-body L.S term

The obvious coupling scheme to be used in the calculation of 1-body spin-orbit operator matrix elements is again the Russel-Saunders (LS) coupling scheme. Therefore, we start from:

$$\begin{aligned}
 (jj_\alpha J|V_{\text{central}}(\vec{r}, \vec{r}') \vec{L} \cdot \vec{S} |j'j_\beta J) = \sum_{\substack{LS \\ L'S'}} \widehat{j} \widehat{j}_\alpha \widehat{L} \widehat{S} \widehat{j}' \widehat{j}_\beta \widehat{L}' \widehat{S}' \begin{Bmatrix} l & l_\alpha & L \\ \frac{1}{2} & \frac{1}{2} & S \\ j & j_\alpha & J \end{Bmatrix} \begin{Bmatrix} l' & l_\beta & L' \\ \frac{1}{2} & \frac{1}{2} & S' \\ j' & j_\beta & J \end{Bmatrix} \\
 \times (ll_\alpha LSJ|V_{\text{central}}(\vec{r}, \vec{r}') \vec{L} \cdot \vec{S} |l'l_\beta L'S'J)
 \end{aligned}
 \tag{D.2.2}$$

The total angular momentum of the system is defined by $\vec{J} = \vec{L} + \vec{S}$. Therefore, we can write the scalar product of the total angular orbital momentum and the total spin as $\vec{L} \cdot \vec{S} = \frac{J^2 - L^2 - S^2}{2}$. We will use this form to further expand the matrix elements' expression:

$$(jj_\alpha J | V_{\text{central}}(\vec{r}, \vec{r}') \vec{L} \cdot \vec{S} | j' j_\beta J) = \sum_{\substack{LS \\ L'S'}} \widehat{j} \widehat{j}_\alpha \widehat{L} \widehat{S} \widehat{j}' \widehat{j}_\beta \widehat{L}' \widehat{S}' \begin{Bmatrix} l & l_\alpha & L \\ \frac{1}{2} & \frac{1}{2} & S \\ j & j_\alpha & J \end{Bmatrix} \begin{Bmatrix} l' & l_\beta & L' \\ \frac{1}{2} & \frac{1}{2} & S' \\ j' & j_\beta & J \end{Bmatrix} \\ \times (l_\alpha LSJ | V_{\text{central}}(\vec{r}, \vec{r}') \frac{J^2 - L^2 - S^2}{2} | l' l_\beta L' S' J) \quad (\text{D.2.3})$$

By properties of the angular momentum (similar expressions can be derived for L^2 and S^2):

$$(l_\alpha LSJ | V_{\text{central}}(\vec{r}, \vec{r}') J^2 | l' l_\beta L' S' J) = J(J+1) \sum_{\substack{m_L m_S \\ m_{L'} m_{S'}}} \langle L S m_L m_S | J M \rangle \langle L' S' m_{L'} m_{S'} | J M \rangle \\ \langle S m_S | S' m_{S'} \rangle \\ (l_\alpha L m_L | V_k(r, r') \overline{C}_k(1) \cdot \overline{C}_k(2) | l' l_\beta L' m_{L'})$$

and matrix elements $(l_\alpha L m_L | V_k(r, r') \overline{C}_k(1) \cdot \overline{C}_k(2) | l' l_\beta L' m_{L'})$ have already been given in the derivation of central spin-dependent terms. Therefore we can give the fully expanded matrix elements of the 1-body spin-orbit operator:

$$(jj_\alpha J | V_{\text{central}}(\vec{r}, \vec{r}') \vec{L} \cdot \vec{S} | j' j_\beta J) = \sum_{LSk} (-)^{l+l'+L} \widehat{j} \widehat{j}_\alpha \widehat{j}' \widehat{j}_\beta \widehat{L}^2 \widehat{S}^2 \widehat{l} \widehat{l}_\alpha \widehat{l}_\beta \begin{Bmatrix} l & l_\alpha & L \\ \frac{1}{2} & \frac{1}{2} & S \\ j & j_\alpha & J \end{Bmatrix} \begin{Bmatrix} l' & l_\beta & L' \\ \frac{1}{2} & \frac{1}{2} & S' \\ j' & j_\beta & J \end{Bmatrix} \\ \frac{J(J+1) - L(L+1) - S(S+1)}{2} \begin{Bmatrix} l & l_\alpha & L \\ l_\beta & l' & k \end{Bmatrix} \\ \begin{pmatrix} l & k & l' \\ 0 & 0 & 0 \end{pmatrix} \begin{pmatrix} l_\alpha & k & l_\beta \\ 0 & 0 & 0 \end{pmatrix} \quad (\text{D.2.4})$$

D.2.2 Derivative term

The operator we labeled as derivative will be shown to consist of a tensor operator of rank 1. We will first give an appropriate expression of the operator before proceeding with the matrix elements expansion. The so-called derivative operator's expression is:

$$V_{\text{derivative}} = \mathbf{i} \vec{n}_1 \wedge \vec{n}_2 \left(r_1 \frac{\partial}{\partial r_2} - r_2 \frac{\partial}{\partial r_1} \right) \cdot \vec{S} \quad (\text{D.2.5})$$

A vector product of unitary vectors can be expressed as a tensor product of rank 1 of spherical harmonics:

$$\mathbf{i} \vec{n}_1 \wedge \vec{n}_2 = \sqrt{2} \left[\overline{C}_1(1) \otimes \overline{C}_1(2) \right]^1 \quad (\text{D.2.6})$$

and the 2-body interaction itself can be extended on a spherical harmonics basis which, combined with the previous equation yields:

$$\begin{aligned}
 V_{\text{derivative}} &= \sum_k \sqrt{2} \left(\overline{C}_k(1) \cdot \overline{C}_k(2) \right) \left[\overline{C}_1(1) \otimes \overline{C}_1(2) \right]^1 \cdot \vec{S} \\
 &= \sqrt{2} \sum_{kk_1k_2} (-)^{k_1} \widehat{k}_1 \widehat{k}_2 \begin{Bmatrix} k_1 & k & 1 \\ 1 & 1 & k_2 \end{Bmatrix} \left[\left[\overline{C}_k(1) \otimes \overline{C}_1(1) \right]^{k_1} \otimes \left[\overline{C}_k(2) \otimes \overline{C}_1(2) \right]^{k_2} \right]^1 \cdot \vec{S} \\
 &= \sqrt{2} \sum_{kk_1k_2} (-)^{k_1} \widehat{k}_1 \widehat{k}_2 \begin{Bmatrix} k_1 & k & 1 \\ 1 & 1 & k_2 \end{Bmatrix} (-)^{k-1} \widehat{k}_1 \begin{pmatrix} k & 1 & k_1 \\ 0 & 0 & 0 \end{pmatrix} (-)^{k-1} \widehat{k}_2 \begin{pmatrix} k & 1 & k_2 \\ 0 & 0 & 0 \end{pmatrix} \\
 &\hspace{20em} \left[\overline{C}_{k_1}(1) \otimes \overline{C}_{k_2}(2) \right]^1 \cdot \vec{S}
 \end{aligned}$$

which, after simplification of the phases, yields the general tensor expression of the spin-orbit derivative operator:

$$V_{\text{derivative}} = \sqrt{2} \sum_{kk_1k_2} (-)^{k_1} \widehat{k}_1^2 \widehat{k}_2^2 \begin{Bmatrix} k_1 & k & 1 \\ 1 & 1 & k_2 \end{Bmatrix} \begin{pmatrix} k & 1 & k_1 \\ 0 & 0 & 0 \end{pmatrix} \begin{pmatrix} k & 1 & k_2 \\ 0 & 0 & 0 \end{pmatrix} \left[\overline{C}_{k_1}(1) \otimes \overline{C}_{k_2}(2) \right]^1 \cdot \vec{S} \quad (\text{D.2.7})$$

This form is suitable for calculating matrix elements in the Russel-Saunders coupling scheme:

$$\begin{aligned}
 (jj_\alpha J | V_{\text{derivative}} | j'j_\beta J) &= \sum_{\substack{kk_1k_2 \\ LL'SS'}} (-)^{k_1} \widehat{k}_1^2 \widehat{k}_2^2 \widehat{j} \widehat{j}_\alpha \widehat{L} \widehat{S} \widehat{j}' \widehat{j}_\beta \widehat{L}' \widehat{S}' \begin{Bmatrix} k_1 & k & 1 \\ 1 & 1 & k_2 \end{Bmatrix} \begin{pmatrix} k & 1 & k_1 \\ 0 & 0 & 0 \end{pmatrix} \begin{pmatrix} k & 1 & k_2 \\ 0 & 0 & 0 \end{pmatrix} \\
 &\quad \left\{ \begin{matrix} l & l_\alpha & L \\ \frac{1}{2} & \frac{1}{2} & S \\ j & j_\alpha & J \end{matrix} \right\} \left\{ \begin{matrix} l' & l_\beta & L' \\ \frac{1}{2} & \frac{1}{2} & S' \\ j' & j_\beta & J \end{matrix} \right\} (ll_\alpha LSJ | \left[\overline{C}_{k_1}(1) \otimes \overline{C}_{k_2}(2) \right]^1 \cdot \vec{S} | l'l_\beta L'S'J)
 \end{aligned}$$

We separate the total spin operator from the spherical harmonic tensors:

$$\begin{aligned}
 (ll_\alpha LSJ | \left[\overline{C}_{k_1}(1) \otimes \overline{C}_{k_2}(2) \right]^1 \cdot \vec{S} | l'l_\beta L'S'J) &= (-)^{L+S'+J} \begin{Bmatrix} S & L & J \\ L' & S' & 1 \end{Bmatrix} \langle S | \vec{S} | S' \rangle (ll_\alpha L | \\
 &\hspace{15em} \left[\overline{C}_{k_1}(1) \otimes \overline{C}_{k_2}(2) \right]^1 | l'l_\beta L')
 \end{aligned}$$

We use the general result stating that $\langle S | \vec{S} | S' \rangle = \sqrt{S(S+1)(2S+1)} \delta_{SS'}$, and we can uncouple L and L' to calculate the harmonic tensors matrix elements:

$$\begin{aligned}
 (ll_\alpha L | \left[\overline{C}_{k_1}(1) \otimes \overline{C}_{k_2}(2) \right]^1 | l'l_\beta L') &= \widehat{L} \widehat{L}' \widehat{1} \begin{Bmatrix} l & l_\alpha & L \\ l' & l_\beta & L' \\ k_1 & k_2 & 1 \end{Bmatrix} \langle l | \overline{C}_{k_1}(1) | l' \rangle \langle l_\alpha \overline{C}_{k_2}(2) | l_\beta \rangle \\
 &= \widehat{L} \widehat{L}' \widehat{1} \begin{Bmatrix} l & l_\alpha & L \\ l' & l_\beta & L' \\ k_1 & k_2 & 1 \end{Bmatrix} (-)^{l+l_\alpha} \widehat{l} \widehat{l}' \widehat{l}_\alpha \widehat{l}_\beta \begin{pmatrix} l & k_1 & l' \\ 0 & 0 & 0 \end{pmatrix} \begin{pmatrix} l_\alpha & k_2 & l_\beta \\ 0 & 0 & 0 \end{pmatrix}
 \end{aligned}$$

Reuniting these expressions, we can write the full expansion of the direct derivative operator matrix elements:

$$\begin{aligned}
 (jj_\alpha J | V_{\text{derivative}} | j'j_\beta J) = & \sum_{\substack{kk_1k_2 \\ LL'SS'}} (-)^{L+S+J+k_1+l+l_\beta} \widehat{k}_1^2 \widehat{k}_2^2 \widehat{j} \widehat{j}_\alpha \widehat{j}' \widehat{j}_\beta \widehat{L}^2 \widehat{L}'^2 \widehat{S}^2 \sqrt{S(S+1)(2S+1)} \\
 & \widehat{1} \widehat{l} \widehat{l}' \widehat{l}_\alpha \widehat{l}_\beta \begin{Bmatrix} l & l_\alpha & L \\ \frac{1}{2} & \frac{1}{2} & S \\ j & j_\alpha & J \end{Bmatrix} \begin{Bmatrix} l' & l_\beta & L' \\ \frac{1}{2} & \frac{1}{2} & S \\ j' & j_\beta & J \end{Bmatrix} \begin{Bmatrix} l & l_\alpha & L \\ l' & l_\beta & L' \\ k_1 & k_2 & 1 \end{Bmatrix} \begin{Bmatrix} k_1 & k & 1 \\ 1 & 1 & k_2 \end{Bmatrix} \\
 & \begin{Bmatrix} S & L & J \\ L' & S & 1 \end{Bmatrix} \begin{pmatrix} k & 1 & k_1 \\ 0 & 0 & 0 \end{pmatrix} \begin{pmatrix} k & 1 & k_2 \\ 0 & 0 & 0 \end{pmatrix} \begin{pmatrix} l & k_1 & l' \\ 0 & 0 & 0 \end{pmatrix} \begin{pmatrix} l_\alpha & k_2 & l_\beta \\ 0 & 0 & 0 \end{pmatrix}
 \end{aligned} \tag{D.2.8}$$

D.2.3 X12 and X21 terms

These operators can be shown to reduce to a scalar product between a rank 1 tensor operator and \vec{S} . Following the same procedure as for the derivative term, we will first write the operator into a suitable tensor form, and afterwards express matrix elements. We remind the reader that we do not treat radial components here. The X12 term reads:

$$X_{12} = \vec{n}_1 \wedge (\vec{n}_2 \wedge \vec{l}_2) \cdot \vec{S} \frac{r_1}{r_2} \tag{D.2.9}$$

Writing this operator in terms of tensor products leads to (we omit the purely radial factor):

$$\begin{aligned}
 X_{12} &= -i\sqrt{2}\vec{n}_1 \wedge [\overline{C}_1(2) \otimes \overline{l}_2]^1 \cdot \vec{S} \\
 &= -i\sqrt{2} \times (-i\sqrt{2}) \left[\overline{C}_1(1) \otimes [\overline{C}_1(2) \otimes \overline{l}_2]^1 \right]^1 \cdot \vec{S} \\
 &= -2 \left[\overline{C}_1(1) \otimes [\overline{C}_1(2) \otimes \overline{l}_2]^1 \right]^1 \cdot \vec{S}
 \end{aligned}$$

We develop the 2-body interaction on a spherical harmonic basis and unite it with X_{12} :

$$\begin{aligned}
 V_{12} &= -2 \sum_k (\overline{C}_k(1) \cdot \overline{C}_k(2)) \left[\overline{C}_1(1) \otimes [\overline{C}_1(2) \otimes \overline{l}_2]^1 \right]^1 \cdot \vec{S} \\
 &= -2 \sum_{kk_1k_2} (-)^{k_1} \widehat{k}_1 \widehat{k}_2 \begin{Bmatrix} k_1 & k & 1 \\ 1 & 1 & k_2 \end{Bmatrix} \left[[\overline{C}_k(1) \otimes \overline{C}_1(1)]^{k_1} \otimes [\overline{C}_k(2) \otimes [\overline{C}_1(2) \otimes \overline{l}_2]^1]^{k_2} \right]^1 \cdot \vec{S} \\
 &= -2 \sum_{kk_1k_2} (-)^{k_1} \widehat{k}_1 \widehat{k}_2 \begin{Bmatrix} k_1 & k & 1 \\ 1 & 1 & k_2 \end{Bmatrix} (-)^{k-1} \widehat{k}_1 \begin{pmatrix} k & 1 & k_1 \\ 0 & 0 & 0 \end{pmatrix} \left[\overline{C}_{k_1}(1) \otimes [\overline{C}_k(2) \otimes [\overline{C}_1(2) \otimes \overline{l}_2]^1]^{k_2} \right]^1 \cdot \vec{S} \\
 &= -2 \sum_{kk_1k_2} (-)^{k_1+k-1} \widehat{k}_1^2 \widehat{k}_2 \begin{Bmatrix} k_1 & k & 1 \\ 1 & 1 & k_2 \end{Bmatrix} \begin{pmatrix} k & 1 & k_1 \\ 0 & 0 & 0 \end{pmatrix} \sum_{k_0} \widehat{k}_0^2 (-)^{k_2-1} \begin{pmatrix} k & 1 & k_0 \\ 0 & 0 & 0 \end{pmatrix} \begin{Bmatrix} k & 1 & k_0 \\ 1 & k_2 & 1 \end{Bmatrix} \\
 & \quad \left[\overline{C}_{k_1}(1) \otimes [\overline{C}_{k_0}(2) \otimes \overline{l}_2]^{k_2} \right]^1 \cdot \vec{S}
 \end{aligned}$$

which, after simplification, yields an appropriate expression of the V_{12} operator to be used to calculate its matrix elements:

$$V_{12} = -2 \sum_{\substack{k k_0 \\ k_1 k_2}} (-)^{k_1+k+k_2} \widehat{1} \widehat{k_0}^2 \widehat{k_1}^2 \widehat{k_2} \begin{Bmatrix} k_1 & k & 1 \\ 1 & 1 & k_2 \end{Bmatrix} \begin{Bmatrix} k & 1 & k_0 \\ 1 & k_2 & 1 \end{Bmatrix} \begin{pmatrix} k & 1 & k_1 \\ 0 & 0 & 0 \end{pmatrix} \begin{pmatrix} k & 1 & k_0 \\ 0 & 0 & 0 \end{pmatrix} \\ \left[\overline{\overline{C}}_{k_1}(1) \otimes \left[\overline{\overline{C}}_{k_0}(2) \otimes \overline{\overline{l}}_2 \right]^{k_2} \right]^1 \cdot \vec{S}$$

We now insert this operator in the Russel-Saunders coupling scheme:

$$(j j_\alpha J | V_{12} | j' j_\beta J) = \sum_{\substack{k k_0 k_1 k_2 \\ L L' S S'}} (-)^{k_1+k+k_2} \widehat{1} \widehat{k_0}^2 \widehat{k_1}^2 \widehat{k_2} \widehat{j} \widehat{j_\alpha} \widehat{L} \widehat{S} \widehat{j'} \widehat{j_\beta} \widehat{L'} \widehat{S'} \begin{Bmatrix} k_1 & k & 1 \\ 1 & 1 & k_2 \end{Bmatrix} \begin{Bmatrix} k & 1 & k_0 \\ 1 & k_2 & 1 \end{Bmatrix} \\ \begin{pmatrix} k & 1 & k_1 \\ 0 & 0 & 0 \end{pmatrix} \begin{pmatrix} k & 1 & k_0 \\ 0 & 0 & 0 \end{pmatrix} \begin{Bmatrix} l & l_\alpha & L \\ \frac{1}{2} & \frac{1}{2} & S \end{Bmatrix} \begin{Bmatrix} l' & l_\beta & L' \\ \frac{1}{2} & \frac{1}{2} & S' \end{Bmatrix} \\ (l l_\alpha L S J | \left[\overline{\overline{C}}_{k_1}(1) \otimes \left[\overline{\overline{C}}_{k_0}(2) \otimes \overline{\overline{l}}_2 \right]^{k_2} \right]^1 \cdot \vec{S} | l' l_\beta L' S' J)$$

The remaining matrix element can be simplified in three steps:

- First, we separate the spin operator from the orbital operator
- Then we uncouple the orbital angular momenta
- And finally we use tensor algebra to express the matrix elements of the remaining operators.

Let us apply this procedure to our case:

$$(l l_\alpha L S J | \left[\overline{\overline{C}}_{k_1}(1) \otimes \left[\overline{\overline{C}}_{k_0}(2) \otimes \overline{\overline{l}}_2 \right]^{k_2} \right]^1 \cdot \vec{S} | l' l_\beta L' S' J) \\ = (-)^{L+S'+J} \begin{Bmatrix} S & L & J \\ L' & S' & 1 \end{Bmatrix} \langle S | \vec{S} | S' \rangle (l l_\alpha L | \left[\overline{\overline{C}}_{k_1}(1) \otimes \left[\overline{\overline{C}}_{k_0}(2) \otimes \overline{\overline{l}}_2 \right]^{k_2} \right]^1 | l' l_\beta L') \\ = (-)^{L+S'+J} \begin{Bmatrix} S & L & J \\ L' & S' & 1 \end{Bmatrix} \sqrt{S(S+1)(2S+1)} \delta_{SS'} \widehat{1} \widehat{L} \widehat{L'} \begin{Bmatrix} l & l_\alpha & L \\ l' & l_\beta & L' \\ k_1 & k_2 & 1 \end{Bmatrix} \langle l | \overline{\overline{C}}_{k_1}(1) | l' \rangle \\ (l_\alpha | \left[\overline{\overline{C}}_{k_0}(2) \otimes \overline{\overline{L}}_2 \right]^{k_2} | l_\beta) \\ = (-)^{L+S'+J} \begin{Bmatrix} S & L & J \\ L' & S' & 1 \end{Bmatrix} \sqrt{S(S+1)(2S+1)} \delta_{SS'} \widehat{1} \widehat{L} \widehat{L'} \begin{Bmatrix} l & l_\alpha & L \\ l' & l_\beta & L' \\ k_1 & k_2 & 1 \end{Bmatrix} (-)^{l \widetilde{l'}} \begin{pmatrix} l & k_1 & l' \\ 0 & 0 & 0 \end{pmatrix} \\ (l_\alpha | \left[\overline{\overline{C}}_{k_0}(2) \otimes \overline{\overline{L}}_2 \right]^{k_2} | l_\beta)$$

The remaining matrix element reads:

$$\begin{aligned}
 (l_\alpha | \left[\overline{C}_{k_0}(2) \otimes \overline{L}_2 \right]^{k_2} | l_\beta) &= (-)^{l_\alpha + l_\beta + k_2} \widehat{k}_2 \sum_\lambda \langle l_\alpha | \overline{C}_{k_0}(2) | \lambda \rangle \langle \lambda | \overline{L}_2 | l_\beta \rangle \begin{Bmatrix} k_0 & 1 & k_2 \\ l_\beta & l_\alpha & \lambda \end{Bmatrix} \\
 &= (-)^{l_\alpha + l_\beta + k_2} \widehat{k}_2 \sum_\lambda (-)^{l_\alpha} \widehat{l}_\alpha \widehat{\lambda} \begin{pmatrix} l_\alpha & k_0 & \lambda \\ 0 & 0 & 0 \end{pmatrix} \sqrt{l_\beta(l_\beta + 1)(2l_\beta + 1)} \delta_{l_\beta \lambda} \\
 &\quad \begin{Bmatrix} k_0 & 1 & k_2 \\ l_\beta & l_\alpha & \lambda \end{Bmatrix} \\
 &= (-)^{2l_\alpha + l_\beta + k_2} \widehat{k}_2 \widehat{l}_\alpha \widehat{l}_\beta \begin{pmatrix} l_\alpha & k_0 & l_\beta \\ 0 & 0 & 0 \end{pmatrix} \sqrt{l_\beta(l_\beta + 1)(2l_\beta + 1)} \begin{Bmatrix} k_0 & 1 & k_2 \\ l_\beta & l_\alpha & l_\beta \end{Bmatrix}
 \end{aligned}$$

Finally, we may simplify some phasis and write the complete expression of V12 matrix element:

$$\begin{aligned}
 (jj_\alpha J | V_{12} | j'j_\beta J) &= -2 \sum_{\substack{k_0 \\ k_1 k_2 \\ LL'}} (-)^{L+S+J+k+k_1+l+l_\beta} \widehat{1}^2 \widehat{k}_0^2 \widehat{k}_1^2 \widehat{k}_2^2 \widehat{j} \widehat{j}_\alpha \widehat{j}' \widehat{j}_\beta \widehat{L}^2 \widehat{L}'^2 \widehat{S}^2 \sqrt{S(S+1)(2S+1)} \\
 &\quad \widehat{l}' \widehat{l}_\alpha \widehat{l}_\beta \sqrt{l_\beta(l_\beta + 1)(2l_\beta + 1)} \begin{Bmatrix} l & l_\alpha & L \\ \frac{1}{2} & \frac{1}{2} & S \end{Bmatrix} \begin{Bmatrix} l' & l_\beta & L' \\ \frac{1}{2} & \frac{1}{2} & S' \end{Bmatrix} \begin{Bmatrix} l & l_\alpha & L \\ k_1 & k_2 & 1 \end{Bmatrix} \\
 &\quad \begin{Bmatrix} S & L & J \\ L' & S' & 1 \end{Bmatrix} \begin{Bmatrix} k_1 & k & 1 \\ 1 & 1 & k_2 \end{Bmatrix} \begin{Bmatrix} k & 1 & k_0 \\ 1 & k_2 & 1 \end{Bmatrix} \begin{Bmatrix} k_0 & 1 & k_2 \\ l_\beta & l_\alpha & l_\beta \end{Bmatrix} \\
 &\quad \begin{pmatrix} k & 1 & k_1 \\ 0 & 0 & 0 \end{pmatrix} \begin{pmatrix} k & 1 & k_0 \\ 0 & 0 & 0 \end{pmatrix} \begin{pmatrix} l & k_1 & l' \\ 0 & 0 & 0 \end{pmatrix} \begin{pmatrix} l_\alpha & k_0 & l_\beta \\ 0 & 0 & 0 \end{pmatrix}
 \end{aligned} \tag{D.2.10}$$

The derivation of the V21 term, though very similar to V12, introduces some order changes. Therefore, we have chosen to give the full derivation here:

$$X_{21} = \vec{n}_2 \wedge (\vec{n}_1 \wedge \vec{l}_1) \cdot \vec{S} \frac{r_2}{r_1} \tag{D.2.11}$$

Writing this operator as tensor products leads to (omitting the purely radial factor):

$$\begin{aligned}
 X_{21} &= -i \sqrt{2} \vec{n}_2 \wedge \left[\overline{C}_1(1) \otimes \overline{l}_1 \right]^1 \cdot \vec{S} \\
 &= -i \sqrt{2} \times (-i \sqrt{2}) \left[\overline{C}_1(2) \otimes \left[\overline{C}_1(1) \otimes \overline{l}_1 \right]^1 \right]^1 \cdot \vec{S} \\
 &= -2 \left[\overline{C}_1(2) \otimes \left[\overline{C}_1(1) \otimes \overline{l}_1 \right]^1 \right]^1 \cdot \vec{S}
 \end{aligned}$$

Under this form, we can see that the X21 operator interchanges particle 1 and particle 2. Therefore, when we write down the matrix elements, instead of having the quantum numbers of particle 1 on the left, it will be those of particle 2. As for the V12 term, we develop the 2-body interaction on a spherical harmonic basis and unite it with X21 without any radial

term:

$$\begin{aligned}
 V_{21} &= -2 \sum_k \left(\overline{C}_k(1) \cdot \overline{C}_k(2) \right) \left[\overline{C}_1(2) \otimes \left[\overline{C}_1(1) \otimes \overline{l}_1 \right]^1 \right]^1 \cdot \vec{S} \\
 &= -2 \sum_{kk_1k_2} (-)^{k_2} \widehat{k}_1 \widehat{k}_2 \begin{Bmatrix} k_2 & k & 1 \\ 1 & 1 & k_1 \end{Bmatrix} \left[\left[\overline{C}_k(2) \otimes \overline{C}_1(2) \right]^{k_2} \otimes \left[\overline{C}_k(1) \otimes \left[\overline{C}_1(1) \otimes \overline{l}_1 \right]^1 \right]^{k_1} \right]^1 \cdot \vec{S} \\
 &= -2 \sum_{kk_1k_2} (-)^{k_2} \widehat{k}_1 \widehat{k}_2 \begin{Bmatrix} k_2 & k & 1 \\ 1 & 1 & k_1 \end{Bmatrix} (-)^{k-1} \widehat{k}_1 \begin{pmatrix} k & 1 & k_2 \\ 0 & 0 & 0 \end{pmatrix} \left[\overline{C}_{k_2}(2) \otimes \left[\overline{C}_k(1) \otimes \left[\overline{C}_1(1) \otimes \overline{l}_1 \right]^1 \right]^{k_1} \right]^1 \cdot \vec{S} \\
 &= -2 \sum_{kk_1k_2} (-)^{k_2+k-1} \widehat{k}_2^2 \widehat{k}_1 \begin{Bmatrix} k_2 & k & 1 \\ 1 & 1 & k_1 \end{Bmatrix} \begin{pmatrix} k & 1 & k_2 \\ 0 & 0 & 0 \end{pmatrix} \sum_{k_0} \widehat{k}_0^2 (-)^{k_1-1} \begin{pmatrix} k & 1 & k_0 \\ 0 & 0 & 0 \end{pmatrix} \begin{Bmatrix} k & 1 & k_0 \\ 1 & k_1 & 1 \end{Bmatrix} \\
 &\quad \left[\overline{C}_{k_2}(2) \otimes \left[\overline{C}_{k_0}(1) \otimes \overline{l}_1 \right]^{k_1} \right]^1 \cdot \vec{S}
 \end{aligned}$$

which, after simplification, yields an appropriate expression of the V_{21} operator which also exhibits the interchange of particle 1 with particle 2:

$$\begin{aligned}
 V_{21} &= -2 \sum_{\substack{kk_0 \\ k_1k_2}} (-)^{k_1+k+k_2} \widehat{1} \widehat{k}_0^2 \widehat{k}_1 \widehat{k}_2^2 \begin{Bmatrix} k_2 & k & 1 \\ 1 & 1 & k_1 \end{Bmatrix} \begin{Bmatrix} k & 1 & k_0 \\ 1 & k_1 & 1 \end{Bmatrix} \begin{pmatrix} k & 1 & k_2 \\ 0 & 0 & 0 \end{pmatrix} \begin{pmatrix} k & 1 & k_0 \\ 0 & 0 & 0 \end{pmatrix} \\
 &\quad \left[\overline{C}_{k_2}(2) \otimes \left[\overline{C}_{k_0}(1) \otimes \overline{l}_1 \right]^{k_1} \right]^1 \cdot \vec{S}
 \end{aligned}$$

Given this interchange, we no longer calculate $\langle jj_\alpha J | V_{21} | j' j_\beta J \rangle$ but $\langle j_\alpha j J | V_{21} | j_\beta j' J \rangle$ instead. In the Russel-Saunders coupling scheme:

$$\begin{aligned}
 \langle j_\alpha j J | V_{21} | j_\beta j' J \rangle &= \sum_{\substack{kk_0k_1k_2 \\ LL'SS'}} (-)^{k_1+k+k_2} \widehat{1} \widehat{k}_0^2 \widehat{k}_1 \widehat{k}_2^2 \widehat{j} \widehat{j}_\alpha \widehat{L} \widehat{S} \widehat{j}' \widehat{j}_\beta \widehat{L}' \widehat{S}' \begin{Bmatrix} k_2 & k & 1 \\ 1 & 1 & k_1 \end{Bmatrix} \begin{Bmatrix} k & 1 & k_0 \\ 1 & k_1 & 1 \end{Bmatrix} \\
 &\quad \begin{pmatrix} k & 1 & k_2 \\ 0 & 0 & 0 \end{pmatrix} \begin{pmatrix} k & 1 & k_0 \\ 0 & 0 & 0 \end{pmatrix} \begin{Bmatrix} l_\alpha & l & L \\ \frac{1}{2} & \frac{1}{2} & S \end{Bmatrix} \begin{Bmatrix} l_\beta & l' & L' \\ \frac{1}{2} & \frac{1}{2} & S' \end{Bmatrix} \\
 &\quad \langle l_\alpha l L S J | \left[\overline{C}_{k_2}(2) \otimes \left[\overline{C}_{k_0}(1) \otimes \overline{l}_1 \right]^{k_1} \right]^1 \cdot \vec{S} | l_\beta l' L' S' J \rangle
 \end{aligned}$$

We now simplify the remaining matrix element:

$$\begin{aligned}
 & (l_\alpha l L S J | \left[\overline{\overline{C_{k_2}}}(2) \otimes \left[\overline{\overline{C_{k_0}}}(1) \otimes \overline{\overline{l_1}} \right]^{k_1} \right]^1 \cdot \vec{S} | l_\beta l' L' S' J \rangle \\
 &= (-)^{L+S'+J} \left\{ \begin{matrix} S & L & J \\ L' & S' & 1 \end{matrix} \right\} \langle S | \vec{S} | S' \rangle (l_\alpha l L | \left[\overline{\overline{C_{k_2}}}(2) \otimes \left[\overline{\overline{C_{k_0}}}(1) \otimes \overline{\overline{l_1}} \right]^{k_1} \right]^1 | l_\beta l' L' \rangle \\
 &= (-)^{L+S'+J} \left\{ \begin{matrix} S & L & J \\ L' & S' & 1 \end{matrix} \right\} \sqrt{S(S+1)(2S+1)} \delta_{SS'} \widehat{1} \widehat{L} \widehat{L}' \left\{ \begin{matrix} l_\alpha & l & L \\ l_\beta & l' & L' \\ k_2 & k_1 & 1 \end{matrix} \right\} \langle l_\alpha | \overline{\overline{C_{k_1}}}(1) | l_\beta \rangle \\
 & \hspace{20em} (l | \left[\overline{\overline{C_{k_0}}}(1) \otimes \overline{\overline{L_1}} \right]^{k_1} | l' \rangle \\
 &= (-)^{L+S'+J} \left\{ \begin{matrix} S & L & J \\ L' & S' & 1 \end{matrix} \right\} \sqrt{S(S+1)(2S+1)} \delta_{SS'} \widehat{1} \widehat{L} \widehat{L}' \left\{ \begin{matrix} l_\alpha & l & L \\ l_\beta & l' & L' \\ k_2 & k_1 & 1 \end{matrix} \right\} (-)^{l_\alpha} \widehat{l} \widehat{l}' \begin{pmatrix} l_\alpha & k_2 & l_\beta \\ 0 & 0 & 0 \end{pmatrix} \\
 & \hspace{20em} (l | \left[\overline{\overline{C_{k_0}}}(1) \otimes \overline{\overline{L_1}} \right]^{k_1} | l' \rangle
 \end{aligned}$$

The last unexpanded element reads:

$$\begin{aligned}
 (l | \left[\overline{\overline{C_{k_0}}}(1) \otimes \overline{\overline{L_1}} \right]^{k_1} | l' \rangle &= (-)^{l+l'+k_1} \widehat{k_1} \sum_\lambda \langle l | \overline{\overline{C_{k_0}}}(1) | \lambda \rangle \langle \lambda | \overline{\overline{L_1}} | l' \rangle \left\{ \begin{matrix} k_0 & 1 & k_1 \\ l' & l & \lambda \end{matrix} \right\} \\
 &= (-)^{l+l'+k_1} \widehat{k_1} \sum_\lambda (-)^{l'} \widehat{l} \widehat{\lambda} \begin{pmatrix} l & k_0 & \lambda \\ 0 & 0 & 0 \end{pmatrix} \sqrt{l'(l'+1)(2l'+1)} \delta_{l'\lambda} \left\{ \begin{matrix} k_0 & 1 & k_1 \\ l' & l & \lambda \end{matrix} \right\} \\
 &= (-)^{2l+l'+k_1} \widehat{k_1} \widehat{l} \widehat{l}' \begin{pmatrix} l & k_0 & l' \\ 0 & 0 & 0 \end{pmatrix} \sqrt{l'(l'+1)(2l'+1)} \left\{ \begin{matrix} k_0 & 1 & k_1 \\ l' & l & l' \end{matrix} \right\}
 \end{aligned}$$

We finally obtain the entire formula by combining all pieces together. The result is given here with the standard form $(j j_\alpha J | V_{21} | j' j_\beta J)$ but it is to be remembered that the V_{21} operator inverses the order of particle 1 and particle 2:

$$\boxed{
 \begin{aligned}
 (j j_\alpha J | V_{21} | j' j_\beta J) &= -2 \sum_{\substack{kk_0 \\ k_1 k_2 \\ LL'}} (-)^{L+S+J+k+k_2+l'+l_\alpha} \widehat{1}^2 \widehat{k_0}^2 \widehat{k_1}^2 \widehat{k_2}^2 \widehat{j} \widehat{j_\alpha} \widehat{j'} \widehat{j_\beta} \widehat{L}^2 \widehat{L'}^2 \widehat{S}^2 \sqrt{S(S+1)(2S+1)} \\
 & \quad \widehat{l} \widehat{l}' \widehat{l}_\alpha \widehat{l}_\beta \sqrt{l'(l'+1)(2l'+1)} \left\{ \begin{matrix} l_\alpha & l & L \\ \frac{1}{2} & \frac{1}{2} & S \\ j_\alpha & j & J \end{matrix} \right\} \left\{ \begin{matrix} l_\beta & l' & L' \\ \frac{1}{2} & \frac{1}{2} & S' \\ j_\beta & j' & J \end{matrix} \right\} \left\{ \begin{matrix} l_\alpha & l & L \\ l_\beta & l' & L' \\ k_2 & k_1 & 1 \end{matrix} \right\} \\
 & \quad \left\{ \begin{matrix} S & L & J \\ L' & S' & 1 \end{matrix} \right\} \left\{ \begin{matrix} k_2 & k & 1 \\ 1 & 1 & k_1 \end{matrix} \right\} \left\{ \begin{matrix} k & 1 & k_0 \\ 1 & k_1 & 1 \end{matrix} \right\} \left\{ \begin{matrix} k_0 & 1 & k_1 \\ l' & l & l' \end{matrix} \right\} \\
 & \quad \begin{pmatrix} k & 1 & k_2 \\ 0 & 0 & 0 \end{pmatrix} \begin{pmatrix} k & 1 & k_0 \\ 0 & 0 & 0 \end{pmatrix} \begin{pmatrix} l_\alpha & k_2 & l_\beta \\ 0 & 0 & 0 \end{pmatrix} \begin{pmatrix} l & k_0 & l' \\ 0 & 0 & 0 \end{pmatrix}
 \end{aligned}
 }$$

(D.2.12)

Appendix E

Demonstrations for uncorrelated 2p2h state

We have gathered here the demonstrations for the computation of reduced density matrix elements between an initial 1p1h state $|\psi_{N_i} \in J_{N_i} M_{N_i} \Pi_{N_i}\rangle$ and a 2p2h state for the four terms appearing in the expansion given in chapter 6.

The demonstration for the term ρ_1 reads:

$$\begin{aligned}
\rho_{\alpha\beta}^{N_i \rightarrow N_3, J} &= \sum_{\text{all } m_i} (-)^{j_{p_1} + j_{p_i} + j_{p_2} + j_\alpha + J_2 - J_1 + M_1 + M_i + M_2 + M_3 + M - m_{h_1} - m_{h_i} - m_{h_2} - m_\beta} \widehat{J}_1 \widehat{J}_i \widehat{J}_2 \widehat{J}_3 \widehat{J} \\
&\quad \frac{\delta_{p_2\alpha} \delta_{h_2\beta} \delta_{p_1 p_i} \delta_{h_1 h_i}}{\langle J_i M_i J M | J_3 M_3 \rangle \widehat{J}_3^{-1}} \begin{pmatrix} j_{p_1} & j_{h_1} & J_1 \\ m_{p_1} & -m_{h_1} & -M_1 \end{pmatrix} \begin{pmatrix} j_{p_2} & j_{h_2} & J_2 \\ m_{p_2} & -m_{h_2} & -M_2 \end{pmatrix} \\
&\quad \begin{pmatrix} J_2 & J_1 & J_3 \\ M_2 & M_1 & -M_3 \end{pmatrix} \begin{pmatrix} j_{p_i} & j_{h_i} & J_i \\ m_{p_i} & -m_{h_i} & -M_i \end{pmatrix} \begin{pmatrix} j_\alpha & j_\beta & J \\ m_\alpha & -m_\beta & -M \end{pmatrix} \\
&= \sum_{\text{all } m_i} (-)^{2j_{p_1} + 2j_{p_2} + J_2 - J_1 + M_1 + M_i + M_2 + M_3 + M - 2m_{h_1} - 2m_{h_2}} \widehat{J}_1 \widehat{J}_i \widehat{J}_2 \widehat{J}_3 \widehat{J} \\
&\quad \frac{\delta_{p_2\alpha} \delta_{h_2\beta}}{\langle J_i M_i J M | J_3 M_3 \rangle \widehat{J}_3^{-1}} \begin{pmatrix} j_{p_1} & j_{h_1} & J_1 \\ m_{p_1} & -m_{h_1} & -M_1 \end{pmatrix} \begin{pmatrix} j_{p_2} & j_{h_2} & J_2 \\ m_{p_2} & -m_{h_2} & -M_2 \end{pmatrix} \\
&\quad \begin{pmatrix} J_2 & J_1 & J_3 \\ M_2 & M_1 & -M_3 \end{pmatrix} \begin{pmatrix} j_{p_1} & j_{h_1} & J_i \\ m_{p_1} & -m_{h_1} & -M_i \end{pmatrix} \begin{pmatrix} j_{p_2} & j_{h_2} & J \\ m_{p_2} & -m_{h_2} & -M \end{pmatrix} \\
&= \sum_{\text{all } m_i} (-)^{J_2 - J_1 + M_1 + M_i + M_2 + M_3 + M} \widehat{J}_1 \widehat{J}_i \widehat{J}_2 \widehat{J}_3 \widehat{J} \frac{\delta_{p_2\alpha} \delta_{h_2\beta}}{\langle J_i M_i J M | J_3 M_3 \rangle \widehat{J}_3^{-1}} \\
&\quad \begin{pmatrix} j_{p_1} & j_{h_1} & J_1 \\ m_{p_1} & -m_{h_1} & -M_1 \end{pmatrix} \begin{pmatrix} j_{p_1} & j_{h_1} & J_i \\ m_{p_1} & -m_{h_1} & -M_i \end{pmatrix} \begin{pmatrix} J_2 & J_1 & J_3 \\ M_2 & M_1 & -M_3 \end{pmatrix} \\
&\quad \begin{pmatrix} j_{p_2} & j_{h_2} & J_2 \\ m_{p_2} & -m_{h_2} & -M_2 \end{pmatrix} \begin{pmatrix} j_{p_2} & j_{h_2} & J \\ m_{p_2} & -m_{h_2} & -M \end{pmatrix}
\end{aligned}$$

We sum over m_{p_2} and m_{h_2} and use the closure relation of Wigner 3J coefficients (A.0.10):

$$\begin{aligned}
 \rho_{\alpha\beta}^{N_i \rightarrow N_3, J} &= \sum (-)^{J_2 - J_1 + M_1 + M_i + M_3} \widehat{J}_1 \widehat{J}_i \widehat{J}_3 \frac{\delta_{p_2\alpha} \delta_{h_2\beta} \delta_{JJ_2}}{\langle J_i M_i J_2 M_2 | J_3 M_3 \rangle \widehat{J}_3^{-1}} \\
 &\quad \begin{pmatrix} j_{p_1} & j_{h_1} & J_1 \\ m_{p_1} & -m_{h_1} & -M_1 \end{pmatrix} \begin{pmatrix} j_{p_1} & j_{h_1} & J_i \\ m_{p_1} & -m_{h_1} & -M_i \end{pmatrix} \begin{pmatrix} J_2 & J_1 & J_3 \\ M_2 & M_1 & -M_3 \end{pmatrix} \\
 &= \sum (-)^{J_2 - J_1 + M_1 + M_i + M_3} \widehat{J}_1 \widehat{J}_i \widehat{J}_3 \frac{\delta_{p_2\alpha} \delta_{h_2\beta} \delta_{JJ_2}}{(-)^{J_i + J_2 - J_3} \langle J_2 M_2 J_i M_i | J_3 M_3 \rangle \widehat{J}_3^{-1}} \\
 &\quad \begin{pmatrix} j_{p_1} & j_{h_1} & J_1 \\ m_{p_1} & -m_{h_1} & -M_1 \end{pmatrix} \begin{pmatrix} j_{p_1} & j_{h_1} & J_i \\ m_{p_1} & -m_{h_1} & -M_i \end{pmatrix} \begin{pmatrix} J_2 & J_1 & J_3 \\ M_2 & M_1 & -M_3 \end{pmatrix} \\
 &= \sum (-)^{-J_1 - J_i + J_3 + M_1 + M_i + M_3} \widehat{J}_1 \widehat{J}_i \widehat{J}_3 \frac{\delta_{p_2\alpha} \delta_{h_2\beta} \delta_{JJ_2}}{\langle J_2 M_2 J_i M_i | J_3 M_3 \rangle \widehat{J}_3^{-1}} \\
 &\quad \begin{pmatrix} j_{p_1} & j_{h_1} & J_1 \\ m_{p_1} & -m_{h_1} & -M_1 \end{pmatrix} \begin{pmatrix} j_{p_1} & j_{h_1} & J_i \\ m_{p_1} & -m_{h_1} & -M_i \end{pmatrix} \begin{pmatrix} J_2 & J_1 & J_3 \\ M_2 & M_1 & -M_3 \end{pmatrix}
 \end{aligned}$$

where the sums run over m_{p_1} , m_{h_1} , and M_1 . We use again the closure relation on Wigner 3J coefficients to obtain:

$$\begin{aligned}
 \rho_{\alpha\beta}^{N_i \rightarrow N_3, J} &= (-)^{-J_1 - J_i + J_3 + M_1 + M_i + M_3} \widehat{J}_3 \frac{\delta_{p_2\alpha} \delta_{h_2\beta} \delta_{JJ_2} \delta_{J_1 J_i} \delta_{M_1 M_i} \widehat{J}_3^{-1}}{\langle J_2 M_2 J_i M_i | J_3 M_3 \rangle} \begin{pmatrix} J_2 & J_1 & J_3 \\ M_2 & M_1 & -M_3 \end{pmatrix} \\
 &= (-)^{J_3 + M_3} \widehat{J}_3 \frac{\delta_{p_2\alpha} \delta_{h_2\beta} \delta_{JJ_2}}{\langle J_2 M_2 J_1 M_1 | J_3 M_3 \rangle \widehat{J}_3^{-1}} \begin{pmatrix} J_2 & J_1 & J_3 \\ M_2 & M_1 & -M_3 \end{pmatrix}
 \end{aligned}$$

Finally, we expand the Clebsch-Gordan coefficient at the denominator in terms of Wigner 3J symbol, and simplify the formula:

$$\rho_{\alpha\beta,1}^{N_1 \rightarrow N_3, J} = (-)^{J_1 - J_2 + J_3} \widehat{J}_3 \delta_{p_2\alpha} \delta_{h_2\beta} \delta_{JJ_2} \quad (\text{E.0.1})$$

The demonstration for the term ρ_4 is similar to that of ρ_1 and leads with no particular difficulty to the result:

$$\rho_{\alpha\beta,4}^{N_2 \rightarrow N_3, J} = \widehat{J}_3 \delta_{p_1\alpha} \delta_{h_1\beta} \delta_{JJ_1} \quad (\text{E.0.2})$$

The demonstration for ρ_2 and ρ_3 is similar and leads to the same result for both terms, except for a difference in the phasis. We write the demonstration for ρ_2 here. First, we apply the conditions embodied by the δ signs to angular momenta of the initial state:

$$\begin{aligned}
 \rho_{\alpha\beta}^{N_i \rightarrow N_3, J} &= \sum_{\text{all } m_i} (-)^{2j_{p_1} + 2j_{p_2} + J_2 - J_1 + M_1 + M_i + M_2 + M_3 + M - 2m_{h_1} - 2m_{h_2}} \widehat{J}_1 \widehat{J}_i \widehat{J}_2 \widehat{J}_3 \widehat{J} \frac{\delta_{p_2\alpha} \delta_{h_2 h_i} \delta_{h_1\beta} \delta_{p_1 p_i}}{\langle J_i M_i J M | J_3 M_3 \rangle \widehat{J}_3^{-1}} \\
 &\quad \begin{pmatrix} j_{p_1} & j_{h_1} & J_1 \\ m_{p_1} & -m_{h_1} & -M_1 \end{pmatrix} \begin{pmatrix} j_{p_2} & j_{h_2} & J_2 \\ m_{p_2} & -m_{h_2} & -M_2 \end{pmatrix} \begin{pmatrix} J_2 & J_1 & J_3 \\ M_2 & M_1 & -M_3 \end{pmatrix} \\
 &\quad \begin{pmatrix} j_{p_1} & j_{h_2} & J_i \\ m_{p_1} & -m_{h_2} & -M_i \end{pmatrix} \begin{pmatrix} j_{p_2} & j_{h_1} & J \\ m_{p_2} & -m_{h_1} & -M \end{pmatrix}
 \end{aligned} \quad (\text{E.0.3})$$

then we simplify the phasis and reorder some terms in the Wigner 3J coefficients:

$$\begin{aligned} \rho_{\alpha\beta}^{N_i \rightarrow N_3, J} = & \sum_{\text{all } m_i} (-)^{J_2 - J_1 + M_i + 2M_3 + M} \widehat{J}_1 \widehat{J}_i \widehat{J}_2 \widehat{J}_3 \widehat{J} \frac{1}{\langle J_i M_i J M | J_3 M_3 \rangle \widehat{J}_3^{-1}} \\ & (-)^{j_{p_1} + j_{h_1} + J_1} \begin{pmatrix} j_{p_1} & j_{h_1} & J_1 \\ -m_{p_1} & m_{h_1} & M_1 \end{pmatrix} \begin{pmatrix} j_{h_2} & j_{p_2} & J_2 \\ m_{h_2} & -m_{p_2} & M_2 \end{pmatrix} \begin{pmatrix} J_3 & J_2 & J_1 \\ -M_3 & M_2 & M_1 \end{pmatrix} \\ & \begin{pmatrix} J_i & j_{h_2} & j_{p_1} \\ M_i & m_{h_2} & -m_{p_1} \end{pmatrix} (-)^{J + j_{p_2} + j_{h_1}} \begin{pmatrix} J & j_{p_2} & j_{h_1} \\ M & -m_{p_2} & m_{h_1} \end{pmatrix} \end{aligned} \quad (\text{E.0.4})$$

Using the definition of the Wigner 9J coefficient (A.0.15), we can write:

$$\rho_{\alpha\beta}^{N_i \rightarrow N_3, J} = \frac{(-)^{J_2 + M_i + 2M_3 + M + j_{p_1} + 2j_{h_1} + J + j_{p_2}}}{\langle J_i M_i J M | J_3 M_3 \rangle \widehat{J}_3^{-1}} \widehat{J}_1 \widehat{J}_i \widehat{J}_2 \widehat{J}_3 \widehat{J} \begin{pmatrix} J_i & J & J_3 \\ M_i & M & -M_3 \end{pmatrix} \begin{Bmatrix} J_i & J & J_3 \\ j_{h_2} & j_{p_2} & J_2 \\ j_{p_1} & j_{h_1} & J_1 \end{Bmatrix} \quad (\text{E.0.5})$$

and finally we expand the denominator in terms of Wigner 3J coefficients and simplify the equation to obtain:

$$\rho_{\alpha\beta}^{N_i \rightarrow N_3, J} = (-)^{J_2 + 2J - J_i + j_{p_1} + 2j_{h_1} + j_{p_2}} \widehat{J}_1 \widehat{J}_i \widehat{J}_2 \widehat{J}_3 \widehat{J} \begin{Bmatrix} J_i & J & J_3 \\ j_{h_2} & j_{p_2} & J_2 \\ j_{p_1} & j_{h_1} & J_1 \end{Bmatrix} \quad (\text{E.0.6})$$

$$-\rho_{\alpha\beta}^{N_i \rightarrow N_3, J} = (-)^{J_2 - J_i + j_{p_1} + j_{p_2}} \widehat{J}_1 \widehat{J}_i \widehat{J}_2 \widehat{J}_3 \widehat{J} \begin{Bmatrix} J_i & J & J_3 \\ j_{h_2} & j_{p_2} & J_2 \\ j_{p_1} & j_{h_1} & J_1 \end{Bmatrix} \quad (\text{E.0.7})$$

Appendix F

The Wigner-Eckart Theorem

Following the definition of Talmi [80], we write Wigner-Eckart theorem that allow us to separate, for a spherical tensor operator, the part of its matrix elements that is purely geometric from the reduced matrix elements. Let T_M^J be a tensor operator rank J and projection M . Let $|\Psi_i\rangle = |\alpha_i J_i M_i\rangle$ be a state with total angular momentum J_i , spin projection M_i and other internal variables α_i , and Let $|\Psi_f\rangle = |\alpha_f J_f M_f\rangle$ another state with similar labeling. The Wigner-Eckart theorem reads:

$$\begin{aligned} \langle \alpha_f J_f M_f | T_M^J | \alpha_i J_i M_i \rangle &= (-)^{J-M} \begin{pmatrix} J_f & J & J_i \\ -M_f & M & M_i \end{pmatrix} \langle \alpha_f J_f || T^J || \alpha_i J_i \rangle \\ &= \frac{(-)^{2J_f+2J-M_f}}{\widehat{J}_f} \langle J_i M_i J M | J_f M_f \rangle \langle \alpha_f J_f || T^J || \alpha_i J_i \rangle \end{aligned} \quad (\text{F.0.1})$$

If the spins and the rank of the tensor are integers, the phase before the Clebsch-Gordan coefficient is simply equal to 1:

$$\langle \alpha_f J_f M_f | T_M^J | \alpha_i J_i M_i \rangle = \frac{1}{\widehat{J}_f} \langle J_i M_i J M | J_f M_f \rangle \langle \alpha_f J_f || T^J || \alpha_i J_i \rangle \quad (\text{F.0.2})$$

Appendix G

Coulomb wave functions and Riccati-Bessel functions

The regular Coulomb wave function F and the irregular G are solutions of the Schrödinger equation with a point-charge Coulomb potential:

$$\frac{d^2 f_l(z)}{dz^2} + \left(1 - \frac{2\eta}{z} - \frac{l(l+1)}{z^2}\right) f_l(z) = 0 \quad (\text{G.0.1})$$

When the Sommerfeld parameter η is equal to zero, F and G are simply Riccati-Bessel functions, related to spherical Bessel functions or the first kind j_l and of the second kind y_l by:

$$\begin{aligned} F_l(z) &\equiv z j_l(z) \\ G_l(z) &\equiv z y_l(z) \end{aligned} \quad (\text{G.0.2})$$

The Hankel functions are defined by:

$$H_l(z) = G_l(z) + iF_l(z) \quad (\text{G.0.3})$$

Appendix H

Resume in French

Une grande partie des processus de réaction nucléaire met en jeu un nucléon incident mis en collision avec un noyau cible. L'un des phénomènes physiques pouvant se produire alors est la diffusion du projectile par la cible, accompagnée ou non d'un échange d'énergie et/ou de moment angulaire. Pour une énergie incidente suffisamment élevée, ces mêmes diffusions se décomposent en plusieurs processus physiques: une partie directe caractérisée par sa brièveté ($< 10^{-21}$ s), une partie dans laquelle le projectile et la cible forment une seule entité appelée noyau composé, dont le temps de vie est beaucoup plus long, et d'une partie hybride entre les deux appelée pré-équilibre. Une bonne description de la partie directe est cruciale pour décrire les observables de diffusion au-delà d'environ 1 MeV, mais aussi car certaines des données d'entrée requises par les modèles décrivant les autres processus de réaction proviennent directement des calculs pour la partie directe. Beaucoup d'efforts ont été mis dans la modélisation précise de ces réactions, mais la complexité du problème à N corps qu'elles constituent fait qu'à ce jour, après plus de 70 ans d'études, la description de ces réactions directes demeure un domaine de recherche intensive au niveau mondial.

Parmi les différentes approches développées depuis plus d'un-demi siècle, l'un des modèles les plus répandus pour décrire les diffusions élastique et inélastique directes de type nucléon-noyau est le modèle optique. Ce modèle se base sur la réduction du problème à N corps en un problème à 1 corps. L'effet de toutes les interactions entre les nucléons de la cible et le projectile est moyenné au travers d'un potentiel complexe, la partie imaginaire servant à représenter l'absorption de flux de la voie élastique vers d'autres voies énergétiquement accessibles. Il est possible de généraliser cette approche en considérant explicitement la diffusion élastique et une sélection de diffusions inélastiques menant à des états excités prédéfinis de la cible. La formulation mathématique du problème de diffusion dans le cadre du modèle optique mène à un système d'équations couplées comme l'équation (3.2.3). Dans ce système, les potentiels représentés par les symboles U contiennent la physique des interactions entre le nucléon incident et la cible dans son état fondamental et un certain nombre de ses états excités. La première équation concerne spécifiquement la voie de diffusion élastique, la seconde équation est pour une voie inélastique notée $|N\rangle$.

Si l'on considère que le potentiel de couplage entre la voie d'entrée et elle-même U^{00} - qui n'est autre que le potentiel optique - est largement supérieur aux potentiels de couplage de la voie d'entrée avec les autres voies de réactions U^{0i} , alors on peut choisir de négliger ces termes ce qui donne:

$$\mathcal{S} : \left\{ \begin{array}{l} \left(E + \frac{\hbar^2}{2\mu} \left(\frac{d^2}{dr^2} - \frac{l'(l'+1)}{r^2} \right) \right) \phi_{[(l'\frac{1}{2})j', J_0], [(l'\frac{1}{2})j', J_0]}^{I,0}(r) - \\ \sum_{jl} \int U_{[(l'\frac{1}{2})j', J_0], [(l\frac{1}{2})j, J_0]}^{I,00}(r, r') \phi_{[(l'\frac{1}{2})j', J_0], [(l\frac{1}{2})j, J_0]}^{I,0}(r') rr' dr' \approx 0 \\ \left(E' + \frac{\hbar^2}{2\mu} \left(\frac{d^2}{dr^2} - \frac{l'(l'+1)}{r^2} \right) \right) \phi_{[(l'\frac{1}{2})j', J_N], [(l'\frac{1}{2})j', J_N]}^{I,N}(r) - \\ \sum_{jl} \int U_{[(l'\frac{1}{2})j', J_N], [(l\frac{1}{2})j, J_N]}^{I,NN}(r, r') \phi_{[(l'\frac{1}{2})j', J_N], [(l\frac{1}{2})j, J_N]}^{I,N}(r') rr' dr' = \\ \sum_{i \neq N} \sum_{jl} \int U_{[(l'\frac{1}{2})j', J_N], [(l\frac{1}{2})j, J_i]}^{I, Ni}(r, r') \phi_{[(l'\frac{1}{2})j', J_N], [(l\frac{1}{2})j, J_i]}^{I,i}(r') rr' dr' \end{array} \right. \quad (\text{H.0.1})$$

Dans cette nouvelle écriture du système, l'équation décrivant la diffusion élastique est découplée de celle décrivant la diffusion inélastique vers l'état $|N\rangle$. Nous pouvons aussi considérer dans ce système que le couplage de la voie inélastique aux autres voies inélastiques U^{Ni} , $i \neq 0$ est pris en compte dans la partie imaginaire du potentiel et donc on se retrouve avec

$$\mathcal{S} : \left\{ \begin{array}{l} \left(E + \frac{\hbar^2}{2\mu} \left(\frac{d^2}{dr^2} - \frac{l'(l'+1)}{r^2} \right) \right) \phi_{[(l'\frac{1}{2})j', J_0], [(l'\frac{1}{2})j', J_0]}^{I,0}(r) - \\ \sum_{jl} \int U_{[(l'\frac{1}{2})j', J_0], [(l\frac{1}{2})j, J_0]}^{I,00}(r, r') \phi_{[(l'\frac{1}{2})j', J_0], [(l\frac{1}{2})j, J_0]}^{I,0}(r') rr' dr' \approx 0 \\ \left(E' + \frac{\hbar^2}{2\mu} \left(\frac{d^2}{dr^2} - \frac{l'(l'+1)}{r^2} \right) \right) \phi_{[(l'\frac{1}{2})j', J_N], [(l'\frac{1}{2})j', J_N]}^{I,N}(r) - \\ \sum_{jl} \int U_{[(l'\frac{1}{2})j', J_N], [(l\frac{1}{2})j, J_N]}^{I,NN}(r, r') \phi_{[(l'\frac{1}{2})j', J_N], [(l\frac{1}{2})j, J_N]}^{I,N}(r') rr' dr' = \\ \sum_{jl} \int U_{[(l'\frac{1}{2})j', J_N], [(l\frac{1}{2})j, J_0]}^{I, N0}(r, r') \phi_{[(l'\frac{1}{2})j', J_N], [(l\frac{1}{2})j, J_0]}^{I,0}(r') rr' dr' \end{array} \right. \quad (\text{H.0.2})$$

Il est dès lors possible de résoudre tout d'abord l'équation pour la diffusion élastique et d'obtenir la fonction d'onde solution de ce problème, puis d'introduire cette solution dans l'équation pour la voie inélastique $|N\rangle$ et de la résoudre. Cette approche est appelée l'Approximation des Ondes Distordues de Born (DWBA). Cette approximation est valide du moment que les potentiels de couplage négligés sont effectivement très petits devant le potentiel optique. Cela est effectivement le cas pour des noyaux sphériques comme le ^{208}Pb mais ce n'est pas le cas pour des noyaux déformés comme l' ^{238}U . Par conséquent, il est nécessaire d'utiliser les voies couplées pour pouvoir traiter correctement le plus grand nombre de noyaux.

La dérivation formelle des équations couplées pour la diffusion nucléon-noyau ayant mené à l'écriture du système \mathcal{S} implique la définition des potentiels de couplage, qui permettent le traitement explicite de la voie élastique et d'une sélection de voies inélastiques, et qui tiennent compte du couplage aux autres voies de manière effective. Ces potentiels obtenus formellement dépendent de l'énergie et ont la particularité d'être non locaux: en coordonnées

position, ils ne sont pas diagonaux ce qui se manifeste dans le système \mathcal{S} par leur dépendance en (r, r') . Parmi les sources de cette non localité, nous pouvons citer l'antisymétrisation des fonctions d'onde des nucléons, les effets dynamiques comme le couplage effectif aux voies inélastiques. De ce fait, le système \mathcal{S} est un système d'équations intégral-différentielles couplées et sa résolution est techniquement complexe et numériquement coûteuse. Par conséquent, la grande majorité des analyses de diffusion élastiques et/ou inélastiques s'est faite en utilisant des potentiels locaux équivalents obtenus via une procédure de localisation comme celle de Perey [24, 32], ou à partir de potentiels phénoménologiques locaux.

Le but de ce travail de thèse est de développer les outils nécessaires à l'étude de diffusions élastique et inélastique directes entre un nucléon incident et tout type de noyau cible, pour lesquels des approches de type *ab initio* sont hors de portée. Il s'agit donc de dériver, dans un formalisme et un schéma de couplage cohérents, les équations couplées associées à ces processus de diffusion et les potentiels de couplages. Ensuite, à partir de ces équations, écrire deux codes: le premier pour calculer les potentiels, et le second pour résoudre les équations couplées. Enfin, de démontrer la robustesse de ces nouveaux outils en les utilisant pour une première application physique: l'inclusion d'excitations de type "2-step process" dans le calcul des sections efficaces d'émission de pré-équilibre.

H.1 Dérivation des potentiels

Il existe plusieurs méthodes pour construire les potentiels apparaissant dans le système (H.0.2). L'approche la plus simple consiste à poser une forme fonctionnelle pour ces potentiels avec un certain nombre de paramètres ajustables, puis d'ajuster ces paramètres sur des données expérimentales pour pouvoir les reproduire. Cette approche est dite phénoménologique, et est bien adaptée aux études de diffusion dans les domaines (en énergie, en masse, etc.) où les paramètres ont été ajustés [28–30]. En revanche, il est impossible de connaître a priori leur capacité de prédiction en dehors de leur domaine d'ajustement.

À l'opposé, l'approche dite *ab initio* tente de faire le lien entre les principes premiers de physique hadronique et de chromodynamique quantique, avec la physique nucléaire [5, 6]. L'interaction entre nucléons est calculée à partir des symétries de ces systèmes subnucléaires, et la structure du noyau atomique ainsi que le potentiel optique le liant au projectile sont calculés avec cette interaction. Cette approche fondamentale est extrêmement gourmande en ressources de calcul, et est essentiellement limitée (pour l'instant) aux noyaux légers, mais connaît des avancées conséquentes et de plus en plus de succès [7, 8].

Un autre type d'approche fondamentale consiste dans un premier temps à calculer, à partir d'une interaction effective entre deux nucléons et d'un modèle de structure, une densité nucléaire à un corps. Puis dans un second temps, ces données de structure nucléaire sont convoluées à la même interaction effective afin de générer le potentiel d'interaction entre le projectile et la cible. Cette développée dans les années 70 [39, 41, 45] est appelée méthode de la structure nucléaire et a été appliquée avec succès essentiellement sur des noyaux doublement magiques [43, 44].

Dans un esprit similaire, la méthode de la matière nucléaire se base sur la convolution d'une interaction effective entre 2 nucléons - appelée matrice g , calculée dans la matière nucléaire infinie ou dans un noyau fini, avec des données de structure qui ne sont pas

nécessairement obtenues à partir de la même interaction. Introduite vers la fin des années 50 [84–86], cette méthode a été appliquée avec succès à un large éventail de noyaux cibles allant des faibles masses aux actinides [26, 34–37, 62, 64].

Nous avons choisi d'utiliser la méthode de la matière nucléaire pour notre étude, en convoluant des données de structure obtenues avec une description de la structure du noyau de type champ moyen et au-delà, et la matrice G de Melbourne comme interaction effective. Les données de structure ont été calculées notamment via la théorie Hartree-Fock (HF) et la méthode dite de la “Random Phase Approximation” (RPA) implémentée avec la force de Gogny D1S, décrite dans l'appendice B. Nous avons tout d'abord dérivé les formules permettant de calculer, à partir des ingrédients sus-mentionnés, les potentiels couplant un état initial $|\psi_i \in J_i M_i \Pi_i\rangle$ à un état $|\psi_f \in J_f M_f \Pi_f\rangle$, avec J le spin total de la cible, M sa projection sur l'axe de quantification et Π sa parité totale. Dans sa forme finale, la formule pour la partie locale des potentiels de couplage est donnée dans l'équation (4.6.7) et la formule pour la partie non locale dans l'équation (4.6.12). Nous avons ensuite écrit le code de calcul MINOLOP - Microscopic NonLocal Potentials - pour calculer numériquement ces potentiels.

H.2 Résolution des équations couplées

Un fois les potentiels définis, il reste à résoudre le système d'équations couplées (3.2.3). Reprenant une méthode développée et appliquée avec succès par notre collaborateur H. Arellano aux réactions d'échange de charge [62], nous avons étendu le formalisme qu'il a proposé aux diffusions avec transfert d'énergie et de spin quelconques. Sa méthode se base sur la transformation du système d'équations couplées en un problème matriciel, et sur sa résolution avec des outils d'algèbre linéaire habituelle. Nous avons repris cette idée et l'avons étendue aux cas de diffusion pertinents pour notre étude. Nous avons notamment découpé le problème matriciel en sous-problèmes, en utilisant le fait que le moment angulaire total et la parité totale du système sont conservés au cours de la réaction. Nous avons également ajouté des corrections numériques dans la résolution du système d'équations. Le code que nous avons ainsi écrit est baptisé ECANOL - Equations Couplées Avec Non Localité. Nous avons ensuite procédé à la validation de nos codes.

H.3 Validation des codes de calcul

Une importante difficulté que nous avons rencontré pendant la validation de nos codes était l'absence de code de référence. En effet, le premier code de résolution des équations du problème en voies couplées a été publié en 2016 [58] et n'a été utilisé jusqu'à présent - à notre connaissance - que pour des calculs *ab initio*. En revanche, d'autres codes qualifiés et utilisés pour de nombreuses études existent mais sont limités soit au cas des potentiels locaux, soit aux calculs DWBA. Les codes FRESCO [59] ou ECIS-06 [60] sont des exemples de codes qui traitent les voies couplées mais avec des potentiels locaux, et DWBA98 [61] et NLAT [63] sont des exemples de codes qui traitent explicitement la non localité mais uniquement dans la limite de la DWBA.

Nous avons donc tout d'abord implémenté dans le code ECANOL la possibilité de faire un calcul en DWBA. Cela consiste en pratique à ne remplir que la diagonale et la partie

triangulaire inférieure des matrices comme celle donnée à la fin du chapitre 3 de ce document. Ainsi, il n'y a fondamentalement pas de différence au niveau du traitement numérique effectué par ECANOL entre un calcul en voies couplées et un calcul DWBA. Par conséquent, la validation des calculs avec potentiels non locaux à la limite de l'approximation des ondes distordues de Born permet aussi de valider le même calcul mais en voies couplées.

Ensuite, nous avons commencé la validation du code MINOLOP. Pour se faire nous avons extrait du code DWBA98, qui utilise les mêmes ingrédients microscopiques que notre code, le potentiel optique pour un noyau dont l'état fondamental est un 0^+ . Nous avons ensuite comparé ce potentiel avec celui obtenu via MINOLOP. Sur la figure 5.6, nous avons tracé le résultat des deux programmes informatiques. On voit que l'accord est excellent pour la partie locale, et l'accord est similaire pour la partie non locale.

Nous nous sommes ensuite intéressés aux potentiels de couplage entre deux états quelconques. Dans le code DWBA98, les seuls potentiels de couplages considérés en dehors du potentiel optique sont les potentiels de transition entre l'état fondamental et un état excité. Nous avons pu extraire la partie directe de ces potentiels mais pas la partie d'échange, donc nous n'avons pu valider par comparaison directe que la partie directe. La comparaison avec les calculs fait avec MINOLOP donne le même type d'accord que pour le potentiel optique. Mais le terme d'échange des potentiels de transition n'a donc pas pu être validé par comparaison directe.

Nous avons procédé à la validation d'ECANOL pour pouvoir ensuite revenir à MINOLOP. Tout d'abord, nous avons validé ECANOL pour la diffusion élastique avec les potentiels microscopiques non locaux. L'accord avec DWBA98 est excellent comme montré sur la figure 5.7. Ensuite, nous avons travaillé sur la validation d'ECANOL pour les voies inélastiques. À la limite DWBA, nous avons pu valider ECANOL pour des potentiels locaux en utilisant la partie directe des potentiels de transition.

Ensuite, dans le cadre des voies couplées, nous avons utilisé le code ECIS-06 comme référence pour nos validations. Dans ce code de calcul, il est possible d'utiliser aisément le modèle macroscopique vibrationnel pour calculer les potentiels locaux de couplage. Nous avons donc implémenté dans ECANOL le même modèle (uniquement le terme central, pas les termes spin-orbite et tenseur). Ensuite, nous avons étudié la convergence du code ECIS-06 en fonction du rayon de coupure du calcul et du pas utilisé pour le maillage radial de l'espace. Nos résultats sont présentés sur les figures 5.3 et 5.4. Nous avons établi comme paramètres du calcul de référence un rayon maximal de 20 fermis et un pas de 0,01 fermi, et nous avons montré que pour obtenir une bonne précision à un coût raisonnable en temps de calcul, nous pouvons utiliser un rayon maximal de 15 fermis et un pas de 0,2 fermi.

Ensuite nous avons comparé les calculs en voies couplées et en DWBA faits par ECANOL aux calculs de référence faits avec ECIS-06, comme montré sur la figure 5.5. On voit que malgré des différences de traitement numérique, les deux codes donnent des résultats remarquablement proches, et nous validons ainsi ECANOL pour des calculs en voies couplées avec des potentiels locaux. De plus, pour compléter la validation faite par rapport au code DWBA98 pour les potentiels de transition microscopiques locaux, nous avons dérivé les équations pour le modèle vibrationnel ainsi que pour la partie centrale indépendante du spin de la matrice G de Melbourne, et nous les avons écrites sous une forme directement comparable. Nous avons ensuite grossièrement ajusté les paramètres du modèle vibrationnel pour reproduire le potentiel microscopique et avons fait un calcul avec ECIS-06 et ECANOL. Malgré un ajustement très grossier des paramètres, le résultat des deux codes est en accord

à quelques pour cents près.

Enfin, nous avons utilisé les potentiels de couplage microscopiques non locaux dans ECANOL et avons comparé nos résultats à ceux de DWBA98 comme montré dans la figure 5.8. Quelques différences numériques persistent mais l'accord global est satisfaisant, ce qui nous permet de valider le code ECANOL pour des diffusions inélastiques ainsi que MINOLOP pour des potentiels de couplage non locaux.

H.4 Applications

Nous avons utilisé nos nouveaux outils pour faire une première application physique d'intérêt: l'étude des émissions de pré-équilibre due à des processus du second ordre (dits 2-step processes). Nous avons considéré les excitations à 2 phonons construites à partir d'états à 1 phonon prédits par la RPA sur le ^{90}Zr , et avons comparé la contribution de ces états issus de processus d'excitation en 2 étapes à ceux en 1 étape (les états à 1 phonon). Pour mener ces calculs, nous avons utilisé plusieurs approximations: l'approximation dite de non-retour, qui suppose que le flux dans la voie élastique ne peut être qu'absorbé pour alimenter les états à 1 phonon, et que les états à 2 phonons ne peuvent qu'être alimentés par les états à 1 phonon. La situation est résumée par les grosses flèches sur la figure 6.2. Nous avons également négligé les couplages entre états à 1 phonon, et avons supposé qu'un seul état à 1 phonon à la fois pouvait alimenter l'état à 2 phonons. Ces approximations ainsi que leurs effets concrets sur les calculs sont résumées dans les équations (6.2.2) à (6.2.5).

En considérant explicitement tous les états à 2 phonons de parité naturelle (jusqu'à 20 MeV d'énergie d'excitation) construits à partir des états à 1 phonon de parité naturelle jusque 20 MeV d'énergie d'excitation, on voit sur les figures 6.8 et 6.9 que les états à 2 phonons ont une contribution non négligeable, surtout aux angles arrières, et ce même pour de faibles énergies d'excitation.

Afin de mesurer l'effet de la collectivité des états prédits avec la théorie RPA et l'impact des approximations utilisées lors des dérivations des densités à un corps, nous avons effectué un calcul similaire dans le cas d'excitations de type particule-trou non corrélées sur l'état fondamental Hartree-Fock. Les résultats de nos calculs montrent qu'aux angles avant d'émission, la section efficace obtenue avec les états collectifs est plus grande que celle obtenue avec les excitations particule-trou plus simples. En revanche, cette différence s'amenuise à mesure que l'angle d'émission augmente, et la tendance observée lors de la comparaison entre 1 et 2 phonons se retrouve avec le calcul non corrélé.

Mais dans le calcul des densités à 1 corps pour les états à 2 phonons, nous avons utilisé l'approximation dite des quasi bosons. Cette approximation mène à une violation importante du principe d'exclusion de Pauli, et à une surestimation des contributions venant des états à 2 phonons. Les calculs que nous avons faits avec les états excités non corrélés ne nous permettent pas de faire une discrimination entre les effets dus à la collectivité, et ceux provenant de l'approximation des quasi bosons.

H.5 Conclusion

Au cours de ce travail de thèse, les équations couplées pour l'étude de diffusions directes (élastique et inélastique) d'un nucléon sur un noyau quelconque ont été dérivées. Des formules pour calculer les potentiels de couplage intervenant dans ces équations ont été dérivées, en utilisant l'approche de la matière nucléaire avec une interaction effective à 2 corps de portée finie et une description microscopique de la structure du noyau cible de type champ moyen et au-delà. À partir de ces formules, deux codes de calcul ont été écrits, MINOLOP pour calculer les potentiels et ECANOL pour résoudre les équations en voies couplées. Ces deux codes ont été validés en comparant leurs prédictions à celles faites par les codes DWBA98 et ECIS-06, deux outils connus et qualifiés. Une première application, démontrant la robustesse des outils ainsi que de l'approche théorique, a été faite sur les émissions de pré-équilibre dues à des processus du second ordre sur le ^{90}Zr .

Afin de compléter ces outils, et de pouvoir comparer des calculs à des données expérimentales, il reste à implémenter et valider les parties spin-orbite et tenseur de l'interaction effective dans MINOLOP. Il reste aussi à implémenter la partie Coulombienne et valider son traitement par ECANOL. Une autre extension possible pour ces codes est l'utilisation du maillage de Lagrange, qui peut fortement réduire le nombre de points requis pour un calcul et pour lequel il existe un code disponible en libre accès [58].

Ces nouveaux outils ouvrent les portes à de nombreuses nouvelles études, allant de l'extension de calculs faits avec la méthode de la structure nucléaire pour des diffusions inélastiques [44], à l'étude de l'impact du traitement explicite de la non localité dans le formalisme des voies couplées. Une application envisageable à moyen terme concerne la description de la bande rotationnelle de l'état fondamental d'un actinide tel que l' ^{238}U . En effet, des approches semi microscopiques ont déjà été utilisée avec succès pour décrire les premiers états excités de basse énergie de l' ^{238}U [26]. Avec MINOLOP, ECANOL, une description microscopique du noyau de type Hartree-Fock-Bogoliubov ou Quasi-particle Random Phase Approximation et une interaction effective comme la matrice G de Melbourne, il serait possible de progresser encore plus vers une description microscopique de la diffusion sur des cibles déformées telles que les actinides.

Bibliography

- [1] R. W. Finlay, J. R. M. Annand, T. S. Cheema, J. Rapaport, and F. S. Dietrich. Energy dependence of neutron scattering from ^{208}Pb in the energy range 7–50 MeV. *Phys. Rev. C*, 30:796–806, Sep 1984.
- [2] A. A. Cowley, A. van Kent, J. J. Lawrie, S. V. Försch, D. M. Whittal, J. V. Pilcher, F. D. Smit, W. A. Richter, R. Lindsay, I. J. van Heerden, R. Bonetti, and P. E. Hodgson. Preequilibrium proton emission induced by 80 and 120 MeV protons incident on ^{90}Zr . *Phys. Rev. C*, 43:678–686, Feb 1991.
- [3] W. A. Richter, A. A. Cowley, G. C. Hillhouse, J. A. Stander, J. W. Koen, S. W. Steyn, R. Lindsay, R. E. Julies, J. J. Lawrie, J. V. Pilcher, and P. E. Hodgson. Preequilibrium (p,p') measurements and calculations for ^{90}Zr and neighboring nuclei for incident energies up to 200 MeV. *Phys. Rev. C*, 49:1001–1011, Feb 1994.
- [4] S. Quaglioni and P. Navrátil. Ab initio many-body calculations of $n-^3\text{H}$, $n-^4\text{He}$, $p-^3,4\text{He}$, and $n-^{10}\text{Be}$ scattering. *Phys. Rev. Lett.*, 101:092501, Aug 2008.
- [5] Y. Jaganathen, N. Michel, and M. Płoszajczak. Gamow shell model description of proton scattering on ^{18}Ne . *Phys. Rev. C*, 89:034624, Mar 2014.
- [6] G. Hupin, J. Langhammer, P. Navrátil, S. Quaglioni, A. Calci, and R. Roth. Ab initio many-body calculations of nucleon- ^4He scattering with three-nucleon forces. *Phys. Rev. C*, 88:054622, Nov 2013.
- [7] G. Hupin, S. Quaglioni, and P. Navrátil. Unified description of ^6Li structure and deuterium- ^4He dynamics with chiral two- and three-nucleon forces. *Phys. Rev. Lett.*, 114:212502, May 2015.
- [8] K. Fosse, N. Michel, M. Płoszajczak, Y. Jaganathen, and R. M. Id Betan. Description of the proton and neutron radiative capture reactions in the gamow shell model. *Phys. Rev. C*, 91:034609, Mar 2015.
- [9] K. Bennaceur, N. Michel, F. Nowacki, J. Okołowicz, and M. Płoszajczak. Shell model description of $^{16}\text{O}(p,\gamma)^{17}\text{F}$ and $^{16}\text{O}(p,p)^{16}\text{O}$ reactions. *Physics Letters B*, 488(1):75 – 82, 2000.
- [10] R. Shyam, K. Bennaceur, J. Okołowicz, and M. Płoszajczak. Structure effects on the Coulomb dissociation of ^8B at relativistic energies. *Nuclear Physics A*, 669(1):65 – 80, 2000.
- [11] J. Okołowicz, M. Płoszajczak, and I. Rotter. Dynamics of quantum systems embedded in a continuum. *Physics Reports*, 374(4):271 – 383, 2003.

-
- [12] J. Rotureau, P. Danielewicz, G. Hagen, F. M. Nunes, and T. Papenbrock. Optical potential from first principles. *Phys. Rev. C*, 95:024315, Feb 2017.
- [13] P. E. Hodgson. The nuclear optical potential. *Rep. Prog. Phys.*, 34:765, 1971.
- [14] H. A. Bethe. Theory of disintegration of nuclei by neutrons. *Phys. Rev.*, 47:747–759, May 1935.
- [15] S. Fernbach, R. Serber, and T. B. Taylor. The scattering of high energy neutrons by nuclei. *Phys. Rev.*, 75:1352–1355, May 1949.
- [16] H. Feshbach, C. E. Porter, and V. F. Weisskopf. Model for nuclear reactions with neutrons. *Phys. Rev.*, 96:448–464, Oct 1954.
- [17] H. Feshbach. Unified theory of nuclear reactions. *Annals of Physics*, 5(4):357 – 390, 1958.
- [18] H. Feshbach. A unified theory of nuclear reactions. II. *Annals of Physics*, 19(2):287 – 313, 1962.
- [19] H. Feshbach. The unified theory of nuclear reactions: III. overlapping resonances. *Annals of Physics*, 43(3):410 – 420, 1967.
- [20] H. Feshbach. The optical model and its justification. *Ann. Rev. of Nucl. Sci.*, 8:49–104, 1958.
- [21] E. Rost and N. Austern. Inelastic diffraction scattering. *Phys. Rev.*, 120:1375–1387, Nov 1960.
- [22] N. K. Glendenning. Theory of direct-interaction inelastic scattering. *Phys. Rev.*, 114:1297–1311, Jun 1959.
- [23] M. Dupuis, S. Karataglidis, E. Bauge, J. P. Delaroche, and D. Gogny. Correlations in microscopic optical model for nucleon elastic scattering off doubly closed-shell nuclei. *Phys. Rev. C*, 73:014605, Jan 2006.
- [24] F. Perey and G. R. Satchler. Validity of the DWBA for inelastic scattering from nuclei. *Physics Letters*, 5(3):212 – 215, 1963.
- [25] B. Buck. Calculation of elastic and inelastic proton scattering with a generalized optical model. *Phys. Rev.*, 130:712–726, Apr 1963.
- [26] M. Dupuis, E. Bauge, S. Hilaire, F. Lechaftois, S. Péru, N. Pillet, and C. Robin. Progress in microscopic direct reaction modeling of nucleon induced reactions. *The European Physical Journal A*, 51(12):168, Dec 2015.
- [27] P. Ring and P. Schuck. *The nuclear many-body problem*. Springer-Verlag, New York, 1980.
- [28] B. Morillon and P. Romain. Bound single-particle states and scattering of nucleons on spherical nuclei with a global optical model. *Phys. Rev. C*, 76:044601, Oct 2007.
- [29] A.J. Koning and J.P. Delaroche. Local and global nucleon optical models from 1 keV to 200 MeV. *Nuclear Physics A*, 713(3):231 – 310, 2003.

-
- [30] R.L. Varner, W.J. Thompson, T.L. McAbee, E.J. Ludwig, and T.B. Clegg. A global nucleon optical model potential. *Physics Reports*, 201(2):57 – 119, 1991.
- [31] C. Barbieri, R.J. Charity, W.H. Dickhoff, and L.G. Sobotka. Toward a global dispersive optical model for the driplines. *Nuclear Physics A*, 834(1):788c – 791c, 2010. The 10th International Conference on Nucleus-Nucleus Collisions (NN2009).
- [32] F. Perey and B. Buck. A non-local potential model for the scattering of neutrons by nuclei. *Nuclear Physics*, 32:353 – 380, 1962.
- [33] W. H. Dickhoff, D. Van Neck, S. J. Waldecker, R. J. Charity, and L. G. Sobotka. Nonlocal extension of the dispersive optical model to describe data below the Fermi energy. *Phys. Rev. C*, 82:054306, Nov 2010.
- [34] F. A. Brieva and J. R. Rook. Nucleon-nucleus optical model potential: (1). nuclear matter approach. *Nuclear Physics A*, 291(2):299 – 316, 1977.
- [35] H. F. Arellano, F. A. Brieva, and W. G. Love. Full-folding-model description of elastic scattering at intermediate energies. *Phys. Rev. Lett.*, 63:605–608, Aug 1989.
- [36] R. Crespo, R. C. Johnson, and J. A. Tostevin. Full folding calculations for proton-nucleus elastic scattering at intermediate energies. *Phys. Rev. C*, 41:2257–2262, May 1990.
- [37] K. Amos, P. J. Dortmans, H. V. Von Geramb, S. Karataglidis, and J. Raynal. Nucleon-nucleus scattering, a microscopic nonrelativistic approach. *Adv. Nucl. Phys.*, 25:275–540, 2000.
- [38] H. F. Arellano and E. Bauge. 7d-folding integral in a density-dependent microscopic optical model potential for nucleon-nucleus scattering. *Phys. Rev. C*, 84:034606, Sep 2011.
- [39] N. Vin Mauh. Theory of nuclear structure. *IAEA Vienna*, page 931, 1970.
- [40] N.Vinh Mau and A. Bouyssy. Optical potential for low-energy neutrons: Imaginary potential for neutron-40ca elastic scattering. *Nuclear Physics A*, 257(2):189 – 220, 1976.
- [41] F. Osterfeld, J. Wambach, and V. A. Madsen. Antisymmetrized, microscopic calculation for the $^{40}\text{Ca}(n, n)$ optical potential. *Phys. Rev. C*, 23:179–193, Jan 1981.
- [42] A. Bouyssy, H. Ngô, and N.Vinh Mau. A nuclear structure approach to the nucleon-nucleus optical potential at low energy. *Nuclear Physics A*, 371(2):173 – 209, 1981.
- [43] G. Blanchon, M. Dupuis, H. F. Arellano, and N. Vinh Mau. Microscopic positive-energy potential based on the Gogny interaction. *Phys. Rev. C*, 91:014612, Jan 2015.
- [44] G. Blanchon, M. Dupuis, R. N. Bernard, and H. F. Arellano. Asymmetry dependence of Gogny-based optical potential. *Eur. Phys. J. A*, 53(5):88, 2017.
- [45] V. Bernard and Nguyen Van Giai. Microscopic optical potential for ^{208}Pb in the nuclear structure approach. *Nuclear Physics A*, 327(2):397 – 418, 1979.

-
- [46] K. Mizuyama and K. Ogata. Self-consistent microscopic description of neutron scattering by ^{16}O based on the continuum particle-vibration coupling method. *Phys. Rev. C*, 86:041603, Oct 2012.
- [47] L. Canton, G. Pisent, J. P. Svenne, D. van der Knijff, K. Amos, and S. Karataglidis. Role of the Pauli principle in collective-model coupled-channel calculations. *Phys. Rev. Lett.*, 94:122503, Apr 2005.
- [48] P. Fraser, K. Amos, S. Karataglidis, L. Canton, G. Pisent, and J. P. Svenne. Two causes of nonlocalities in nucleon-nucleus potentials and their effects in nucleon-nucleus scattering. *The European Physical Journal A*, 35(1):69–80, Jan 2008.
- [49] R. Crespo, R. C. Johnson, and J. A. Tostevin. Mean field calculations of nucleon-nucleus scattering. *Phys. Rev. C*, 53:3022–3031, Jun 1996.
- [50] K. M. Watson. Multiple scattering by quantum-mechanical systems. *Phys. Rev.*, 105:1388–1398, Feb 1957.
- [51] C. L. Rao, M. Reeves, and G. R. Satchler. Target excitations and the optical potential for protons scattering from nuclei. *Nuclear Physics A*, 207(1):182 – 208, 1973.
- [52] G. H. Rawitscher. The microscopic Feshbach optical potential for a schematic coupled channel example. *Nuclear Physics A*, 475(3):519 – 547, 1987.
- [53] N. Vinh Mau, J. L. Ferrero, J. C. Pacheco, and B. Bilwes. Comment on “Dynamical polarization potential due to the excitation of collective states”. *Phys. Rev. C*, 47:899–901, Feb 1993.
- [54] N. Keeley and R. S. Mackintosh. Dynamic polarization potential and dynamical nonlocality in nuclear potentials: Nucleon-nucleus potential. *Phys. Rev. C*, 90:044602, Oct 2014.
- [55] W.G. Love. A study of the local Slater-exchange approximation for nucleon and heavy-ion scattering. *Nuclear Physics A*, 312(1):160 – 176, 1978.
- [56] N. Austern. Wave functions of nonlocal potentials: The Perey effect. *Phys. Rev.*, 137:B752–B757, Feb 1965.
- [57] L. J. Titus and F. M. Nunes. Testing the Perey effect. *Phys. Rev. C*, 89:034609, Mar 2014.
- [58] P. Descouvemont. An R-matrix package for coupled-channel problems in nuclear physics. *Computer Physics Communications*, 200:199 – 219, 2016.
- [59] I. J. Thompson. Coupled reaction channels calculations in nuclear physics. *Computer Physics Reports*, 7(4):167 – 212, 1988.
- [60] J. Raynal. Notes on ECIS94. *Tech. Rep. CEA-N-2772*, pages 1–145, 1994.
- [61] J. Raynal. computer code DWBA98. *NEA*, 1999.
- [62] H. F. Arellano and W. G. Love. In-medium full-folding model approach to quasielastic (p, n) charge-exchange reactions. *Phys. Rev. C*, 76:014616, Jul 2007.

-
- [63] L.J. Titus, A. Ross, and F.M. Nunes. Transfer reaction code with nonlocal interactions. *Computer Physics Communications*, 207:499 – 517, 2016.
- [64] M. Dupuis, S. Karataglidis, E. Bauge, J.-P. Delaroche, and D. Gogny. Challenging nuclear structure models through a microscopic description of proton inelastic scattering off ^{208}Pb . *Physics Letters B*, 665(4):152 – 156, 2008.
- [65] N. Austern. *Direct Nuclear Reaction Theories*. Interscience monographs and texts in physics and astronomy, v. 25. Wiley-Interscience, 1970.
- [66] P. E. Hodgson. The dispersive optical model. In Syed M. Qaim, editor, *Nuclear Data for Science and Technology*, pages 768–774, Berlin, Heidelberg, 1992. Springer Berlin Heidelberg.
- [67] M. H. Mahzoon, R. J. Charity, W. H. Dickhoff, H. Dussan, and S. J. Waldecker. Forging the link between nuclear reactions and nuclear structure. *Phys. Rev. Lett.*, 112:162503, Apr 2014.
- [68] B. Morillon and P. Romain. Dispersive and global spherical optical model with a local energy approximation for the scattering of neutrons by nuclei from 1 keV to 200 MeV. *Phys. Rev. C*, 70:014601, Jul 2004.
- [69] E. Sh. Soukhovitskiĭ, R. Capote, J. M. Quesada, S. Chiba, and D. S. Martyanov. Nucleon scattering on actinides using a dispersive optical model with extended couplings. *Phys. Rev. C*, 94:064605, Dec 2016.
- [70] A. Idini, C. Barbieri, and P. Navrátil. Ab initio optical potentials and nucleon scattering on medium mass nuclei. *Journal of Physics: Conference Series*, 981(1):012005, 2018.
- [71] C. Mahaux and R. Sartor. Dispersive versus constant-geometry models of the neutron- ^{208}Pb mean field. *Nuclear Physics A*, 516(2):285 – 303, 1990.
- [72] G.R. Satchler. *Direct Nuclear Reactions*, p61.
- [73] G.R. Satchler. *Direct Nuclear Reactions*, p56-58.
- [74] C Cohen-Tannoudji, B Diu, and F Laloe. *Mécanique Quantique, tome II*.
- [75] I. J. Thompson and F. M. Nunes. *Nuclear Reactions for Astrophysics*, p77.
- [76] G.R. Satchler. *Direct Nuclear Reactions*, p132.
- [77] C.J. Joachain. *Quantum collision theory*. 1975.
- [78] H. F. Arellano. Private communication.
- [79] M. Dupuis. Microscopic description of elastic and direct inelastic nucleon scattering off spherical nuclei. *The European Physical Journal A*, 53(5):111, May 2017.
- [80] I. Talmi. *Simple Models of Complex Nuclei: The Shell Model and Interacting Boson Model*. Beitrage Zur Wirtschaftsinformatik. Harwood Academic Publishers, 1993.
- [81] R. B. Wiringa, V. G. J. Stoks, and R. Schiavilla. Accurate nucleon-nucleon potential with charge-independence breaking. *Phys. Rev. C*, 51:38–51, Jan 1995.

-
- [82] V. G. J. Stoks, R. A. M. Klomp, C. P. F. Terheggen, and J. J. de Swart. Construction of high-quality NN potential models. *Phys. Rev. C*, 49:2950–2962, Jun 1994.
- [83] R. Machleidt. High-precision, charge-dependent Bonn nucleon-nucleon potential. *Phys. Rev. C*, 63:024001, Jan 2001.
- [84] K. A. Brueckner, C. A. Levinson, and H. M. Mahmoud. Two-body forces and nuclear saturation. i. central forces. *Phys. Rev.*, 95:217–228, Jul 1954.
- [85] H. A. Bethe. Nuclear many-body problem. *Phys. Rev.*, 103:1353–1390, Sep 1956.
- [86] Derivation of the Brueckner many-body theory. *Proceedings of the Royal Society of London A: Mathematical, Physical and Engineering Sciences*, 239(1217):267–279, 1957.
- [87] W. H. Dickhoff and D. Van Neck. *Many Body theory exposed! eq 16.59*. World Scientific, 2008.
- [88] R. Machleidt, K. Holinde, and Ch. Elster. The Bonn meson-exchange model for the nucleon-nucleon interaction. *Physics Reports*, 149(1):1 – 89, 1987.
- [89] S. Karataglidis. Melbourne G matrix on a density mesh.
- [90] J.P. Blaizot and D. Gogny. Theory of elementary excitations in closed shell nuclei. *Nuclear Physics A*, 284(3):429 – 460, 1977.
- [91] D. R. Hartree. The wave mechanics of an atom with a non-Coulomb central field. part i. theory and methods. *Mathematical Proceedings of the Cambridge Philosophical Society*, 24(1):89–110, 1928.
- [92] V. Fock. Näherungsmethode zur lösung des quantenmechanischen mehrkörperproblems. *Zeitschrift für Physik*, 61(1):126–148, Jan 1930.
- [93] J.F. Berger, M. Girod, and D. Gogny. Time-dependent quantum collective dynamics applied to nuclear fission. *Computer Physics Communications*, 63(1):365 – 374, 1991.
- [94] D. Gogny and P. L. Lions. Hartree-Fock theory in nuclear physics. *RAIRO, Modélisation Math. Anal. Numér.*, 20:571–637, 1986.
- [95] M. Dupuis. *Modèles de réactions directes et de pré-équilibre quantique pour la diffusion de nucléons sur des noyaux sphériques.*. PhD thesis, University Of Bordeaux, 2006.
- [96] P.J. Ellis. RPA ground state correlations from perturbation theory. *Nuclear Physics A*, 155(2):625 – 643, 1970.
- [97] M. H. Mahzoon, M. C. Atkinson, R. J. Charity, and W. H. Dickhoff. Neutron skin thickness of ^{48}Ca from a nonlocal dispersive optical-model analysis. *Phys. Rev. Lett.*, 119:222503, Nov 2017.
- [98] J. B. Campbell. On Temme’s algorithm for the modified Bessel function of the third kind. *ACM Trans. Math. Softw.*, 6(4):581–586, December 1980.
- [99] W. J. Cody. Algorithm 597: Sequence of modified Bessel functions of the first kind. *ACM Trans. Math. Softw.*, 9(2):242–245, June 1983.

-
- [100] J. M. Blatt and L. C. Biedenharn. The angular distribution of scattering and reaction cross sections. *Rev. Mod. Phys.*, 24:258–272, Oct 1952.
- [101] G.R. Satchler. *Direct Nuclear Reactions, chapter 14*.
- [102] M.N. Harakeh and A. Woude. *Giant Resonances: Fundamental High-frequency Modes of Nuclear Excitation*. Oxford science publications. Oxford University Press, 2001.
- [103] N. Bohr. Neutron capture and nuclear constitution. *Nature*, 137:344–348, 1936.
- [104] J. J. Griffin. Statistical model of intermediate structure. *Phys. Rev. Lett.*, 17:478–481, Aug 1966.
- [105] J.J. Griffin. Energy dependence of average direct reaction cross sections and partial nuclear level densities. *Physics Letters B*, 24(1):5 – 7, 1967.
- [106] C. Kalbach. Isospin conservation in preequilibrium reactions. *Phys. Rev. C*, 72:024607, Aug 2005.
- [107] A.J. Koning and M.C. Duijvestijn. A global pre-equilibrium analysis from 7 to 200 MeV based on the optical model potential. *Nuclear Physics A*, 744:15 – 76, 2004.
- [108] H. Feshbach, A. Kerman, and S. Koonin. The statistical theory of multi-step compound and direct reactions. *Annals of Physics*, 125(2):429 – 476, 1980.
- [109] T. Tamura, T. Udagawa, and H. Lenske. Multistep direct reaction analysis of continuum spectra in reactions induced by light ions. *Phys. Rev. C*, 26:379–404, Aug 1982.
- [110] H. Nishioka, H. A. Weidenmüller, and S. Yoshida. Statistical theory of precompound reactions: The multistep direct process. *Annals of Physics*, 183(1):166 – 187, 1988.
- [111] E. Gadioli and P.E. Hodgson. *Pre-equilibrium nuclear reactions*. Oxford studies in nuclear physics. Clarendon Press, 1992.
- [112] A. J. Koning and J. M. Akkermans. Intercomparison of multi-step direct reaction models. In Syed M. Qaim, editor, *Nuclear Data for Science and Technology*, pages 891–893, Berlin, Heidelberg, 1992. Springer Berlin Heidelberg.
- [113] T. Kawano and S. Yoshida. Interference effect in the scattering amplitudes for nucleon-induced two-step direct process using the sudden approximation. *Phys. Rev. C*, 64:024603, Jun 2001.
- [114] M. Dupuis, T. Kawano, J.-P. Delaroche, and E. Bauge. Microscopic model approach to (n, xn) pre-equilibrium reactions for medium-energy neutrons. *Phys. Rev. C*, 83:014602, Jan 2011.
- [115] E. Boeker. Two-particle-two-hole states in ^{16}O . *Physica*, 32(4):669 – 688, 1966.
- [116] D. Gambacurta, M. Grasso, F. Catara, and M. Sambataro. Extension of the second random-phase approximation. *Phys. Rev. C*, 73:024319, Feb 2006.
- [117] D. Gambacurta, M. Grasso, and J. Engel. Subtraction method in the second random-phase approximation: First applications with a Skyrme energy functional. *Phys. Rev. C*, 92:034303, Sep 2015.

-
- [118] S. Péru and H. Goutte. Role of deformation on giant resonances within the quasiparticle random-phase approximation and the Gogny force. *Phys. Rev. C*, 77:044313, Apr 2008.
- [119] S. Péru and M. Martini. Mean field based calculations with the Gogny force: Some theoretical tools to explore the nuclear structure. *The European Physical Journal A*, 50(5):88, May 2014.
- [120] M.B. Chadwick, E. Dupont, E. Bauge, A. Blokhin, O. Bouland, D.A. Brown, R. Capote, A. Carlson, Y. Danon, C. De Saint Jean, M. Dunn, U. Fischer, R.A. Forrest, S.C. Frankle, T. Fukahori, Z. Ge, S.M. Grimes, G.M. Hale, M. Herman, A. Ignatyuk, M. Ishikawa, N. Iwamoto, O. Iwamoto, M. Jandel, R. Jacqmin, T. Kawano, S. Kunieda, A. Kahler, B. Kiedrowski, I. Kodeli, A.J. Koning, L. Leal, Y.O. Lee, J.P. Lestone, C. Lubitz, M. MacInnes, D. McNabb, R. McKnight, M. Moxon, S. Mughabghab, G. Noguere, G. Palmiotti, A. Plompen, B. Pritychenko, V. Pronyaev, D. Rochman, P. Romain, D. Roubtsov, P. Schillebeeckx, M. Salvatores, S. Simakov, E.Sh. Soukhovitskii, J.C. Sublet, P. Talou, I. Thompson, A. Trkov, R. Vogt, and S. van der Marck. The CIELO collaboration: Neutron reactions on ^1H , ^{16}O , ^{56}Fe , $^{235,238}\text{U}$, and ^{239}Pu . *Nuclear Data Sheets*, 118:1 – 25, 2014.
- [121] A. Santamarina, D. Bernard, P. Leconte, and J.-F. Vidal. Improvement of ^{238}U inelastic scattering cross section for an accurate calculation of large commercial reactors. *Nuclear Data Sheets*, 118:118 – 121, 2014.
- [122] H. F. Arellano and G. Blanchon. Irreducible nonlocality of optical model potentials based on realistic NN interactions. to be published.
- [123] J. E. Escher, I. J. Thompson, G. Arbanas, Ch. Elster, V. Eremenko, L. Hlophe, and F. M. Nunes. Reexamining surface-integral formulations for one-nucleon transfers to bound and resonance states. *Phys. Rev. C*, 89:054605, May 2014.
- [124] L. Hlophe, V. Eremenko, Ch. Elster, F. M. Nunes, G. Arbanas, J. E. Escher, and I. J. Thompson. Separable representation of proton-nucleus optical potentials. *Phys. Rev. C*, 90:061602, Dec 2014.
- [125] A.J. Koning, S. Hilaire, and M.C. Duijvestijn. Talys-1.0: Making nuclear data libraries using TALYS. *International Nuclear Data Conference for Science and Technology*, pages 211–214, 2007.
- [126] G.N. Watson. *A Treatise on the Theory of Bessel Functions*.
- [127] G. Blanchon, M. Dupuis, H. F. Arellano, and N. Vinh Mau. Diffusion élastique de nucléons par un noyau à couches fermées dans l’approximation HF+RPA avec l’interaction de Gogny. *CEA report*, (nb OTP A22D0000102001), 2012.

Titre: Potentiels microscopiques non locaux pour l'étude des observables de diffusion de nucléons dans le formalisme des voies couplées

Mots clés: réactions nucléaires, structure nucléaire, modèle optique, non localité, voies couplées

Résumé: Une bonne compréhension et une bonne capacité de prédiction de la section efficace de diffusion de neutron sont essentielles à un grand nombre de technologies nucléaires, parmi lesquelles les réacteurs à fission. Pour les noyaux déformés, le calcul de ces observables pour la voie élastique et les premiers états excités de basse énergie requiert l'utilisation de calculs en voies couplées. Des potentiels optique et de transition phénoménologiques locaux sont le plus couramment utilisés dans les analyses par voies couplées, mais leur précision en dehors de leur domaine d'ajustement est imprévisible. Des approches microscopiques sont en cours de développement pour augmenter les capacités prédictives et résoudre les problèmes d'extrapolation. Un potentiel obtenu microscopiquement est non local, et de récentes études ont souligné l'importance de traiter cette non localité explicitement, sans passer par une procédure de localisation. Notre but dans ce travail est de développer les outils nécessaires à l'étude, dans un cadre microscopique sans

paramètre ajustable, de l'impact de la non localité des potentiels sur les observables de diffusion de nucléon. Pour pouvoir étudier tout type de noyau (sphérique ou déformé), nous menons notre étude dans le formalisme des voies couplées. La première partie de ce document contient la dérivation, faite dans un cadre unique et cohérent, des équations couplées pour la diffusion de nucléons d'une part, et des potentiels microscopiques obtenues avec la matrice G de Melbourne représentant l'interaction entre le projectile et un nucléon de la cible, et une description de cette dernière via la RPA. La deuxième partie est dédiée à la présentation des codes que nous avons développés durant ce projet de thèse : MINOLOP pour le calcul de potentiels microscopiques à partir de la matrice G de Melbourne et d'informations de structure données sous la forme d'une densité à 1 corps, et ECANOL pour la résolution des équations en voies couplées avec des potentiels non locaux en entrée. Enfin, nous présentons nos premières applications basées sur ces deux codes : l'étude d'émission de pré-équilibre due à des excitations à 2 phonons dans le ^{90}Zr .

Title: Microscopic nonlocal potentials for the study of scattering observables of nucleons within the coupled channel framework

Keywords: Nuclear reactions, nuclear structure, optical model, nonlocality, coupled channels

Abstract: A good understanding and prediction capacity of neutron scattering cross sections is crucial to many nuclear technologies, among which all kinds of reactors based on fission process. For deformed nuclei, the computation of scattering observables for the elastic channel and the first, low-lying excited states requires coupled channel calculations. Local, phenomenological optical and macroscopic transition potentials are the most commonly used in coupled channel analyses, but their accuracy outside of their fitting range remains unpredictable. Microscopic approaches are being developed in order to improve prediction power and solve the extrapolation issue. Potentials obtained microscopically are nonlocal, and recent studies have emphasized the importance of treating explicitly this nonlocality, without using a localization procedure. Our goal in the present work is to develop the tools required to study in a quantum framework with no adjustable

parameter, the impact of the nonlocality of potentials on scattering observables of nucleon-nucleus reactions. In order to be able to study any kind of nucleus (spherical or deformed), we do our study in the coupled channel framework. The first part of this paper is dedicated to the derivation in a unique, consistent scope of coupled equations for nucleon-nucleus scattering and of the potentials obtained with the Melbourne G matrix (representing the interaction between the projectile and one nucleon of the target) and RPA structure input. Secondly, we describe the codes which we wrote during this Ph.D. project : MINOLOP for the computation of microscopic potentials using the Melbourne G matrix and structure inputs given in terms of a 1-body density, and ECANOL for the resolution of coupled channel equations using nonlocal potentials as input. Eventually, we present our first applications using these two codes to study pre-equilibrium emissions due to 2-phonon excitations in ^{90}Zr .

